WL-TR-95-2062

ELECTRON DETACHMENT AND GAS
DIELECTRIC PHENOMENA

L.G. CHRISTOPHOROU
P.G. DATSKOS
L.A. PINNADUWAGE
J.G. CARTER

UNIVERSITY OF TENNESSEE
KNOXVILLE TN 37996

MAY 1995

FINAL REPORT FOR 04/01/92-04/01/95

APPROVED FOR PUBLIC RELEASE; DISTRIBUTION IS UNLIMITED.

19960322 004

AEROPROPULSION AND POWER DIRECTORATE
WRIGHT LABORATORY
AIR FORCE MATERIEL COMMAND
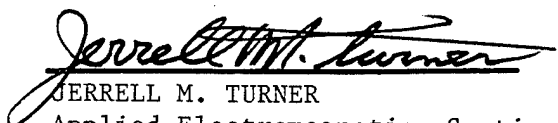WRIGHT PATTERSON AFB OH 45433-7251

DTIC QUALITY INSPECTED 1

NOTICE

WHEN GOVERNMENT DRAWINGS, SPECIFICATIONS, OR OTHER DATA ARE USED FOR ANY PURPOSE OTHER THAN IN CONNECTION WITH A DEFINITE GOVERNMENT-RELATED PROCUREMENT, THE UNITED STATES GOVERNMENT INCURS NO RESPONSIBILITY OR ANY OBLIGATION WHATSOEVER. THE FACT THAT THE GOVERNMENT MAY HAVE FORMULATED OR IN ANY WAY SUPPLIED THE SAID DRAWINGS, SPECIFICATIONS, OR OTHER DATA, IS NOT TO BE REGARDED BY IMPLICATION, OR OTHERWISE IN ANY MANNER CONSTRUED, AS LICENSING THE HOLDER, OR ANY OTHER PERSON OR CORPORATION; OR AS CONVEYING ANY RIGHTS OR PERMISSION TO MANUFACTURE, USE, OR SELL ANY PATENTED INVENTION THAT MAY IN ANY WAY BE RELATED THERETO.

THIS REPORT IS RELEASABLE TO THE NATIONAL TECHNICAL INFORMATION SERVICE (NTIS). AT NTIS, IT WILL BE AVAILABLE TO THE GENERAL PUBLIC, INCLUDING FOREIGN NATIONS.

THIS TECHNICAL REPORT HAS BEEN REVIEWED AND IS APPROVED FOR PUBLICATION.

JERRELL M. TURNER
Applied Electromagnetics Section
Advanced Power Systems Branch
Aerospace Power Division
Aero Propulsion and Power Directorate

MICHAEL A. MARCINIAK, Major, USAF
Power Semiconductor Technology Section
Power Components Branch
Aerospace Power Division
Aero Propulsion and Power Directorate

MICHAEL D. BRAYDICH, Lt Col., USAF
Chief
Aerospace Power Division

IF YOUR ADDRESS HAS CHANGED, IF YOU WISH TO BE REMOVED FROM OUR MAILING LIST, OR IF THE ADDRESSEE IS NO LONGER EMPLOYED BY YOUR ORGANIZATION PLEASE NOTIFY WL/POOC WRIGHT-PATTERSON AFB OH 45433-7919 TO HELP MAINTAIN A CURRENT MAILING LIST.

Copies of this report should not be returned unless return is required by security considerations, contractual obligations, or notice on a specific document.

REPORT DOCUMENTATION PAGE

Public reporting burden for this collection of information is estimated to average 1 hour per response, including the time for reviewing instructions, searching existing data sources, gathering and maintaining the data needed, and completing and reviewing the collection of information. Send comments regarding this burden estimate or any other aspect of this collection of information, including suggestions for reducing this burden, to Washington Headquarters Services, Directorate for Information Operations and Reports, 1215 Jefferson Davis Highway, Suite 1204, Arlington, VA 22202-4302, and to the Office of Management and Budget, Paperwork Reduction Project (0704-0188), Washington, DC 20503.

1. AGENCY USE ONLY (Leave blank)	2. REPORT DATE MAY 1995	3. REPORT TYPE AND DATES COVERED FINAL 04/01/92--04/01/95

4. TITLE AND SUBTITLE ELECTRON DETACHMENT AND GAS DIELECTRIC PHENOMENA

5. FUNDING NUMBERS
C F33615-92-C-2221
PE 61102
PR 2301
TA DW
WU 00

6. AUTHOR(S)

L. G. Christophorou, P. G. Datskos, L. A. Pinnaduwage, and J. G. Carter

7. PERFORMING ORGANIZATION NAME(S) AND ADDRESS(ES)

UNIVERSITY OF TENNESSEE
Knoxville, TN 37996

8. PERFORMING ORGANIZATION REPORT NUMBER

9. SPONSORING/MONITORING AGENCY NAME(S) AND ADDRESS(ES)
AEROPROPULSION AND POWER DIRECTORATE
WRIGHT LABORATORY
AIR FORCE MATERIEL COMMAND
WRIGHT PATTERSON AFB OH 45433-7251

10. SPONSORING/MONITORING AGENCY REPORT NUMBER

WL-TR-95-2062

11. SUPPLEMENTARY NOTES

12a. DISTRIBUTION/AVAILABILITY STATEMENT
APPROVED FOR PUBLIC RELEASE; DISTRIBUTION IS UNLIMITED.

12b. DISTRIBUTION CODE

13. ABSTRACT (Maximum 200 words)

Measurements are reported on the rate constants and cross sections of electron attachment to SF_6, c-C_4F_6, and C_6F_6 as a function of temperature in the range 300 to 600 K. Measurements are reported, also, of the rate constant for the temperature-enhanced autodetachment from SF_6^-, c-$C_4F_6^-$, and $C_6F_6^-$ in the same temperature range. New techniques are described for the accurate measurement of the effect of temperature on electron attachment and detachment processes and on the photodetachment of anions in dense fluids. Photodetachment measurements on SF_6^- and $C_6F_6^-$ are reported and discussed. Optically-enhanced electron attachment has been observed in laser-irradiated H_2, SiH_4 and CH_4. The usefulness of these findings in understanding gas dielecrtic phenomena and plasma processes in gas-discharge-based technologies is discussed.

14. SUBJECT TERMS
Electron attachment; electron detachment; photodetachment; optically-enhanced attachment; dielectric phenomena; plasma processing; sulfur hexafluoride; hydrogen; silane

15. NUMBER OF PAGES
143

16. PRICE CODE

17. SECURITY CLASSIFICATION OF REPORT UNCLASSIFIED	18. SECURITY CLASSIFICATION OF THIS PAGE UNCLASSIFIED	19. SECURITY CLASSIFICATION OF ABSTRACT UNCLASSIFIED	20. LIMITATION OF ABSTRACT SAR

TABLE OF CONTENTS

1. Summary

In this report are summarized the results of a 3-year research effort on electron detachment and gas dielectric phenomena. The research focused on understanding the basic processes involved in gas breakdown and gas discharges, and the properties of systems of direct interest to gas insulation and gas-discharge-based technologies.

Measurements are reported on the rate constants and cross sections of electron attachment to SF_6, c-C_4F_8, and C_6F_6 as a function of temperature from 300 to 600 K. Measurements are reported, also, of the rate constant for temperature-enhanced autodetachment from SF_6^-, c-$C_4F_8^-$, and $C_6F_6^-$ in the same temperature range. These findings have been understood in terms of the internal energy of the neutral molecule and its electron affinity, and in terms of the internal energy of the parent anion. Consistent with the high value of the electron affinity of SF_6, no significant autodetachment in the temperature range 300 to 600 K has been observed in SF_6 / N_2 mixtures. The dielectric strength of SF_6 was found to increase with temperature in the range 300 to 600 K and this is explained on the basis of the effect of temperature on electron attachment to SF_6 at high energies.

New techniques for accurate measurement of the effect of temperature on electron attachment and detachment processes in electronegative gases, and the photodetachment threshold and photodetachment cross section of negative ions in dense gases (and in liquids) are described. Accurate measurements have been made of the photodetachment cross section and energetics for SF_6^- in N_2 and CH_4 buffer gases. Similar measurements were made for $C_6F_6^-$ in both the gaseous and the condense phase.

Optically-enhanced electron attachment has been observed in hydrogen, silane, and methane.

The results obtained aided our understanding of uniform and non-uniform field breakdown characteristics of dielectric gases ,and, also, our understanding of phenomena observed in plasma processing of materials, negative ion sources, and lasing systems.

1

2. Introduction

This report describes the work that has been conducted under the project entitled " *Electron Detachment and Dielectric Phenomena*" during a 3-year period from April 14, 1992 to April 23, 1995. This research was performed under the auspices of the Wright Laboratory, Wright-Patterson Air Force Base of the Department of the Air Force, Contract Number F3361592-C-2221; the Air Force Contact was Dr. Alan Garscadden.

The research performed under this contract focused on understanding the basic processes involved in gas breakdown and gas discharges in order to pave the way for improvements in the reliability of Gas-Insulated Systems (GIS) and gas-discharge-based technologies. The principal goals of the present work were:

(i) The quantification and understanding of electron detachment from negative ions in dielectric gases / gas mixtures under varied experimental conditions of applied electric field, gas pressure and temperature;

(ii) The investigation of the effect of temperature on the electron attachment to molecules and electron autodetachment from parent negative ions of interest to gaseous dielectrics.

(iii) The accurate measurement of the photodetachment thresholds and the absolute photodetachment cross section for SF_6^- and other anions of interest to gas-discharge technologies and the effect of the medium on this process.

(iv) Electron attachment to electronically excited molecules.

The major accomplishments of this project can be summarized as follows:

(1). Measurements of the rate constants and cross sections of electron attachment to SF_6, c-C_4F_8, and C_6F_6 as a function of temperature (and, also, as a function of applied electric field and gas pressure) from room temperature to about 600 K.

(2). Measurement of the rate constant for temperature-enhanced autodetachment from SF_6^-, c-$C_4F_8^-$, and $C_6F_6^-$ from room temperature to about 600 K.

(3). Development of an understanding of the effect of temperature on electron attachment and

2

autodetachment in terms of the internal energy of the neutral molecule and its electron affinity, and in terms of the internal energy of the parent anion.

(4). Establishment of a new technique which allows simultaneous study of the effect of internal ro-vibrational energy of molecules on the formation of parent anions and of the effect of ro-vibrational energy on the autodechment of the parent anions.

(5). Development of a sensitive method which allows the accurate measurement of the photodetachment thresholds and the photodetachment cross sections as a function of photon energy above threshold in low- and high-pressure gases and in liquids.

(6). Measurement of the photodetachment threshold and the photodetachment cross section of SF_6^- in high pressure nitrogen and in high pressure methane.

(7). Measurement of the photodetachment threshold and the photodetachment cross section for a prototypical anion, namely $C_6F_6^-$, in both the gaseous and the condensed phases of matter in an effort to quantify and understand the effect of the medium on the photodetachment process and its energetics.

(8). The finding that SF_6 / N_2 exhibit no significant autodetachment in the temperature range 300 to 600 K. This is consistent with the high value of the electron affinity of the SF_6 molecule.

(9) The finding that the uniform field dielectric strength of SF_6 increases with increasing temperature in the range 300 to 600 K. This is consistent with the effect of temperature on the electron attachment properties of the SF_6 molecule at high energies.

(10). Confirmation of the formation of H^- in UV-laser irradiated hydrogen by *in situ* photodetachment measurements and by measurement of the negative ion mobilities.

(11). Observation of optically-enhanced electron attachment in laser-irradiated silicon and in laser-irradiated methane.

(12). Utilization of the results obtained on the effects of internal energy of molecules and anions on their electron attachment and detachment properties to aid the understanding of uniform and nonuniform field breakdown characteristics of dielectric gases and other gas-discharge-based technologies such as those involved in plasma processing of materials, negative ion sources, and lasing systems.

The results of these investigations have been fully described in 16 open literature publications. These are listed in Section 2 of this report. In Section 2 of the report are also listed the papers which have been presented at scientific meetings and which are based on work conducted in part under this contract. Two of the review papers partially sponsored by this contract are given as Appendix A and as Appendix B.

3. Open Literature Publications and Presentations at Scientific Conferences

3.1. Open Literature Publications

1. P. G. Datskos, L. G. Christophorou, and J. G. Carter, "Temperature-Enhanced Electron Detachment From $C_6F_6^-$ Negative Ions," J. Chem. Phys. **98**, 7875-7882 (1993).

2. P. G. Datskos, L. G. Christophorou, and J. G. Carter, "Temperature Dependence of Electron Attachment and Detachment in SF_6 and $c-C_4F_6$, " J. Chem. Phys. **99**, 8607-8616 (1993).

3. L. G. Christophorou, L. A. Pinnaduwage, and P. G. Datskos, "Electron Attachment to Excited Molecules," In <u>Linking the Gaseous and the Condensed Phases of Matter: The Behavior of Slow Electrons</u>, L. G. Christophorou, E. Illenberger, and W. F. Schmidt (Eds.), Plenum Press, New York, 1994, pp. 415-442.

4. L. A. Pinnaduwage and L. G. Christophorou, "Verification of H^- Formation in UV-Laser-Irradiated Hydrogen: Implications for Negative Ion and Neutral Beam Technologies," J. Appl. Phys. **79**, 46-54 (1994).

5. T. Kielkopf, L. A. Pinnaduwage, and L. G. Christophorou, "Lasing in Aluminum Following Photoionization and Neutralization in the Presence of H_2: The Role of H^-," Phys. Rev. **A49**, 2675-2680 (1994).

6. L. G. Christophorou, "Linking the Gaseous and the Condensed Phases of Matter: The Slow Electron and its Interactions," In <u>Linking the Gaseous and the Condensed Phases of Matter: The Behavior of Slow Electrons</u>, L. G. Christophorou, E. Illenberger, and W. F. Schmidt (Eds.), NATO ASI Series, Plenum Press, 1994, pp. 3-30.

7. L. G. Christophorou, P. G. Datskos, and H. Faidas, "Photodetachment in the Gaseous, Liquid,

and Solid States of Matter," J. Chem. Phys. **101**, 6728-6742 (1994).

8. L. A. Pinnaduwage and L. G. Christophorou, "On the Mechanism of Enhancement of Non-Uniform Field Breakdown Characteristics Due to Additive Gases," In Gaseous Dielectrics VII, L. G. Christophorou and D. R. James (Eds.), Plenum Press, 1994, pp. 123-130.

9. P. G. Datskos, L. G. Christophorou, and J. G. Carter, "Attachment of Low-Energy Electrons to "Hot" SF_6 Molecules," In Gaseous Dielectrics VII, L. G. Christophorou and D. R. James (Eds.), Plenum Press, 1994, pp. 23-30.

10. P. G. Datskos, L. G. Christophorou, and J. G. Carter, "Effect of Temperature on the Electron Attachment and Detachment Properties of c-C_4F_6," In Gaseous Dielectrics VII, L. G. Christophorou and D. R. James (Eds.), Plenum Press, 1994, pp. 13-20.

11. L. A. Pinnaduwage, M. Z. Martin, and L. G. Christophorou, "Enhanced Negative Ion Formation in UV-Laser-Irradiated Silane; Implications for Plasma Deposition of Amorphous Silicon," Appl. Phys. Letts. **65**, 2571-2573 (1994).

12. L. G. Christophorou, P. G. Datskos, and J. G. Carter, "Response to "Comment on "Temperature-Enhanced Electron Detachment from $C_6F_6^-$ Negative Ions," J. Chem. Phys. **100**, 6983 (1994).

13. P. G. Datskos, J. G. Carter and L. G. Christophorou, "Photodetachment of SF_6^-," Chem. Phys. Letts. (In Press).

14. L. G. Christophorou and P. G. Datskos, "Effect of Temperature on the Formation and Autodestruction of Parent Anions," International. Journal of Mass Spectrometry and Ion Processes (Accepted for Publication).

15. L. A. Pinnaduwage, M. Z. Martin, and L. G. Christophorou, "Enhanced Negative Ion Formation in ArF-Laser-Irradiated Mathane: Possible Implications for Plasma Processing Discharges," Contributions to Plasma Physics (Accepted for Publication).

16. L. G. Christophorou, R. Van Brunt, and J. Olthoff, "Fundamental Processes in Gas Discharges," Invited Lectures, Proceedings XIth International Conference on Gas Discharges and Their Applications, Tokyo, Japan, September 11-15, 1995.

3.2. Presentations at Scientific Meetings

1. L. G. Christophorou, "Linking the Gaseous and the Condensed Phases of Matter: The Slow Electron and Its Interactions," NATO ASI, Patras, Greece, September 5-18, 1993.

2. L. G. Christophorou, L. A. Pinnaduwage, and P. G. Datskos, "Electron Attachment to Excited Molecules," NATO ASI, Patras, Greece, September 5-18, 1993.

3. P. G. Datskos, L. G. Christophorou, and J. G. Carter, "Temperature-Enhanced Detachment from Polyatomic Parent Negative Ions," NATO ASI, Patras, Greece, September 5-18, 1993.

4. J. F. Kielkopf, L. A. Pinnaduwage, and L. G. Christophorou, "Production of the 4s $^2S_{1/2}$ State of Al and Stimulated Emission at 3962 A by $Al^+ + H^-$ Charge Neutralization Collisions," American Physical Society Meeting, Crystal City, Virginia, April 18-22, 1994.

5. L. A. Pinnaduwage and L. G. Christophorou, "On the Mechanism of Enhancement of Non-Uniform Field Breakdown Characteristics Due to Additive Gases," Seventh International Symposium on Gaseous Dielectrics, Knoxville, Tennessee, April 24-28, 1994.

6. P. G. Datskos, L. G. Christophorou, and J. G. Carter, "Effect of Temperature on the Low-

7

Energy Electron Attachment and Detachment Properties of c-C_4F_6," Seventh International Symposium on Gaseous Dielectrics, Knoxville, Tennessee, April 24-28, 1994.

7. P. G. Datskos, L. G. Christophorou, and J. G. Carter, "Attachment of Low-Energy Electrons to "Hot" SF_6 Molecules," Seventh international Symposium on Gaseous Dielectrics, Knoxville, Tennessee, April 24-28, 1994.

8. L. A. Pinnaduwage, M. Z. Martin, and L. G. Christophorou, "Efficient Negative Ion Formation in UV-Laser -Irradiated Silane: Implications for Plasma Deposition of Amorphous Silicon," 47th Annual Gaseous Electronics Conference, Gaithersburg, Maryland, October 18-21, 1994.

9. P. G. Datskos, L. G. Christophorou, and J. G. Carter, "Photodetachment of SF_6^- and $C_6F_6^-$ Negative Ions in the Gaseous Phase," 47th Annual Gaseous Electronics Conference, Gaithersburg, Maryland, October 18-21, 1994.

10. L. G. Christophorou, "Electron Attachment to Excited Molecules," International Symposium on Electron- and Photon- Molecule Collisions and Swarms, Berkeley, CA, July 22-25, 1995.

11. L. G. Christophorou, "Fundamental Processes in Gas Discharges," XIth International Conference on Gas Discharges and Their Applications, Tokyo, Japan, September 11-15, 1995.

4. Photodetachment in Low-Pressure Gases, High-Pressure Gases And in Liquids

4.1. Photodetachment of H$^-$ in Mixtures of H$_2$ and He

A technique has been developed to conduct *in situ* photodetachment studies of negative ions in high-pressure gases (1 to 1000 Torr). This is important for gas-insulated systems and gas discharges, since the method yields cross sections which are for species which are actually present in the system. The initial measurements were made for H$^-$ ions for which the photodetachment cross section is well established. These photodetachment and auxiliary ion mobility measurements also served another purpose: they identified the negative ion species in laser-irradiated hydrogen. Both the method and the results are fully described in a paper published in the Journal of Applied Physics which is reproduced below (pages 10-18).

Verification of H⁻ formation in ultraviolet-laser-irradiated hydr⌐ Implications for negative ion and neutral beam technologies

L. A. Pinnaduwage and L. G. Christophorou
Atomic, Molecular, and High Voltage Physics Group, Health Sciences Research Division, Oak Ridge National Laboratory, P.O. Box 2008, Oak Ridge, Tennessee 37831-6122, and Department of Physics, University of Tennessee, Knoxville, Tennessee 37996

Photodetachment and ion mobility measurements are reported confirming the efficient H⁻ formation in UV-laser-irradiated H_2 reported earlier [L. A. Pinnaduwage and L. G. Christophorou, Phys. Rev. Lett. **70**, 754 (1993)]. The implications of the efficienct H⁻ formation in UV-laser-irradiated H_2 (and other types of negative ions in UV-laser-irradiated gases) for negative ion and neutral particle beam technologies are discussed. Also, the possible contribution to H⁻ formation in H_2 discharge sources from electron attachment to high-lying electronically excited states of H_2 is indicated.

I. INTRODUCTION

A. Efficient H⁻ formation in ArF-laser-irradiated H_2

Recently we reported[1] experimental evidence for efficient H⁻ formation in ArF-excimer-laser-irradiated H_2. Due to the coincidence of the two-photon energy at this laser line with the $E,F\ ^1\Sigma_g^+$ (v=6) state of H_2, an efficient transition to energies above the ionization threshold was achieved via a (2+1) resonance enhanced multiphoton ionization (REMPI) process. Electrons produced via photoionization were shown to attach to the concomitantly produced superexcited states (electronically excited states lying above the ionization threshold, SES) of H_2 or some other electron attaching species produced via SES. Since electron attachment to the ground $X\ ^1\Sigma_g^+$ (v=0) state—which is the only state populated at room temperature—is extremely weak [maximum electron attachment rate constant $\sim 10^{-13}$ cm³ s⁻¹ (Ref. 2)], electron attachment must have occurred inside the laser-irradiated region. Since electron attachment to the high-vibrational states of the ground $X\ ^1\Sigma_g^+$ state (hereafter denoted by HV states) is known to be orders of magnitude larger[3,4] compared to the $X\ ^1\Sigma_g^+$ (v=0) state, a possible mechanism for the observed H⁻ formation was electron attachment to HV states produced indirectly via the $E,F\ ^1\Sigma_g^+\rightarrow B\ ^1\Sigma_u^+\rightarrow X\ ^1\Sigma_g^+$ radiative transitions. This possibility was ruled out by the observed laser fluence dependencies;[1] also the estimated rate constant for the observed electron attachment process was much larger compared to electron attachment to the HV states; see below.

The electron attachment rate constant associated with the observations of Ref. 1 could not be evaluated since the lifetime of the electron attaching species was not known. However, an indirect measure of the efficiency of H⁻ formation can be obtained by calculating the electron attachment rate constant involved if it were due to the long-lived (lifetimes $\sim 10^5$ s) HV states produced indirectly via the above-mentioned radiative transitions. Even if this process occurred with 100% efficiency, the electron attachment rate constant would have to be $\sim 10^{-6}$ cm³ s⁻¹ to explain the observed H⁻ formation; see Fig. 1.[1] The maximum electron attachment rate constant for the HV states is $\sim 10^{-8}$ cm³ s⁻¹.[5,6] Since the maximum conversion efficiency for HV states formation via

$E,F\ ^1\Sigma_g\rightarrow B\ ^1\Sigma_g^+\rightarrow X\ ^1\Sigma_g^+$ radiative transitions is $\sim 3\%$,[7] it is safe to conclude that the actual electron attachment rate constant involved (for short-lived electronically excited states) is several orders of magnitude larger compared to the HV states. The H⁻ number density corresponding to the high-laser-intensity data of Fig. 1 is $\sim 10^9$ ions/cm³.

In the experiments of Ref. 1, the positive ions produced via laser photoionization were rejected and only the negative ions and the unattached electrons from the laser-irradiated region were extracted to the detection region by using a three-electrode arrangement. The voltage signals induced by the motion of the negative ions and electrons in the detection region were monitored; the signals due to the negative ions and the electrons were distinguished by their vastly different drift velocities (see the signal wave form no. 1 in Fig. 3 in Sec. II). Therefore, the evidence for H⁻ formation in Ref. 1 was indirect; although H⁻ was the only possible negative ion from H_2, we did not have independent confirmation of the identity of the negative ion. In order to confirm the formation of H⁻ ions, we conducted (i) a photodetachment study where, the photodetachment cross section of the negative ions was measured at the XeCl excimer laser line; (ii) an ion mobility study where the mobilities of the negative ions (and concomitantly produced positive ions) were measured; these studies are described in Sec. II. The only remote possibility of producing negative ions of other species would be due to the presence of O_2 or water vapor (which was highly unlikely with our vacuum system of base pressure $\sim 5\times 10^{-6}$ Pa); one could expect O⁻, O_2^-; or OH⁻ ions if those impurities were present. Our measured photodetachment and ion mobility parameters lie well outside the corresponding parameters for these ions; see below. We also note that the previously unexplained observation[8] of lasing in Al at the $3s4s\ ^2S_{1/2}\rightarrow 3s3p\ ^2P_{3/2}$ transitions following ArF laser irradiation of Al in the presence of H_2 has recently been shown[9] to be due to the population of Al ($3s3p\ ^2P_{3/2}$) via charge neutralization of Al⁺ (produced via photoionization of Al with ArF laser) by H⁻ (produced via the mechanism reported in Ref. 1).
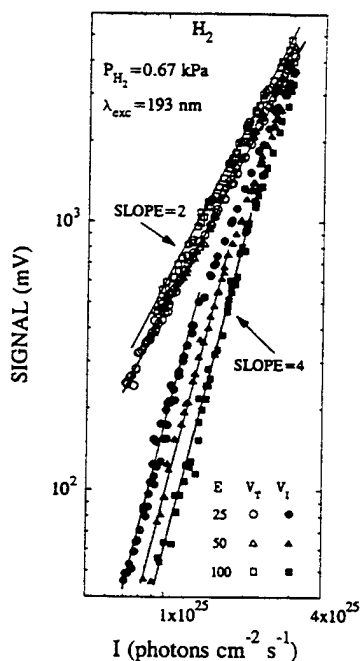
FIG. 1. Laser intensity I, dependence of the measured total V_T, and negative ion V_I signals for the experimental parameters indicated in the figure; E is the applied electric field in $V\,cm^{-1}$. V_T is proportional to the number density of electrons initially produced via photoionization; the slope of 2 for the V_T curve indicates effective two-photon ionization for the (2+1) REMPI process due to strong photon absorption from the intermediate $E.F\ ^1\Sigma_g^+$ ($v=6$) state. The fraction of electrons converted to negative ions increases with increasing I, and at high I almost all the electrons are converted to negative ions.

B. Negative ion and neutral beam technologies

Negative ions, notably H^- ions, play special roles in particle accelerators[10] and also in generating neutral beams for magnetic fusion energy research.[11] This is due to the high efficiencies with which negative ions can be converted to neutrals and positive ions. For example, in tandem accelerators negative ions are accelerated to a given voltage V, and at the high-voltage terminal are transformed to positive ions by passage though a stripping foil; thus the resulting positive ions are effectively accelerated to 2 eV energy by the time they arrive at the ground potential terminal. Also, injection and extraction problems of charged particles in circular accelerators can be overcome by using negative ions. For the production of neutral beams for fusion energy research, negative ions have become indispensable due to their high neutralization efficiencies at high energies compared to positive ions.[11,12] It is expected that a 1.3 MeV, 16 A of D^0 or H^0 beam of pulse length of two weeks will be needed when the International Thermonuclear Experimental Reactor (ITER) goes into operation.[13] The currently available H^- beams (from sources which are variations of volume discharge sources) fall far short of this goal: 10 A at 50 keV and 0.1 s pulse length, 0.25 A at 50 keV and 8.6×10^4 s pulse length are two examples.[13]

The possibility of exploiting the observed efficient H^- formation in ArF-excimer-laser-irradiated H_2 (Ref. 1) in a new type of ion source is discussed in Sec. III A. Such a source will be able to generate a wide variety of negative ions (including D^- and O^-), since besides H^- formation in H_2 we have observed the formation of other negative ions in several molecular species (e.g., NO) irradiated by UV lasers.[14,15]

As pointed out in Sec. I A, the mechanism of H^- formation reported in Ref. 1 is also new. In Sec. III B we will discuss the possible involvement of this mechanism for H^- formation in currently popular H_2 discharge sources. It is generally believed[16,17] that dissociative attachment of slow electrons to vibrationally excited molecules is responsible for the formation of H^- in a hydrogen discharge; however, recent studies[17,18] indicate that the measured number densities of vibrationally excited H_2 molecules in such discharges are not large enough to account for the measured H^- number densities. It is possible that the new mechanism reported in Ref. 1 partially contributes to the formation of H^- in hydrogen discharge sources.

II. EXPERIMENTAL VERIFICATION OF H⁻ FORMATION

A. Photodetachment experiment

Direct photodetachment studies on H^- ions have been conducted by Smith and Burch[19] which yielded relative cross sections for the wavelength range of 426–1301 nm. These measurements were consistent with theoretical calculations[20] when normalized to the calculated cross section at 528 nm. Absolute photodetachment cross sections for H^- in the wavelength range of 500–1600 nm have been determined by Popp and Kruse[21] using the H^- emission continuum from a hydrogen arc. These measurements were also consistent with the theoretical calculations.[20]

The high-pressure experimental apparatus employed in the present and in the preliminary experiments on H_2 (Ref. 1) was described in detail earlier.[14] The experimental setup for the present photodetachment studies is shown in Fig. 2. The excimer laser 1 was operated at the ArF line and produced negative ions in the irradiated region.[1] These negative ions and the unattached electrons were directed to the detection region (located between the bottom two electrodes), through a grid in the middle electrode, by an applied electric field.[1] Since the electron attachment rate constant for the $v=0$ level of the ground electronic state of H_2—which is the only vibrational level populated at room temperature—has a peak value of only $\sim10^{-13}\ cm^3\,s^{-1}$,[2] the electron attachment which occurred outside the ArF-laser-irradiated region was negligible. Thus, except for the spreading due to space-charge effects (see Sec. III), the negative ions drifted as a single pulse (swarm) to the detection region. Helium buffer gas was mixed with H_2 in the chamber in order to lower the effective E/N (E is the applied electric field and N is the total gas number density), and thus to obtain distinctly separated electron and ion components in the signal wave forms (see Fig. 3 below).

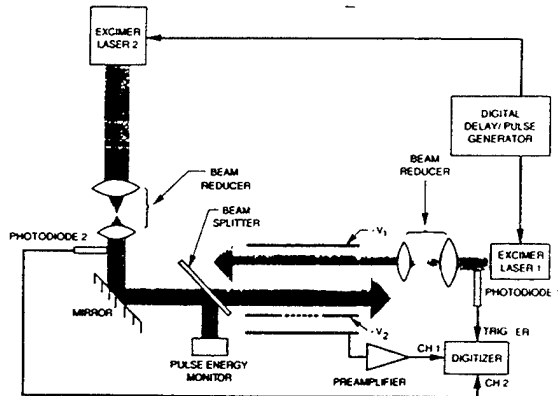The negative ion swarm was intercepted by the detaching pulse from the excimer laser 2 (see Fig. 2) operating at

11

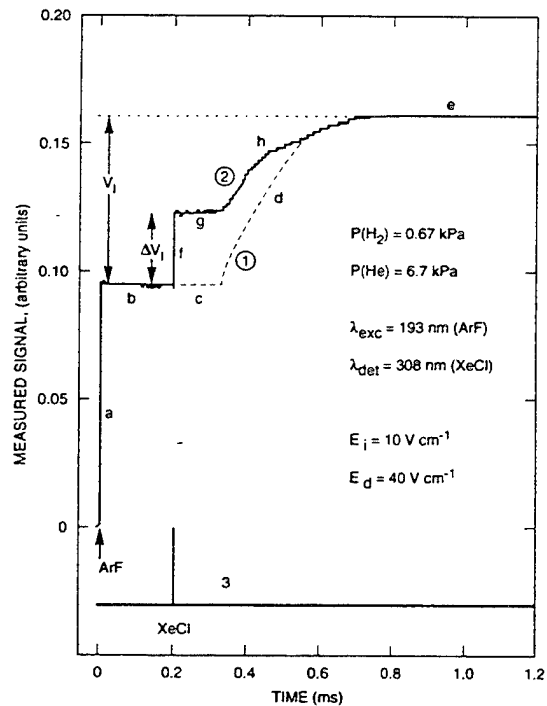FIG. 2. Schematic diagram of the experimental arrangement employed in the photodetachment experiments.

FIG. 3. Typical signal wave forms from a photodetachment experiment, for the experimental parameters indicated in the figure: The ArF laser, producing electrons and negative ions (indirectly), is fired at $t = 0$. The resulting wave form would have looked like wave form 1 (the dashed sections, c,d, were hand drawn) in the absence of the photodetaching XeCl pulse. The initial sharp rise (a) is due to unattached electrons; V_l indicates the magnitude of the slow component of the wave form, i.e., the signal due to negative ions produced by the ArF pulse. Wave form 2 is the actual signal recorded with the firing of both lasers, where the sharp jump in signal ΔV_l in synchronization with the XeCl pulse (shown in wave form 3) is due to the electrons released by photodetachment.

the XeCl (308 nm) line. In order to ensure that all negative ions were intercepted by the detaching laser pulse, (i) the two laser beams were aligned to overlap, and (ii) the cross section of the detaching laser pulse (XeCl) was made larger compared to the ArF pulse. The geometrical cross sections of the XeCl and ArF pulses were 0.8×0.3 and 0.6×0.2 cm², respectively. The XeCl pulse energy was monitored using a beam splitter as shown in Fig. 2; the monitored energy was calibrated with respect to the actual pulse energies in the interaction region. Two Molectron J-25 probes were employed for pulse energy monitoring and calibration. Lumonics model TE-860-4 and EX-500 excimer lasers were employed to provide the ArF and XeCl lines, respectively; the respective pulse durations were ~10 and ~15 ns. The time delay between the two laser pulses was varied using a Stanford Research GD 535 delay/pulse generator. The signal wave forms were recorded with a Nicolet 450 transient digitizer.

Typical signal wave forms are shown in Fig. 3. The wave form labeled 1 (along a, b, c, d, e, where sections c and d were hand drawn) shows how the electron and ion signals due to the ArF laser pulse, fired at $t = 0$, would have looked like in the absence of a detaching pulse. The initial fast rise, a, in the signal is due to the unattached electrons; the drift time for electrons is a few μs and thus the rise in the signal is vertical on this ms time scale. The signal of wave form 1 remains at this level (bc) until the negative ions arrive in the detection region after ~0.35 ms. Then the signal rises slowly (d) due to the motion of the ions in the detection region. The detaching XeCl excimer laser pulse was fired ~0.2 ms after the ArF pulse as shown by the bottom wave form labeled 3; this was the signal from photodiode 2 of Fig. 2, which monitored the arrival of the XeCl pulse. The wave form labeled 2 (along a, b, f, g, h, e) was the actual signal due to electrons and negative ions when the ArF and XeCl pulses were fired with ~0.2 ms delay between them; the additional fast rise in the wave form (f), coincident with the arrival of the XeCl pulse in the interaction region, is due to the electrons detached from the negative ions. For the wave form shown in

Fig. 3, ~40% of the negative ions were detached by the XeCl pulse.

The number of ions photodetached by a laser pulse of intensity I and duration τ_L is given by

$$\int_{n_{io}}^{n_{if}} dn_i = -\int_o^{\tau_L} n_i \sigma_d I \, dt, \tag{1}$$

where n_{io} and n_{if} are the number of negative ions before and after the firing of the detaching pulse, and σ_d is the photodetachment cross section. From Eq.(1) we have

$$\frac{n_{io} - n_{if}}{n_{io}} = 1 - e^{-\sigma_d F} \tag{2}$$

where $F = I\tau_L$ is the laser fluence.

Since photodetachment occurs before the detection region (see Fig. 2), the "photodetachment signal" ΔV_l and the negative ion signal due to ArF pulse, V_l (see Fig. 3), are proportional to the number of ions photodetached by the XeCl pulse and the total number of negative ions produced by the ArF pulse, respectively.
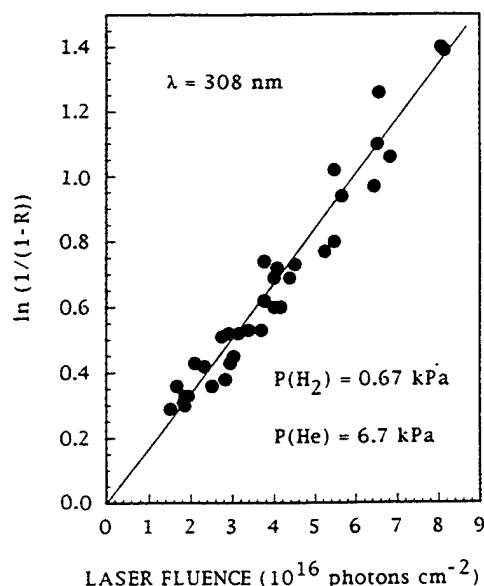
L. A. Pinnaduwage and L. G. Christophorou

12

λ = 308 nm

P(H₂) = 0.67 kPa

P(He) = 6.7 kPa

LASER FLUENCE (10^{16} photons cm^{-2})

FIG. 4. The quantity $\ln[1/(1-R)]$, where $R = \Delta V_I/V_I$ (ΔV_I is the photodetachment signal and V_I is the negative ion signal due to the ArF pulse), is plotted vs the fluence of the photodetaching XeCl laser pulse.

Thus

$$R = \frac{\Delta V_I}{V_I} = 1 - e^{-\sigma_d F}, \qquad (3)$$

$$\ln\left(\frac{1}{1-R}\right) = \sigma_d F. \qquad (4)$$

A plot of $\ln[1/(1-R)]$ vs F for the data taken at the XeCl laser line (wavelength=308 nm) is shown in Fig. 4. From the gradient of the graph, we determined a photodetachment cross section σ_d of $(1.7\pm0.2)\times10^{-17}$ cm^2 in good agreement with the expected value of $\sim1.7\times10^{-17}$ cm^2.[19–21] In the unlikely event of having large amounts of O_2 or water vapor impurities in the system, O^-, O_2^-, or OH^- may constitute the negative ion component. Photodetachment cross sections for those ions at 308 nm are not available, but the measured cross-section values (for wavelengths longer than 400 nm) lie in the 10^{-18} cm^2 range.[22]

B. Ion mobility measurements

Measurements of the mobilities of ions due to H_2 in H_2 gas have been reported by several groups,[23–25] and those results have been summarized.[26]

The present ion mobility measurements were conducted in the same apparatus that was used for the photodetachment experiments (see Fig. 2); however, only the excimer laser 1 was needed in the mobility experiments. A light pulse from this laser produced electrons and positive ions via photoionization of H_2. The electrons attached to the excited species same produced concomitantly by the laser pulse.[1] By applying suitably oriented electric fields in the ion production and detection regions (located between the top two and the bot-

tom two electrodes, respectively; see Fig. 2), either the negative ions or the positive ions could be directed to the detection region. The current due to the motion of the charged particles in the detection region was integrated using an external RC circuit with $RC\sim5$ s; the resulting (linearly) rising voltage pulse was recorded with a Nicolet model 450 transient digitizer. For the ion mobility experiments the interelectrode gaps in the ion production and ion detection regions were (1.00 ± 0.02) and (2.29 ± 0.03) cm, respectively, and the diameter of the grid in the middle electrode, through which the ions were extracted into the detection region, was ~7.6 cm; the chamber was filled with H_2 (no buffer gas was used).

A typical signal wave form in the negative mode (i.e., the signal due to the unattached electrons and the negative ions) is shown in Fig. 5. The initial fast rise in the signal is due to the unattached electrons. The plateau following the initial rise indicates the time taken by the negative ions to reach the grid and the subsequent slow rise is due to the motion of the negative ions in the detection region. It is important to note that electron attachment occurred only inside the laser-irradiated volume; the maximum electron attachment rate constant for the zero vibrational state of the ground electronic state of H_2 is only $\sim10^{-13}$ cm^3 s^{-1},[2] and thus virtually no negative ions would be produced outside the laser-irradiated volume. The geometrical cross section of the laser pulse was $\sim0.1\times0.5$ cm^2 and thus the "width" (i.e., the dimension along the drift direction) of the ion (and electron) pulses was ~0.1 cm.

The slow component representing the motion of the negative ions in Fig. 5 is not a straight line, as would be expected from a narrow ion pulse. The rounding at the edges is mainly due to space-charge effects. It must be noted that a signal level of ~100 mV roughly corresponded to $\sim10^8$ ions/cm^3. It has been shown[27] that space-charge effects can be non-negligible even at ion densities of 10^5 ions/cm^3. We define the drift time τ_d as the time interval between the intersections of a straight line drawn symmetrically on the rising curve with the initial and final signal levels indicated by the two arrows in Fig. 5. It was found that $\tau_d(E/N)$ depended on the signal level for a given E/N value. The mea-
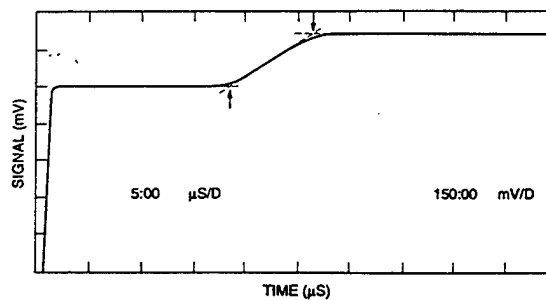

FIG. 5. A typical signal wave form in the "negative" mode consisting of a fast component due to (unattached) electrons and a slow component due to negative ions. The rounding of the negative ion signal at the edges was mainly due to space-charge effects; the drift time was defined as the time between the intersections of the straight line drawn symmetrically on the rising curve and the initial and final signal levels, as indicated by the arrows.

J. Appl. Phys., Vol. 76. No. 1, 1 July 1994

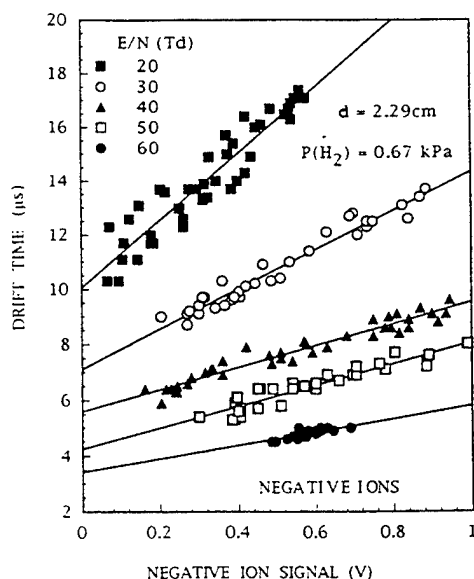L. A. Pinnaduwage and L. G. Christophorou   49

13

FIG. 6. Measured negative ion drift times vs negative ion signals for the five E/N values indicated in the figure. The space-charge-free drift times were taken to be the extrapolated values at zero signal levels. The E/N is given in units of Td ($=10^{-17}$ V cm^2).

sured drift times for different negative ion signal strengths are shown in Fig. 6 for five values of E/N. The dependence of the drift time on the signal strength is due mainly to space-charge effects, i.e., due to the local E/N being different from the applied E/N value. As can be expected, the space-charge effects become smaller at larger E/N values and smaller signal levels. The "space-charge-free" drift times were taken to be the drift times extrapolated to zero signal levels (see Fig. 6).

The space-charge-free drift times, together with the measured drift distance of (2.29 ± 0.03) cm in the detection region were used to calculate the ionic drift velocities. Our measurements are compared with the published[26] drift velocities for H$^-$ ions in H$_2$ in Table I.

We also measured the drift velocities of the positive ions produced, by reversing the applied electric field. The measured positive ion drift times are shown in Fig. 7 for different positive ion signal levels. The space-charge effects are apparently smaller for positive ions. The reason for this is not entirely understood, although it could be rationalized as follows: Equal numbers of positive ions and electrons are produced in the laser-irradiated volume in the interaction region and a fraction of the electrons are converted to negative ions. The electrons come out of this plasma very quickly, and therefore there is a charge imbalance in the plasma (i.e., the laser-irradiated volume) before the positive and negative ions begin to move in opposite directions. As the positive and negative ions start to separate,the positive charges "hold back" the departing negative ions, making the negative ion pulse broader. This effect will be larger at smaller applied electric fields comparable to space-charge fields due to positive ions. On the other hand, such an effect on the positive

TABLE I. Comparison of the drift velocities measured for negative ions in pure H$_2$ in the present experiments with the published values for H$^-$ ions in H$_2$.

| E/N (Td) | Negative ion drift velocity (10^4 cm s^{-1}) | | |
	H$^-$ (Ref. 26) (Total error: $\pm3\%$)	Present measurements (Total error: $\pm7\%$)	Difference[a]
20	22.7	22.7	0%
30	33.0	32.3	-2%
40	42.7	40.9	-4%
50	52.0	53.9	$+4\%$
60	60.9	66.6	$+9\%$

[a]Percent difference between our measurements and the published values (see Ref. 26) for H$^-$ ions.

ions by the negative ions will be smaller, since the negative ion density is smaller.

The present positive ion drift velocities are compared with the published[26] drift velocities for H$_3^+$ ions in H$_2$ gas in Table II. It must be noted that virtually all the H$_2^+$ ions produced via photoionization in the ion production region are converted to H$_3^+$ ions via ion-molecule reactions before they arrive in the detection region. The reaction

$$H_2^+ + H_2 \rightarrow H_3^+ + H \tag{5}$$

has a cross section of $\sim 10^{-14}$ cm^2.[28]

It can be seen from Tables I and II that the present measured values of the drift velocities of negative and positive ions are within a few percent of the published values for H$^-$ and H$_3^+$ ions; also see Fig. 8. This confirms that the negative ions produced via ArF laser irradiation of H$_2$ gas are indeed H$^-$ ions. Any other negative ion certainly would have drift
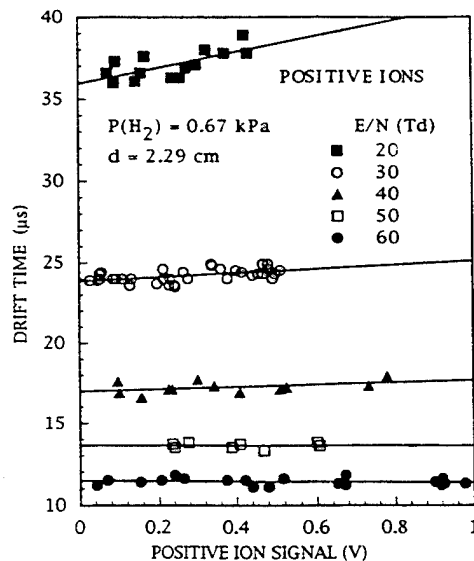

FIG. 7. Measured positive ion drift times vs positive ion signals for the five E/N values indicated in the figure. The space-charge-free drift times were taken to be the drift times extrapolated to zero signal levels. The E/N is given in units of Td ($=10^{-17}$ V cm^2).

L. A. Pinnaduwage and L. G. Christophorou

14

TABLE II. Comparison of the drift velocities measured for positive ions in pure H_2 in the present experiments with the published values for H_3^+ ions in H_2.

E/N (Td)	Positive ion drift velocity (10^4 cm s^{-1})		
	H_3^+ (Ref. 26) (Total error: ±2%)	Present measurements (Total error: ±7%)	Difference[a]
20	6.07	6.4	+5%
30	9.11	9.6	+5%
40	12.3	13.4	+9%
50	15.7	16.8	+7%
60	19.5	19.9	+2%

[a]Percent difference between our measurements and the published values (see Ref. 26) for H_3^+ ions.

velocities lower than the measured values and the differences would have been more than 10%. For example, one can rule out the impurity ions O^-, O_2^-, and OH^- although the drift velocities of these ions in H_2 are not available. This can be done by noting that the drift velocities of O^-, O_2^-, and OH^- ions (Ref. 26) in He at $E/N = 10$ Td (1 Td$= 10^{-17}$ V cm^2) are 7.12, 5.67, and 6.48$\times 10^4$ cm s^{-1}, respectively, compared to the value of 9.86$\times 10^4$ cm s^{-1} for H^- ions in He; the differences are more than 40%.

C. Lasing in Al following photoionization and charge neutralization in the presence of H_2

Kielkopf had reported[8] observation of lasing in Al at the $3s4s\ ^2S_{1/2}$-$3s3p\ ^2P_{3/2}$ transition following ArF-excimer-laser irradiation of Al in the presence of H_2 or D_2. Aluminum was shown[8] to be efficiently ionized by the ArF laser radiation: In addition to the photoionization of the outer electron, there is resonant inner-shell excitation ($3s3p$-$3p^2$) followed by autoionization. Thus, it had been pointed out[8] that charge neutralization of Al^+ by electrons or $H^-(D^-)$ could be the mechanism for the efficient formation of the Al ($3s4s\ ^2S_{1/2}$) state and thus the creation of a population inversion with

FIG. 8. Published values (Ref. 26) and the present measurements for the drift velocities of the H_3^+ and the H^- ions in H_2 as a function of the E/N value. From the straight lines drawn through the origin and the present data, we calculate a thermal "reduced mobility" K_0 of ~12.3 cm^2 V^{-1} s^{-1} for H_3^+ ions and ~40.3 cm^2 V^{-1} s^{-1} for H^- ions.

respect to the ground $3s3p\ ^2P_{3/2}$ state. Following our preliminary studies[1] on H^- formation in ArF-laser-irradiated H_2, additional experiments were conducted which confirmed[9] that the neutralization agent was indeed $H^-(D^-)$ formed efficiently via the mechanism of Ref. 1. For example, the laser emission in Al could be extinguished by destroying the H^- ions via photodetachment by a Nd:YAG laser.[9]

To summarize, we have three independent sources of information that confirm the formation of H^- ions in ArF-laser-irradiated H_2: (i) the photodetachment cross section measurement at 308 nm (Sec. II A); (ii) the ion mobility measurements (Sec. II B); and (iii) the observation of lasing in ArF-laser-irradiated Al in the presence of H_2 where the lasing state has been shown[8,9] to be populated via charge neutralization of Ar^+ by H^-. Furthermore, the electron attachment rate constant involved is $>10^{-6}$ cm^3 s^{-1}, and large H^- ion densities are produced via this mechanism.

III. IMPLICATIONS FOR NEGATIVE ION (AND NEUTRAL) BEAM TECHNOLOGIES

A. Possible new type of negative ion and neutral beam source

The observed efficient H^- formation in ArF-excimer-laser-irradiated H_2 points to the possibility that this scheme can be used in a new type of a H^- ion source. Furthermore, we have observed efficient formation of negative ions in UV-laser-irradiated saturated tertiary amines,[14] nitric oxide,[15] deuterium (D^- formation in ArF-excimer-laser-irradiated D_2 is qualitatively similar to H^- formation in H_2), and a few other gases that are currently being studied. Therefore, by utilizing different gases (and laser lines), it may be possible to generate different kinds of negative ions such as H^-, D^-, O^-, and so on.[29] Since negative ion beams can be easily converted to neutrals, neutral beams can also be generated.

Based on our studies of electron attachment to electronically excited molecules,[1,14,15] we believe that efficient electron attachment to a molecule excited to energies above its ionization threshold can be expected when (i) the efficiency for direct ionization is <1 (i.e., SES are populated), and (ii) at least one of the possible molecular fragments has a positive electron affinity. Since the attaching electrons are produced by the same laser pulse, it is also necessary to have sufficient number of electrons produced via either direct ionization or preionization of SES.[14] Normally, we choose a laser line which yields sufficient ionization for a given gas; as long as the total excitation energy lies within a few eV of the ionization threshold, condition (i) above is satisfied. However, regarding our basic measurements, two points need to be clarified: (a) The attaching electrons are produced via photoionization by the same laser pulse that produces the electron attaching excited molecules; hence, at high laser intensities the formation of negative ions is limited by the available electrons (see Fig. 1); (b) The closer the energy of the populated SES to the ionization threshold, the more efficient is the electron attachment [this is related to (i) above]. Depending on the nature of the multiphoton process (order of the process, whether or not any real intermediate states are involved) needed to excite the molecules to energies above
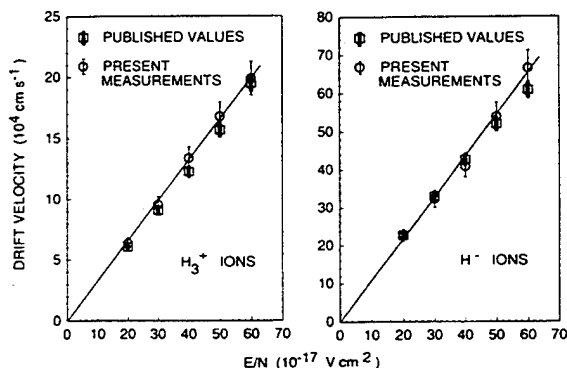
J. Appl. Phys., Vol. 76, No. 1, 1 July 1994

L. A. Pinnaduwage and L. G. Christophorou   51

15

their ionization thresholds, we have observed negative ion formation at laser intensity levels ranging from 10^{23} to 10^{26} photons/cm^2 s^{-1}.[1,14,15] From the molecules we have studied so far, only N_2 did not yield negative ions,[1] which is consistent with (ii) above since the electron affinity of the N atom is negative, i.e., it cannot bind an electron (in its ground state).

In the studies we have conducted to date on electron attachment to electronically excited molecules, we routinely obtained negative ion densities of 10^9 ions/cm^3 without any attempts of optimization; this number density corresponds to a signal level of 1000 mV in Fig. 1. (In fact, in these studies we deliberately keep the signal level small in order to avoid saturation of the preamplifier.) For comparison, the H$^-$ density in a H_2 discharge source is $\sim10^{10}$ ions/cm^3.[30] We also note that with the present mechanism the negative ion formation at high laser intensities is limited by the number of electrons (available for attachment) provided via laser photoionization; if $V_T \propto I^n$ then $V_I \propto I^{2n}$ (for the data of Fig. 1, $n=2$), and hence the ion signal V_I rises faster than the precursor electron signal ($\propto V_T$) due to photoionization. Thus, larger negative ion signals may be obtained simply by making more electrons available for attachment; for example, additional electrons may be provided by a heated filament located close to the laser interaction region.

Since D$^-$ ion beams have a special significance for fusion energy research, let us take a closer look at D$^-$ formation via ArF-laser-irradiated D_2. While photoionization of H_2 via (2+1) REMPI at the ArF laser line has been studied extensively (see the references in Ref. 1), such studies on D_2 have not been conducted to our knowledge. The $J=0$, 1, 2, 3, and 4 levels of the $v=0$ state of the ground X $^1\Sigma_g^+$ state of D_2 are populated at 300 K with relative abundances of 1.0, 2.6, 2.4, 1.4, and 0.6. The rotational energies of the $J=1$, 2, 3, and 4 states with respect to the $J=0$ state are 60.9, 182.7, 365.3, and 608.9 cm^{-1}, respectively; the energies of the rovibrational states of the E, F $^1\Sigma_g^+$ state of D_2 are given in Refs. 31 and 32. The two-photon energies of the free-running ArF laser used in our experiments lie in the range of $\sim103\,200$ to $\sim103\,600$ cm^{-1}. Therefore, $Q(3)$ and $Q(4)$ transitions and several O and S transitions to the E,F $^1\Sigma_g^+$, $v=8$ ($v_F=5$) level of D_2 should occur. Even though the outer F well is not directly accessible via Franck–Condon transitions, due to the significant tunneling between the inner and outer wells close to the top of the barrier,[33] such transitions do occur, but are somewhat weaker[34] than transitions to the inner E well; on the other hand, photoionization from the outer F well is more efficient.[34] In our experiments, the photoionization signal in D_2 was ~10 times smaller (and hence the D$^-$ signal at high laser intensities was proportionally smaller) compared to H_2. Furthermore, in the experiments of Kielkopf,[8] Al emission via charge neutralization of Al$^+$ with D$^-$ (produced via ArF-laser-irradiated D_2) has been observed with somewhat smaller efficiency compared to the Al emission when D_2 was replaced by H_2 (also see Ref. 9).

We also note that it is possible to tune the ArF laser emission in the range from ~192.6 to ~194.2 nm (with a linewidth of ~0.1 nm) using an intracavity prism[35] or an oscillator/amplifier configuration (commercially available) and thus to obtain two photon energies in the range $\sim103\,000$ to $\sim103\,800$ cm^{-1}. Thus, it is possible to induce individual $Q(1)$ through $Q(4)$ transitions to the E,F $^1\Sigma_g^+$ ($v=8$) level or $Q(4)$ transition to the E,F $^1\Sigma_g^+$ ($v=9$) level. Thus, larger ionization signals should be possible with a tunable ArF laser especially via the $Q(1)$ and $Q(2)$ transitions to the E,F state.

The importance of negative ion beams in fusion energy research and in particle accelerators was pointed out in Sec. I. Traditionally, positive ion beams have been used for many other ion beam applications,[10,36–38] including semiconductor material doping, surface modification (rate of ware, friction, lubrication) by ion implantation, ion-beam lithography, and as probe beams for material analysis (mass spectrometry and surface analysis). This has been mainly due to the availability of comparatively intense positive ion beams. However, judging by the number density of negative ions we routinely encounter in our studies on electron attachment to laser-irradiated gases,[1,14,15] it is likely that intense negative ion beams can be produced by the proposed method. Additionally, negative ion beams may have some advantages over positive ion beams in certain applications. For example, negative ion beams could be used advantageously to minimize surface charging effects in ion implantation of insulators.[39] Also, positive ion beams of energy 2 eV can be obtained by accelerating negative ion beams to a voltage V and stripping two electrons from each negative ion at the high-voltage terminal, as in tandem accelerators;[10] thus, even for applications which may require positive ion beams, starting off with a negative ion beam doubles the beam energy.

For ion source applications, the crucial parameters are the ion beam intensity and the ion energy spread. Thus, even though the basic measurements[1,14,15] of negative ion formation are encouraging, it is important to determine the intensities and intrinsic energy spread of ion beams extracted from the laser plasma, prior to considering practical applications for this scheme. In this regard, we are planning to extract a H$^-$ beam from the ArF-laser-irradiated H_2, and to measure the H$^-$ beam intensity and energy spread. If the outcome is favorable, this mechanism will provide a versatile ion source capable of providing a wide variety of ion beams [for example, O$^-$ ions can be produced via laser irradiation of NO (Ref. 15)]. The main disadvantage of such a source will be the cost of a laser system.

It must be noted that there does not exist a one-to-one correspondence between the duration of an ion pulse extracted from this type of a source to the duration of the laser pulse that created the ions. In ion sources electric fields in the source region are minimized in order to avoid beam energy spread; the ions are directed toward the extraction aperture by a magnetic field, and they drift essentially with thermal velocities. Taking an ion velocity of $\sim10^4$ cm s^{-1} and an ion source length of 10 cm, the "ion pulse" due to a given laser pulse will be ~1 ms long. Since commercial excimer lasers with 500 Hz repetition rate are available, a continuous ion beam may be possible with a single laser; otherwise, two or more lasers operating out of phase with each other may have to be used.

L. A. Pinnaduwage and L. G. Christophorou

16

B. Possible new electron attachment mechanism for hydrogen discharge sources

Currently there is considerable activity on a H^- volume source (hydrogen discharge)[11,16,17] due to its possible application in a neutral beam injector for fusion energy research. The efficient production of H^- ions in a hydrogen discharge is not yet fully understood, but is generally attributed to the attachment of slow electrons to high-vibrational (HV) states of H_2 produced directly or indirectly via electron impact. The other mechanisms that have been considered up to now are: (i) electron attachment to the metastable $c\ ^3\Pi_u$ state; (ii) dissociative recombination of electrons with H_3^+ ions that are abundant in a hydrogen discharge; and (iii) polar dissociation of highly excited H_2 (ion-pair formation). These three processes have been shown[16] to yield H^- ions with a lower efficiency than electron attachment to the HV states of H_2. Furthermore, the measured H^- densities in discharge sources seem to be larger than the values expected from model calculations based on electron attachment to HV states.[17,18]

As discussed in Sec. I, our observation on efficient H^- formation in ArF-excimer-laser-irradiated H_2 cannot be explained by electron attachment to HV states that may be indirectly populated under our experimental conditions; the other possible mechanisms discussed in the above paragraph were also ruled out.[1] Also, it was shown that the electron attachment rate constant corresponding to the H^- formation in ArF-laser-irradiated H_2 was orders of magnitude larger than the rate constants associated with any of these processes. The experimental observations were shown to be consistent with electron attachment to SES of H_2 or some other electron attaching species produced indirectly via the SES.[1] In the following we discuss the possible contribution of such a mechanism to the H^- formation in a H_2 discharge source.

Direct electron attachment to the SES of H_2 populated via electron impact in a discharge source is less likely due to (i) the smaller number densities of SES populated, and (ii) the sub-ns lifetimes expected for SES. Another possibility discussed in Ref. 1 was the long-lived, highly excited Rydberg (HR) states of H_2 populated via collisional stabilization of SES. In a hydrogen discharge, such HR states can be populated directly via electron impact; H_2 (HR) states produced via electron impact have been observed with lifetimes of $\sim 100\ \mu s$ (Ref. 40) at background pressures of $\sim 10^{-3}$ Pa. Such long-lived HR states are thought to be high orbital angular momentum (high-l) states produced via electron impact at near threshold energies.[40,41]

Since the gas pressure in a hydrogen discharge source is ~ 1 Pa, one needs to consider possible quenching of such HR states prior to electron attachment. It has been shown[42] that for quenching of Rydberg atoms by neutrals, the quenching cross section initially increases with the increasing of the principal quantum number n of the Rydberg state, but it starts decreasing at high n, where the excited electron is essentially "free;" also, the quenching efficiency by rare gas atoms and quadrupolar molecules such as H_2 and N_2 is much smaller compared to that by polar molecules. It is thus quite possible that the HR states of H_2 live long enough in a hydrogen discharge for electron attachment to occur, especially

since electron attachment to such states is likely to be very efficient, and thus the electron attachment time to be small. In view of this evidence, the need for a reexamination of the processes responsible for the observed efficient H^- formation in hydrogen discharges is indicated.

IV. CONCLUSIONS

Efficient H^- formation in ArF-excimer-laser-irradiated H_2 (Ref. 1) was confirmed by photodetachment and ion mobility measurements.

Based on the mechanisms for the H^- formation in ArF-laser-irradiated H_2,[1] it was pointed out that electron attachment to high-lying electronically excited states of H_2 (populated via electron impact) could be a significant channel for H^- formation in hydrogen discharge sources.

A new type of negative ion source capable of generating a variety of negative ion (and neutral particle) beams was proposed based on the observed efficient negative ion formation in laser-irradiated H_2 (Ref. 1) and other gases.[14,15]

[1] L. A. Pinnaduwage and L. G. Christophorou, Phys. Rev. Lett. 70, 754 (1993).
[2] G. J. Schulz and R. K. Asundi, Phys. Rev. Lett. 158, 25 (1967).
[3] M. Allan and S. F. Wong, Phys. Rev. Lett. 41, 1791 (1978).
[4] J. M. Wadehra and J. N. Bardsley, Phys. Rev. Lett. 41, 1795 (1978).
[5] J. M. Wadehra, Phys. Rev. A 29, 106 (1984).
[6] A. P. Hickman, Phys. Rev. A 43, 3495 (1991).
[7] H. Pummer, H. Egger, T. S. Luk, T. Srinivasan, and C. K. Rhodes, Phys. Rev. A 28, 795 (1983).
[8] J. F. Kielkopf, J. Opt. Soc. Am. B 8, 212 (1991).
[9] J. F. Kielkopf, L. A. Pinnaduwage, and L. G. Christophorou, Phys. Rev. A 49, 2675 (1994).
[10] G. W. Hamilton and M. Bacal, IEEE Trans. Plasma Sci. 19, 1143 (1991).
[11] K. W. Ehlers, J. Vac. Sci. Technol. A 1, 974 (1983).
[12] K. H. Berkner, R. V. Pyle, and J. W. Stearns, Nucl. Fusion 15, 249 (1975).
[13] W. S. Cooper, Phys. Fluids B 4, 2300 (1992).
[14] L. A. Pinnaduwage, L. G. Christophorou, and A. P. Bitouni, J. Chem. Phys. 95, 274 (1991).
[15] L. A. Pinnaduwage and L. G. Christophorou, Chem. Phys. Lett. 186, 4 (1991); Chem. Phys. Lett. 189, 486(E) (1992).
[16] J. R. Hiskes, Comments At. Mol. Phys. 19, 59 (1987); M. Bacal and D. A. Skinner, ibid. 23, 283 (1990).
[17] P. Berlemont, D. A. Skinner, and M. Bacal, Rev. Sci. Instrum. 64, 2721 (1993).
[18] A. T. Young, P. Chen, K. N. Leung, and G. C. Stutzin, in Proceedings of the 6th International Symposium on Laser-Aided Plasma Diagnostics (1993), pp. 178–183.
[19] S. J. Smith and D. S. Burch, Phys. Rev. 116, 1125 (1959).
[20] J. T. Broad and W. P. Reinhardt, Phys. Rev. A 14, 2159 (1976), and references therein.
[21] H. P. Popp and S. Kruse, J. Quant. Spectrosc. Radiat. Transf. 16, 683 (1976).
[22] L. G. Christophorou, Atomic and Molecular Radiation Physics (Wiley, New York, 1971) pp. 527–537.
[23] D. L. Albritton, T. M. Miller, D. W. Martin, and E. W. McDaniel, Phys. Rev. 171, 94 (1968).

17

[24] E. Graham, D. R. James, W. C. Keever, D. L. Albritton, and E. W. McDaniel, J. Chem. Phys. **59**, 3477 (1973).

[25] M. McFarland, D. L. Albritton, F. C. Fehsenfeld, E. E. Ferguson, and A. L. Schmeltekopf, J. Chem. Phys. **59**, 6610 (1973).

[26] H. W. Ellis, R. Y. Pai, E. W. McDaniel, E. A. Mason, and L. A. Vienland, At. Data Nucl. Data Tables **17**, 177 (1976).

[27] E. A. Mason and E. W. McDaniel, Transport Properties of Ions in Gases (Wiley, New York, 1988), p. 7; also see the footnote on the same page by R. Johnsen.

[28] D. P. Stevenson and D. O. Schissler, J. Chem. Phys. **29**, 282 (1958).

[29] L. A. Pinnaduwage and L. G. Christophorou, patent application submitted, 1994.

[30] P. J. Eenshuistra, M. Gochitashvilli, R. Becker, A. W. Kleyn, and H. J. Hopman, J. Appl. Phys. **67**, 85 (1990).

[31] L. Wolniewicz and K. Dressler, J. Chem. Phys. **82**, 3292 (1985).

[32] P. Senn, P. Quadrelli, K. Dressler, and G. Herzberg, J. Chem. Phys. **85**, 2384 (1986).

[33] W. Kolos and L. Wolniewicz, J. Chem. Phys. **50**, 3228 (1969).

[34] E. E. Marinero, R. Vasudev, and R. N. Zare, J. Chem. Phys. **78**, 692 (1983).

[35] D. J. Kliger, J. Bokor, and C. K. Rhodes, Phys. Rev. A **21**, 607 (1980).

[36] A. T. Forrester, Large Ion Beams (Wiley, New York), 1988.

[37] *The Physics and Technology of Ion Sources,* edited by I. G. Brown (Wiley, New York, 1989).

[38] G. D. Alton, Nucl. Instrum. Methods B **73**, 221 (1993).

[39] J. H. Freeman, in *Ion Implantation,* edited by G. Dearnaley, J. H. Freeman, R. S. Nelson, and J. Stephen (North-Holland, Amsterdam, 1973), p. 366.

[40] S. M. Tarr, J. A. Shiavone, and R. S. Freund, Phys. Rev. Lett. **44**, 1660 (1980); J. Chem. Phys. **74**, 2869 (1981).

[41] U. Fano, J. Phys. B **17**, L401 (1974).

[42] *Rydberg States of Atoms and Molecules,* edited by R. F. Stebbings and F. B. Dunning (Cambridge University Press, Cambridge, 1983).

18

4.2. Photodetachment of $C_6F_6^-$ in the Gaseous Phase; Effect of Medium on Photodetachment

In an effort to understand and to quantify the role of photodetachment in gas dielectric behavior we have modified further the method we developed earlier for the study of photodetachment in dielectric liquids so that similar studies can be made in the gaseous phase. This was a rather involved process, but the new method is an important tool in these studies. We used the new method to make absolute measurements of the cross section of laser photodetachment of $C_6F_6^-$ ions embedded in gaseous tetramethylsilane (TMS). These measurements were considered essential since they would allow a comparison of the results at low densities with similar measurements made earlier by us in nonpolar liquids, and with measurements made by others in clusters and solids.

The measurements indicate that the photodetachment cross section of $C_6F_6^-$ in gaseous TMS is about three times larger than in liquid TMS. This is rationalized by considering the effect of the medium on both the photoabsorption and the autodetachment process. The photoabsorption cross section in both the gas and the liquid exhibits (at least) two maxima due to autodetaching negative ion states. We argued that these are due to σ^* σ^* transitions in $C_6F_6^-$. The relative positions of these "superexcited" anionic states did not change appreciably in going from the gas to the liquid and the solid indicating similar influences of the medium on them. As expected, the photodetachment threshold in the condensed phase is shifted to higher energies compared to the gaseous phase. The shift is consistent with recent photoelectron studies of photodetachment of $C_6F_6^-$ clusters. These measurements clearly show that the potodetachment from negative ions embedded in all states of matter proceeds directly or indirectly via negative ion states and that for nonpolar media the effect of the medium can be accounted for by considering the macroscopic properties of the medium described by its dielectric constant or the refractive index of the medium.

A full account of these unique studies has been published and below we reproduce the pertinent publication (pages 20-34).

Photodetachment in the gaseous, liquid, and solid states of matter

L. G. Christophorou, P. G. Datskos, and H. Faidas[a]

Atomic, Molecular, and High Voltage Physics Group, Health Sciences Research Division, Oak Ridge National Laboratory, P.O. Box 2008, Oak Ridge, Tennessee 37831-6122 and Department of Physics, University of Tennessee, Knoxville, Tennessee 37996

We have made absolute cross section measurements of laser photodetachment of $C_6F_6^-$ ions embedded in gaseous tetramethylsilane (TMS) and compared the results at low gas densities with measurements in nonpolar liquids and solids. The measurements indicate that the photodetachment cross section of $C_6F_6^-$ in gaseous TMS is about three times larger than in liquid TMS. This is rationalized by considering the effect of the medium on both the photoabsorption and the autodetachment processes. The photodetachment cross section in both the gas and the liquid exhibits (at least) two maxima due to autodetaching negative ion states. It is argued that these are due to $\sigma^* \rightarrow \sigma^*$ transitions in $C_6F_6^-$. The relative positions of these "superexcited" anionic states did not change appreciably in going from the gas to the liquid and the solid, indicating similar influences of the medium on them. As expected, the photodetachment threshold in the condensed phase is shifted to higher energies compared to the gaseous phase. This shift is consistent with recent photoelectron studies of photodetachment of $C_6F_6^-$ clusters. The present study clearly shows that the photodetachment from negative ions embedded in all states of matter proceeds directly or indirectly via negative ion autodetaching states, and that for nonpolar media, the effect of the medium can be accounted for by considering the macroscopic properties of the medium described by its dielectric constant ϵ and refractive index n.

I. INTRODUCTION

There have been a number of studies recently aiming at linking the gaseous and condensed phases of matter.[1] A fundamental component of this effort to interface the phases of matter is the study of the interactions of slow electrons and photons in the gaseous and the condensed phases and in the interphase region between the phases that includes the behavior of slow electrons in low- and high-pressure gases and in clusters.[1,2] At our laboratory, we conducted over a period of many years interphase studies on electron attachment,[2-5] electron drift,[4-8] and photoionization.[2,8-10] We also studied the photodetachment of $C_6F_6^-$ in liquid TMS (Ref. 11).

In an effort to understand the effect of the medium and the state of matter on the process of photodetachment, we have measured the photodetachment cross section of $C_6F_6^-$ in gaseous TMS. These measurements are reported in this paper and the energetics of the process as well as the structure and absolute magnitude of the measured cross section are compared with those in nonpolar liquids.[11-13] The energetics of the photodetachment process in all phases of matter[11-18] and in $C_6F_6^-$ clusters[19] are discussed, and so is the structure observed in the photodetachment cross section of $C_6F_6^-$ embedded in a gaseous or a liquid[11-13] medium and the structure in the photoabsorption cross section of $C_6F_6^-$ embedded in a liquid[12,15] or a solid (glass)[16-18] medium. The findings on $C_6F_6^-$ are compared with those on O_2^- in gases[20-24] and in nonpolar liquids[4,13,25,26] and aromatic anions in nonpolar liquids.[27,28]

Hexafluorobenzene (C_6F_6) attaches near-zero energy electrons very strongly in all phases of matter. The rate con-

stant for electron attachment is 1.2×10^{14} $M^{-1} s^{-1}$ in liquid tetramethylsilane (TMS) and 5.6×10^{13} $M^{-1} s^{-1}$ in liquid isooctane[15] ($M^{-1} s^{-1} = 1.66 \times 10^{-21}$ cm^3 $molecule^{-1} s^{-1}$). In both the liquid[15] and the solid,[17,18] it has been established that electron attachment is due to the formation of $C_6F_6^-$.

In the gaseous phase, the C_6F_6 molecule has been studied rather well with regard to its electron attachment, detachment, and scattering properties. Thus, electron swarm studies have shown that C_6F_6 attaches slow electrons (≤ 1.5 eV) very efficiently.[29-32] At room temperature (~300 K), the thermal electron attachment rate constant is 1×10^{-7} cm^3 $molecule^{-1} s^{-1}$ (Refs. 29-31). The apparent electron attachment rate constant below ~1 eV decreases with increasing gas temperature T (see Refs. 31 and 33-36) and this has been shown to be due to thermally enhanced autodetachment.[37,38] Mass spectrometric studies have shown that at near thermal energies, the parent anion $C_6F_6^-$ is the only anion formed upon electron collision[39-42] and time-of-flight mass spectroscopic studies have determined the autodetachment lifetime of the isolated $C_6F_6^{-*}$ to be ~12 μs.[40] Fragment anions (F^-, $C_5F_3^-$, and $C_6F_5^-$) were observed[41] at energies ≥ 4 eV, but besides the ~0.0 eV $C_6F_6^-$ resonance, no other electron attachment resonances were found below 4 eV, although peaks due to dissociative electron attachment processes of the form $M + e \rightarrow (M-H)^- + H$ or $M + e \rightarrow (M-HF)^- + HF$ (M = molecular mass) were found in the energy range ~1.8–2.5 eV for some of the multiply fluorinated benzenes.[41] [The dissociation energy $D(C_6F_5-F)$ is ~5.5 eV (Refs. 32 and 43)].

The findings of electron attachment studies referred to in the preceding paragraph are consistent with those of electron scattering. Thus, low-energy electron transmission studies[44] have shown the existence of three negative ion states below
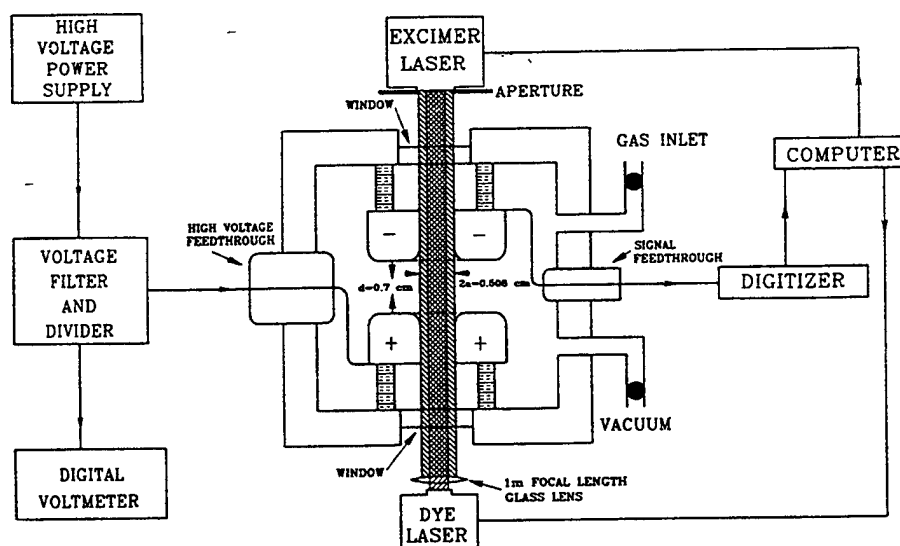
FIG. 1. A schematic diagram of the two-laser photodetachment technique.

~5 eV. The first two are degenerate and are located at ~0.4 eV and the third one is located at 4.5 eV. These negative ion states are associated with electron capture into the lowest three π_4^*, π_5^*, and π_6^* empty π orbitals of C_6F_6. The C_6F_6 molecule is planar and, as benzene, has a D_{6h} symmetry. However, $C_6F_6^-$ is thought to be nonplanar and to have a puckered-ring structure.[45]

The negative ion state responsible for the formation of the long-lived $C_6F_6^-{}^*$ at ~0.0 eV involves electron capture into a σ^* orbital (or a combination of σ^* and π^* orbitals) (see Refs. 14 and 45–50); the lowest σ^* symmetry e_{1u} or e_{2g} is still in question.[50] The electron affinity E.A. of C_6F_6 has been reported to be between 0.52 and >1.8 eV (see Refs. 32 and 51), although the more recent measurements cluster around 0.8 eV [0.86±0.03 (Ref. 32); 0.83±0.2 (Ref. 52); 0.8±0.1 (Ref. 19); 0.603 (Ref. 38); 0.52 (Ref. 53)].

II. PHOTODETACHMENT OF $C_6F_6^-$ IN GASEOUS TMS

A. Experimental method

The experimental method used in the present studies is similar to that described earlier.[11] A schematic of the experimental arrangement employed is shown in Fig. 1. The cell consisted of a six-way stainless-steel cube with two windows and electrical feedthroughs at opposite sides. The two parallel electrodes had a gridded circular area and were held at a distance d of 0.7 cm. The cell was filled with small quantities of C_6F_6 gas in a buffer gas of tetramethylsilane (TMS). The TMS gas number density N_T was varied from 1.77×10^{19} to 1.87×10^{19} molecules cm^{-3} and the C_6F_6 gas number density N_a was varied from 1.94×10^{14} to 9.1×10^{14} molecules cm^{-3}. An excimer laser beam [$\lambda=308$ nm; full width at half-maximum (FWHM) ~15×10^{-9} s] enters the cell through a circular aperture ($2a=0.508$ cm in diameter) and produces an electron swarm photoelectrically from the gridded part of

the cathode electrode. The electrons in the swarm move towards the anode under the influence of an externally applied electric field and are totally depleted at distances $z<d/2$, forming parent $C_6F_6^-$ anions via
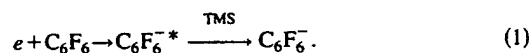
$$e + C_6F_6 \rightarrow C_6F_6^-{}^* \xrightarrow{\text{TMS}} C_6F_6^-. \tag{1}$$

A second, counterpropagating laser beam (FWHM~6×10^{-10} s) from the tunable dye laser enters the cell coaxially and with a time delay of ~3.5×10^{-6} s from the first laser pulse. Photons from this second tunable dye-laser beam with energies in excess of the photodetachment threshold E_{th} photodetach the parent negative ions, giving rise to a photodetached electron swarm. As this electron swarm moves towards the anode, electrons are depleted again by forming $C_6F_6^-$ anions which are finally collected at the anode electrode.

The circular aperture with diameter $2a$ allowed a practically constant (flat) intensity profile [$I_e(r)$=constant, with r being the radial direction along a plane parallel to that of the aperture] of the excimer laser beam to strike the gridded cathode thus producing an electron swarm with a number density which is constant across r and proportional in magnitude to the excimer laser intensity, i.e., $n_e(r,z=0)=AI_e(r)$=constant. These electrons are depleted by attaching to C_6F_6 molecules. The electron number density $n_e(r,z)$ and the negative ion number density $n_i(r,z)$ for times t less than the electron drift time t_e ($100<t_e<200$ ns) are described by

$$n_e(r,z) = AI_e(r)e^{-\eta z}, \tag{2}$$

$$n_i(r,z) = AI_e(r)(1-e^{-\eta z}), \tag{3}$$

21

where η is the electron attachment coefficient of C_6F_6. Under our experimental conditions and for the concentrations of C_6F_6 used, the electrons are depleted entirely within times $t \leqslant t_e/2$ or for distances $z = z_0 \leqslant d/2$.

The dye-laser beam which had a Gaussian intensity profile $I_d(r)$ with a spatial opening less than $2a$ enters the interaction region between the two electrodes $\sim 3.5 \times 10^{-6}$ s after the excimer laser and well after all of the electrons were attached, i.e., at $t > t_e$. For photon energies $h\nu = E > E_{th}$, this gives rise to photodetached electrons. Under the conditions that the photodetached electron number density $n_{ed}(r,z)$ is much smaller than the negative ion number density $n_i(r,z)$, $n_{ed}(r,z)$ is given by

$$n_{ed}(r,z) = \sigma_{pd}(E) n_i(r,z) I_d(r), \tag{4}$$

where $\sigma_{pd}(E)$ is the photodetachment cross section and $I_d(r)$ is the number of photons per unit area per dye-laser pulse. The total number N_{ed} of photodetached electrons is then obtained by integrating over the interaction volume between the two circular electrodes

$$\int_0^{z_0} \int_0^{2\pi} \int_0^a n_{ed}(r,z) r \, dr \, d\theta \, dz$$

$$= \int_0^{z_0} \int_0^{2\pi} \int_0^a \sigma_{pd}(E) n_i(r,z) I_d(r) r \, dr \, d\theta \, dz, \tag{5}$$

$$2\pi \frac{a^2}{2} N_{ed} = \sigma_{pd}(E) N_i \int_0^{2\pi} \int_0^a I_d(r) r \, dr \, d\theta, \tag{6}$$

$$N_{ed} = \sigma_{pd}(E) N_i I_t / \pi a^2, \tag{7}$$

where N_i is the initial number of negative ions (equal to the initial number of photoelectrons N_e) and I_t is the total number of electron detaching photons that enter the interaction region, i.e., the volume defined by the gridded part of the two circular electrodes. From Eq. (7), the photodetachment cross section can be determined as

$$\sigma_{pd}(E) = \frac{N_{ed}}{N_i} \frac{\pi a^2}{I_t}, \tag{8}$$

i.e., from a measurement of the ratio N_{ed}/N_i [see Fig. 2(A)] and the total number of photons I_t in the dye-laser pulse since the area πa^2 is known ($=0.203$ cm^2).

As the electrons produced by the excimer laser pulse from the cathode electrode drift towards the anode, their motion induces a transient voltage in the anode electrode which is detected as a fast initial drop in the measured voltage waveform [see Fig. 2(A)]. This drop stops when all of the electrons have been attached to C_6F_6. The magnitude of the voltage drop is proportional to the number of electrons N_e in the gap, which is the same as the total number of ions N_i formed. The slowly changing (dropping) portion of the waveform is due to the slow motion of the $C_6F_6^-$ anions for which the drift time is of the order of 10^{-3} s. The second light pulse from the tunable dye-laser illuminates the negative ions present in the gap and detaches electrons (whenever $h\nu > E_{th}$) inducing a second fast drop in the voltage waveform, but smaller in magnitude than the initial one, followed by yet another slowly changing portion of the total voltage

waveform when all of the detached electrons were captured again. From such waveforms, the ratio N_{ed}/N_i is measured and used in the determination of $\sigma_{pd}(E)$.

The present technique, although similar to that used earlier to measure $\sigma_{pd}(E)$ of $C_6F_6^-$ in liquid TMS (Ref. 11) differs in the way the initial electron swarm is produced. In the present arrangement [Fig. 2(B)], the electron swarm is produced monophotonically from a gridded cathode, while in the earlier arrangement [Fig. 2(C)], it is produced biphotonically from two-photon ionization of the medium. In the present technique, the electrons drift towards the anode electrode along the laser beam axis and always remain within the interaction volume; in the earlier technique,[11] the electrons drift laterally to the laser beam axis, and depending on their drift velocity, attachment rate and time delay between the excimer and dye-laser pulses can move outside the interaction volume [Fig. 2(C)] and so care must be taken for them to attach very quickly (within $<10^{-9}$ s).

In the present studies, the ratio N_{ed}/N_i was kept small (<0.04), and for the dye-laser intensities used, it had a linear dependence on I_t (Fig. 3). All the measurements were made at a temperature $T \approx 300$ K. The E/N values ranged between 2.3×10^{-16} and 4.6×10^{-16} V cm^2 and the applied voltage was varied from 3000 to 6000 V. The induced voltage signals were fed directly in the 1 MΩ input of a LeCroy 9420 digitizer. The signal due to the motion of the initially produced photoelectrons was typically between 20 and 30 mV and that due to the photodetached electrons was between 100 and 700 μV.

B. Results

The photodetachment cross section for $C_6F_6^-$ as a function of the photon energy $E = h\nu$ measured as described in Sec. II A is shown in Fig. 4. The error of the measurements varies from 5% to 10% depending on the wavelength; it comes principally from the measurement of I_t. The cross section has two maxima at 2.31 and 3.03 eV and possibly a third one at ~ 3.5 eV. Unfortunately, we could not extend our measurements to shorter wavelengths to better identify the position of the third maximum. We were also limited by low signal levels in making measurements at photon energies below 1.39 eV. Thus, we were unable to determine accurately a threshold value for $C_6F_6^-$ photodetachment. However, we plotted the experimental measurements at the lower photon energies employed as $(\sigma_{pd}/E)^{2/3}$ vs E (see Sec. II C) and from linear least squares fits over various ranges we determined threshold energies that varied from 0.56 to 0.83 eV (see Table I). Clearly, while more measurements closer to the threshold are needed to determine accurately the threshold energy, the intercept of 0.83 eV obtained for the fit of the data in the lowest energy range is consistent with the accepted value of the electron affinity of C_6F_6 (Sec. I).

C. Discussion

1. Direct vs indirect photodetachment

In the discussion that follows, we shall assume that in all the photodetachment and photoabsorption studies of $C_6F_6^-$ under consideration, the $C_6F_6^-$ ion is in the ground electronic
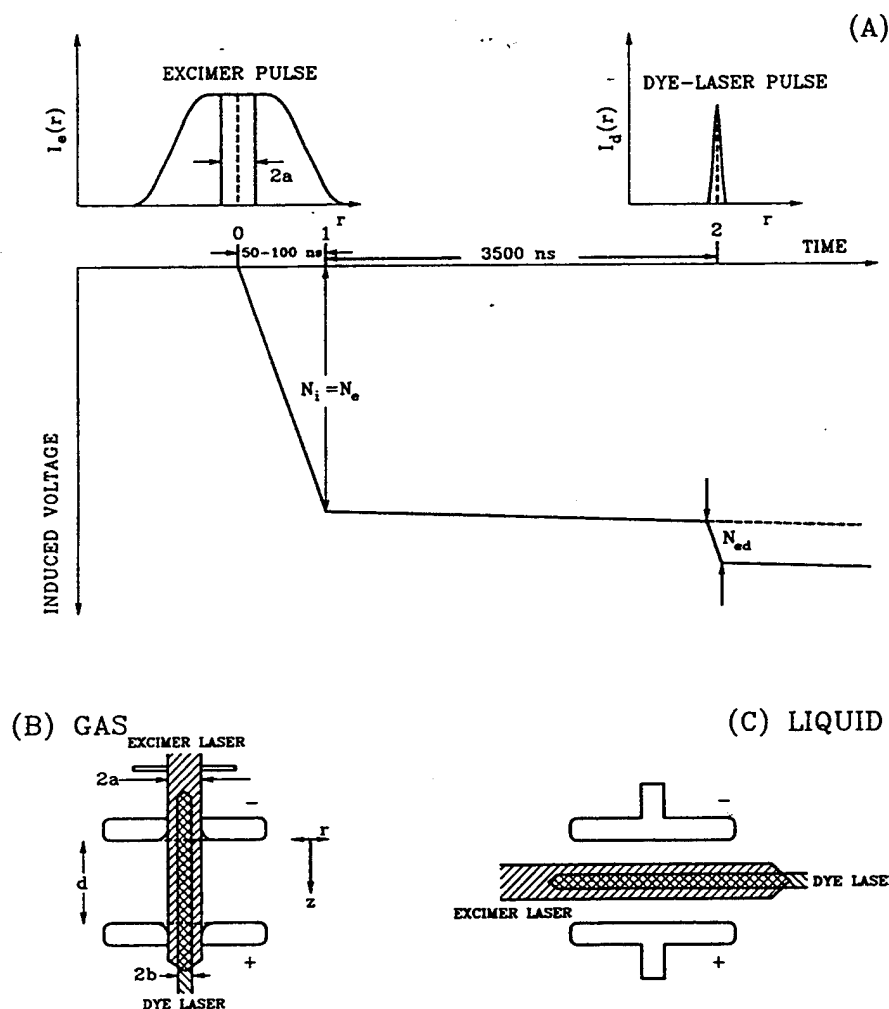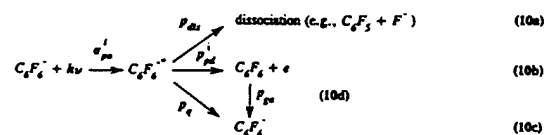
22

FIG. 2. Schematics of the two-laser photodetachment technique illustrating (A) the spatial profiles of the excimer and tunable dye-laser pulses and typical induced voltage waveforms. The time scale is as follows: ~50–100 ns between the excimer laser pulse (point 0) and the complete depletion of the photoelectrons (point 1); ~3.5 μs between the excimer laser pulse (point 0) and the dye-laser pulse (point 2). The photoelectron signal was between 20 and 30 mV and the photodetached electron signal was between 100 to 700 μV; (B) the geometry of the present technique used to measure $\sigma_{pd}^G(E)$ for $C_6F_6^-$ in gaseous TMS; and (C) the geometry of the technique used earlier to measure $\sigma_{pd}^L(E)$ for $C_6F_6^-$ in liquid TMS.

state prior to photodetachment independently of the state of the medium in which it is embedded. This is because both in the gaseous and the condensed-phase studies under consideration, the conditions are such that the time between collisions of $C_6F_6^{-*}$ and the molecules of the medium are much shorter than the autodetachment lifetime of the isolated $C_6F_6^{-*}$.

In analogy to the photoionization of a neutral molecule in a low-pressure gas, we can distinguish between direct transitions to the continuum, viz.,

$$C_6F_6^- + h\nu \xrightarrow{\sigma_{pd}^d} C_6F_6 + e \qquad (9)$$
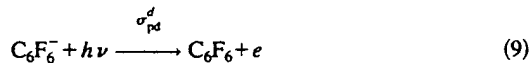
and indirect transitions to the continuum via a superexcited state of the anion (i.e., an electronic state which lies above the photodetachment threshold), viz.,

$$C_6F_6^- + h\nu \xrightarrow{\sigma_{pa}^i} C_6F_6^{-*} \begin{array}{l} \xrightarrow[P_{da}]{\text{dissociation (e.g., } C_6F_5 + F^-)} \qquad (10a) \\ \xrightarrow{P_{pd}} C_6F_6 + e \qquad (10b) \\ \xrightarrow[P_q]{} \downarrow P_{pa} \qquad (10d) \\ C_6F_6^- \qquad (10c) \end{array}$$

Processes (10a), (10b), and (10c) are, respectively, anionic dissociation, indirect photodetachment, and quenching (i.e., radiationless conversion of $C_6F_6^{-*}$ to lower-energy states) of
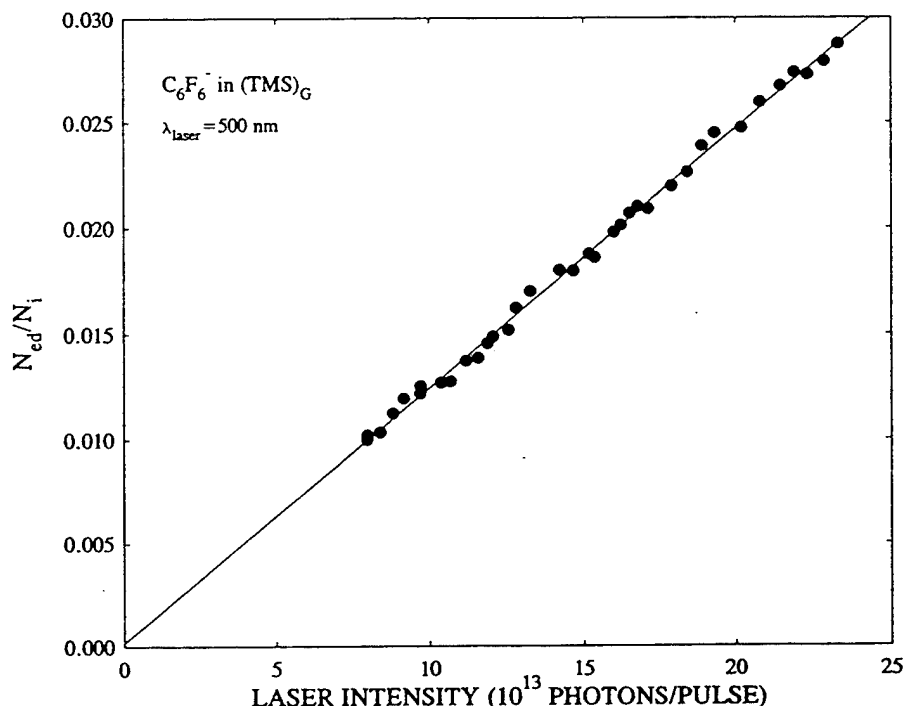
J. Chem. Phys., Vol. 101, No. 8, 15 October 1994

23

FIG. 3. The ratio N_{ed}/N_i for $C_6F_6^-$ in gaseous TMS as a function of the intensity of the electron detaching laser pulse (at $\lambda = 500$ nm).

$C_6F_6^-{}^*$ with respective probabilities p_{dis}, p_{pd}^i, and p_q. Process (10d) can be thought of as *geminate attachment* and is unlikely to occur in gases; its probability is small even in liquids.[12,54] If we take $p_{ga} = 0$, we can write for the overall photodetachment cross section at a particular photon energy $E = h\nu$,

$$\sigma_{pd}(E) = \sigma_{pd}^d(E) + \sigma_{pd}^i(E) = \sigma_{pa}^d(E) + \sigma_{pa}^i(E)\,\frac{p_{pd}^i}{p_{pd}^i + p_q + p_{dis}}$$

$$= \sigma_{pa}^d(E) + \sigma_{pa}^i(E)R(E). \qquad (11)$$

In Eq. (11), the cross section σ_{pd}^d for direct photodetachment [process (9)] is equal to the cross section σ_{pa}^d for direct photoabsorption, and the cross section σ_{pd}^i for indirect photodetachment is less than the cross section σ_{pa}^i for indirect photoabsorption by a factor R. If we take the dissociation energy $D(C_6F_5-F) = 5.5$ eV and the electron affinity of the fluorine atom E.A.$_G$(F) = 3.45 eV (see Ref. 51), we see that the dissociation of $C_6F_6^-{}^*$ into $C_6F_5 + F^-$ requires a minimum energy of E.A.$(C_6F_6) + D(C_6F_6-F) - $ E.A.$_G$(F) = 0.86 + 5.5 $ $-3.45 = 2.9$ eV. Thus, we expect p_{dis} to be small. Furthermore, from studies of the dependence of the autodetachment frequency t_d^{-1} of $C_6F_6^-$ on the temperature T (and thus on the internal energy of the anion $\langle\epsilon\rangle_{int}$),[38] one can infer that t_d^{-1} is $> 10^{13}$ s^{-1} at $\langle\epsilon\rangle_{int} \gtrsim 2.0$ eV. For the number densities of TMS employed in the present gaseous experiment, we estimate that the mean time τ_c between collisions of $C_6F_6^-{}^*$ and TMS molecules is $\sim 10^{-10}$ s. Therefore, the autodetachment time

of $C_6F_6^-{}^*$ ($E \gtrsim 2$ eV) in the present experiments is very much smaller than τ_c and we may take $p_q \rightarrow 0$. In Eq. (11), then $R \rightarrow 1$ and

$$\sigma_{pd}(E) = \sigma_{pd}^d(E) + \sigma_{pd}^i(E) = \sigma_{pa}^d(E) + \sigma_{pa}^i(E) = \sigma_{pa}^{tot}(E), \quad (12)$$

i.e., in the gaseous phase, the measured photodetachment cross section $\sigma_{pd}(E)$ is equal to the total photoabsorption cross section $\sigma_{pa}(E)$. The photodetachment cross section in Fig. 4 should, then, be identical with the photoabsorption cross section in the gaseous phase. No measurements of the latter are at present available (see, however, the discussion in Sec. III).

2. The structure of $\sigma_{pd}(E)$ and the excited states of $C_6F_6^-$

To understand the observed structure in $\sigma_{pd}(E)$, we need to refer to the knowledge we summarized in the Introduction with regard to the structure of C_6F_6 and $C_6F_6^-$, and the negative ion states of C_6F_6 as they are observed by the various methods. Clearly, electron attachment studies have shown the existence of a resonance at ~ 0.0 eV due to long-lived $C_6F_6^-{}^*$ which is probably a σ^* resonance located at ~ -0.8 eV (see Fig. 5 and Table II). Besides this resonance, electron attachment and electron transmission studies revealed π^* negative ion states at ~ 0.4 and ~ 4.5 eV (Fig. 5). Interestingly, no negative ion states of C_6F_6 were detected by the use of these methods in the energy region between 4.5 eV (the
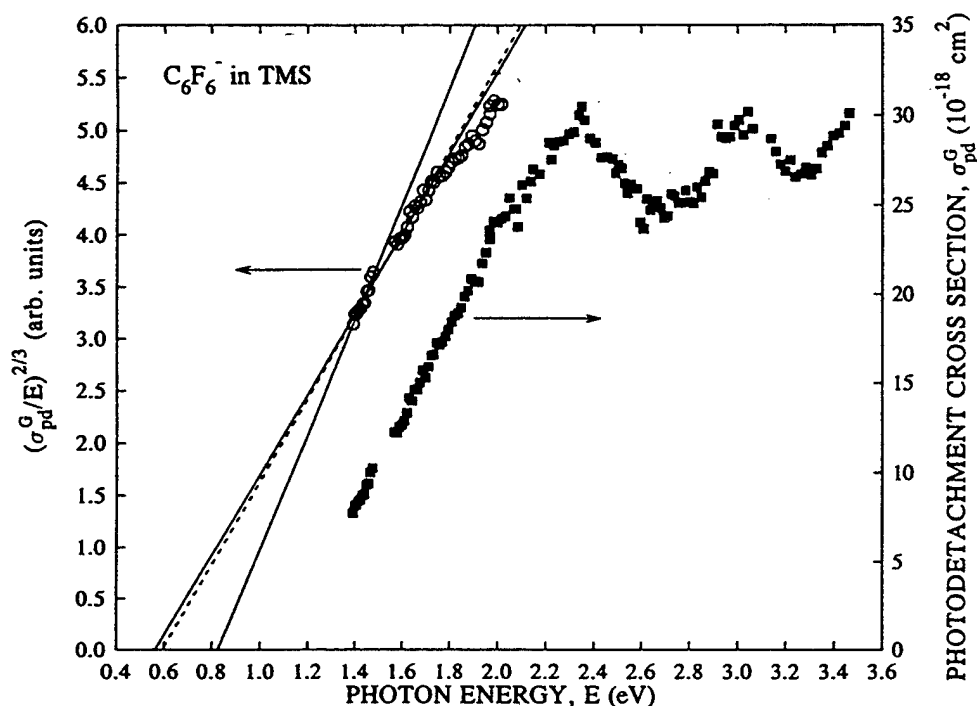
24

FIG. 4. (■) The cross section $\sigma_{pd}^G(E)$ for photodetachment of $C_6F_6^-$ in TMS buffer gas as a function of the photon energy E. (O) A plot of $(\sigma_{pd}^G/E)^{2/3}$ vs photon energy. The different lines are linear least squares fits to the measurements over different energy ranges (see the text and Table I).

position of the π_6^* resonance) and 0.4 eV (the position of the $\pi_{4,5}^*$ degenerate resonances). However, calculations[55,56] on and electron transmission studies[57,58] of a number of substituted benzenes (e.g., chlorobenzenes, dihalobenzenes, and benzene thioderivatives) uncovered a number of σ^* resonances halfway between the energy position of the π_4^* and $\pi_{5,6}^*$ negative ion resonances. Also, dissociative electron attachment studies on multiply substituted fluorobenzenes showed[41] the existence of resonances in the energy range ~ 1.8–~ 2.5 eV due to reactions of the form $M + e \rightarrow (M-H)^- + H$ and for some of the fluorobenzenes, due to reactions of the form $M + e \rightarrow (M-HF)^- + F$ (M is the molecular mass). However, no such reactions were reported for C_6F_6. From the results of these studies, therefore, it can be inferred that σ^* states of $C_6F_6^-$ are not "seen" in electron transmission experiments or in dissociative electron attachment studies.

If we consider the positions of the peaks in $\sigma_{pd}(E)$ in Fig. 4 (see also Table II) and the fact that these represent transition energies from the ground state of $C_6F_6^-$ to the excited states of $C_6F_6^-$, we can conclude that besides the π^* negative ion states "seen" in electron transmission experiments, there exist two (and possibly three) negative ion states of $C_6F_6^-$ located at ~ 1.6 and 2.3 eV (and the third one at ~ 2.8 eV) (see Fig. 5). The fact that these states are not seen in dissociative electron attachment studies or in electron transmission experiments leads us to conclude that σ^* negative ion states are probed in the present photodetachment

experiments [and in negative ion photoabsorption studies (see Sec. III)] confirming the σ^* character of the ground state of $C_6F_6^-$. Their observation in the photodetachment and photoabsorption studies rules out the possibility that their absence in electron transmission spectra is due to their short lifetimes. It rather seems that the transition probabilities are different between the photodetachment/photoabsorption studies on the one hand and the electron attachment/electron transmission studies on the other. Our findings are consistent with the lowest state of $C_6F_6^-$ being σ^*.

Two types of transitions involving σ and σ^* orbitals are envisioned as shown in Fig. 6: (i) one-particle $\sigma^* \rightarrow \sigma^*$ transitions in which the attached electron is excited from a partially filled σ^* orbital to a higher empty σ^* orbital; and (ii) two-particle/one-hole $\sigma \rightarrow \sigma^*$ transitions in which a valence electron is excited from the highest filled σ orbital to an

TABLE I. Estimates of the photodetachment threshold E_{th}^G of $C_6F_6^-$ in gaseous TMS and corresponding correlation coefficients for three energy ranges.

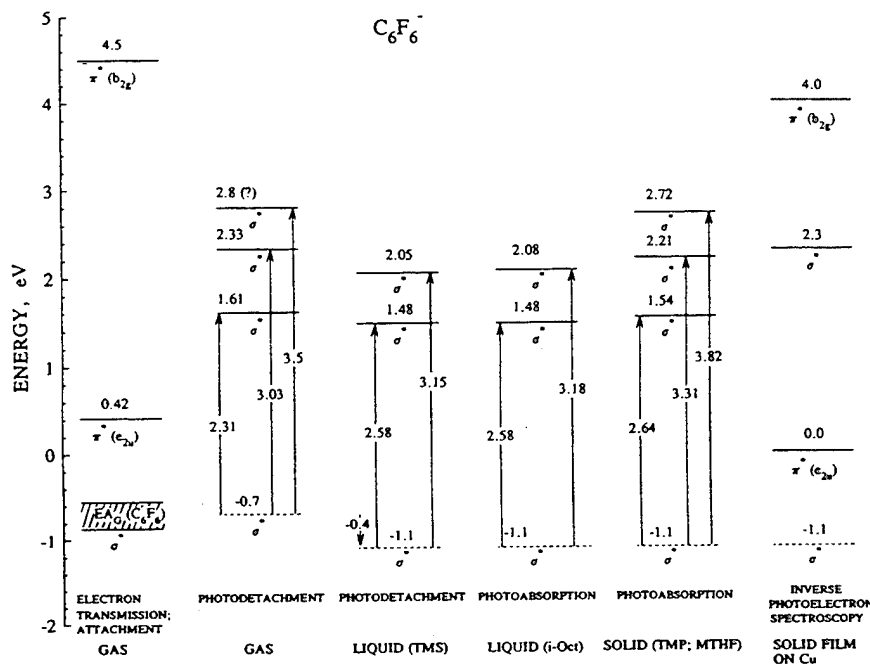| Energy range (eV)	E_{th}^G (eV)	Correlation coefficient
1.393–1.476	0.825	0.9701
1.393–1.675	0.592	0.9925
1.393–1.771	0.562	0.9940

FIG. 5. Energy positions of the negative ion states of $C_6F_6^-$ determined in the various states of matter by various methods: electron transmission/attachment in the gaseous phase; photodetachment in the gaseous phase; photodetachment in the liquid phase (liquid TMS); photoabsorption in the liquid phase (liquid i-oct); photoabsorption in the solid phase (solid TMP and solid MTHF); and inverse photoelectron spectroscopy (solid film of $C_6F_6^-$ on Cu substrate) (see the text). We took a value of 0.7 eV for $E.A._G(C_6F_6)$ so that a lowering by 0.4 eV in the condensed phase will bring the position of the σ^* resonance in coincidence with the value determined for solid C_6F_6 on Cu substrates.

occupied, but not filled σ^* orbital. The transition energies involved in the present experiments are consistent with the first mechanism, i.e., they are due to single particle $\sigma^* \rightarrow \sigma^*$ transitions. Clearly then photodetachment studies show that higher σ^* negative ion states of $C_6F_6^-$ can be probed by photodetachment spectroscopy via $\sigma^* \rightarrow \sigma^*$ transitions. Two-particle/one-hole transitions are possible, but they lie at higher energies where mixing with other configurations can hinder their identification. This situation seems to be similar to that for aromatic hydrocarbon anions (see Sec. IV B and Ref. 59), except that for those anions, the transitions involved are $\pi^* \rightarrow \pi^*$ and $\pi \rightarrow \pi^*$ (the former lying at lower energies than the latter).

The energy positions of the σ^* resonances observed in the present study of the photodetachment of $C_6F_6^-$ in the gaseous phase are in agreement with those inferred from photodetachment[11-13] and photoabsorption[12,15] studies of $C_6F_6^-$ in liquids and from photoabsorption studies of $C_6F_6^-$ in solids.[16-18] Also, a study of inverse photoelectron spectra of condensed films of C_6F_6 on a Cu surface revealed[14] a σ^* resonance of $C_6F_6^-$ at ~2.30 eV (see Fig. 5 and Sec. III). The photoabsorption spectra of $C_6F_6^-$ in nonpolar solids (glasses)[16] clearly show a third σ^* resonance at ~2.8 eV (Fig. 5 and Table II). The photodetachment spectrum in Fig. 4 is consistent with the existence of a third peak at about this energy. All other photodetachment/photoabsorption studies of $C_6F_6^-$ in the liquid phase did not extend to this energy

range. It seems, however, desirable to extend the energy range of the photodetachment/photoabsorption studies to both lower and higher energies and search for the π^* resonances of $C_6F_6^-$. It must be noted, however, that earlier comparisons[59] of electron transmission and optical absorp-
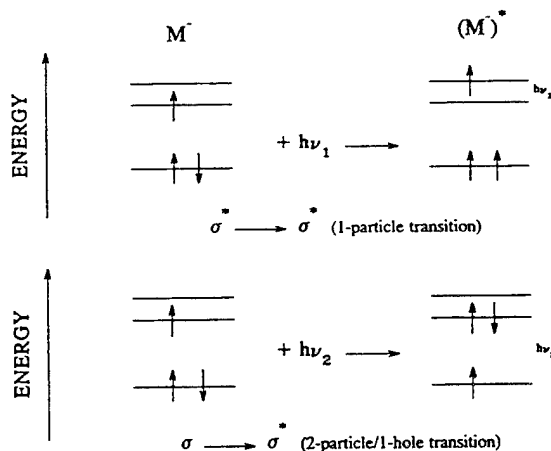

FIG. 6. An illustration of $\sigma^* \rightarrow \sigma^*$ (one-particle) and $\sigma \rightarrow \sigma^*$ (two-particle/one-hole) transitions in the reaction $M^- + h\nu \rightarrow (M^-)^*$ (see the text).

J. Chem. Phys., Vol. 101, No. 8, 15 October 1994

26

TABLE II. Electron affinity of C_6F_6 and photodetachment thresholds and transition energies to autodetaching excited states of $C_6F_6^-$.

Quantity	Gas	Cluster	Liquid	Solid (glass)
Electron affinity E.A. (eV)[a]	0.86 ± 0.03[b]			
	0.83 ± 0.2[c]			
	0.80 ± 0.1[d]			
	0.603[e]			
	0.520[f]			
Photodetachment threshold E_{pd}^{th} (eV)	$0.83(?)$[g]	$n=1$; 0.8 (1.56)[d,h]	1.51 (TMS)[i,j]	
		$n=2$; 0.93 (1.76)	1.61 (TMS)[i,j]	
		$n=3$; 1.28 (1.90)	1.82 $(n$-B)[l,m]	
		$n=4$; 1.47 (2.12)	1.97 $(n$-P)[l,n]	
		$n=5$; 1.36 (2.24)	1.67 (neo-P)[l,o]	
		$n=6$; 1.52 (2.34)	1.88 $(c$-P)[l,p]	
		$n=7$; 1.70 (2.48)	1.72 (neo-H)[l,q]	
		$n=8$; 1.64 (2.54)	1.90 (TMP)[l,r]	
			Photodetachment studies E_{pd}^{AS}	
Transition energies to autodetaching states (eV)	2.31[g]		2.58 (TMS)[j], 2.60 (TMS)[k]	
	3.03[g]		3.15 (TMS)[j]	
	$\sim3.5(?)$[g]		—	
			Photoabsorption studies E_{pa}^{AS}	Photoabsorption studies E_{pa}^{AS}
			2.58 $(i$-oct)[s,t]; 2.60 (TeMP)[t,u]	2.64 (TMP;MTHF)[v,w]
			3.10 (TeMP)[t,u]; 3.18 $(i$-oct)[s,t]	3.31 (TMP;MTHF)[v,w]
				3.82 (TMP;MTHF)[v,w]

[a]See other values in Refs. 32 and 51.
[b]Reference 32.
[c]Reference 52.
[d]Reference 19.
[e]Reference 38.
[f]Reference 53.
[g]Present work.
[h]$n=1,2,...,8$ refers to the cluster size; values in parentheses are the vertical detachment energies. The thresholds were obtained from the measured photoelectron spectra and correspond to an estimate of the upper limit of the adiabatic electron affinity.
[i]TMS=tetramethylsilane; $T=296$ K [$V_0=-0.58$ eV (Ref. 4)].
[j]Reference 11.
[k]Reference 12.
[l]Reference 13.
[m]n-B=n-butane; $T=296$ K [$V_0=0.12$ eV (Ref. 4)].
[n]n-P=n-pentane; $T=296$ K [$V_0=\sim0.01$ eV (Ref. 4)].
[o]neo-P=neopentane (2,2-dimethylpropane); $T=296$ K [$V_0=-0.43$ eV (Ref. 4)].
[p]c-P=cyclopentane; $T=296$ K [$V_0=-0.22$ eV (Ref. 4)].
[q]neo-H=neohexane (2,2-dimethylbutane); $T=296$ K [$V_0=-0.22$ eV (Ref. 4)].
[r]TMP=2,2,4-trimethylpentane (isooctane); $T=296$ K [$V_0=-0.17$ eV (Ref. 4)].
[s]i-oct=isooctane; $T=296$ K.
[t]Reference 15.
[u]TeMP=2,2,4,4-tetramethylpentane; $T=296$ K [$V_0=-0.35$ eV (Ref. 4)].
[v]MTHF=2-methyltetrahydrofuran; $T=77$ K.
[w]Reference 16.

tion spectra of ground-state anions in solution revealed several differences. For example, strong peaks in electron transmission spectra are often absent (or very weak) in optical absorption spectra when they are due to transitions which are dipole forbidden from the ground state anion. Conversely, strong peaks in the absorption spectrum due to excitation of dipole-allowed two-particle/one-hole states from the ground state anion are absent or weak in the electron transmission spectrum because they require a two-electron process.

3. The photodetachment threshold and the threshold behavior of $\sigma_{pd}(E)$

See the discussion in Sec. III.

III. PHOTODETACHMENT OF $C_6F_6^-$ AS A FUNCTION OF STATE

A. Threshold energetics

In low-pressure gases, the relation between the photodetachment threshold E_{th}^G for the process

$$M_G^- + h\nu \rightarrow M_G + e_G \qquad (13)$$

and the electron affinity E.A.$_G$ of the molecule M and the vertical detachment energy[60] VDE$_G$ for the anion M^- is

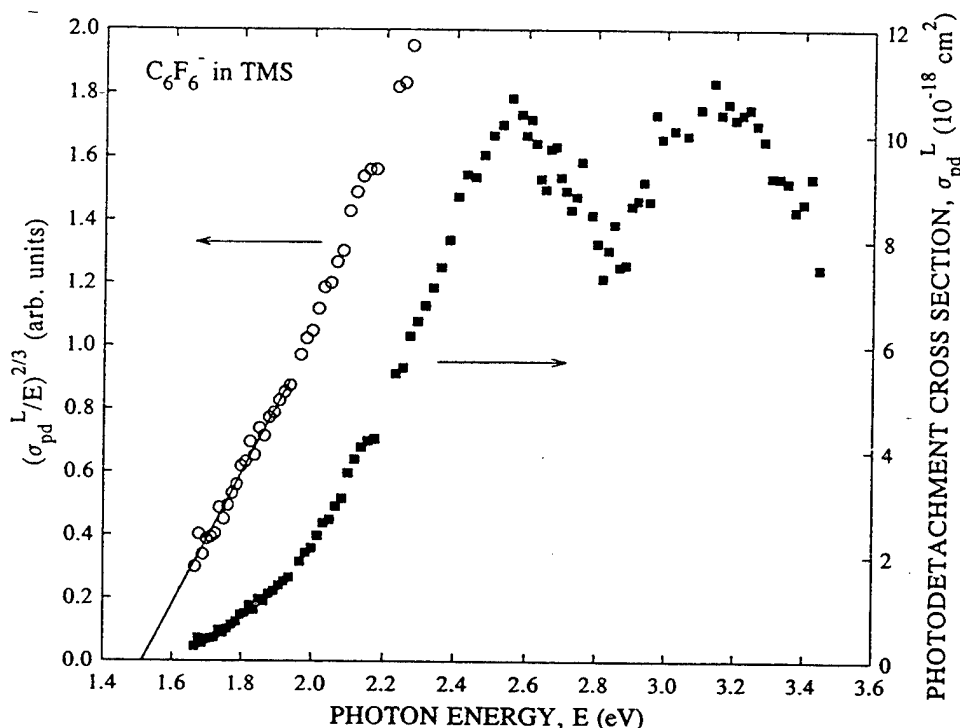$$E_{th}^G = VDE_G = E.A._{\cdot G} + \Delta E_G. \qquad (14)$$

27

FIG. 7. The absolute photodetachment cross section $\sigma_{pd}^L(E)$ (right-hand side Y axis) of $C_6F_6^-$ in liquid TMS as a function of the photon energy E, and a linear least squares fit of $(\sigma_{pd}^L/E)^{2/3}$ (left-hand side Y axis) for $E < 1.95$ eV. The intercept with the X axis gives a threshold energy E_{th}^L of 1.51 eV (Ref. 11).

In Eq. (14), E_{th}^G normally exceeds E.A.$_G$ by an amount ΔE_G due to differences in the equilibrium positions of the energy curves (surfaces) of M and M^-.

In dense gases, liquids, solids, and large clusters, the photodetachment process for the molecular anions is complicated by the effect of the medium principally on the anion and the released electron. Let us consider the photodetachment process in a liquid as an example and let us rewrite Eqs. (13) and (14) as[2,4,11]

$$M_L^- + h\nu \rightarrow M_L + e_L \qquad (15)$$

and

$$E_{th}^L = VDE_L = E.A._L + \Delta E_L = E.A._G + V_0 - P^- + \Delta E_L. \qquad (16)$$

In contrast with process (13), where e_G is essentially in the vacuum level, in process (15) the electron is ejected and stays in the liquid, its energy at the bottom of the liquid conduction band being V_0. In Eq. (16), P^- is the polarization energy of the negative ion in the liquid and E_{th}^L, VDE_L, E.A.$_L (= E.A._G + V_0 - P^-)$, and ΔE_L are, respectively, the photodetachment threshold, vertical detachment energy, electron affinity, and the value of ΔE in the liquid; the effect of the medium on the neutral molecule was considered small and was neglected in the energetics.

Implicit in the preceding discussion is the assumption that the anion M^- is in its lowest state of excitation in all states of matter prior to photodetachment. This seems likely to be the case in the experiments under consideration in this paper (see the earlier discussion in Sec. II).

In Fig. 7 is shown $\sigma_{pd}^L(E)$ as a function of the photon energy E for $C_6F_6^-$ in liquid TMS ($T = 298$ K) as measured by Faidas et al.[11] using a two-laser photodetachment technique similar to the one employed in the present study. The photodetachment threshold E_{th}^L for $C_6F_6^-$ was determined by fitting the experimental measurements close to the threshold to

$$(\sigma_{pd}^L/E)^{1/n} = B(E - E_{th}^L). \qquad (17)$$

The best fit was obtained[11] for $n = 3/2$ and $E_{th}^L = 1.51$ eV. Equation (17) is based on an earlier expression for the threshold behavior of σ_{pd}^G for atomic anions,[61,62] viz.,

$$\sigma_{pd}^G(E) = B' E(E - E_{th}^G)^{(2l+1)/2}, \qquad (18)$$

where B' is a constant and l is the angular momentum of the photoejected electron.

In the present study, the gaseous measurements of $\sigma_{pd}^G(E)$ could not be made sufficiently close to E_{th}^G to allow an accurate determination of E_{th}^G and n. Nonetheless, we plotted the gaseous $\sigma_{pd}^G(E)$ in the manner suggested by Eq. (17). From a linear least squares fit to plots of $(\sigma_{pd}^G/E)^{2/3}$ vs E, the threshold E_{th}^G was determined using measurements extending to various energy ranges above the lowest energy at
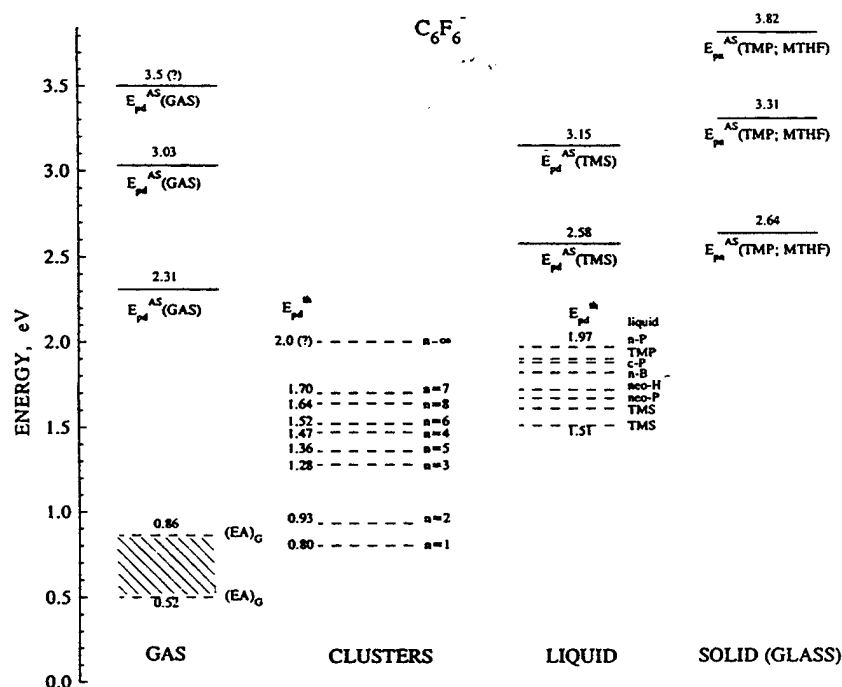
28

FIG. 8. An energy level diagram showing the positions of the electron affinity E.A.$_G$ and autodetaching states AS, as determined in the present study of C_6F_6 photodetachment in gaseous TMS, E_{pd}^{AS}(GAS) with the photodetachment thresholds, E_{pd}^{th} for $(C_6F_6^-)_n$ $(n=1-8)$ clusters (E_{pd}^{th} for $n\to\infty$ was determined as discussed in the text). Similarly, photodetachment thresholds E_{pd}^{th} for $C_6F_6^-$ in various liquids are shown along with the energy position of autodetaching states determined from photodetachment studies in liquid TMS. The last column is the positions of autodetaching states of $C_6F_6^-$ determined from photoabsorption studies in TMP and MTHF glasses. [The energy positions were the same in both media (see the text).] (---) Positions of photodetachment thresholds; (—) positions of autodetaching states.

which measurements were made (see Table I). For the energy range closest to the threshold, E_{th}^G was estimated to be 0.83 eV. This value is consistent with the accepted values for the electron affinity of the C_6F_6 molecule and is 0.68 eV lower than the photodetachment threshold $E_{th}^L = 1.51$ eV estimated by Faidas et al.[11] for $C_6F_6^-$ in liquid TMS. From Eqs. (14) and (16),

$$E_{th}^L - E_{th}^G = V_0 - P^- + (\Delta E_L - \Delta E_G).\qquad(19)$$

If we take as did the authors of Ref. 11 for liquid TMS $V_0 = -0.51$ eV (Ref. 12) and $P^- = -0.92$ eV (Ref 12), then $V_0 - P^- = 0.41$ eV, which implies that $\Delta E_L - \Delta E_G = 0.27$ eV. In view of the uncertainty in E_{th}^G and in the values of the other quantities involved, it is difficult to say whether this indicated difference between ΔE_L and ΔE_G is genuine.

Faidas et al.[11] found that the E.A. of C_6F_6 in liquid TMS was E.A.$_{TMS}(C_6F_6) = 1.27$ eV, i.e., it exceeds its isolated molecule (gaseous) E.A.$_G(C_6F_6) = 0.86$ eV by 0.41 eV. This energy shift (0.41 eV) in the electron affinity of C_6F_6 is almost identical to the energy shift observed[14] between the energy positions of the negative ion states in C_6F_6 in the gas phase and in C_6F_6 films on Cu substrates.

Finally, it is interesting to note the increase in the photodetachment thresholds of $(C_6F_6^-)_n$ clusters with increasing cluster size and to see how these compare with the photodetachment thresholds of $C_6F_6^-$ in the gas and in the dielectric

liquids (see Fig. 8). If we assume that when $n\to\infty$, the photodetachment threshold for $(C_6F_6^-)_{n\to\infty}$ would be equal to the sum of E.A.$_G(C_6F_6)$ and the polarization energy P^- of $C_6F_6^-$ in C_6F_6, we find that $(E_{pd}^{th})_{n\to\infty} = (0.86+1.14)$ eV$=2.0$ eV. The value of P^- was determined from the Born equation[63] using the values of 2.03 (Ref. 64) and 3.2 Å (Ref. 15) for the dielectric constant ϵ of liquid C_6F_6 and the radius R of $C_6F_6^-$. The value of 2.0 eV is not incompatible with the photodetachment thresholds of $C_6F_6^-$ in dielectric liquids (see Fig. 8); the latter vary according to the value of the V_0 of the liquid. In estimating $(E_{pd}^{th})_{n\to\infty}$ for $(C_6F_6^-)_{n\to\infty}$, we neglected V_0. It is interesting to note that the gradual rise in the energy position of all three autoionizing states of $C_6F_6^-$ in going from the gas to the liquid and solid. This trend is also clearly seen in comparing the E.A.$_G$ of the C_6F_6 molecule with the photodetachment thresholds E_{pd}^{th} of $(C_6F_6^-)_n$ clusters and of $C_6F_6^-$ in dielectric liquids (Fig. 8).

B. Negative ion states

In Sec. II C, we have seen that negative ion states of C_6F_6 due to π^* and σ^* orbitals are present in all states of matter. Their energies in the gas phase, however, are shifted to lower energy by ~0.4 eV in the condensed phase. Thus (see Fig. 5), the energy position of the π_6^* negative ion resonance at 4.5 eV in the gas phase can be correlated with the
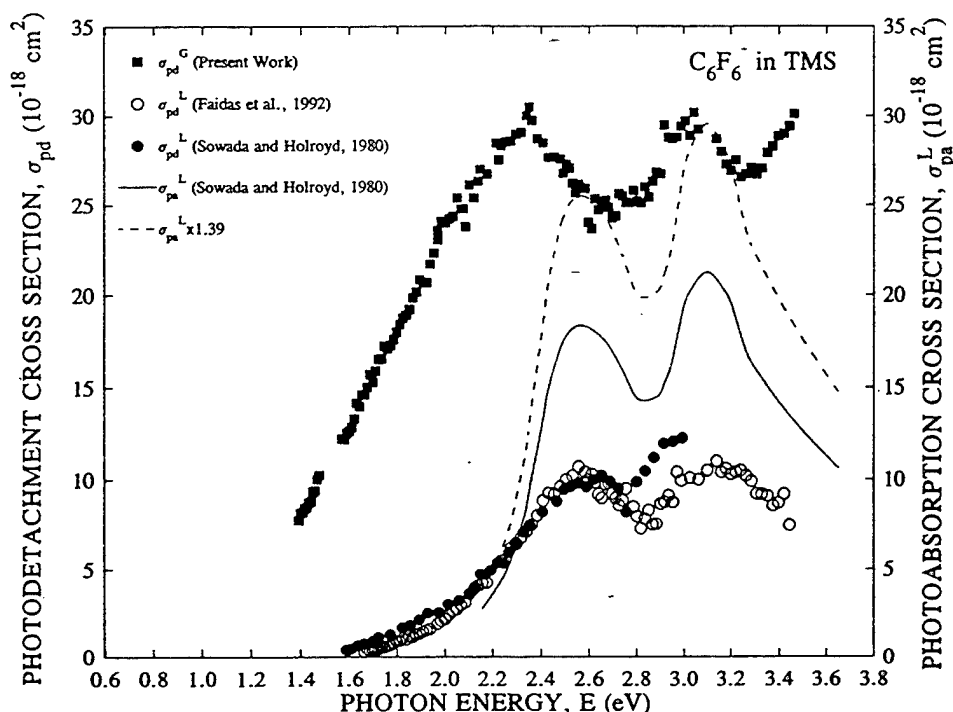
29

FIG. 9. Photodetachment cross section σ_{pd}^G of $C_6F_6^-$ in gaseous TMS [■ (present work)] and σ_{pd}^L in liquid TMS [O (Ref. 11); ● (Ref. 12)]. The solid line (—) is the photoabsorption cross section σ_{pa}^L of $C_6F_6^-$ in liquid 2,2,4,4-tetramethylpentane (Ref. 12) and the broken line (---) is this cross section multiplied by a factor of 1.39 (see the text).

peak observed in the solid film at ~4.0 eV. Similarly, the energy position of the $\pi_{4,5}^*$ resonance observed at ~0.4 eV in the gas can be correlated with that at ~0.0 eV in the solid, and the ground state σ^* resonance at ~−0.7 eV can be correlated to that in the solid at −1.1 eV. Similarly, the energy positions of the negative ion states due to σ^* orbitals as determined in gaseous photodetachment experiments correlate nicely with those from similar studies in liquids (and glasses), although the downward shift is somewhat smaller (see Fig. 5).

In such comparisons, efforts should be made to ensure the same identity of the anion in both the gaseous and the condensed phases. Dissociative attachment processes which are not energetically possible in the gaseous phase may become energetically possible in the condensed phase, especially when anions of small radii are produced which are embedded in media of high dielectric constants. However, such a situation does not appear to be involved in the present study. For example, the threshold E_{th} for process (10a) (i.e., $C_6F_6^- + h\nu \rightarrow C_6F_5 + F^-$) in TMS is

$$E_{th} = D(C-F) + E.A._G(C_6F_6) - P_{TMS}^-(C_6F_6^-) - E.A._G(F)$$

$$+ P_{TMS}^-(F^-). \tag{20}$$

If we take $D(C-F)=5.5$ eV (Ref. 32), $E.A._G(C_6F_6)=0.86$ eV (Ref. 32), $P_{TMS}^-(C_6F_6^-)=-1.03$ eV, $E.A._G(F)=3.45$ eV (Ref. 51), and $P_{TMS}^-(F^-)=-2.47$ eV, Eq. (20) gives $E_{th}=1.5$ eV.

The values of $P_{TMS}^-(C_6F_6^-)$ and $P_{TMS}^-(F^-)$ were determined from the Born equation[63] using 3.2 Å for the effective radius of $C_6F_6^-$ (Ref. 15), 1.33 Å for the F^- radius,[65] and 1.84 for the dielectric constant of TMS (Ref. 26).

C. The magnitude of the photodetachment cross section and its dependence on the state of matter

The present measurements of $\sigma_{pd}^G(E)$ combined with those of $\sigma_{pd}^L(E)$ and $\sigma_{pa}^L(E)$ offer the opportunity to assess the role of the medium on the magnitude of the photodetachment cross section. In Fig 9 are plotted the following cross section measurements for $C_6F_6^-$: the photodetachment cross section $\sigma_{pd}^G(E)$ for $C_6F_6^-$ in gaseous TMS, the photodetachment cross section $\sigma_{pd}^L(E)$ for $C_6F_6^-$ in liquid TMS, and the photoabsorption cross section $\sigma_{pa}^L(E)$ for $C_6F_6^-$ in liquid 2,2,4,4-tetramethylpentane.[12] $\sigma_{pd}^L(E)$ of Ref. 12 in various dielectric liquids exhibits similar behavior (Fig. 10) and shows a peak at about the same energy which coincides with the first maximum in $\sigma_{pa}^L(E)$ (see Fig. 10). The photoabsorption cross section, however, extends to higher energies and shows a second maximum (see Table II and Fig. 10). The photoabsorption cross section in the solid[16] which extends to even higher energies shows a third maximum (see Fig. 10) which is consistent with the present measurements (see Table II and Fig. 8); all these absorption maxima were attributed to light absorption by the $C_6F_6^-$ anion.
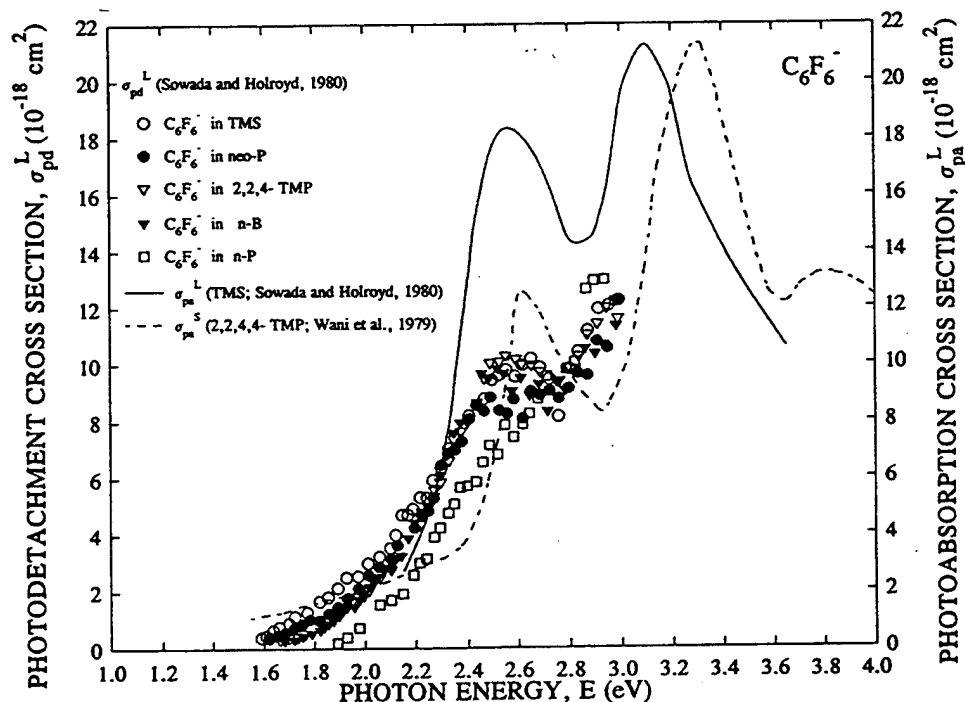
J. Chem. Phys., Vol. 101, No. 8, 15 October 1994

30

FIG. 10. Photodetachment cross section of $C_6F_6^-$ as a function of photon energy $\sigma_{pd}^L(E)$ in various dielectric liquids (O—TMS; ●—neo-P; ∇—2,2,4-TMP; ▼—n-B; □—n-P) (data of Ref. 12). Photoabsorption cross section of $C_6F_6^-$ as a function of photon energy in liquid TMS, $\sigma_{pa}^L(E)$ [TMS (Ref. 12)], and in solid 2,2,4-TMP, $\sigma_{pa}^s(E)$ [2,2,4-TMP (Ref. 16)].

It is seen from the data in Fig. 9 that $\sigma_{pd}^G(E)$ ~ $3\sigma_{pd}^L(E)$ and that in general $\sigma_{pd}^L(E) < \sigma_{pa}^L(E)$. We thus have to understand (i) the differences between $\sigma_{pa}^L(E)$ and $\sigma_{pd}^L(E)$ in the liquid (condensed) phase and (ii) the differences between $\sigma_{pd}^G(E)$ in the gas and $\sigma_{pd}^L(E)$ in the liquid. The understanding of (ii) requires an understanding of (i). Let us then go back to reaction (10) and the discussion in Sec. II on the relation of $\sigma_{pd}^G(E)$ to $\sigma_{pa}^G(E)$ in the gas. We have concluded in that section that

$$\sigma_{pd}^G(E) = \sigma_{pa}^G(E), \tag{21}$$

i.e., that the "photodetachment quantum yield" in the gas phase $q_{pd}^G(E)$ is unity. In the liquid, however, the photodetachment quantum yield $q_{pd}^L(E)$ for $C_6F_6^-$ was found[12] to be between 0.39 and 0.68 depending on the liquid and the photon energy; $q_{pd}^L(E)$ was larger at $E=3.0$ eV than at $E=2.6$ eV (Ref. 12) and this is consistent with the increase in the photoionization efficiency with increasing photon energy in the case of neutral molecules.[66]

If processes (10a)–(10c) are assumed for $C_6F_6^-$ in both the gaseous and the condensed phases, one can attribute the difference in the magnitudes of $\sigma_{pd}^L(E)$ and $\sigma_{pa}^L(E)$ in the liquid phase to the fast quenching of $C_6F_6^-$* by the bulk medium, i.e., to channel (10c); the dependence of $q_{pd}^L(E)$ on E can be rationalized by assuming that p_{pd}^i increases with E. As discussed earlier, channel (10a) is not energetically possible for the nonpolar solvents considered in this work for

$E<1.5$ eV and is neglected. We also neglect channel (10d) based on the work of Refs. 12 and 54. Thus, values of $q_{pd}^L(E)$ less than unity in liquids are attributed to the internal quenching of $C_6F_6^-$* [channel (10c)]; i.e., a fraction of the excited $C_6F_6^-$* anions internally convert to lower states at rates comparable to those of autodetachment. This process is absent in the gaseous experiments as we have indicated in Sec. III. We may then consider rationalizing the finding that $\sigma_{pd}^G(E) > \sigma_{pd}^L(E)$ as arising from the quenching process (10c). This is, however, only partly correct. The difference between the magnitudes of $\sigma_{pd}^G(E)$ and $\sigma_{pd}^L(E)$ is much larger than can be accounted for by such a consideration. Thus even if we take $q_{pd}^L(E) = 1$ [i.e., even if we take $\sigma_{pd}^L(E) = \sigma_{pa}^L(E)$], it is clear from the data in Fig. 9 that still

$$\sigma_{pd}^G(E) = \sigma_{pa}^G(E) > \sigma_{pa}^L(E). \tag{22}$$

What is, then responsible for the missing cross section?

Clearly one has to consider the effect of the medium on the photoabsorption process itself. The effect of the medium on the properties of the electronic spectra of molecules during the gradual transition from low pressure gas to condensed matter has a long history of investigation (e.g., see Refs. 67 and 68). Generally, the effects are separated into two types;[67-69] due to (i) the universal, collective action of the dielectric medium on the dissolved species and (ii) the specific interactions between the dissolved species and one or more particles in its surrounding. For nonpolar liquids

J. Chem. Phys., Vol. 101, No. 8, 15 October 1994

31

under consideration in this paper, we neglect (ii) and attempt to understand the differences between the magnitudes of $\sigma_{pd}^{G}(E)$ and $\sigma_{pd}^{L}(E)$ by considering the effect of (i) with the aid of the macroscopic characteristics of the liquid, i.e., the static dielectric constant ϵ and the refractive index n.

Let us then write

$$\sigma_{pd}^{G}(E) = \sigma_{pa}^{G}(E) = \sigma_{pa}^{L}(E)\phi(n)^{-1}, \tag{23}$$

where $\phi(n) \leq 1$ is a function of n. Following Neporent et al.,[69,70] we may express the photoabsorption cross section σ_{pa}^{L} for a given transition of a molecule immersed in a liquid to its gaseous value σ_{pa}^{G} as

$$\sigma_{pa}^{L}(E) = \sigma_{pa}^{G}(E)\phi(n), \tag{24}$$

where

$$\phi(n) = \frac{(2n^2+1)^2}{9n^3}\left(1 - \frac{\alpha}{R^3}\frac{2n^2-2}{2n^2+1}\right)^2 \tag{25}$$

represents a correction taking account the effect of the universal action of the medium. In expression (25), α is the average polarizability of the molecule in the region of the electronic transition and R is the Onsager cavity radius (practically equal to the molecular radius).[69,70] Experimental measurements as a function of the gas number density N have shown (e.g., see Refs. 69 and 70) that $\phi(n) \leq 1$ and that it decreases with increasing N.

While the preceding discussion is in accord with our observation, to quantify the relation between $\sigma_{pd}^{G}(E)$ and $\sigma_{pd}^{L}(E)$, we need to evaluate $\phi(n)$, and for this we need reliable values of n_{TMS}, $R_{C_6F_6^-}$ and $\alpha_{C_6F_6^-}$. For ϵ_{TMS} and $R_{C_6F_6^-}$, we can employ the values of 1.84 and 3.2 Å we used earlier. However, we have no knowledge of $\alpha_{C_6F_6^-}$. The values of the static polarizabilities of benzene, fluorobenzene, and m-difluorobenzene are about the same and equal to[71] 10.3×10^{-24} cm^3 and that of C_6F_6 is equal to 10.47×10^{-24} cm^3 (Refs. 64 and 72). Assuming such a value of 10.47×10^{-24} cm^3 for $C_6F_6^-$ along with the values of ϵ_{TMS} and $R_{C_6F_6^-}$ quoted above, we find from Eq. (25) that $\phi(n) = 0.76$. If now $\sigma_{pa}^{L}(E)$ is multiplied by $\phi(n)^{-1}(=1.32)$, it brings $\sigma_{pd}^{L}(E)$ and $\sigma_{pd}^{G}(E)$ into comfortable agreement. Actually, the best fit is obtained for $\phi(n)^{-1} \approx 1.39$ (see Fig. 9); this value is easily obtained if, e.g., $\alpha_{C_6F_6^-} \approx 13 \times 10^{-24}$ cm^3.

Finally, the comparison of the cross sections in Fig. 9 suggests that the peaks in the photoabsorption cross section $\sigma_{pa}^{L}(E)$ are narrower than the photodetachment peaks in either $\sigma_{pd}^{L}(E)$ or $\sigma_{pd}^{G}(E)$. This can be seen by considering the fact that while the width of $\sigma_{pa}^{L}(E)$ is determined exclusively by the Franck–Condon factors involved, the width of $\sigma_{pd}^{L}(E)$ is also influenced by the rapid decay (autodetachment) process(es). One might also expect the peaks of $\sigma_{pd}^{G}(E)$ to be somewhat broader than the peaks of $\sigma_{pd}^{L}(E)$ since the liquid stabilizes (increases the lifetime of) the high-lying anionic states [for the ground state naphthalene anion, e.g., the lifetime is 2.6×10^{-14} s in the gas phase[73] and 4×10^{-8} s in liquid TMS (Ref. 74)].

IV. THE BEHAVIOR OF OTHER ANIONS

The study of $C_6F_6^-$ as outlined in the preceding sections appears to be the most detailed to date. There exist only a handful of measurements on the photodetachment of other anions—absolute cross section measurements of the photodetachment of O_2^- in gases[20-24] and in nonpolar liquids,[4,13,25,26] and measurements of the photodetachment and photoabsorption cross sections for some aromatic anions in nonpolar liquids.[27,28] These measurements are briefly discussed in this section. They corroborate the conclusions reached in this paper on the photodetachment of $C_6F_6^-$ in the various states of matter.

A. $\sigma_{pd}^{G}(E)$ and $\sigma_{pd}^{L}(E)$ for O_2^-

In Fig. 11 are compared the experimental measurements of $\sigma_{pd}^{G}(E)$ of Burch et al.[20] for O_2^- in a low-pressure gas with experimental measurements of $\sigma_{pd}^{L}(E)$ for O_2^- in liquid TMS (296 K).[26] While from the measurements on $\sigma_{pd}^{G}(E)$ in Fig. 11 we cannot discern the photodetachment threshold energy, it is well known that the electron affinity of O_2^- is 0.44 eV (Ref. 51). The photodetachment threshold of O_2^- in various dielectric liquids lies at higher energies (see Fig. 11 for O_2^- in TMS)[26] and is a function of the liquid medium[13,26,75] [2.08 eV in TMS (Refs. 13, 26, and 75); 2.02 eV in 2,2-dimethylpropane (Ref. 26); 2.55 eV in 2,2,4-TMP (Refs. 13, 26 and 75)]; it depends on the value[76] of the liquid conduction band energy V_0.

Close to the photodetachment threshold, the variation of $\sigma_{pd}^{L}(E)$ with E followed an $E^{3/2}$ power law for all these liquids as is to be expected[13,26,77] from Eq. (18). In the gas phase, the photodetachment of O_2^- involves the transition from a π-electron orbital to a plane wave in the continuum. In the liquid, the same transition ejects the electron in the conduction band. Previous authors[26,77] assumed an "equivalency" in the two situations, although the electron in the latter case is quasifree and undergoes frequent scattering. In the work of Sowada and Holroyd,[26] the slopes B of the $[\sigma_{pd}^{L}(E)/E]^{2/3}$ vs E lines near the threshold were found to be independent of the liquid and smaller than their gaseous value by a factor of ~ 3. It can be seen from Fig. 11 that at the same value of $(E - E_{th})$ above the photodetachment threshold, the magnitude of σ_{pd}^{G} is about twice that of σ_{pd}^{L}. A rationalization of this difference in the magnitude of the photodetachment cross section in the gas and the liquid was attempted[78] by simply considering the effective mass m^* of the photodetached electron in the conduction band of the liquids. We believe that the differences can be accounted for to a large extent in a fashion similar to that we discussed in the previous section for the case of $C_6F_6^-$. If we use Eq. (25) with $\epsilon_{TMS} = 1.84$, $R_{O_2^-} = 1.54$ Å (Ref. 26), and $\alpha_{O_2^-} = 2.45 \times 10^{-24}$ cm^3 (Ref. 79), we find that $\phi(n) = 0.7$. To our knowledge, no $\sigma_{pa}(E)$'s exist for O_2^- in either the gaseous or the liquid (nonpolar) state that would allow a similar analysis as was possible for $C_6F_6^-$. If, however, we multiply the $\sigma_{pd}^{L}(E)$ for O_2^- by $\phi(n)^{-1} = 1.43$, the ratio $\sigma_{pd}^{L}(E) \times 1.43/\sigma_{pd}^{G}(E)$ would give an estimate of the photodetachment quantum yield for O_2^- in liquid TMS. This is found to be ~ 0.71 for $0.3 \leq (E - E_{th}) \leq 0.9$ eV.
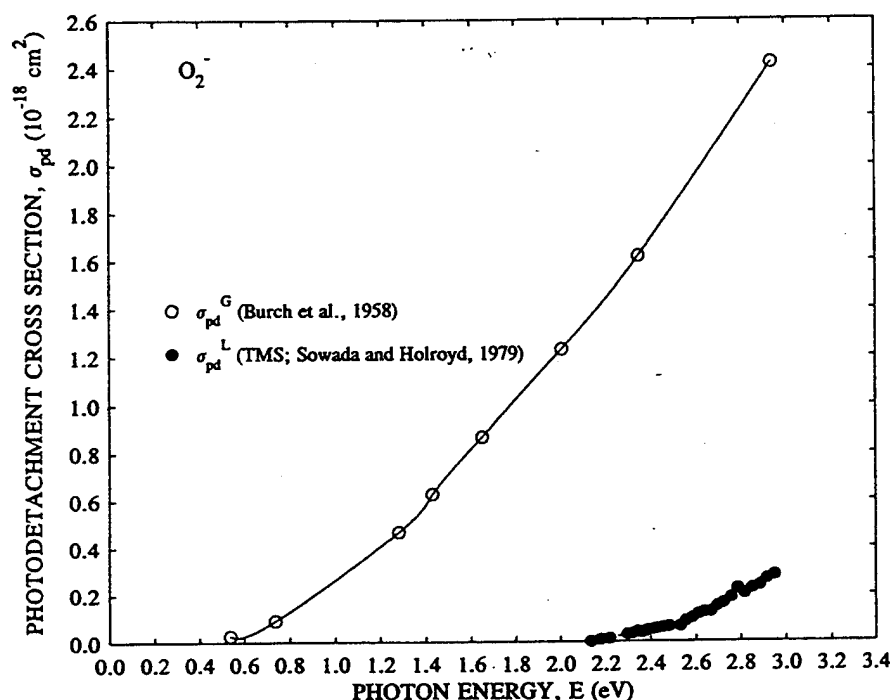
32

FIG. 11. Photodetachment cross section for O_2^- in a low-pressure gas [$\sigma_{pd}^G(E)$: O (Ref. 20)] and in liquid TMS (298 K) [$\sigma_{pd}^L(E)$: ● (Ref. 26)].

B. Aromatic anions in condensed matter (nonpolar liquids and glasses)

The conclusions reached in this paper regarding the photodetachment of $C_6F_6^-$ in the various states of matter are corroborated by the findings of a number of earlier studies on the photodetachment[27,28] and photoabsorption[28,80,81] of aromatic anions in nonpolar liquids (and frozen solutions). Especially, the investigations of Sowada and Holroyd[28] showed that photodetachment is a major process that ensues photoabsorption by aromatic anions [their measured $\sigma_{pd}^L(E)$ have peak values of ~ 1 Å^2]. The photodetachment quantum yield q_{pd}^L, however, is <1 (e.g., $q_{pd}^L = 0.09$ for perylene^{-*} in liquid n-P and 0.46 for perylene^{-*} in liquid TMS), and this was interpreted[28] in terms of autoionizing states which also convert internally to ground state anions. This interpretation is consistent with the failure of earlier studies[81] to measure fluorescence emission from such excited anions due possibly to the conversion into vibrational levels of the ground state. The liquid (solvent) is thus seen to stabilize the excited anion, making its lifetime longer in the liquid than in the gas, a conclusion also reached by theory.[82] Theoretical studies indicated also that for aromatic ("circular") anions, the spacing and the width of the autodetaching levels are determined principally by the potential of the extra electron in the molecule itself and not much by the (nonpolar) medium. In spite of the large electrostatic forces between the molecules of the liquid and the anions that are embedded in it, the small influence of the nonpolar liquid on the electronic absorption

spectra of the anions can be attributed to the small radii of the orbitals of the aromatic molecule's autodetaching states (probably about the same as those of the neutral molecule), i.e., by the limited range of the outermost electron's potential. Calculations showed also that the widths of the autodetaching levels (and hence their decay rates) become larger, the higher the energy level and the smaller the range of the interaction potential,[83] and depend noticeably on the angular momentum of the captured electron.[84]

[1] *Linking the Gaseous and the Condensed Phases of Matter: The Slow Electron and Its Interactions*, edited by L. G. Christophorou, E. Illenberger, and W. F. Schmidt (Plenum, New York, 1994).
[2] L. G. Christophorou, in *Linking the Gaseous and the Condensed Phases of Matter: The Slow Electron and Its Interactions*, edited by L. G. Christophorou, E. Illenberger, and W. F. Schmidt (Plenum, New York, 1994), pp. 3-30.
[3] L. G. Christophorou, Chem. Rev. 76, 409 (1976).
[4] L. G. Christophorou and K. Siomos, in *Electron–Molecule Interactions and Their Applications*, edited by L. G. Christophorou (Academic, New York, 1984), Vol. 2, Chap. 4.
[5] L. G. Christophorou, in *The Liquid State and Its Electrical Properties*,

J. Chem. Phys., Vol. 101, No. 8, 15 October 1994

33

edited by E. E. Kunhardt, L. G. Christophorou, and L. H. Luessen (Plenum, New York, 1988), pp. 283–316.

[6] L. G. Christophorou, Int. J. Radiat. Phys. Chem. 7, 205 (1975).

[7] S. R. Hunter and L. G. Christophorou, in *Electron–Molecule Interactions and Their Applications*, edited by L. G. Christophorou (Academic, New York, 1984), Vol. 2, Chap. 3.

[8] L. G. Christophorou, in *Physical and Chemical Mechanisms in Molecular Biology*, edited by W. A. Glass and M. N. Varma (Plenum, New York, 1991), pp. 183–230.

[9] H. Faidas and L. G. Christophorou, Radiat. Phys. Chem. 32, 433 (1988).

[10] H. Faidas, L. G. Christophorou, P. G. Datskos, and D. L. McCorkle, J. Chem. Phys. 90, 6619 (1989)

[11] H. Faidas, L. G. Christophorou, and D. L. McCorkle, Chem. Phys. Lett. 193, 487 (1992).

[12] U. Sowada and R. A. Holroyd, J. Phys. Chem. 84, 1150 (1980).

[13] U. Sowada, in *Proceedings of the 7th International Conference on Conduction and Breakdown in Dielectric Liquids, Berlin, July 27–31*, edited by W. F. Schmidt (Hahn–Meitner Institute, Berlin, 1981), p. 79.

[14] R. Dudde, B. Reihl, and A. Otto, J. Chem. Phys. 92, 3930 (1990); see a review of "inverse photoemission" by Smith [N. V. Smith, Rep. Prog. Phys. 51, 1227 (1988)].

[15] C. A. M. van den Ende, L. Nyikos, J. M. Warman, and A. Hummel, Radiat. Phys. Chem. 19, 297 (1982).

[16] A. M. Wani, T. Mukherjee, and J. P. Mittal, Radiat. Effects Lett. 43, 13 (1979).

[17] L. C. T. Shoute and J. P. Mittal, Radiat. Phys. Chem. 30, 105 (1987).

[18] L. C. T. Shoute and J. P. Mittal, J. Radiat. Phys. Chem. 97, 379 (1993).

[19] A. Nakajima, T. Taguwa, K. Hoshino, T. Sugioka, T. Naganuma, F. Ono, K. Watanabe, K. Nakao, Y. Konishi, R. Kishi, and K. Kaya, Chem. Phys. Lett. 214, 22 (1993).

[20] D. S. Burch, S. J. Smith, and L. M. Branscomb, Phys. Rev. 112, 171 (1958).

[21] R. A. Beyer and J. A. Vanderhoff, J. Chem. Phys. 65, 2313 (1976).

[22] P. C. Cosby, R. A. Bennett, J. R. Peterson, and J. T. Moseley, J. Chem. Phys. 63, 1612 (1975).

[23] P. C. Cosby, J. H. Ling, J. R. Peterson, and J. T. Moseley, J. Chem. Phys. 65, 5267 (1976).

[24] L. G. Christophorou, Contrib. Plasma Phys. 27, 237 (1987).

[25] L. V. Lukin and B. S. Yakovlev, Chem. Phys. Lett. 42, 307 (1976).

[26] U. Sowada and R. A. Holroyd, J. Chem. Phys. 70, 3586 (1979).

[27] A. A. Balakin, L. V. Lukin, A. V. Tolmachev, and B. S. Yakovlev, Opt. Spectrosc. 50, 161 (1981).

[28] U. Sowada and R. A. Holroyd, J. Chem. Phys. 85, 541 (1981).

[29] K. S. Gant and L. G. Christophorou, J. Chem. Phys. 65, 2977 (1976).

[30] F. J. Davis, R. N. Compton, and D. R. Nelson, J. Chem. Phys. 59, 2324 (1973).

[31] N. G. Adams, D. Smith, E. Alge, and J. Burdon, Chem. Phys. Lett. 116, 460 (1985).

[32] W. E. Wentworth, T. Limero, and E. C. M. Chen, J. Phys. Chem. 91, 241 (1987).

[33] N. Hernandez-Gil, W. E. Wentworth, T. Limero, and E. C. M. Chen, J. Chromatogr. 312, 31 (1984).

[34] E. C. M. Chen, W. E. Wentworth, and T. Limero, J. Chem. Phys. 83, 6541 (1985).

[35] S. M. Spyrou and L. G. Christophorou, J. Chem. Phys. 82, 1048 (1985).

[36] L. G. Christophorou, J. Chem. Phys. 83, 6543 (1985).

[37] W. B. Knighton, J. A. Bognar, and E. P. Grimsrud, Chem. Phys. Lett. 192, 522 (1992).

[38] P. G. Datskos, L. G. Christophorou, and J. G. Carter, J. Chem. Phys. 98, 7875 (1993).

[39] V. H. Dibeler, R. M. Reese, and F. L. Mohler, J. Chem. Phys. 26, 304 (1957).

[40] W. T. Naff, C. D. Cooper, and R. N. Compton, J. Chem. Phys. 49, 2784 (1968).

[41] H.-P. Fenzlaff and E. Illenberger, Int. J. Mass Spectrom. Ion Processes 59, 185 (1984).

[42] T. Oster, A. Kühn, and E. Illenberger, Int. J. Mass Spectrom. Ion Processes 89, 1 (1989).

[43] K. Y. Choo, G. D. Mendenhall, D. M. Golden, and S. W. Benson, Int. J. Chem. Kinet. 6, 813 (1974).

[44] J. R. Frazier, L. G. Christophorou, J. G. Carter, and H. C. Schweinler, J. Chem. Phys. 69, 3807 (1978).

[45] M. C. R. Symons, R. C. Selby, I. G. Smith, and S. W. Bratt, Chem. Phys. Lett. 48, 100 (1977).

[46] M. B. Yim and D. E. Wood, J. Am. Chem. Soc. 98, 2053 (1976).

[47] J. T. Wang and F. Williams, Chem. Phys. Lett. 71, 471 (1980).

[48] C. B. Duke, K. L. Yip, G. P. Ceasar, A. W. Potts, and D. G. Streets, J. Chem. Phys. 66, 256 (1977).

[49] L. N. Shchegoleva, I. I. Bilkis, and P. V. Schastnev, Chem. Phys. 82, 343 (1983).

[50] A. P. Hitchcock, P. Fischer, A. Gedanken, and M. B. Robin, J. Phys. Chem. 91, 531 (1987).

[51] A. A. Christodoulides, D. L. McCorkle, and L. G. Christophorou, in *Electron–Molecule Interactions and Their Applications*, edited by L. G. Christophorou (Academic, Orlando, FL, 1984), Vol. 2, Chap. 6.

[52] E. C. M. Chen, J. R. Wiley, C. F. Batten, and W. E. Wentworth, J. Phys. Chem. 98, 88 (1994).

[53] S. Chowdhury, E. P. Grimsrud, T. Heinis, and P. Kebarle, J. Am. Chem. Soc. 108, 3630 (1986).

[54] G. J. Hoijtink, Chem. Phys. Lett. 29, 154 (1974).

[55] M. Guerra, G. Distefano, D. Jones, F. P. Colonna, and A. Modelli, Chem. Phys. 91, 383 (1984).

[56] J. C. Giordan, J. H. Moore, and J. A. Tossell, J. Am. Chem. Soc. 106, 7397 (1984).

[57] A. Modelli, D. Jones, F. P. Colonna, and G. Distefano, Chem. Phys. 77, 153 (1983).

[58] P. D. Burrow, A. Modelli, and K. D. Jordan, Chem. Phys. Lett. 132, 441 (1986).

[59] P. D. Burrow, J. A. Michejda, and K. D. Jordan, J. Chem. Phys. 86, 9 (1987).

[60] The vertical detachment energy is defined (Ref. 61) as the minimum energy required to eject the extra electron from the anion in its ground electronic and molecular state without changing the internuclear separation.

[61] L. G. Christophorou, *Atomic and Molecular Radiation Physics* (Wiley-Interscience, New York, 1971), Chap. 7.

[62] S. Geltman, Phys. Rev. 112, 176 (1958).

[63]

$$P^- = -\frac{e^2}{2R}\left(1 - \frac{1}{\epsilon}\right) = -\frac{7.2}{R}\left(1 - \frac{1}{\epsilon}\right),$$

where P^- is in electron volts and the effective radius of the anion R is in Å; ϵ is the dielectric constant of the medium in which the anion is embedded.

[64] M. E. Baur, D. A. Horsma, C. M. Knobler, and P. Perez, J. Phys. Chem. 73, 641 (1969).

[65] *Handbook of Chemistry and Physics*, 70th ed. (CRC Boca Raton, FL, 1989–1990), p. F187.

[66] L. G. Christophorou, *Atomic and Molecular Radiation Physics* (Wiley-Interscience, New York, 1971), Chap. 3.

[67] J. B. Birks, *Photophysics of Aromatic Molecules* (Wiley-Interscience, London, 1970), pp. 109–119.

[68] M. B. Robin, *Higher Excited States of Polyatomic Molecules* (Academic, New York, 1974), Vol. 1, Chaps. 1 and 2.

[69] B. S. Neporent, N. B. Bakhshiev, V. A. Lavrov, and S. M. Korotkov, Opt. Spectrosc. 13, 18 (1962).

[70] B. S. Neporent and N. G. Bakhshiev, Opt. Spectrosc. 5, 634 (1958).

[71] *Handbook of Chemistry and Physics*, 70th ed. (CRC Boca Raton, FL, 1989–1990), pp. E75 and E76.

[72] M. P. Bogaard, A. D. Buckingham, M. G. Corfield, D. A. Dunmur, and A. H. White, Chem. Phys. Lett. 12, 558 (1972).

[73] K. D. Jordan and P. D. Burrow, Acc. Chem. Res. 11, 341 (1978).

[74] R. A. Holroyd, Ber. Bunsenges. Phys. Chem. 81, 298 (1977).

[75] The photodetachment thresholds of O_2^- in TMS and 2,2,4-TMP reported in Ref. 25 are, respectively, 2.3 and 2.4 eV. While these threshold values are consistent with those of Ref. 26, the magnitude of the photodetachment cross section reported in Ref. 25 is more than two orders of magnitude larger than that reported in Ref. 26, and is clearly in error.

[76] See footnotes to Table II.

[77] J. K. Baird and T. P. Schuman, Radiat. Phys. Chem. 32, 493 (1988).

[78] J. K. Baird, J. Chem. Phys. 79, 316 (1983).

[79] M. Bösch and R. Hofmann, J. Phys. Chem. Solids 36, 1077 (1975).

[80] T. Shida and S. Iwata, J. Am. Chem. Soc. 95, 3473 (1973).

[81] G. J. Hoijtink, N. H. Velthorst, and P. J. Zandstra, J. Mol. Phys. 3, 533 (1960).

[82] A. Banerjee and J. Simons, J. Chem. Phys. 69, 5538 (1978).

[83] H. Tsubomura and S. Sunakawa, Bull. Chem. Soc. Jpn. 40, 2468 (1967).

[84] T. Watanabe, T. Shida, and S. Iwata, Chem. Phys. 13, 65 (1967).

34

4.3. Photodetachment of SF_6^- in Nitrogen and Methane

Having established the photodetachment method we developed for the study of the photodetachment process in liquids and in gases, we began a detailed study of the photodetachment process for SF_6^- embedded in a nitrogen buffer gas at room temperature. The initial measurements of the photodetachment cross section, $\sigma_{pd}(E)$, of SF_6^- ions in N_2 buffer gas as a function of the photon energy E put the threshold for the process $SF_6^- + h\nu \rightarrow SF_6 + e$ at about 3.2 eV. The photodetachment cross section was found to increase monotonically with increasing photon energy E above the threshold. However, for E > 3 eV it was found that there is a contribution to the photodetachment signal from electrons released from the cathode by the photodetaching laser pulse via a two-photon process. It is then important to separate any such contribution to the measured photodetachment signal, especially when, as in the case of SF_6^-, the photodetachment cross section is small.

Our efforts to quantify the photodetachment cross section involving the SF_6^- anion have been hindered by the fact that the photodetachment cross section as a function of photon energy E is small (10^{-20} - 10^{-19} cm^2) below 3.3 eV, and by the fact that the photodetachment threshold for this anion is unusually large (about 3.2 eV) compared to the electron affinity of the SF_6 molecule (about 1 eV). In our technique, the measurement of σ_{pd} (E) relies on the experimental determination of the ratio N_{pd} / N_e where N_{pd} is the number of the photodetached electrons and N_e is the total number of electrons photoinjected into the gas (from a gridded cathode) by a laser pulse; all of these electrons attach to SF_6 forming SF_6^-. The measurement of the ratio N_{pd} / N_e is based on the determination of the induced voltages in the circuit caused by the motion of the photodetached electrons and the total number of negative ions (equal to the total number of photoinjected electrons N_e). An improvement in the accuracy of the measurement of these induced voltages would translate into an improvement in the measurement of σ_{pd} (E). In our efforts to achieve this, we replaced N_2 as the buffer gas. Instead of N_2, we used CH_4 for which-- at the operating E / N values-- the electron drift velocity is more than 20 times higher than in N_2. Since the induced voltage signal is proportional to the drift velocity of the electrons, we achieved

35

a considerable increase in the signal intensity. This has resulted in a better signal-to-noise ratio and a more accurate determination of the ratio N_{pd} / N_e. Thus, it has become possible to make accurate measurements of both the photodetachment cross section and the photodetachment threshold. These important results have been accepted for publication in Chemical Physics Letters. The new technique, the measurements and their analysis, and the interpretation of the results are fully described in this paper which is reproduced below (pages 36-48).

PHOTODETACHMENT OF SF$_6^-$[#]

P. G. Datskos, J. G. Carter, and L. G. Christophorou[1]

Atomic, Molecular, and High Voltage Physics Group
Health Sciences Research Division
Oak Ridge National Laboratory, P. O. Box 2008, Oak Ridge, TN 37831-6122
and
Department of Physics, University of Tennessee, Knoxville, TN 37996

Abstract

The photodetachment cross section for SF$_6^-$ and the photodetachment threshold for this process have been accurately measured using a newly developed technique. The photodetachment cross section has a threshold at 3.16 eV which is about three times larger than the electron affinity of the SF$_6$ molecule. The magnitude of the photodetachment cross section increases monotonically from the threshold to 1.0×10^{-18} cm^2 at a photon energy of 3.46 eV. The small size of the measured cross section is attributed to the large relaxation in the equilibrium internuclear positions of SF$_6^-$ compared to SF$_6$; the analysis of the data indicates that the photoejected electron has an angular momentum quantum number $\ell = 1$.

1.   Introduction

Sulfur hexafluoride (SF_6) attaches slow electrons very efficiently [1-2]. The large cross section for electron attachment to SF_6 forming parent and fragment negative ions largely accounts for its high dielectric strength [3] and its use in high voltage insulation [4] and other technologies (e.g., plasma etching [5-7]). In these applications, electron detachment from negative ions is also significant (e.g., as a source of avalanche-initiating electrons in SF_6 gas-insulated systems [8-10]). One possible detachment process in such media is photodetachment. Besides its practical significance, the photodetachment process for SF_6^- is also of basic interest; earlier studies [11-15] have indicated that the vertical detachment energy for this anion is much larger than the electron affinity of the SF_6 molecule, suggesting a large internuclear relaxation in SF_6^- compared to SF_6.

In this letter we report an accurate measurement of the threshold of, and the cross section $\sigma_{pd}(E)$ as a function of the photon energy $E = h\upsilon$ for, the process

$$SF_6^- + h\nu \rightarrow SF_6 + e \qquad (1)$$

The photodetachment threshold (representing the vertical detachment energy [1] of SF_6^-) has also been determined accurately and found to be 3.16 eV, i.e., significantly higher than the most recent values (1.05 eV (Ref. 16), 1.07 eV (Ref. 17))[§] of the electron affinity EA of SF_6. The photodetachment cross section $\sigma_{pd}(E)$ has been found to increase monotonically from the threshold to 1×10^{-18} cm^2 at $\bar{}$ 0.30 eV above threshold. The present measurements of the threshold energy and the magnitude of $\sigma_{pd}(E)$ for process (1) are in general agreement with an earlier photodetachment study [19] which employed a "photodetachment-modulated electron capture detector."

---

§See earlier EA values in Ref. 18.

37

2. Experimental Method

The experimental method used in the present study is similar to that we described earlier [20]. A major improvement made in the method lies in the choice of the buffer gas. In the earlier study [20] we used N_2 as the buffer gas. In the present study we used methane (CH_4) in order to improve the sensitivity of the technique (see below) that would allow for a more accurate determination of $\sigma_{pd}(E)$ especially when the size of $\sigma_{pd}(E)$ is small.

A schematic of the experimental arrangement employed is shown in Fig. 1. The cell consists of a six-way stainless-steel cube with two windows and electrical feedthroughs at opposite sides. The two stainless-steel parallel electrodes have a gridded circular area and were held at a distance d = 0.7 cm. The cell was filled with small quantities of SF_6 gas in a buffer gas of CH_4; the CH_4 gas number density was varied from 3.22×10^{19} to 6.44×10^{19} molecules cm^{-3} and the SF_6 gas number density was varied from 3.2×10^{13} to 16.11×10^{13} molecules cm^{-3} to optimize the signal-to-noise ratio. An excimer laser beam (λ = 308 nm; FWHM ~ 15×10^{-9} s) enters the cell through a circular aperture (2a = 0.508 cm in diameter) producing (photoelectrically) an electron swarm from the gridded part of the cathode electrode (Fig. 2). The electrons in the swarm move towards the anode under the influence of an externally applied uniform electric field and for the number densities of SF_6 employed they are totally depleted at drift distances z < d/2, forming SF_6^- via the process (the production of SF_5^- was kept to a minimum by working at low E/N values)
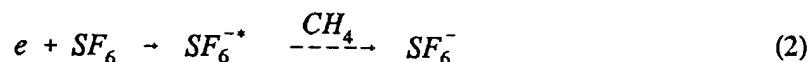
$$e + SF_6 \rightarrow SF_6^{-*} \xrightarrow{\quad CH_4 \quad} SF_6^- \tag{2}$$

A second, counter-propagating laser beam (FWHM ~6×10^{-10} s) from the tunable dye-laser enters the cell coaxially with the excimer laser pulse but with a time delay of ~3.5×10^{-6} s.

Photons from this second tunable dye-laser beam (with energies higher than the photodetachment threshold, E_{th}) photodetach SF_6^- giving rise to a photodetached electron swarm. As this electron swarm moves along the z-axis (Fig. 2) towards the anode, electrons are depleted again by attachment to SF_6 forming SF_6^- which are finally collected at the anode electrode.

A circular aperture with a diameter 2a=0.508 cm, was chosen so that a practically constant intensity profile of the excimer laser beam strikes the gridded anode thus producing an electron swarm with a number density, $n_e(r,z)$, which is constant across the gridded electrode and proportional in magnitude to the excimer laser intensity, i.e., $n_e(r,z=0)=AI_e(r)=$constant. These electrons are depleted by attachment to SF_6 molecules. The electron number density $n_e(r,z)$ and the negative ion number density $n_i(r,z)$, for times t less than the electron drift time, t_e, are described by

$$n_e(r,z)=A\ I_e(r)\ e^{-\eta z} \tag{3}$$

$$n_i(r,z)=A\ I_e(r)\ (1-e^{-\eta z}) \tag{4}$$

where η is the electron attachment coefficient for SF_6. Under the chosen experimental conditions the electrons are depleted entirely within times $t \leq t_e/2$.

The dye-laser beam which had a Gaussian intensity profile, $I_d(r)$, (defined as the number of photons per pulse) with a spatial opening 2b (Fig. 2) less than 2a, entered the interaction region between the two electrodes ~3.5×10^{-6} s after the excimer laser and well after all electrons were attached, i.e., at $t > t_e$. Photons with energies $E(=h\upsilon) > E_{th}$ give rise to photodetached electrons. Under the condition that the photodetached electron number density, $n_{ed}(r,z)$ is much smaller than the negative ion number density $n_i(r,z)$, the $n_{ed}(r,z)$ is given by

$$n_{ed}(r,z) = \sigma_{pd}(E) \ n_i(r,z) \ I_d(r) \qquad (5)$$

where $\sigma_{pd}(E)$ is the photodetachment cross section for photons of energy E. The total number, N_{ed}, of photodetached electrons is then obtained by integrating over the whole volume between the two circular electrodes, viz.,

$$\int_o^d \int_o^{2\pi} \int_o^a n_{ed}(r,z) r dr d\theta dz = \int_o^d \int_o^{2\pi} \int_o^a \sigma_{pd}(E) n_i(r,z) I_d(r) r dr d\theta dz \qquad (6)$$

$$N_{ed} = \sigma_{pd}(E) \frac{N_i}{\pi a^2} \int_o^a I_d(r) dr \qquad (7)$$

$$N_{ed} = \sigma_{pd}(E) N_i I_t / \pi a^2 \qquad (8)$$

where N_i is the initial number of negative ions (equal to the initial number of photoelectrons N_e) and I_t is the total number of electron detaching photons that enter the interaction region, i.e., the volume defined by the gridded part of the two circular electrodes. It can be seen from Eq. (8) that $\sigma_{pd}(E)$ can be determined from

$$\sigma_{pd}(E) = \frac{N_{ed}}{N_i} \frac{\pi a^2}{I_t} \qquad (9)$$

i.e., from a measurement of the ratio N_{ed}/N_i and the total number of photons I_t in the dye-laser pulse since the area πa^2 is known $(=0.203 \ cm^2)$.

As the electrons produced by the excimer laser pulse from the cathode electrode drift towards the anode electrode they induce a transient voltage signal in it which is detected as a fast initial drop in the measured voltage waveform (see Fig. 3). This drop stops when all electrons have been attached to SF_6 molecules; the magnitude of this drop is

proportional to the number of electrons, N_e, in the gap which is the same as the total number of SF_6^- ions, N_i, formed. The motion of the slower (than the electrons) SF_6^- ions (drift times ~10^{-3} s) cause a second drop corresponding to the gradually changing (dropping) portion of the waveform. The second light pulse from the tunable dye-laser illuminates the negative ions present in the gap and detaches electrons (whenever $E >$ E_{th}) inducing a second fast drop in the voltage waveform which is smaller in magnitude than the initial one, followed by yet another slowly dropping portion of the total voltage waveform when all the detached electrons were captured once again. From such waveforms the ratio N_{cd}/N_i is measured and used to determine $\sigma_{pd}(E)$.

The present measurements were made at a temperature $T \approx 300$ K. Due to the small values of $\sigma_{pd}(E)$ near the threshold, the ratio N_{cd}/N_e was small (~0.001). To improve the accuracy of the measurement, we attempted to increase the induced voltage due to N_{pd}. As was stated in the beginning of this section, we achieved considerable improvement in the measurement of N_{pd}/N_e (and thus in $\sigma_{pd}(E)$) by replacing N_2 with CH_4 as the buffer gas. For the operating E/N values (the pressure-reduced electric field E/P_{300} ranged from 0.36 to 0.71 Volt cm^{-1} $Torr^{-1}$) the electron drift velocity in CH_4 is ~ 15 times larger than in N_2 (Ref. 21). Since the induced voltage signal is proportional to the drift velocity of the electrons, we achieved a considerable increase in the signal intensity, which resulted in a better signal-to-noise ratio and a more accurate determination of the ratio N_{pd}/N_e. In spite of this improvement in the measurement, the error was still large (5 to 20% depending on the photon energy above E_{th}) but smaller than that indicated in other published data (Refs. 14 and 19).

3.   Photodetachment Cross Section and Vertical Photodetachment Energy for SF_6^-

In Fig. 4 is shown the photodetachment cross section $\sigma_{pd}(E)$ for SF_6^- for photon energies 3.16 to 3.46 eV. The magnitude of $\sigma_{pd}(E)$ is relatively small; we attribute this to the large difference between the equilibrium internuclear positions of SF_6^- and SF_6. The large relaxation in the equilibrium internuclear positions in SF_6^- is also responsible for the large

41

vertical detachment energy of this anion as given by the photodetachment threshold E_{th}. In this study we have been able to determine accurately the value of E_{th} from the data in Fig. 4. The $\sigma_{pd}(E)$ data, over the entire photon energy range covered, were fitted to the expression [20-22].

$$(\sigma_{pd}/E)^{1/n} = B(E-E_{th}) \tag{10}$$

where B and n are constants. The best fit to the data was obtained for $n = 3/2$ and $E_{th} = 3.16$ eV. The experimental data are plotted in Fig. 4 as $(\sigma_{pd}/E)^{2/3}$ versus E. The broken line through the data represents a least squares fit using Eq. (10) with $n = 3/2$ and $E_{th} = 3.16$ eV. The fit was done for different photon energy ranges above E_{th} and the results are given in Table 1. The 2/3 value of the exponent 1/n is consistent with photodetachment studies on other systems (e.g., see Ref. 20); if we assume n to be given by $(2\ell+1)/2$ (Refs. 20-22), a value of $n = 3/2$ would correspond to an angular momentum value of $\ell = 1$ for the ejected electron. The threshold value of 3.16 eV for process (1) is consistent with earlier estimates of the vertical detachment energy of SF_6^- [2.99 eV (Ref. 13); 3.0 eV (Ref. 12); 3.4 eV (Ref. 11); ≤ 3.25 eV (Ref. 15)] and the E_{th} value of 3.20 eV of Ref. 19.

In conclusion, via a new method which utilizes a fast buffer gas (CH_4) we were able to determine accurately both the absolute value and the threshold for the photodetachment process of SF_6^- over a range of photon energies below 3.46 eV. The photodetachment cross section is small, the photodetachment threshold is determined to be 3.16 eV, and the angular momentum quantum number of the photoejected electron is found to be $\ell=1$. The present measurements can be useful to the modelling of gas discharges and breakdown in SF_6 and the method described can be applied to similar studies especially when the cross section is small.

References

[1]   L. G. Christophorou, D. L. McCorkle, and A. A. Christodoulides in <u>Electron-Molecule Interactions and Their Applications</u>, L. G. Christophorou (Ed.), Academic Press, New York, 1984, Vol. 1, Chapt. 6.

[2]   S. R. Hunter, J. G. Carter, and L. G. Christophorou, *J. Chem. Phys.* **90**, 4879 (1989).

[3]   L. G. Christophorou and S. R. Hunter in <u>Electron-Molecule Interactions and Their Applications</u>, L. G. Christophorou (Ed.), Academic Press, New York, 1984, Vol. 2, Chapt. 5.

[4]   L. G. Christophorou and I. Sauers (Eds), <u>Gaseous Dielectrics VI</u>, Plenum Press, New York, 1991; L. G. Christophorou and D. W. Bouldin (Eds.), <u>Gaseous Dielectrics V</u>, Pergamon Press, New York, 1987; L. G. Christophorou and M. O. Pace (Eds.), <u>Gaseous Dielectrics IV</u>, Pergamon Press, New York, 1984.

[5]   W. W. Brandt and T. Honda, *J. Appl. Phys.* **60**, 1505 (1986).

[6]   R. W. Boswell and D. Henry, *Appl. Phys. Lett.* **47**, 1095 (1985).

[7]   S. Salimian, C. B. Cooper, R. Norton, and J. Bacon, *Appl. Phys. Lett.* **51** 1083 (1987).

[8]   F. Pinnekamp and N. Wiegart, in <u>Gaseous Dielectrics IV</u>, L. G. Christophorou and M. O. Pace (Eds.), Pergamon Press, New York, 1984, p. 91.

[9]   N. Wiegart, *IEEE Trans. Electr. Insul.* **20**, 587 (1985).

[10] J. K. Olthoff, R. J. Van Brunt, Y. Wang, R. L. Champion, and L. D. Doverspike, *J. Chem. Phys.* **91**, 2261 (1989).

[11]   O. J. Orient and A. Chutjian, *Phys. Rev. A* **34**, 1841 (1986).

[12]   A. Chutjian, in Electron-Molecule Collisions and Photoionization Processes, V. McKoy, H. Suzuki, K. Takayanagi, and S. Trajmar (Eds.), Verlag Chemie Int., Deerfield Beach, Florida, 1984, p. 127.

[13]   P. J. Hay, *J. Chem. Phys.* **76**, 502 (1982).

[14]   P. S. Drzaic and J. I. Brauman, *Chem. Phys. Lett.* **83**, 508 (1981); *J. Am. Chem. Soc.* **104**, 13 (1982).

[15]   B. Freiser and J. L. Beauchamp quoted in Refs. 11 and 12.

[16]   E. P. Grimsrud, S. Chowdhury, and P. Kebarle, *J. Chem. Phys.* **83**, 1059 (1985).

[17]   E.C.M. Chen, J. R. Wiley, C. F. Batten, and W. E. Wentworth, *J. Phys. Chem.* **98**, 88 (1994).

[18]   A. A. Christodoulides, D. L. McCorkle, and L. G. Christophorou, in Electron-Molecule Interactions and Their Applications, Academic Press, New York, 1984, Vol. 2, Chapt. 6.

[19]   R. S. Mock and E. P. Grimsrud, *Chem. Phys. Lett.* **184**, 99 (1991).

[20]   L. G. Christophorou, P. G. Datskos, and H. Faidas, *J. Chem. Phys.* **101**, 6728 (1994).

[21]   L. G. Christophorou, Atomic, and Molecular Radiation Physics, Wiley-Interscience, New York, 1971.

[22]   S. Geltman, *Phys. Rev.* **112**, 176 (1958).

Table 1. Estimates of the photodetachment threshold E_{th} for SF_6^- in CH_4 and corresponding correlation coefficients (C.C.) for different photon energy ranges above E_{th}.

Energy Range (eV)	E_{th} (eV)	C. C.
3.179 - 3.458	3.161	0.9918
3.179 - 3.397	3.158	0.9907
3.179 - 3.306	3.159	0.9724
3.179 - 3.241	3.166	0.9713
3.241 - 3.458	3.159	0.9840
	<3.16>	
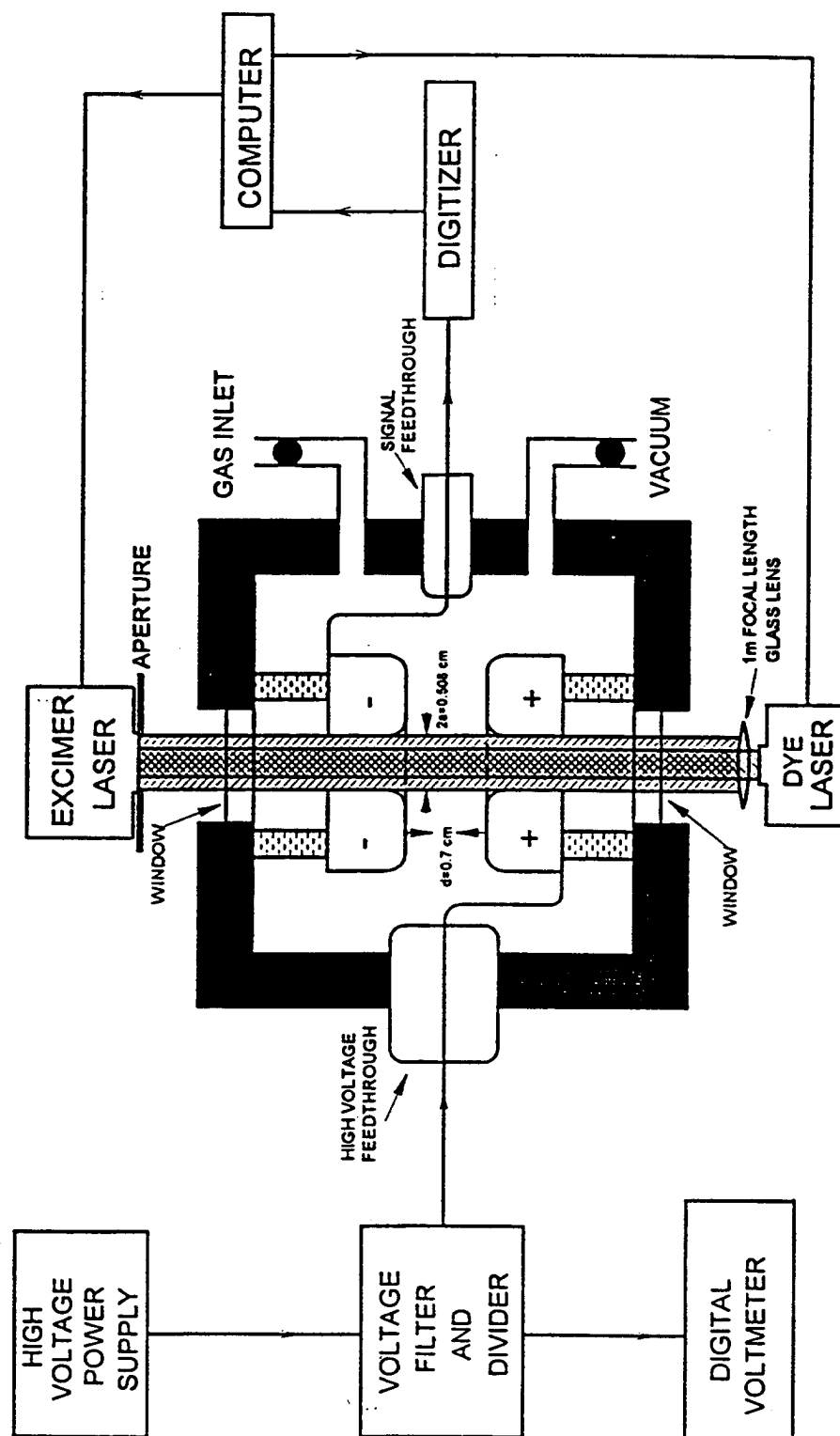
Figure 1: Schematic diagram of the overall arrangement of the two-laser photodetachment technique.
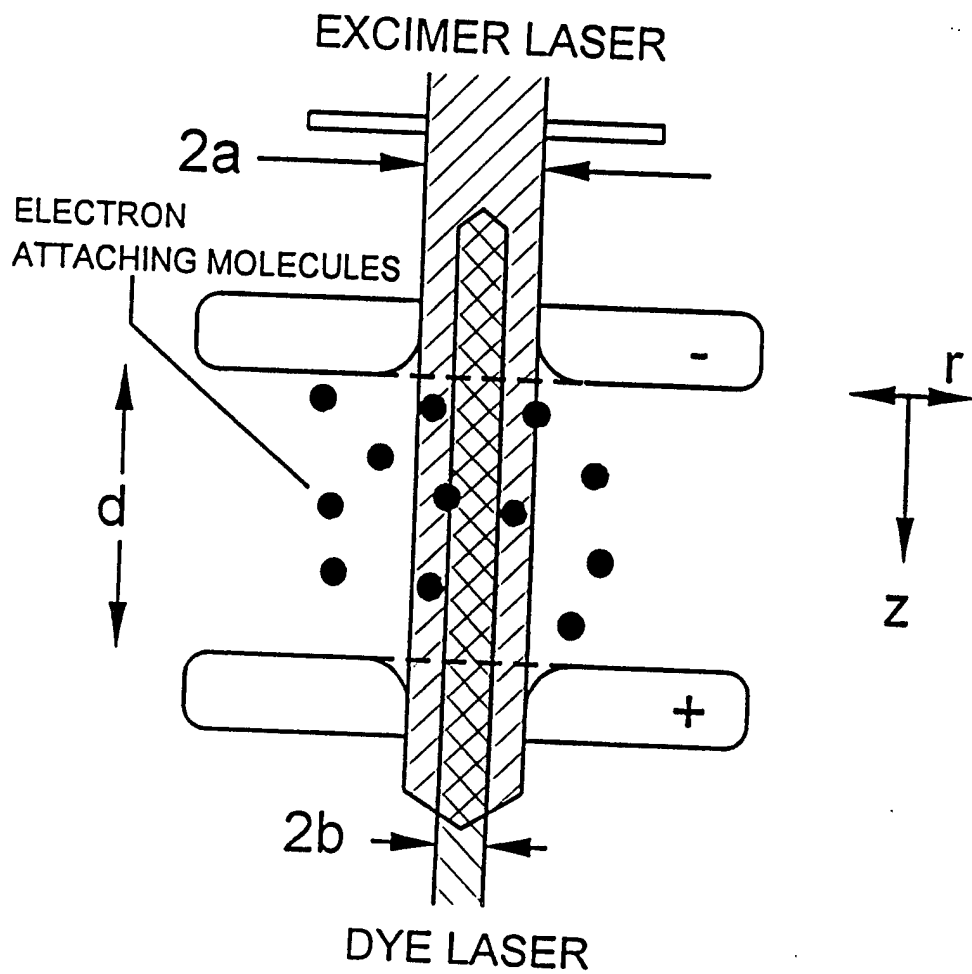
Figure 2: Schematic of the two-laser/electrode geometry arrangement of the photodetachment technique used to measure $\sigma_{pd}(E)$ for SF_6^- in CH_4.
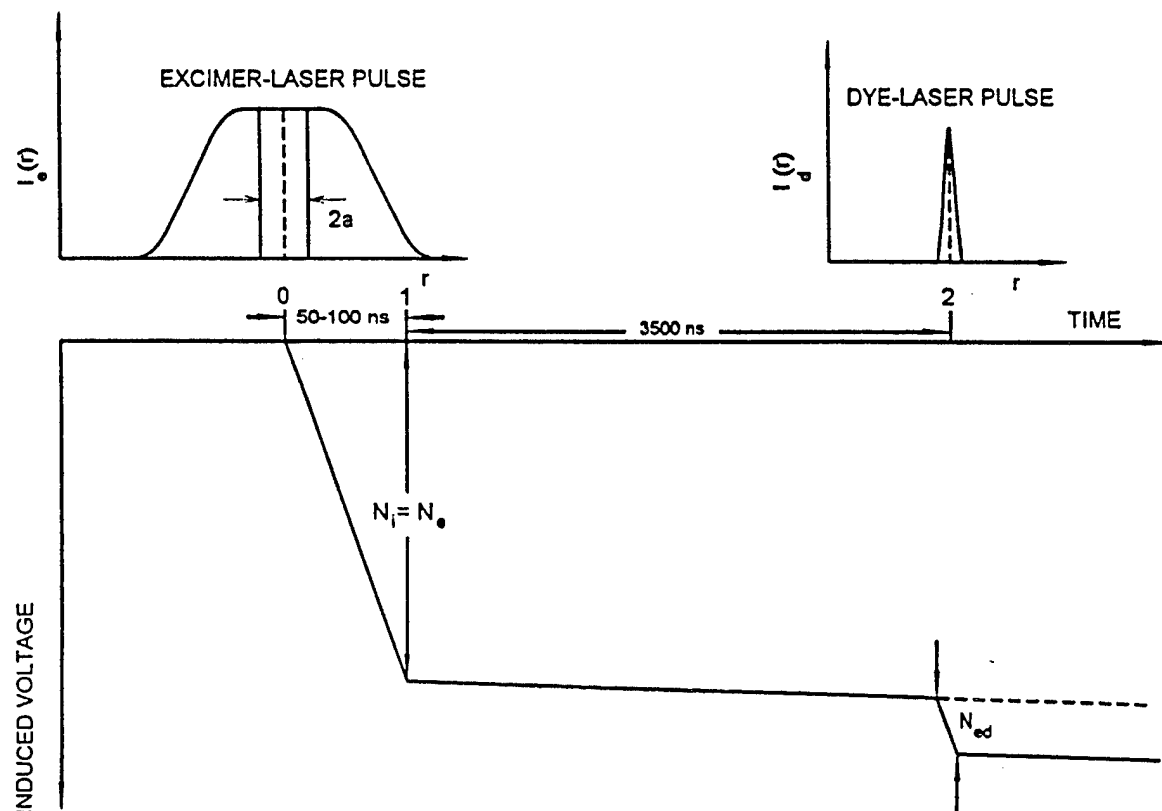
Figure 3: Schematic of the two-laser photodetachment technique illustrating a typical induced voltage waveform and the spatial profiles of the excimer and tunable laser pulses.

48
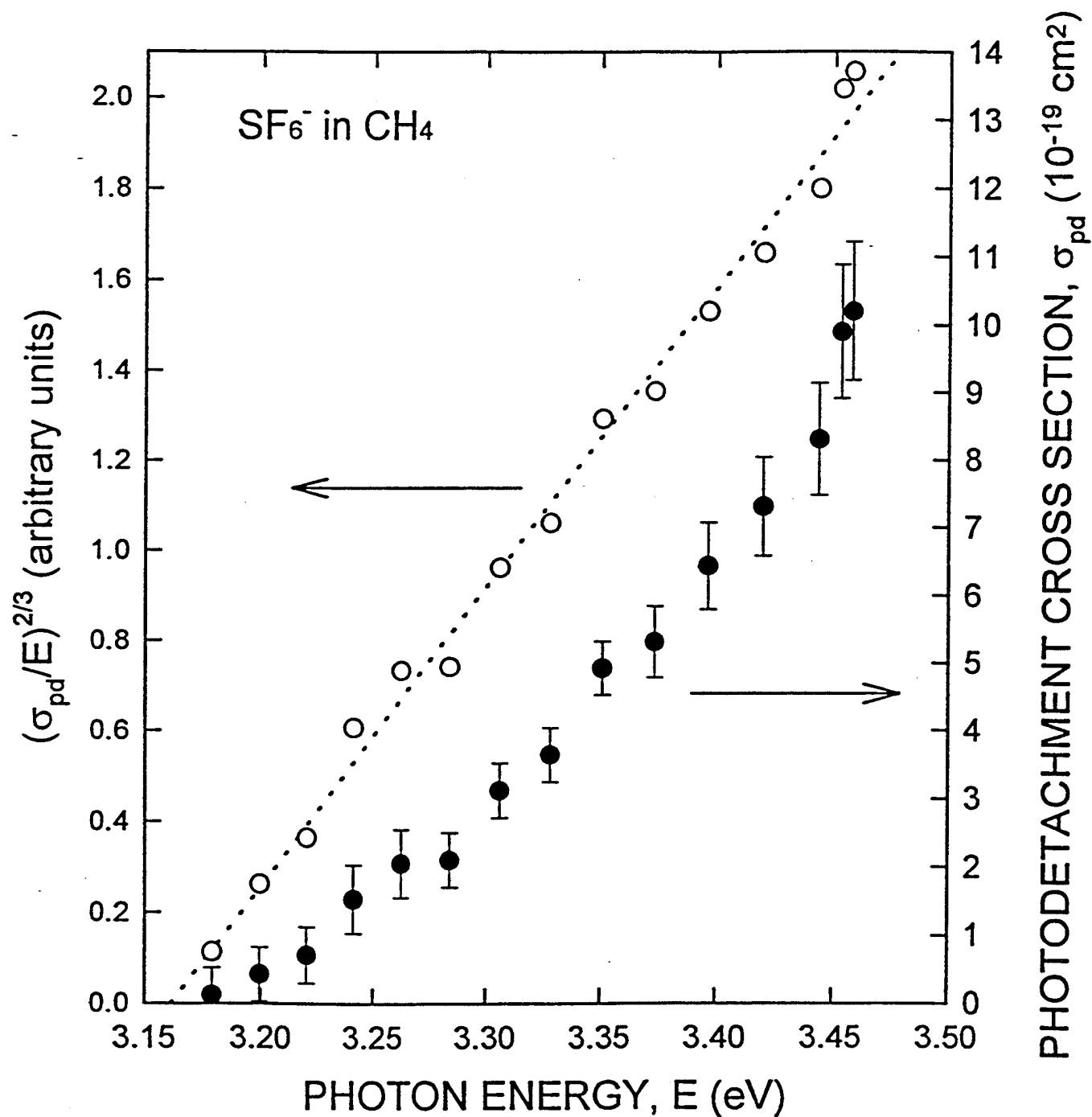
Figure 4: (•) Photodetachment cross section $\sigma_{pd}(E)$ for SF_6^- in CH_4 as a function of photon energy E.(○) A plot of $(\sigma_{pd}(E)/E)^{2/3}$ vs. photon energy.

5. Effect of Temperature on Electron Attachment and Detachment Processes (Thermally-Enhanced Electron Detachment)

5.1.The Time-Resolved Electron Swarm Technique

We have furthered the development of the time-resolved electron swarm technique and applied it to obtain information on electron attachment and detachment processes simultaneously from an analysis of transient electron waveforms. In this method photoelectrons are generated by a short laser pulse at the cathode of a parallel-plate electrode arrangement which are depleted by attachment to the electronegative gas under study (mixed with nitrogen) in the interelectrode space as they drift to the anode under an externally applied uniform electric field. The contribution of the initially produced (prompt) and the delayed (autodetached from the parent anions) electrons to the induced signal in the detector circuit was recorded as a function of time following the laser pulse and also as a function of gas density, applied electric field, and gas temperature, T. From such electron current waveforms the electron attachment and detachment frequencies have been determined as a function of the experimental variables. The technique is very powerful and it provided most valuable information on the effect of internal energy of molecules and parent anions on, respectively, their electron attachment and autodetachment properties. The method has been described in a number of publications (see below and Appendix A). It has been applied in present investigation to the study of the effects of temperature on the electron attachment and detachment properties of electronegative gases which at low electron energies form predominantly parent anions and whose behavior may be prototypical of other gaseous dielectrics

5.2. Temperature-Enhanced Electron Detachment from $C_6F_6^-$ Negative Ions

We have chosen C_6F_6 (hexafluorobenzene) for this investigation because this molecule attaches strongly low-energy (< 1.5 eV) electrons forming parent ($C_6F_6^-$) negative ions. Since the negative

50

ions formed via electron attachment can become a potential source of electrons in a gas dielectric, we investigated the electron attaching properties of C_6F_6 and the electron detaching properties of $C_6F_6^-$ as a function of T above ambient. The behavior of these species may serve as prototypical for those dielectric gases which form parent anions at low-electron energies.

It has been found that increases in T from ambient to 575 K enhance dramatically the autodetachment frequency for $C_6F_6^-$. The heat-activated autodetachment correlates with the increase in the internal energy of the anion and has an activation energy of 0.477 eV. In contrast to this profound increase of the autodetachment rate with T, the electron attachment rate constant producing $C_6F_6^-$ varies very little with T in this temperature range; the attachment rate constant initially increases slightly with increasing T below 500 K and subsequently shows some decline with further increases in T.

The technique, the analysis of the transient waveforms and the results obtained are presented and discussed in a paper which appeared in the Journal of Chemical Physics which is reproduced below (pages 52-59).

Temperature-enhanced electron detachment from $C_6F_6^-$ negative ions

P. G. Datskos,[a] L. G. Christophorou,[a] and J. G. Carter
Atomic, Molecular, and High Voltage Physics Group, Health and Safety Research Division,
Oak Ridge National Laboratory, Oak Ridge, Tennessee 37831-6122

A method is described whereby photoelectrons generated by a short laser pulse at the cathode of a parallel-plate electrode arrangement are depleted by attachment to C_6F_6 molecules mixed with N_2 in the interelectrode space as they drift to the anode under an externally applied electric field. The contribution of the initially produced (prompt) and the delayed (autodetached from $C_6F_6^-$) electrons to the induced signal in the detector circuit is recorded as a function of time following the laser pulse and also as a function of gas number density, applied electric field, and gas temperature, T. Increases in T from ambient to 575 K enhance dramatically the autodetachment frequency, τ_d^{-1}, for $C_6F_6^-$. This heat-activated autodetachment correlates with the increase in the internal energy of the anion and has an activation energy of 0.477 eV. Electron attachment producing $C_6F_6^-$ initially increases slightly with increasing T below 500 K and subsequently decreases with further increases in T.

I. INTRODUCTION

Earlier studies[1-5] have shown that hexafluorobenzene (C_6F_6) captures electrons through both (low lying) nondissociative and (higher lying) dissociative negative ion states. The negative ion resonances (NIRs) observed in C_6F_6 can generally be understood[1,4,5] by considering the capture of the incoming electron into one of the three empty π-orbitals π_4, π_5, and π_6. Electron transmission experiments[1] demonstrated the existence of three NIRs. For the first two degenerate NIRs associated with the π_4, π_5 orbitals, a vertical attachment energy (VAE) of ~0.42 eV was reported and for the third NIR associated with the π_6 orbital the reported value of the VAE is ~4.5 eV. Literature values for the electron affinity (EA) of C_6F_6 vary from 0.52 to more than 1.8 eV.[6-15] Since the dissociation energy $D(C_6F_5-F)$ is ~3.45 eV (Ref. 16) and the EA of the F atom and the C_6F_5 radical are, respectively, 3.4 and 2.7 eV (see Ref. 15) dissociative electron attachment leading to F^- and especially $C_6F_5^-$ is not expected at thermal energies. Hence the negative ions formed at thermal energies are expected to be due to $C_6F_6^-$ parent anions. Indeed electron beam studies[2,3] have shown the formation of F^- and $C_6F_5^-$ at ~4.0 and ~4.5 eV, respectively, and the formation of the parent anion $C_6F_6^-$ at low energies and with the parent anion's intensity rising towards thermal electron energies; electron beam studies using a time of flight mass spectrometer measured[3] the autodetachment lifetime of $C_6F_6^-$* and found it to be ~12 μs at room temperature. Increases in the energy of the captured electron leads to smaller autodetachment lifetimes[17,18] for $C_6F_6^-$*.

Room temperature electron swarm studies[5,19] found that electron attachment to C_6F_6 was very strong at mean electron energies, $\langle\epsilon\rangle$ below 1.5 eV. The electron attachment cross section deduced[5] from the swarm measurements possesses two peaks; one at ~0.0 eV and another at ~0.73 eV. The process responsible for the thermal energy peak was associated with electron capture into the degenerate π_4 and π_5 molecular orbitals, and that at ~0.73 eV with the π_6 NIR. Electron swarm studies[20-24] of the attachment of *thermal* electrons to C_6F_6 at temperatures above ambient have reported that the rate constant for thermal electron attachment decreases profoundly with increasing T; electron swarm studies at mean electron energies from thermal to ~1 eV showed[23] decreases in the attachment rate constant k_a by more than two orders of magnitude as T was raised from 450 to 600 K. It was suggested that the observed decreases in $k_a(T)$ could be due to changes in the capture process[23,24] forming $C_6F_6^-$* and/or due to electron detachment from the parent anion.[22] A more recent study[25] at thermal electron energies reported that the decrease in k_a with increasing T is indeed due to electron detachment from stabilized $C_6F_6^-$ and measured the electron detachment frequency in the temperature range 300–350 K. This was accomplished by monitoring the temporal profile of the $C_6F_6^-$ anions at ms times following the formation of $C_6F_6^-$*. In the present study we determined the electron attachment rate constant and the electron detachment frequency by recording the transient electron current due to prompt and delayed (detached) electrons.

In the present study we measured the electron attachment rate constant for the formation of $C_6F_6^-$ and the electron detachment frequency for $C_6F_6^-$ as a function of T (300–575 K) and $\langle\epsilon\rangle$ (~0.187 to ~1.0 eV). This we accomplished by recording the transient electron current due to prompt and delayed (detached) electrons within microsecond and submicrosecond times following the injection of the initial electrons into the gas from the cathode using a fast laser pulse (see Sec. II). These electrons drift to the anode under an externally applied uniform electric field. The interelectrode space was filled with minute amounts of C_6F_6 in a buffer gas of N_2. For the N_2 number densities used (1.61×10^{19} to 9.66×10^{19} molecules cm^{-3}) the initially produced (prompt) electrons attain quickly

52

(through collisions with the gas molecules) an equilibrium energy distribution $f(\epsilon,\langle\epsilon\rangle,T)$ which is well characterized under our experimental conditions.[26] At each value of the density, N, reduced electric field, E/N, employed the $f(\epsilon,\langle\epsilon\rangle,T)$ is calculated[27] and hence $\langle\epsilon\rangle(E/N,T)$ is determined and therefore the measured attachment rate constant and electron detachment frequency can be obtained as a function of $\langle\epsilon\rangle$ and T. The attachment and detachment processes envisioned are

$$e + C_6F_6 \xrightarrow{k_c} C_6F_6^{-*} \xrightarrow{N_2} C_6F_6^-, \qquad (1)$$

$$C_6F_6^- \xrightarrow{\tau_d^{-1}} C_6F_6 + e, \qquad (2)$$
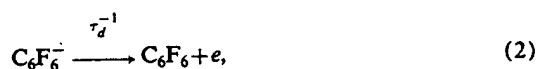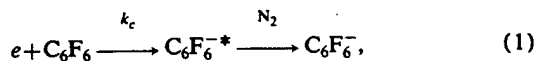
namely, electrons are captured by the C_6F_6 molecules with a rate constant k_c forming transient negative ions $C_6F_6^{-*}$ which are subsequently stabilized via collisions with (primarily) N_2 molecules forming $C_6F_6^-$. Electrons are thermally detached from $C_6F_6^-$ [reaction (2)] with an autodetachment frequency τ_d^{-1}. In this paper we studied reactions (1) and (2) as a function of T and $\langle\epsilon\rangle$ and concluded that the reduction in stable parent anion formation at elevated T is principally due to the large increase in the autodetachment from $C_6F_6^-$ with increasing T.

II. EXPERIMENTAL TECHNIQUE AND MEASUREMENTS

The experimental set up is shown schematically in Fig. 1. The cell used consists of a six way stainless steel cube
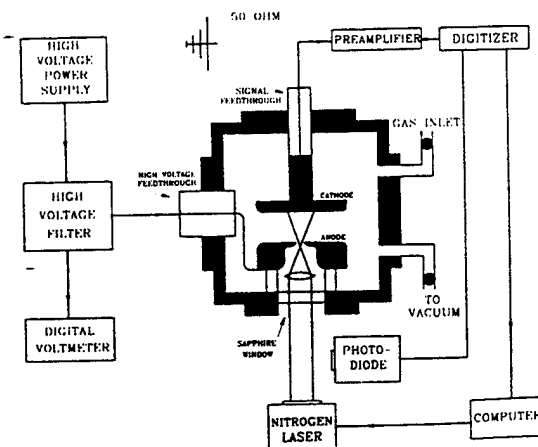
FIG. 1. Schematic diagram of the experimental set up.

with one sapphire window to allow the laser light to enter the cell. The two parallel stainless steel electrodes were circular disks of 3.81 cm in diameter and were held a distance of 0.4183 cm apart. The laser employed to produce the photoelectrons from the cathode was a Laser Photonics model LN 1000 nitrogen laser. The laser wavelength was 337.1 nm and the laser pulse duration (FWHM) was 6×10^{-10} s. The laser light strikes the cathode after going through a 0.1 cm diam hole in the anode electrode. A
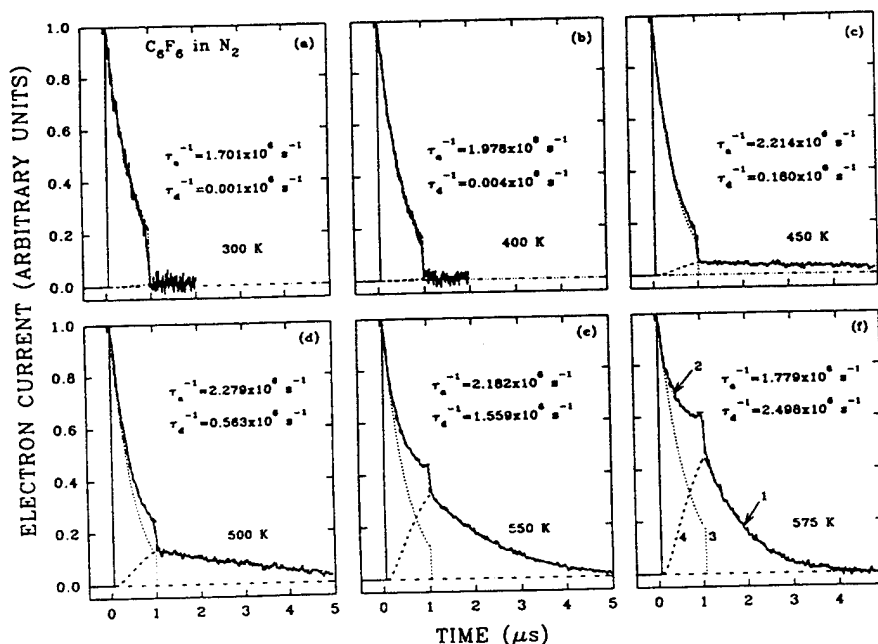
FIG. 2. Electron current waveforms for C_6F_6 at $T=300$, 400, 450, 500, 550, and 575 K. All waveforms are for $E/N=1.087\times10^{-17}$ V cm^2, $N_f=9.66 \times10^{19}$ molecules cm^{-3}, $N_a=5.64\times10^{13}$ molecules cm^{-3}, and $d=0.4183$ cm (see the text). In the figure the solid curves (-) [curve 1 in (f)] are the experimentally measured total electron currents as a function of time; the dash–dot (- - -) curves [curve 2 in (f)] are the calculated electron current waveforms for the τ_a^{-1} and τ_d^{-1} values obtained from the fitting of the model (see the text) to curves 1; the dotted ($\cdots$) curves [curve 3 in (f)] represent the contribution to the total electron current of the initial (prompt) electron swarm when only electron attachment occurs, and the broken (---) curves [curve 4 in (f)] represent the contribution to the total electron current from the autodetached electrons.

J. Chem. Phys., Vol. 98, No. 10, 15 May 1993

53

converging lens is employed to pass the laser beam through the hole to the cathode; the illuminated area on the cathode is ~ 1.5 cm^2.

A uniform electric field was applied to drift the electrons to the anode. The motion of the electrons (and the ions formed) in the interelectrode gap was detected and recorded with a Tektronix 7912 AD digitizer through a 50 Ω resistor to ground. The induced signal in the detection circuit is proportional to the electron and ion currents in the gap which themselves depend on the electron and ion drift velocities and the initial electron number density. However, the contribution to the current in the time scales of interest in this study is solely from the electrons and not from the negative ions.

The experiments were performed using N$_2$ as the buffer gas which was of Matheson ultrahigh purity (99.999%). Before use, the N$_2$ gas was cooled to liquid nitrogen temperature to freeze out any condensible impurities. The C$_6$F$_6$ sample was obtained from Aldrich Chemical Company with a stated purity of 99.9%. The C$_6$F$_6$ sample was subjected to several vacuum distillation cycles prior to the measurements in order to remove any air from the sample. The total gas number density, N_T, was varied from 1.61 to 9.66×10^{19} molecules cm^{-3}, and the attaching gas number density, N_a, was varied from 1.93×10^{13} to 38.64×10^{13} molecules cm^{-3}. A heating jacket was used to maintain the desired temperature which in turn was measured with two thermocouples in the cell.

The time and space evolution of the electron swarm when both electron attachment and detachment (but no ionization) processes are present can be described,[28-31] by

$$\frac{\partial \rho_e(x,t)}{\partial t} + w_e \frac{\partial \rho_e(x,t)}{\partial x} = -\frac{1}{\tau_a}\rho_e(x,t) + \frac{1}{\tau_d}\rho_i(x,t), \quad (3)$$

$$\frac{\partial \rho_i(x,t)}{\partial t} + w_i \frac{\partial \rho_i(x,t)}{\partial x} = \frac{1}{\tau_a}\rho_e(x,t) - \frac{1}{\tau_d}\rho_i(x,t), \quad (4)$$

where $\rho_e(x,t)$ and $\rho_i(x,t)$ is the number density of the electrons and negative ions, respectively, w_e and w_i are their respective drift velocities, and τ_a^{-1} and τ_d^{-1} are, respectively, the electron attachment and detachment frequencies. The solution to Eqs. (3) and (4) when the initial electron swarm is produced by a short duration laser pulse, i.e., for initial conditions $\rho_e(x,0) = n_0\delta(x)$ and $\rho_i(x,0) = 0$ is given by[28-31]

$$\rho_e(x,t) = \frac{n_0}{w_e - w_i}\exp\left[-\frac{1}{\tau_a}\left(\frac{x-w_it}{w_e-w_i}\right) + \frac{1}{\tau_d}\left(\frac{x-w_et}{w_e-w_i}\right)\right]$$
$$\times\left\{\delta\left(\frac{w_et-x}{w_e-w_i}\right) + \sqrt{\frac{1}{\tau_a\tau_d}\frac{x-w_it}{w_et-x}}\right.$$
$$\left.\times I_1\left[\frac{2}{(w_e-w_i)}\sqrt{\frac{1}{\tau_a\tau_d}(w_et-x)(x-w_it)}\right]\right\}, \quad (5)$$

$$\rho_i(x,t) = \frac{n_0}{w_e-w_i}\frac{1}{\tau_a}\exp\left[-\frac{1}{\tau_a}\left(\frac{x-w_it}{w_e-w_i}\right) + \frac{1}{\tau_d}\left(\frac{x-w_et}{w_e-w_i}\right)\right]$$
$$\times I_0\left[\frac{2}{(w_e-w_i)}\sqrt{\frac{1}{\tau_a\tau_d}(w_et-x)(x-w_it)}\right], \quad (6)$$

where n_0 is the initial electron number density, $\delta[(w_et-x)/(w_e-w_i)]$ is the delta function and I_n is the nth order modified Bessel function.

The electron and negative ion currents can be determined from

$$i_e(t) = \frac{ew_e}{d}\int_{w_it}^{\min[w_et,d]}\rho_e(x,t)dx, \quad (7)$$

$$i_i(t) = \frac{ew_i}{d}\int_{w_it}^{\min[w_et,d]}\rho_i(x,t)dx, \quad (8)$$

where d is the interelectrode gap.

We can define the electron attachment and detachment rate constants as

$$k_a\left(=\frac{\eta w_e}{N_a}\right) = (\tau_a N_a)^{-1}, \quad k_d = \tau_d^{-1}, \quad (9)$$

where η is the electron attachment coefficient defined[29,30] as the mean number of attachment collisions for one electron traveling 1 unit length along the direction of the electric field. By a nonlinear least squares fit of Eq. (7) to the experimental waveforms, $\tau_a^{-1}(\langle\epsilon\rangle,T)$ and $\tau_d^{-1}(\langle\epsilon\rangle,T)$ can be determined and from these the electron attachment rate constant $k_a(\langle\epsilon\rangle,T)$ and the autodetachment frequency $\tau_d^{-1}(\langle\epsilon\rangle,T)$. Examples of typical experimental waveforms are shown in Fig. 2 for $T = 300, 400, 450, 500, 550,$ and 575 K. The evolution of the autodetachment process for C$_6$F$_6$ as T is increased can be viewed in Fig. 2. In this figure the solid curves are the experimental waveforms for $\langle\epsilon\rangle \approx 0.38$ eV $(E/N = 1.087 \times 10^{-17}$ V cm^2), $N_T = 9.66 \times 10^{19}$ molecules cm^{-3}, $N_a = 5.64 \times 10^{13}$ molecules cm^{-3} and for a drift gap, d, of 0.4183 cm. The dotted curves represent the contribution to the total electron current when no autodetachment occurs. The difference between the total electron current (solid curves) and the dotted curves represents the contribution of the autodetached ("delayed") electrons (dashed curves). As T is increased this contribution becomes increasingly more significant and the parent anions decay faster.

III. RESULTS AND DISCUSSION

A. Electron attachment rate constant $k_a(\langle\epsilon\rangle,T)$ as a function of $\langle\epsilon\rangle$ and T

As mentioned in the Introduction the electron energy distribution functions $f(\epsilon,\langle\epsilon\rangle,T)$ for N$_2$ are known under our experimental conditions and thus at each value of E/N and T employed, the mean electron energy $\langle\epsilon\rangle(E/N,T)$ can be determined. For a number of $\langle\epsilon\rangle$ values we determined (from waveforms such as in Fig. 2) the $\tau_a^{-1}(\langle\epsilon\rangle,T)$ and $\tau_d^{-1}(\langle\epsilon\rangle,T)$ simultaneously via a nonlinear least squares fit procedure. Typical fits are shown in Fig. 2 for electron current waveforms for C$_6$F$_6$ at $T = 300, 400, 450,$
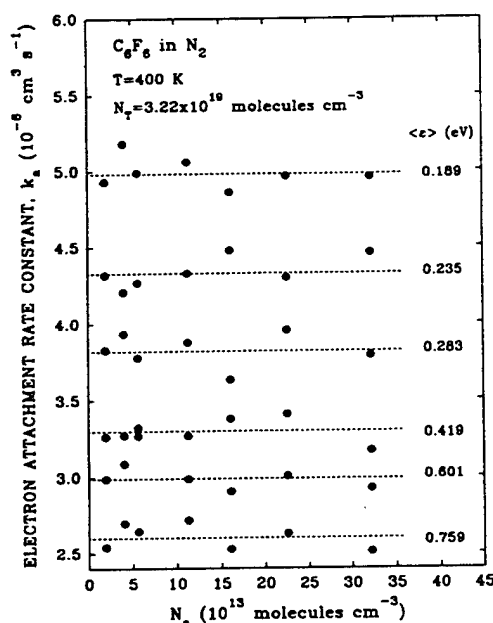
J. Chem. Phys., Vol. 98, No. 10, 15 May 1993

54

FIG. 3. Electron attachment rate constant k_a for C_6F_6 as a function of the attaching gas number density N_a for several values of the mean electron energy $\langle\epsilon\rangle$ and fixed values of T (400 K) and N_T (3.22×10^{19} molecules cm^{-3}).
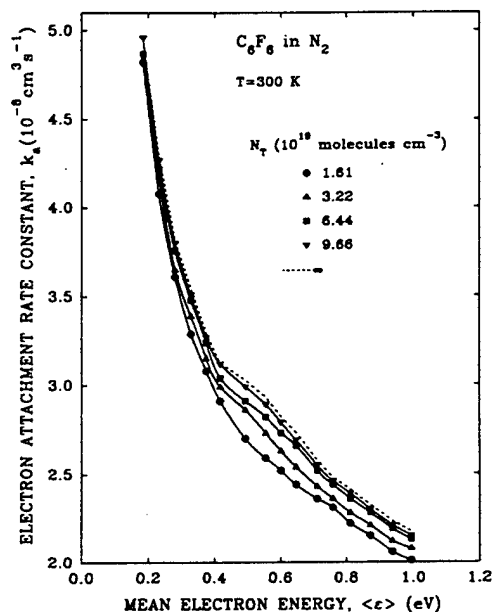

FIG. 4. Electron attachment rate constant k_a (for $N_a\to0$) for C_6F_6 as a function of mean electron energy, $\langle\epsilon\rangle$, and the total gas number density, N_T, at $T=300$ K. The broken curve is the electron attachment rate constant for $N_T\to\infty$.

B. Autodetachment frequency $\tau_d^{-1}(\langle\epsilon\rangle,T)$ as a function of $\langle\epsilon\rangle$ and T

500, 550, and 575 K. In the figure the solid curves (—) [curve 1 in Fig. 2(f)] are the experimentally measured total electron currents as a function of time; the dash-dot (-·-) curves [curve 2 in Fig. 2(f)] are the calculated electron current waveforms for the τ_a^{-1} and τ_d^{-1} values obtained from the fitting of the model to curves 1; the dotted (···) curves [curve 3 in Fig. 2(f)] represent the contribution to the total electron current of the initial electron swarm when only electron attachment occurs, and the broken (—) curves [curve 4 in Fig. 2(f)] represent the contribution to the total electron current from the autodetached electrons. Once $\tau_a^{-1}(\langle\epsilon\rangle,T)$ was determined this way, the total electron attachment rate constant $k_a(\langle\epsilon\rangle,T)$ for C_6F_6 at 300, 400, 450, 500, 550, and 575 K was calculated through Eq. (9). The $k_a(\langle\epsilon\rangle,T)$ was found to be independent of the attaching gas number density N_a at all T (see Fig. 3) but exhibited a small increase with increasing total gas number density, N_T (Fig. 4). The increase in $k_a(\langle\epsilon\rangle,T)$ with increasing N_T is due to the collisional stabilization of the transient $C_6F_6^{-*}$ anions. From data such as in Fig. 4 the values of $\lim_{N_T\to\infty} k_a(\langle\epsilon\rangle,T)$ were determined (by plotting $1/k_a$ as a function of $1/N_T$ and extrapolating $1/N_T$ to 0) at 300, 400, 450, 500, 550, and 575 K. These values of $k_a(\langle\epsilon\rangle,T)$ are plotted in Fig. 5 as a function of $\langle\epsilon\rangle$ for all the temperatures studied. It can be seen that the $k_a(\langle\epsilon\rangle,T)$ initially increases with increasing T (for $T<500$ K) and subsequently decreases for T above 500 K.
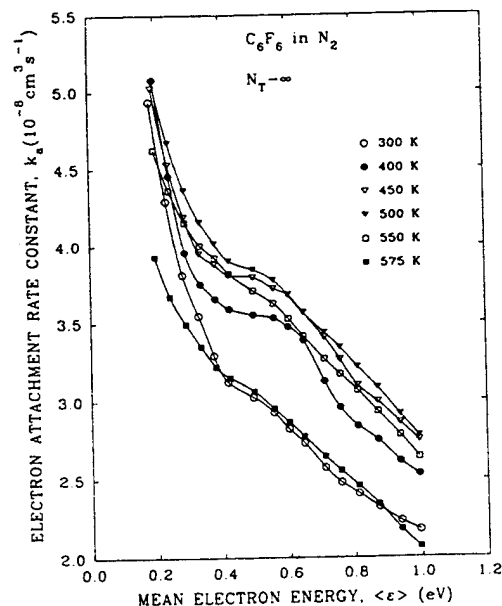
As mentioned above, the present measurements and analysis give simultaneously τ_a^{-1} and τ_d^{-1}. The latter was

FIG. 5. Electron attachment rate constant k_a (for $N_a\to0$ and $N_T\to\infty$) for C_6F_6 as a function of mean electron energy, $\langle\epsilon\rangle$ at temperatures of 300, 400, 450, 500, 550, and 575 K.
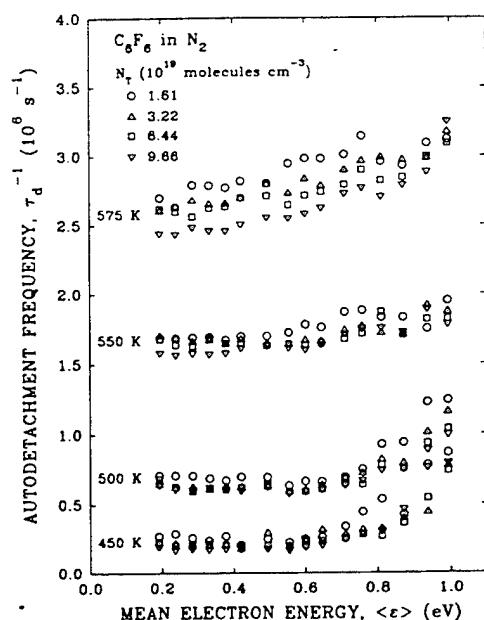
J. Chem. Phys., Vol. 98, No. 10, 15 May 1993

55

FIG. 6. Autodetachment frequency $\tau_d^{-1}(\langle\epsilon\rangle,T)$ for $C_6F_6^-$ (or $C_6F_6^{-*}$ which were not completely stabilized) as a function of mean electron energy, $\langle\epsilon\rangle$ at 450, 500, 550, and 575 K and the total gas number densities, N_T, of (O) 1.61, ($\triangle$) 3.22, ($\square$) 6.44, and (∇) 9.66×10^{19} molecules cm^{-3}.

FIG. 7. Autodetachment frequency $\tau_d^{-1}(\langle\epsilon\rangle,T)$ (for $N_T\rightarrow\infty$) for $C_6F_6^-$ as a function of mean electron energy, $\langle\epsilon\rangle$ at 450, 500, 550, and 575 K. (For T below 450 K the τ_d^{-1} was too small to be measured with the present technique.)

determined as a function of $\langle\epsilon\rangle$ for 450, 500, 550, and 575 K. These are plotted in Fig. 6 for total gas number densities $N_T=1.61$, 3.22, 6.44, and 9.66×10^{19} molecules cm^{-3}. It can be seen from Fig. 6 that τ_d^{-1} increases sharply as T is raised from 450 to 575 K and for a fixed $\langle\epsilon\rangle$ and T it becomes smaller the higher the N_T. The increase of τ_d^{-1} with T is due to the increase in the internal energy of $C_6F_6^-$ as T is raised (see later in this section) and the decrease of τ_d^{-1} with N_T is due to the fact that as N_T is increased progressively a larger number of the initially unstable $C_6F_6^{-*}$ become collisionally stabilized. When $N_T\rightarrow\infty$ all $C_6F_6^{-*}$ formed are fully stabilized giving $C_6F_6^-$ thus requiring more energy to revert back to the neutral molecule plus a free electron [reaction (2)]. In order to obtain the value $\lim\limits_{N_T\rightarrow\infty}[\tau_d^{-1}(\langle\epsilon\rangle,T)]$, the $\tau_d^{-1}(\langle\epsilon\rangle,T)$ was determined as a function of the total gas number density N_T (for sufficiently low values of N_T, $C_6F_6^{-*}$ can decay without being fully stabilized), plotted as a function of $1/N_T$ and extrapolated to $1/N_T\rightarrow0$. The values $\tau_d^{-1}(\langle\epsilon\rangle,T)$ obtained this way correspond to the autodetachment frequency for the fully stabilized parent anions $C_6F_6^-$ and are plotted in Fig. 7. Below 450 K the $\tau_d^{-1}(\langle\epsilon\rangle,T)$ (in the $\langle\epsilon\rangle$ range studied) were very small and the uncertainty in their determination large since there is very little autodetachment taking place.

C. Swarm unfolded electron attachment cross section $\sigma_a(\epsilon,T)$

The small number of attaching gas molecules (compared to that for N_2) employed in the present study, is not expected to change the electron energy distribution func-

tion $f(\epsilon,\langle\epsilon\rangle,T)$ of N_2 which we can assume to be the same for N_2 and for the C_6F_6/N_2 gas mixtures used in this study. This is also evident from Fig. 3 where $k_a(\langle\epsilon\rangle,T)$ shows no overall dependence on N_T. We can then determine the total electron attachment cross section $\sigma_a(\epsilon,T)$ using an iterative electron swarm-unfolding technique[32] to unfold the total electron attachment rate constants $k_a(\langle\epsilon\rangle,T)$ shown in Fig. 5. The swarm-unfolded $\sigma_a(\epsilon,T)$ are plotted as a function of the incident electron energy ϵ for 300, 400, 450, 500, 550, and 575 K in Fig. 8. They show maxima at ~0.0 and at ~0.8 eV. The positions of the maxima are consistent with earlier studies[5] which found the electron attachment cross section for C_6F_6 at 300 K to possess two peaks, one at thermal energies and another at ~0.73 eV and associated the former peak with electron capture into the π_4 or π_5 orbitals and the latter into the π_6 orbital.

D. Variation of the electron attachment and detachment frequencies in C_6F_6 with, respectively, the internal energy of C_6F_6 and $C_6F_6^-$

Clearly the results of this study show that in the temperature range investigated in this paper, the temperature influences profoundly the autodetachment process [reaction (2)] but it has only a small effect on the electron capture process [reaction (1)]. In the present study the transient $C_6F_6^{-*}$ anion formed initially by the capture of an electron, is stabilized by collisions with N_2 molecules (resulting in $C_6F_6^-$). Some anions obviously undergo autodetachment while still excited. As $N_T\rightarrow\infty$ all of the $C_6F_6^{-*}$ anions become stabilized before autoejecting the electron back into the medium. Assuming that the cross section for
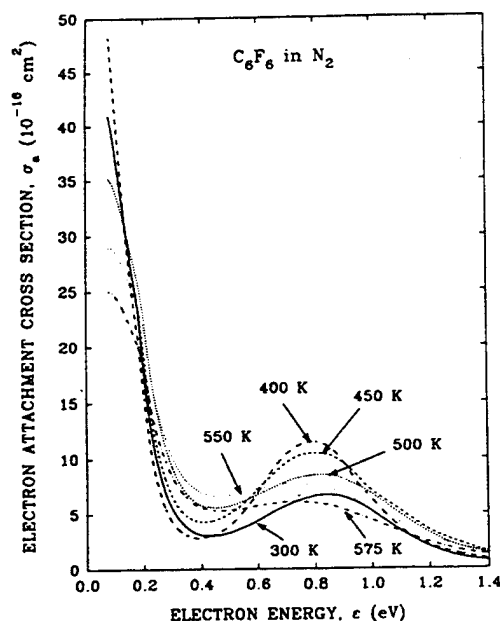
J. Chem. Phys., Vol. 98, No. 10, 15 May 1993

56

FIG. 8. Swarm unfolded total electron attachment cross sections $\sigma_a(\epsilon, T)$ for C_6F_6 at 300, 400, 450, 500, 550, and 575 K.
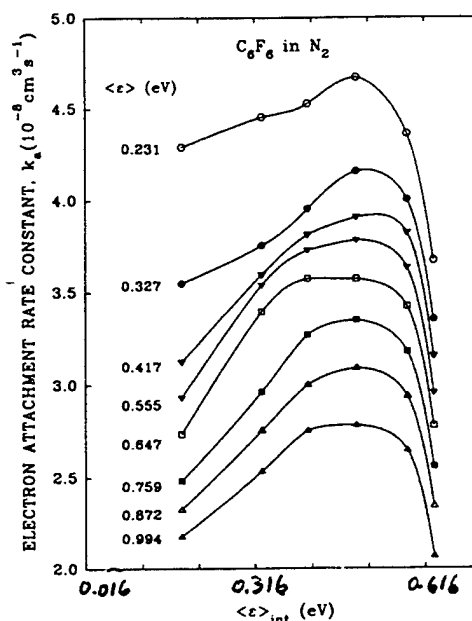

FIG. 9. Electron attachment rate constant, k_a (for $N_T \to \infty$) for $C_6F_6^-$ as a function of $\langle\epsilon\rangle_{int}$ for various values of the mean electron energy.

the collision between $C_6F_6^-{}^*$ and N_2 is given by the classical Langevin expression[33] an estimate for the time τ_c between collisions can be determined from

$$\tau_c = \frac{1}{2\pi N_T}\left(\frac{M_r}{e^2\alpha}\right)^{1/2}, \quad (10)$$

where M_r is the reduced mass of the $C_6F_6^-$, N_2 system and α is the static polarizability of N_2 ($=1.7403\times10^{-24}$ cm^3).[34] For the gas number densities N_T employed in this study τ_c varies from $\sim 10^{-11}$ to $\sim 10^{-10}$ s. That is, the times between collisions of $C_6F_6^-{}^*$ and N_2 are much shorter than the autodetachment lifetime of the isolated $C_6F_6^-{}^*$ anion (for thermal electron capture this lifetime is $\sim 12\ \mu s$) (Refs. 3, 17, and 18).

In an effort to better understand the effect of T on τ_a^{-1} and τ_d^{-1} we estimated at each T employed in the present study the vibrational energy of C_6F_6 in excess of the zero-point energy from

$$\langle\epsilon\rangle_{vib}(T) \approx \sum_{i=1}^{N} \frac{\hbar\omega_i}{e^{\hbar\omega/kT}-1} \quad (11)$$

using the vibrational frequencies listed in Refs. 35–37 and assumed that the total internal energy $\langle\epsilon\rangle_{int}(T)$ of both C_6F_6 and $C_6F_6^-$ is given by this quantity. We then plotted the electron attachment rate constant and the autodetachment frequency as a function of $\langle\epsilon\rangle_{int}$ in Figs. 9 and 10, respectively. The $k_a(\langle\epsilon\rangle, \langle\epsilon\rangle_{int})$ first increases and then decreases with $\langle\epsilon\rangle_{int}$ but the changes are small compared to those of $\tau_d^{-1}(\langle\epsilon\rangle, \langle\epsilon\rangle_{int})$. The autodetachment frequency at all values of $\langle\epsilon\rangle$ increases monotonically with increasing internal energy; by more than one order of magnitude (see Fig. 10) when $\langle\epsilon\rangle_{int}$ increases from ~ 0.409 to ~ 0.633 eV.

If we assume that the autodetachment process requires an activation energy E^* and that τ_d^{-1} is related to T by

$$\tau_d^{-1} = Ae^{-E^*/kT} \quad (12)$$

then E^* can be estimated from a plot of $\ln(\tau_d^{-1})$ as a function of $1/T$. A plot of this nature is shown in Fig. 11.
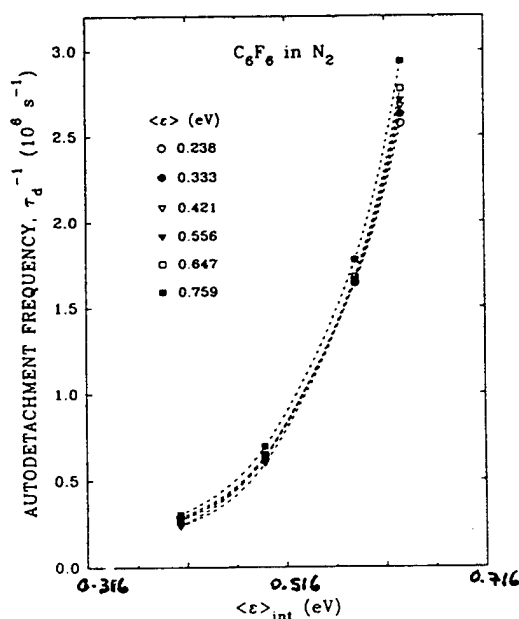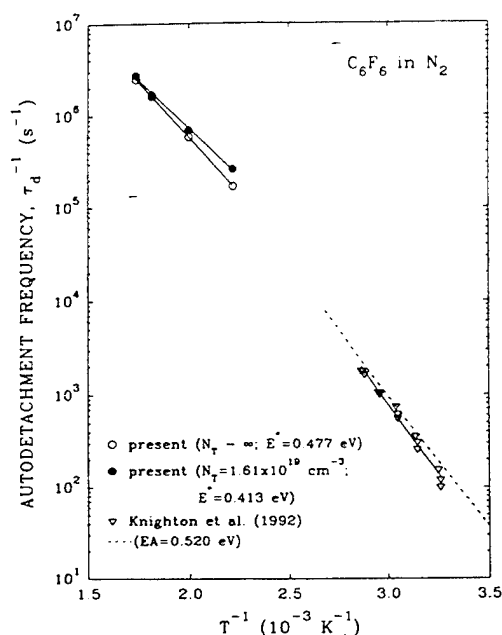

FIG. 10. Autodetachment frequency, τ_d^{-1} (for $N_T \to \infty$) for $C_6F_6^-$ as a function of $\langle\epsilon\rangle_{int}$ for various values of the mean electron energy.

J. Chem. Phys., Vol. 98, No. 10, 15 May 1993

57

FIG. 11. Autodetachment frequency, τ_d^{-1} (for $\langle\epsilon\rangle\rightarrow 3/2kT$) for $C_6F_6^-$ as a function of $1/T$. The open circles are for $N_T\rightarrow\infty$ and the closed circles for $N_T=1.61\times 10^{19}$ molecules cm^{-3}. Also plotted in the figure are the τ_d^{-1} data of Ref. 25 we extracted from Fig. 9 of that paper. The slope of the solid line through their data corresponds to an E^* of 0.603 eV. The broken line through their data corresponds to an E^* value of 0.52 eV which is the value reported by Ref. 13 for the EA of C_6F_6.

The τ_d^{-1} data plotted in Fig. 11 are for thermal electrons and for two values of N_T (see figure caption). From the slope of $\ln(\tau_d^{-1})$ vs $1/T$ for $N_T\rightarrow\infty$ (i.e., completely stabilized $C_6F_6^-$) we estimated E^* to be 0.477 eV. The slope for a similar plot in Fig. 11 for $N_T=1.61\times 10^{19}$ molecules cm^{-3} is 0.413 eV indicating that at this N_T not all $C_6F_6^-$ were in their lowest internal energy state. The value for E^* of $N_T\rightarrow\infty$ would correspond to the case that all negative ions reach adiabatically the ground electronic state for the neutral, from the lowest possible internal energy state of the anion and should compare well—as apparently it does—with the value for the electron affinity of C_6F_6 (EA=0.52 eV) reported in Ref. 13. Both of these values were basically determined by looking at the autodetachment process; the present one by looking at the autodetached electrons at microsecond and submicrosecond times and that of Ref. 13 at the decline of the negative ion density at ms time scales. The E^* values of the present study and the EA of Refs. 13 and 25 are lower than the EA values reported by other workers [i.e., ~ 0.86 eV (Ref. 14), >1.8 eV (Ref. 7)]. Also plotted in Fig. 11 are the data for τ_d^{-1} between 300 and 350 K measured in Ref. 25 for thermal electrons, which at 350 K are almost two orders of magnitude lower than our values for τ_d^{-1} for 450 K. Such small τ_d^{-1} would be undetected in our electron current waveforms and the perturbation of such a process in the measurement of k_a would be increasingly negligible for T

below 450 K. We fitted the data from Ref. 25 with Eq. (12) and the solid line through their points has a slope which corresponds to an activation energy $E^*=0.603$ eV. We also plotted our measured values for $\tau_d^{-1}(T)$ at mean electron energies higher than thermal to see possible effects of the captured electron's energy on E^* The results obtained show that at higher $\langle\epsilon\rangle$ the E^* are somewhat smaller than for $\langle\epsilon\rangle=3/2kT$. For example, when the mean energy of the electron swarm is 0.759 eV fitting of the $\tau_d^{-1}(T)$ to Eq. (12) yields an activation energy 0.425 eV for $N_T\rightarrow\infty$.

Finally, besides the basic significance of the present study the quantitative understanding of the effects of T on the electron attachment and detachment properties of electronegative gases is important in determining the dielectric properties of gaseous dielectrics especially when avalanche initiation is triggered by autodetachment.

ACKNOWLEDGMENTS

[1] J. R. Frazier, L. G. Christophorou, J. G. Carter, and H. C. Schweinler, J. Chem. Phys. 69, 3807 (1978).
[2] V. H. Dibeler, R. M. Reese, and F. L. Mohler, J. Chem. Phys. 26, 304 (1957).
[3] W. T. Naff, C. D. Cooper, and R. N. Compton, J. Chem. Phys. 49, 2784 (1968).
[4] T. Oster, A. Kühn, and E. Illenberger, Int. J. Mass Spectrom. and Ion Processes 89, 1 (1989).
[5] K. S. Gant and L. G. Christophorou, J. Chem. Phys. 65, 2977 (1976).
[6] F. M. Page and G. C. Goode, Negative Ions and the Magnetron (Wiley-Interscience, New York, 1969).
[7] C. Lifschitz, T. O. Tiernan, and B. M. Hughes, J. Chem. Phys. 59, 3182 (1973).
[8] L. J. Rains, H. W. Moore, and R. J. McIver, J. Chem. Phys. 68, 3309 (1978).
[9] R. N. McDonald, A. K. Chowdhury, and D. W. Setser, J. Am. Chem. Soc. 103, 7588 (1981).
[10] U. Sowada and R. A. Holroyd, J. Phys. Chem. 84, 1150 (1984).
[11] E. C. M. Chen, W. E. Wentworth, and T. J. Limero, J. Chem. Phys. 83, 6541 (1985).
[12] P. Kebarle and E. P. Grimsrud, J. Phys. Chem. 90, 2747 (1986).
[13] S. Chowdhury, E. P. Grimsrud, T. Heinis, and P. Kebarle, J. Am. Chem. Soc. 108, 3630 (1986).
[14] W. E. Wentworth, T. Limero, and E. C. M. Chen, J. Phys. Chem. 91, 241 (1987).
[15] A. A. Christodoulides, D. L. McCorkle, and L. G. Christophorou, Electron-Molecule Interactions and Their Applications, edited by L. G. Christophorou (Academic, Orlando, 1984), Vol. 2, Chap. 6.
[16] P. Smith, J. Chem. Phys. 29, 681 (1958).
[17] L. G. Christophorou, Adv. Electron. Electron Phys. 46, 55 (1978).
[18] L. G. Christophorou, K. S. Gant, and V. E. Anderson, J. Chem. Soc. Faraday Trans. II 73, 804 (1977).
[19] F. J. Davis, R. N. Compton, and D. R. Nelson, J. Chem. Phys. 59, 2324 (1973).
[20] N. G. Adams, D. Smith, E. Alge, and J. Burdon, Chem. Phys. Lett. 116, 460 (1985).
[21] N. Hernandez-Gil, W. E. Wentworth, T. Limero, an E. C. M. Chen, J. Chromatogr. 312, 31 (1984).
[22] E. C. M. Chen, W. E. Wentworth, and T. Limero, J. Chem. Phys. 83, 6541 (1985).

58

[23] S. M. Spyrou and L. G. Christophorou, J. Chem. Phys. **82**, 1048 (1985).

[24] L. G. Christophorou, J. Chem. Phys. **83**, 6543 (1985).

[25] W. B. Knighton, J. A. Bognar, and E. P. Grimsrud, Chem. Phys. Lett. **192**, 522 (1992).

[26] L. G. H. Huxley and R. W. Crompton, *The Diffusion and Drift of Electrons in Gases* (Wiley–Interscience, New York, 1974); S. R. Hunter and L. G. Christophorou, *Electron–Molecule Interactions and Their Applications*, edited by L. G. Christophorou (Academic, Orlando, 1984), Vol. 2, Chap. 3.

[27] A. V. Phelps and L. C. Pitchford, Phys. Rev. A **31**, 2932 (1985); S. R. Hunter, J. G. Carter, and L. G. Christophorou, J. Chem. Phys. **90**, 4879 (1989).

[28] L. Frommhold, Fortschr. Phys. **12**, 597 (1964).

[29] C. Wen, Ph.D. dissertation, Eindhoven University of Technology, The Netherlands, 1989.

[30] C. Wen and J. M. Wetzer, IEEE Trans. Electr. Insul. **23**, 999 (1988); **24**, 143 (1989).

[31] T. H. Teich, in *Gaseous Dielectrics VI*, edited by L. G. Christophorou and I. Sauers (Plenum, New York, 1991), pp. 215–229.

[32] L. G. Christophorou, D. L. McCorkle, and V. E. Anderson, J. Phys. **4**, 1163 (1971).

[33] P. Langevin, Ann. Chim. Phys. **5**, 245 (1905).

[34] R. H. Orcutt and R. H. Cole, J. Chem. Phys. **46**, 697 (1967).

[35] D. Steele and D. H. Whiffen, Trans. Faraday Soc. **55**, 369 (1959).

[36] R. A. R. Pearce, D. Steele, and K. Radcliffe, J. Mol. Struct. **15**, 409 (1973).

[37] F. Török, Á. Hegedüs, K. Kósa, and P. Pulay, J. Mol. Struct. **32**, 98 (1976).

J. Chem. Phys., Vol. 98, No. 10, 15 May 1993

59

5.3. Temperature Dependence of Electron Attachment and Detachment in SF_6 and $c-C_4F_6$

In the temperature, T, range of 300 to 600 K and the mean electron energy range of 0.19 to 1.0 eV, the total electron attachment rate constant for SF_6 and $c-C_4F_6$ measured in dilute mixtures with N_2, is virtually independent of T. Under the same experimental conditions the stabilized SF_6^- anion does not undergo autodetachment but the stabilized $c-C_4F_6^-$ anion undergoes a profound increase in autodetachment (by about four orders of magnitude). This difference between the SF_6^- and the $c-C_4F_6^-$ anions is attributed to the larger electron affinity of the SF_6 molecule compared to the $c-C_4F_6^-$ molecule. The heat-activated autodetachment for $c-C_4F_6^-$ is related to increases in the internal energy content of the $c-C_4F_6^-$ anion and was found to have an activation energy of 0.237 eV. The beautiful detailed data on these two dielectric gases are contained in a Journal of Chemical Physics paper which is given below (pages 61-70). This work, as that on C_6F_6 is fundamental in value and indicates that some earlier work [N. G. Adams, D. Smith, E. Alge, and J. Burdon, Chem. Phys. Let. **116**, 460 (1985); E. C. M. Chen, W. E. Wentworth, and T. J. Limero, J. Chem. Phys.**83**, 6541 (1985); S. M. Spyrou and L. G. Christophorou, J. Chem. Phys. **82**, 1048 (1985)] on the effect of temperature on electron attachment may be in error.

Temperature dependence of electron attachment and detachment in SF$_6$ and c-C$_4$F$_6$

P. G. Datskos,[a] L. G. Christophorou,[a] and J. G. Carter
Atomic, Molecular, and High Voltage Physics Group, Health and Safety Research Division, Oak Ridge National Laboratory, Oak Ridge, Tennessee 37831-6122

In the temperature, T, range of 300–600 K and the mean electron energy range $\langle \epsilon \rangle$ of 0.19–1.0 eV, the total electron attachment rate constant for SF$_6$ and c-C$_4$F$_6$ measured in dilute mixtures with N$_2$, is virtually independent of T. Under the same experimental conditions the stabilized SF$_6^-$ anion does not undergo autodetachment but the stabilized c-C$_4$F$_6^-$ anion undergoes a profound increase in autodetachment (by about four orders of magnitude). This difference between the SF$_6^-$ and the c-C$_4$F$_6^-$ anions is attributed to the larger electron affinity of the SF$_6$ molecule compared to the c-C$_4$F$_6$ molecule. The heat-activated autodetachment for c-C$_4$F$_6^-$ is related to increases in the internal energy content of the c-C$_4$F$_6^-$ anion and is found to have an activation energy of 0.237 eV. The "limiting electric field strength" of SF$_6$ was found to increase by ~11% as T was increased from 300 to 600 K.

I. INTRODUCTION

The electron attachment and detachment properties of polyatomic molecules are significant in many applications.[1] For example, the large electron attachment cross sections for sulfur hexafluoride (SF$_6$)[1–15] and hexafluorobutene (c-C$_4$F$_6$)[7,14,16] due to parent and/or fragment negative ion formation are principally responsible for their high dielectric strength (compared, say, to air) and for their use (especially of SF$_6$) in high-voltage insulation and other applications. [e.g., plasma etching of silicon[17] and GaAs based semiconductors.][18] Electron detachment from negative ions in SF$_6$ has been implicated as a source of avalanche-initiating electrons (e.g., see Refs. 19–23).

Electron beam studies at room temperature have shown that at near-zero energy electrons attach to SF$_6$ very efficiently forming parent anions SF$_6^{-*}$ whose autodetachment lifetimes, τ_a, under single-collision conditions are > 1 μs (e.g., see Refs. 2,8,12,24–27) and also fragment anions (e.g., F$^-$, F$_2^-$, SF$_2^-$, SF$_3^-$, SF$_4^-$, and SF$_5^-$).[8,28,29] Similar studies on c-C$_4$F$_6$ have shown[24,30] that electrons with energies below 1 eV attach efficiently to this molecule predominantly producing long-lived c-C$_4$F$_6^{-*}$ whose "isolated ion" τ_a is >7 μs. At electron energies, ϵ, above 1 eV, the fragment ions F$^-$, C$_3$F$_3^-$, and C$_4$F$_5^-$ were observed.[30]

Electron swarm studies at room temperature[6,13] have shown that the total electron attachment rate constant k_a for SF$_6$ is very large for mean electron energies, $\langle \epsilon \rangle$, below 1 eV and that it decreases monotonically with increasing $\langle \epsilon \rangle$ above thermal energies; the value, $(k_a)_{th}$, of k_a at thermal electron energies is 2.3×10^{-7} cm^3 s^{-1} (Ref. 13). Similar swarm measurements showed[16] that the c-C$_4$F$_6$ molecule exhibits the same type of behavior with regard to the dependence of k_a on $\langle \epsilon \rangle$; at room temperature the $(k_a)_{th}$ $\approx 1.5 \times 10^{-7}$ cm^3 s^{-1} for this molecule.[7,16]

Electron beam and electron swarm studies at temperatures, T, above ambient have been reported only for SF$_6$. Electron beam studies have shown[31] that SF$_5^-$ from SF$_6$ at near-zero energy increases by a few orders of magnitude when T is increased from 300 to ~880 K. Another electron beam study has shown[5] that the energy-integrated total electron attachment cross section for SF$_6$ is independent of T (300–1200 K). This finding is consistent with that of electron swarm studies[2,4,11] which found that $(k_a)_{th}$ remains unaffected by changes in T in the temperature range investigated in these studies (300–500 K).[32]

In this paper we report the results of an electron swarm study which allowed the determination of the effect of T on both the electron attachment and the electron detachment processes for SF$_6$ and c-C$_4$F$_6$ at low ($\leqslant 1$ eV) electron energies. We visualize the electron attachment and electron detachment processes for these molecules (M) as

$$e + M \xrightarrow{k_c} M^{-*} \xrightarrow{p} M^- \tag{1}$$

and

$$M^- \xrightarrow{t_d^{-1}} M + e. \tag{2}$$

That is, electrons are captured by the molecule M (SF$_6$ or c-C$_4$F$_6$) with a rate constant k_c forming transient negative ions which are subsequently stabilized with a probability p via collisions with (primarily) N$_2$ molecules giving stable M^- (SF$_6^-$ or c-C$_4$F$_6^-$) ions. The attached electrons can then thermally detach from the stable ion M^- [reaction (2)] with a detachment frequency t_d^{-1}. Reaction (2) should not be confused with the autodetachment of the isolated, initial metastable ion M^{-*}, viz.,

$$M^{-*} \xrightarrow{\tau_a^{-1}} M^{(*)} + e, \tag{3}$$

which is the reaction probed in single-collision beam experiments.

We investigated reactions (1) and (2) for SF$_6$ and c-C$_4$F$_6$ as a function of T (from 300 to 600 K) and $\langle \epsilon \rangle$

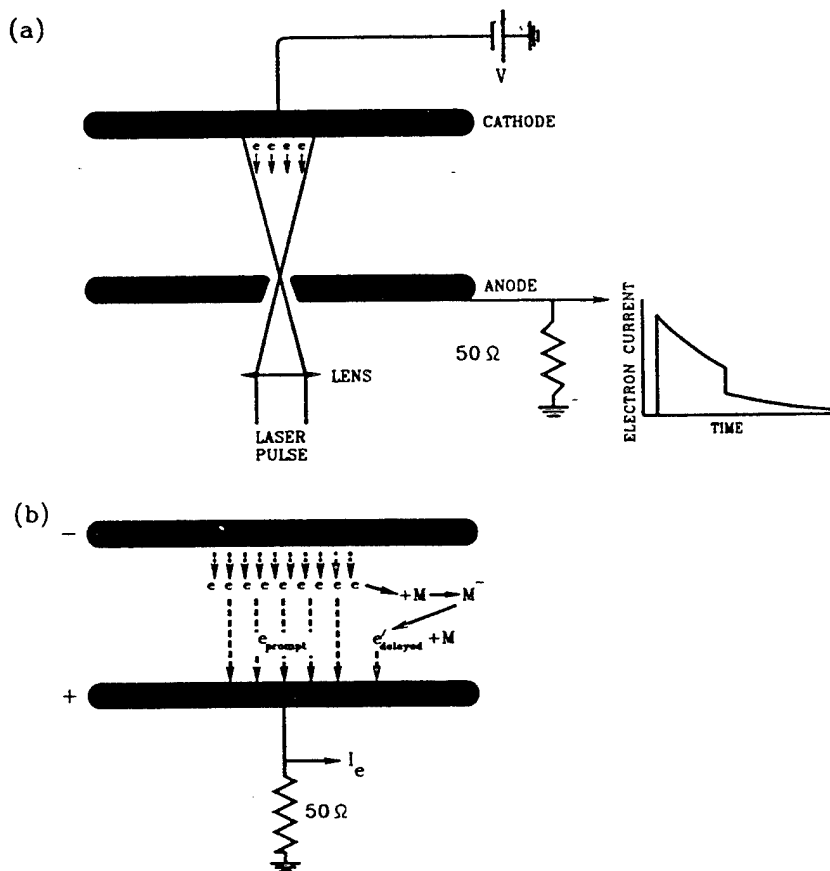[a] Also at The Department of Physics and Astronomy, The University of Tennessee, Knoxville, Tennessee 37996-1200.

FIG. 1. Schematic diagram showing the principle of the time-resolved electron swarm technique (see the text).

from (~ 0.19 to ~ 1.0 eV). We determined the k_a ($\langle \epsilon \rangle,T$) and the t_d^{-1} ($\langle \epsilon \rangle,T$) for SF$_6$ and c-C$_4$F$_6$. Our findings show that there are only minor effects on the low-energy electron attachment to SF$_6$ and c-C$_4$F$_6$ caused by changes in T (from 300 to 600 K). However, the effect of T on electron detachment from c-C$_4$F$_6^-$ is profound; the electron detachment frequency for the parent negative ion increases by more than three orders of magnitude as T is raised from 300 to 600 K. In contrast, the SF$_6^-$ ion was found to be very stable with respect to electron detachment in the same T range.

In the present work, also, we measured the "limiting electric field strength" $(E/N)_{lim}$ for pure SF$_6$ as a function of the gas temperature. Our study shows that the $(E/N)_{lim}$ for SF$_6$ increases monotonically with increasing T in the temperature range investigated (300–600 K).

II. EXPERIMENTAL TECHNIQUE AND MEASUREMENTS

A. Technique

The time-resolved electron swarm technique we employed in the present study has been described earlier.[33] The main chamber consists of a six-way stainless steel cube

with one sapphire window to allow the laser beam to enter the cell. The two parallel stainless steel electrodes were circular disks of 3.81 cm in diameter. The principle of this technique is shown schematically in Fig. 1. The electron swarm is produced by a fast N$_2$ laser pulse [pulse duration (FWHM) $\sim 6 \times 10^{-10}$ s] which strikes the cathode through a 0.1-cm-diam hole in the anode electrode.

The interelectrode space was filled with minute amounts of attaching gas molecules M(SF$_6$ or c-C$_4$F$_6$) in a buffer gas (N$_2$). The number density of the buffer gas was in the range of 1.61×10^{19}–9.66×10^{19} molecules cm^{-3}. For these densities the initially produced (prompt) electrons quickly attain (through collisions with the gas molecules) an equilibrium energy distribution $f(\epsilon,E/N,T)$ which is well defined under the present experimental conditions[34–36] and drift towards the anode under the influence of an externally applied uniform electric field. As they drift, a fraction of them is removed forming unstable parent negative ions which are rapidly stabilized, by collisions with the buffer gas, forming stable negative ions (M^- in Fig. 1). These stabilized anions can subsequently thermally autodetach giving rise to delayed electrons which can be present in the interaction region long after the initial elec-

J. Chem. Phys., Vol. 99, No. 11, 1 December 1993

62

trons have been collected. The motion of the electrons which reach the anode without ever having been captured ("prompt" electrons) and the electrons which have been attached and then thermally released ("delayed" electrons) induces a current in the anode circuit which is observed through a 50 Ω resistor to ground. For the μs time scales of interest in this work and the low E/N values employed, the contribution to the observed total current is solely from the electrons. The contribution of slowly moving species such as the negative ions is negligible and can be neglected.

The electron current wave forms can be described by[33]

$$i_e(t) = \frac{ew_e}{d} \int_{w_i t}^{\min(w_i t, d)} \rho_e(x,t) dx, \qquad (4)$$

where $\rho_e(x,t)$ is the number density of the electrons at a distance x from the cathode and time t, w_e is the electron drift velocity, and d is the drift distance. When the initial electron swarm is produced by a short duration laser pulse, i.e., for initial conditions $\rho_e(x,0) = n_0\delta(x)$ the electron number density is given by[33,37-40]

$$\rho_e(x,t) = \frac{n_0}{w_e - w_i} \exp\left[-\frac{1}{t_a}\left(\frac{x - w_i t}{w_e - w_i}\right) - \frac{1}{t_d}\left(\frac{w_e t - x}{w_e - w_i}\right)\right]$$

$$\times \left[\delta\left(\frac{w_e t - x}{w_e - w_i}\right) + \sqrt{\frac{1}{t_a t_d} \frac{x - w_i t}{w_e t - x}}\right.$$

$$\left. \times I_1\left(\frac{2}{(w_e - w_i)}\sqrt{\frac{1}{t_a t_d}(w_e t - x)(x - w_i t)}\right)\right], \qquad (5)$$

where w_i is the negative ion drift velocity and t_a^{-1} and t_d^{-1} are, respectively, the electron attachment and detachment frequencies. At each value of the gas number density-reduced electric field E/N we employed, the $f(\epsilon, \langle\epsilon\rangle, T)$ was calculated[13,36] and hence the $\langle\epsilon\rangle(E/N,T)$ determined, and therefore the measured electron attachment and detachment frequencies can be obtained as a function of $\langle\epsilon\rangle$ and T. The change in the electron current due to the loss (electron attachment) and gain (electron detachment) of electrons as the temperature is increased above ambient can be seen from the typical experimental wave forms shown for SF$_6$ (at 300, 400, 500, and 550 K) and for c-C$_4$F$_6$ (at 400, 450, 500, 550, and 600 K) in Figs. 2 and 3, respectively. From Fig. 2 it can be seen that no delayed electrons [due to reaction (2)] are present in the SF$_6$/N$_2$ mixtures for temperatures up to 550 K. However, for the c-C$_4$F$_6$/N$_2$ gas mixtures there is an increasingly larger contribution of delayed electrons to the total current (Fig. 3). Using wave forms such as in Figs. 2 and Fig. 3 obtained at a number of E/N and T values, we employed Eq. (4) and a nonlinear least squares fit to determine the t_a^{-1} and t_d^{-1}. In Fig. 2 the solid curves represent the experimental wave forms for $E/N = 3.10 \times 10^{-17}$ V cm^2 ($\langle\epsilon\rangle \approx 0.71$ eV), $N_T = 6.44 \times 10^{19}$ molecules cm^{-3}, and $N_a = 9.66 \times 10^{13}$ molecules cm^{-3}. The dash-dot curves are fits of the experimental wave forms to Eq. (4). In Fig. 3 the evolution of the autodetachment process for c-C$_4$F$_6$ as T is increased can be
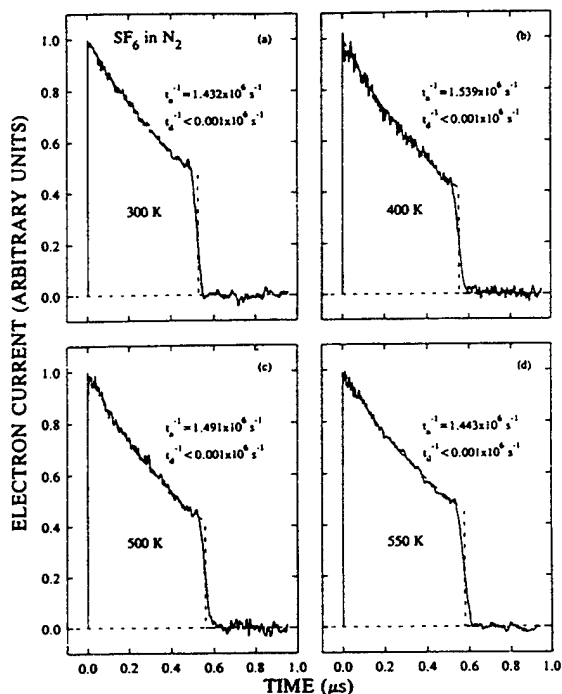

FIG. 2. Electron current wave forms for SF$_6$ in N$_2$ at $T=300$, 400, 500, and 550 K. All wave forms are for $E/N=3.10\times10^{-17}$ V cm^2, $N_T=6.44 \times 10^{19}$ molecules cm^{-3}, $N_a=9.66\times10^{13}$ molecules cm^{-3}. In the figure the solid curves (—) are the experimentally measured total electron currents as a function of time; the dash-dot (- · -) are the calculated electron current wave forms for the t_a^{-1} and t_d^{-1} values obtained from a fit to Eq. (4) (see the text) and shown on the figure. Note that we can obtain only an upper limit to t_d^{-1} of 10^3 s^{-1}.

viewed. In this figure the solid curves are the experimental current wave forms for $E/N=1.24\times10^{-17}$ V cm^2 ($\langle\epsilon\rangle \approx 0.42$ eV), $N_T=6.44\times10^{19}$ molecules cm^{-3}, $N_a=6.44 \times10^{13}$ molecules cm^{-3}. The dotted curves represent the contribution to the total electron current when no autodetachment occurs. The difference between the total electron current (solid curves) and the dotted curves represents the contribution of the autodetached (delayed) electrons (dashed curves). As T is increased this contribution becomes increasingly more significant and the parent anions decay faster (see further discussion in Sec. III).

B. Gases purity

The experiments were performed using Matheson ultrahigh purity N$_2$ as the buffer gas (quoted purity specifications 99.999% or better), instrument purity SF$_6$ from Matheson Gas Products (quoted purity of better than 99.99%), and c-C$_4$F$_6$ with a stated purity of 99%. Before use, the N$_2$ gas was cooled to liquid N$_2$ temperatures to freeze out any condensible impurities. The N$_2$ vapor was then extracted at temperatures just above the boiling point. The SF$_6$ and c-C$_4$F$_6$ sample gases were further purified by subjecting them to numerous freeze-pump-thaw cycles at
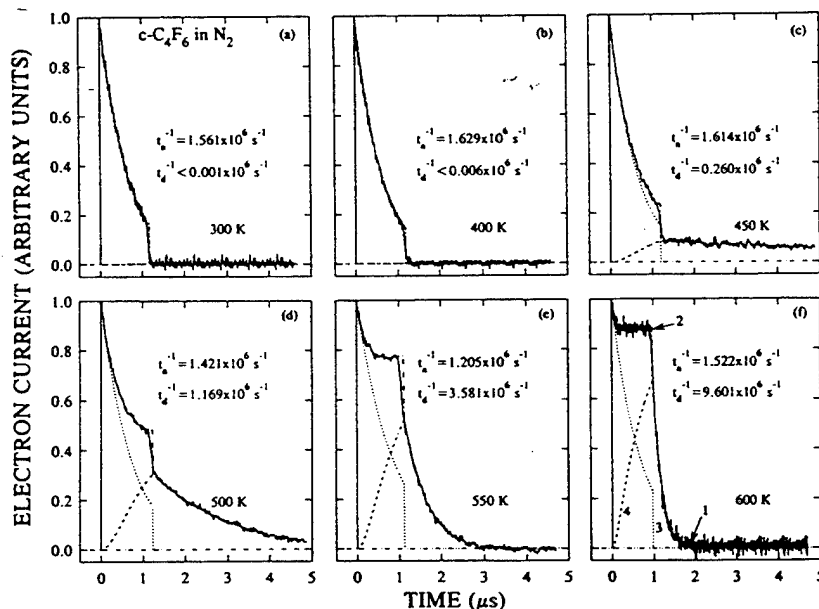
J. Chem. Phys., Vol. 99, No. 11, 1 December 1993

63

FIG. 3. Electron current wave forms for c-C$_4$F$_6$ in N$_2$ at $T=300$, 400, 450, 500, 550, and 600 K. All wave forms are for $E/N=1.24\times10^{-17}$ V cm^2, $N_T=6.44\times10^{19}$ molecules cm^{-3}, $N_a=6.44\times10^{13}$ molecules cm^{-3}. In the figure the solid curves [—; curve 1 in (f)] are the experimentally measured total electron currents as a function of time; the dash–dot (-·-) curves [curve 2; (f)] are the calculated electron current wave forms for the t_a^{-1} and t_d^{-1} values obtained from the fitting of Eq. (4) (see the text and the values of t_a^{-1} and t_d^{-1} given in the figure) to curves 1; the dotted (···) curves [curve 3; (f)] represent the contribution to the total electron current of the initial (prompt) electron swarm when only electron attachment occurs, and the broken (—) curves [curve 4; (f)] represent the contribution to the total electron current from the autodetached electrons.

liquid N$_2$ and dry ice temperatures (in the case of c-C$_4$F$_6$) to remove air and any other impurities not frozen at these temperatures.

The N$_2$ gas number density, N_T, was varied from 1.61 $\times10^{19}$ to 9.66$\times10^{19}$ molecules cm^{-3}, and the attaching gas number density, N_a, was varied from 1.93$\times10^{13}$ to 16.1$\times10^{13}$ molecules cm^{-3} for SF$_6$ and from 1.60$\times10^{13}$ to 64.4$\times10^{13}$ molecules cm^{-3} for c-C$_4$F$_6$.

III. RESULTS AND DISCUSSION

A. Electron attachment rate constant $k_a(\langle\epsilon\rangle,T)$ as a function of $\langle\epsilon\rangle$ and T

As mentioned in Sec. I, the electron energy distribution functions $f(\epsilon,\langle\epsilon\rangle,T)$ for N$_2$ are known under our experimental conditions and thus at each value of E/N and T employed, the mean electron energy $\langle\epsilon\rangle(E/N,T)$ can be determined. For a number of $\langle\epsilon\rangle$ values we determined (from wave forms such as those in Figs. 2 and 3) the $t_a^{-1}(\langle\epsilon\rangle,T)$ and $t_d^{-1}(\langle\epsilon\rangle,T)$ simultaneously via a nonlinear least squares fit procedure to Eq. (4). Once $t_a^{-1}(\langle\epsilon\rangle,T)$ was determined this way, the total electron attachment rate constant $k_a(\langle\epsilon\rangle,T)$ for SF$_6$ and c-C$_4$F$_6$ was calculated through the relationship $k_a=t_a^{-1}/N_a$ where N_a is the attaching gas number density.

In Fig. 4 is shown the $k_a(\langle\epsilon\rangle,T)$ for SF$_6$ as a function of the SF$_6$ gas number density for various mean electron energies and N$_2$ gas number densities; it is seen to be independent of the attaching gas number density N_a and the
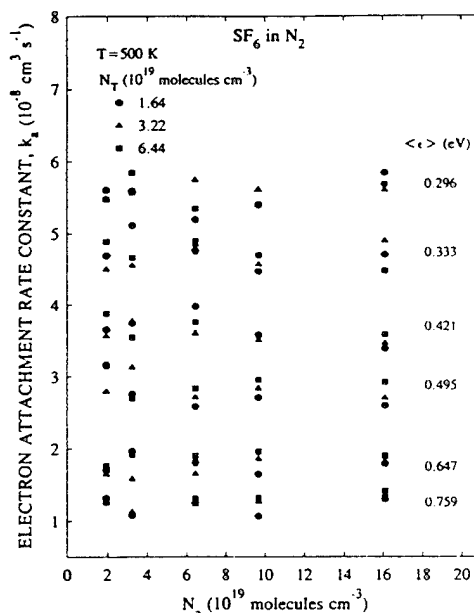
FIG. 4. Electron attachment rate constant k_a for SF$_6$ as a function of the attaching gas number density N_a for several values of the mean electron energy $\langle\epsilon\rangle$ and fixed values of T (500 K). $N_T=1.64\times10^{19}$ (●), 3.22 $\times10^{19}$ (▲), and 6.44$\times10^{19}$ (■) molecules cm^{-3}.
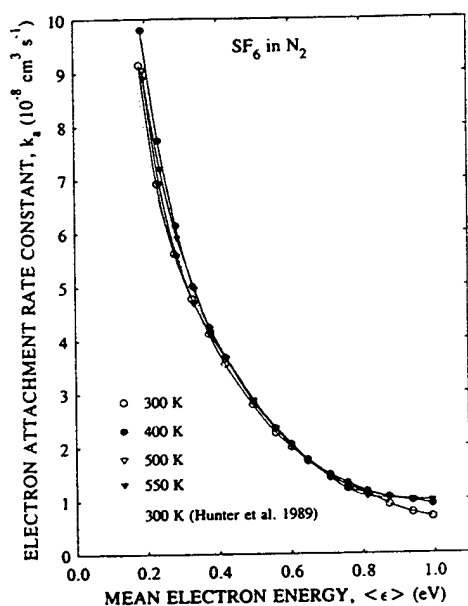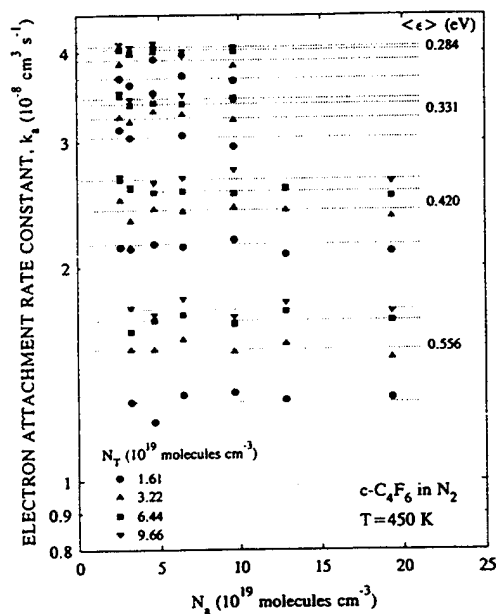
FIG. 5. Electron attachment rate constant k_a (for $N_a \rightarrow 0$) for SF_6 as a function of the mean electron energy, $\langle \epsilon \rangle$, and the total gas number density, N_T, at temperatures of 300 (O), 400 (●), 500 (∇), and 550 (▼) K. The broken curve is the electron attachment rate constant measured in Ref. 13.

FIG. 6. Electron attachment rate constant k_a for c-C_4F_6 as a function of the attaching gas number density N_a for several values of the mean electron energy $\langle \epsilon \rangle$ and a fixed value of T (450 K) and for $N_T = 1.61 \times 10^{19}$ (●), 3.22×10^{19} (▲), 6.44×10^{19} (■), and 9.66×10^{19} (▼) molecules cm^{-3}.

total gas number density N_T at all T studied, suggesting that for the N_T employed the parent SF_6^{-*} anions lose their excess energy (through collisions with N_2 molecules) and become "stabilized." In Fig. 5 the $k_a(\langle \epsilon \rangle, T)$ is plotted as a function of $\langle \epsilon \rangle$ for all the temperatures studied along with the $k_a(T = 300$ K$)$ taken from Ref. 13 for comparison. The $k_a(\langle \epsilon \rangle, T)$ exhibit a rather small dependence on T in the temperature range investigated.

Similarly, the $k_a(\langle \epsilon \rangle, T)$ for c-C_4F_6 was found to be independent of the attaching gas number density N_a at all T studied. However, the $k_a(\langle \epsilon \rangle, T)$ exhibited a small increase with increasing total gas number density, N_T, as can be seen from the data in Fig. 6. The increase in $k_a(\langle \epsilon \rangle, T)$ with increasing N_T is attributed to the collisional stabilization of the transient c-$C_4F_6^{-*}$ anions by N_2 gas molecules. From data such as in Fig. 6 the values of $\lim_{N_T \rightarrow \infty} k_a(\langle \epsilon \rangle, T)$ were determined (by plotting $1/k_a$ as a function of $1/N_T$ and extrapolating $1/N_T$ to 0) at 300, 400, 450, 500, and 600 K. These values of $k_a(\langle \epsilon \rangle, T)$ are plotted in Fig. 7 as a function of $\langle \epsilon \rangle$ for all the temperatures studied. The effect of T on $k_a(\langle \epsilon \rangle, T)$ is rather small for the T range investigated (Fig. 7).

B. Autodetachment frequency $t_d^{-1}(\langle \epsilon \rangle, T)$ as a function of $\langle \epsilon \rangle$ and T

Reaction (2) has been found to be rather insignificant for SF_6^- for $T \leqslant 550$ K. This is demonstrated by the data in Fig. 2 where the total electron current wave forms are shown for fixed N_a for different temperatures; there is no

contribution to the total electron current from delayed (autodetached) electrons. In Fig. 8 are shown the electron current wave forms at $T = 550$ K for SF_6 concentrations ranging from 3.22×10^{13} to 16.10×10^{13} molecules cm^{-3}.
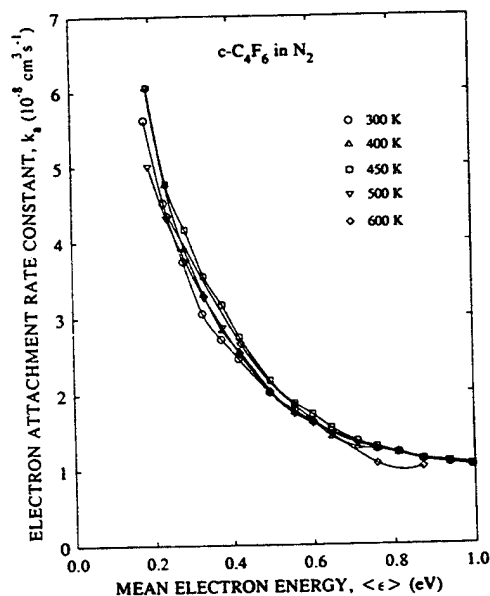

FIG. 7. Electron attachment rate constant k_a (for $N_a \rightarrow 0$ and $N_T \rightarrow \infty$) for c-C_4F_6 as a function of the mean electron energy, $\langle \epsilon \rangle$ at temperatures of 300 (O), 400 (△), 450 (□), 500 (∇), and 600 (◇) K.
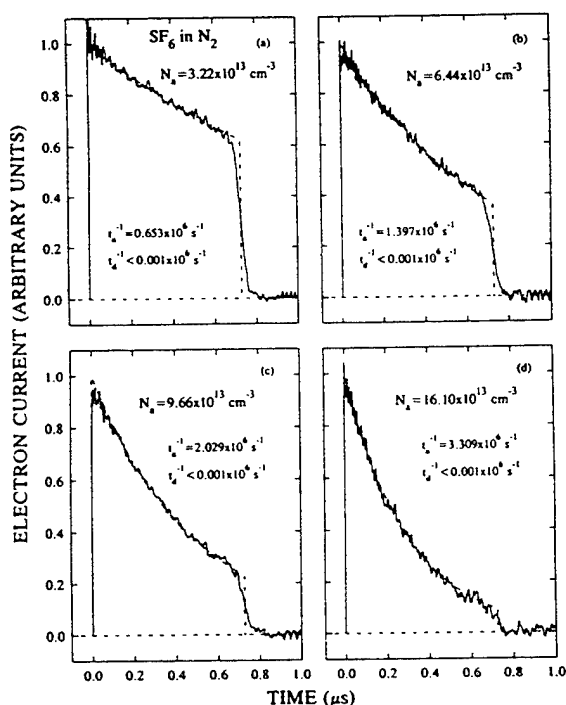
J. Chem. Phys., Vol. 99, No. 11, 1 December 1993

65

FIG. 8. Electron current wave forms for SF_6 in N_2 for N_a=3.22×10^{13}, 6.44×10^{13}, 9.66×10^{13}, and 16.1×10^{13} molecules cm^{-3}. The wave forms were measured at T=550 K, E/N=2.17×10^{-17} V cm^2, and N_T=6.44 ×10^{19} molecules cm^{-3}. In the figure the solid curves (—) are the experimentally measured total electron currents as a function of time; the dash–dot (-·-) curves are the calculated electron current wave forms for the t_a^{-1} and t_d^{-1} values obtained from a fit to Eq. (4) and listed in the figure (see the text).

FIG. 9. Autodetachment frequency $t_d^{-1}(\langle\epsilon\rangle,T)$ (for $N_T\to\infty$) for c-$C_4F_6^-$ as a function of the mean electron energy, $\langle\epsilon\rangle$ at 450 ($\triangledown$), 500 ($\blacktriangledown$), 550 ($\square$), and 600 ($\blacksquare$) K. (For T below 450 K the t_d^{-1} was too small to be detectable with the present technique.)

Even for the largest N_a employed there is still no noticeable contribution to the total electron current from delayed electrons. These measurements put an upper limit to t_d^{-1} for SF_6^-; t_d^{-1} is less than 10^3 s^{-1} at T=550 K.

In sharp contrast to the case of SF_6^-, electron detachment from the c-$C_4F_6^-$ is large and varies profoundly with T in the range investigated (300–600 K). The t_d^{-1} we determined for c-$C_4F_6^-$ is shown in Fig. 9 as a function of $\langle\epsilon\rangle$ for T=450, 500, 550, and 600 K; it increases sharply as T is raised from 450 to 600 K. The increase of t_d^{-1} with T is attributed to the increase in the internal energy of c-$C_4F_6^-$ (see the discussion later). Below 450 K the $t_d^{-1}(\langle\epsilon\rangle,T)$ is very small and only an upper limit can be placed on t_d^{-1} (see Fig. 3).

C. Variation of the k_a and t_d^{-1} for SF_6 and c-C_4F_6 with the internal energy $\langle\epsilon\rangle_{int}$ of the respective neutral and parent negative ion

Our findings clearly demonstrate that there is only a minor effect of the gas temperature on the rate constant for low-energy electron attachment to SF_6 and c-C_4F_6 molecules [reaction (1)]. However, the temperature influences profoundly the autodetachment reaction (2) for the case for the c-$C_4F_6^-$ ion. For the total (buffer) gas number densities used in our experiments, the parent negative ions

formed undergo a large number of collisions with the buffer gas molecules within the lifetime of the "isolated" M^{-*}. An estimate of such a collision time τ_c can be obtained assuming that the cross section for a collision between an anion and a buffer gas molecule is described by the classical Langevin expression.[41] This yields a collision time τ_c between a transient SF_6^{-*} or c-$C_4F_6^{-*}$ ion and a N_2 molecule of $\sim10^{-11}$ to $\sim10^{-10}$ s depending on N_T (actually τ_c is inversely proportional to N_T). This time is at least four orders of magnitude shorter than the lifetime of either of the isolated transient anions (SF_6^{-*} or c-$C_4F_6^{-*}$). We can then assume that the majority of the negative ions are themselves in their lowest vibrational/rotational energy state allowed at each temperature when the electron is thermally detached from the anion.

In an effort to gain a better understanding of the effect of T on k_a and t_d^{-1} we estimated, at each T employed, the vibrational energy of SF_6 and c-C_4F_6 in excess of the zero-point energy from

$$\langle\epsilon\rangle_{vib}(T)\approx\sum_{i=1}^{N}\frac{\hbar\omega_i}{e^{\hbar\omega_i/kT}-1} \tag{6}$$

using the vibrational frequencies found in the literature for SF_6 (Ref. 42) and c-C_4F_6 (Ref. 43). We, then, assumed that the total internal energy content $\langle\epsilon\rangle_{int}(T)$ for both the neutral molecule and the respective parent anion is given by this quantity. The $k_a(\langle\epsilon\rangle,\langle\epsilon\rangle_{int})$ exhibits a rather minor dependence on $\langle\epsilon\rangle_{int}$ for both molecules. In contrast, the $t_d^{-1}(\langle\epsilon\rangle,\langle\epsilon\rangle_{int})$ for c-$C_4F_6^-$ increases dramatically with increasing $\langle\epsilon\rangle_{int}$ (see Fig. 10); $t_d^{-1}(\langle\epsilon\rangle)$ increases by about four orders of magnitude when $\langle\epsilon\rangle_{int}$ increases from

66

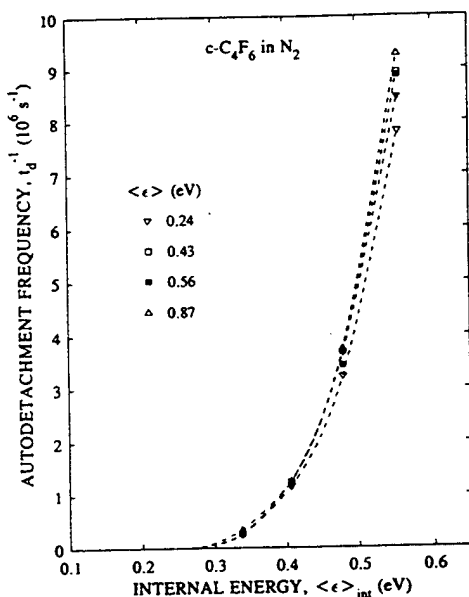FIG. 10. Autodetachment frequency, t_d^{-1} for c-$C_4F_6^-$ as a function of $\langle\epsilon\rangle_{int}$ for four values of the mean electron energy.
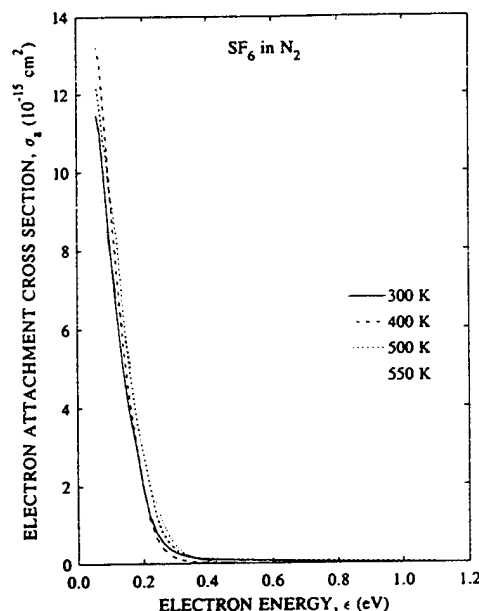

FIG. 12. Swarm unfolded total electron attachment cross section $\sigma_a(\epsilon,T)$ for SF_6 at 300, 400, 500, and 550 K.

$\sim$0.160 to $\sim$0.555 eV. The $t_d^{-1}(\langle\epsilon\rangle)$ for SF_6^- always remains below 10^3 s^{-1} even as $\langle\epsilon\rangle_{int}$ is increased from $\sim$0.074 to $\sim$0.294 eV.

If the electron detachment process (2) has an activa-

FIG. 11. Autodetachment frequency, t_d^{-1} for c-$C_4F_6^-$ as a function of $1/T$ for four values of the mean electron energy. In the figure are also given the values of E^* [Eq. (7)] obtained by a least squares fit to the data at each value of $\langle\epsilon\rangle$.

tion energy E^*, and if t_d^{-1} is related to the gas temperature T and E^* by

$$t_d^{-1} = t_{d\infty}^{-1} e^{-E^*/kT}, \tag{7}$$

where $t_{d\infty}^{-1}$ is the autodetachment frequency when $T\to\infty$, then an estimate of E^* can be obtained from a plot of $\ln(t_d^{-1})$ vs $1/T$. A plot of this nature is shown in Fig. 11 for the case of c-$C_4F_6^-$. From a linear least squares fit to the data in Fig. 11 using Eq. (7) we estimated E^* to be 0.237 eV; this value is independent of $\langle\epsilon\rangle$ (see Fig. 11) which suggests that indeed the majority of the negative ions are vibrationally/rotationally relaxed prior to electron detachment. If we take this value for E^* to represent an estimate of the electron affinity (EA) of c-C_4F_6 we can rationalize the absence of electron detachment from SF_6^- on the basis of the higher electron affinity of SF_6; reported values of EA(SF_6) range from $\sim$0.5 to $\sim$1.5 eV[44] with a recommended value of 1.05 eV.[45]

D. Swarm unfolded electron attachment cross section $\sigma_a(\epsilon,T)$ as a function of ϵ and T

The small number of attaching gas molecules (compared to N_2) used in the present study, does not change the electron energy distribution function $f(\epsilon,\langle\epsilon\rangle,T)$ of the electron swarm in N_2 which can be assumed to be the same for the SF_6/N_2 and c-C_4F_6/N_2 gas mixtures used in this study. We then, determined the total electron attachment cross section $\sigma_a(\epsilon,T)$ using an iterative electron swarm-unfolding technique[46] to unfold the total electron attachment rate constants $k_a(\langle\epsilon\rangle,T)$ we ascertained at different temperatures (Figs. 5 and 7).
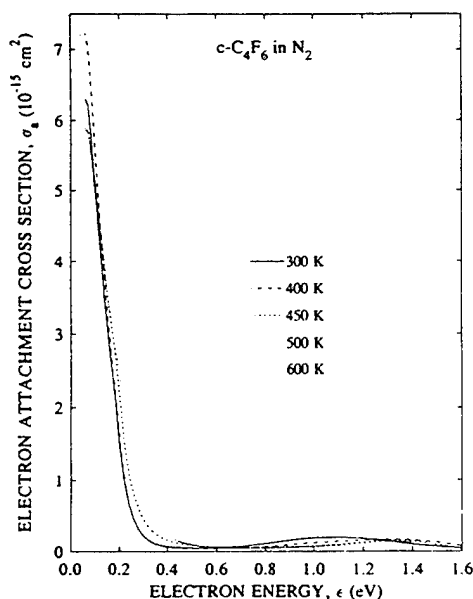
J. Chem. Phys., Vol. 99, No. 11, 1 December 1993

67

FIG. 13. Swarm unfolded total electron attachment cross section $\sigma_a(\epsilon,T)$ for c-C_4F_6 at 300, 400, 450, 500, and 600 K.

The swarm-unfolded $\sigma_a(\epsilon,T)$ for SF_6 and c-C_4F_6 are shown in Figs. 12 and 13, respectively, as a function of the incident electron energy ϵ and temperature T. The $\sigma_a(\epsilon,T)$ for both of these molecules exhibits a sharp increase as $\epsilon \to 0.0$ eV due to the parent anion formation.

E. Limiting electric field strength $(E/N)_{lim}$ as a function of E/N and T

In our study we were able to determine the limiting breakdown field strength, $(E/N)_{lim}$, for pure SF_6 as a function of gas temperature. We define the $(E/N)_{lim}$ as the maximum E/N value—at each temperature—for which the number of electrons reaching the anode is the same as the number of electrons initially ejected from the cathode into the gas medium. That is, the net gain (loss) of electronic charge during the drift of the electrons is zero and thus electrical breakdown is not possible. For the case of an electronegative gas (when no electron detachment processes are present) this represents the situation for which the electron attachment frequency equals the electron ionization frequency.

We determined the $(E/N)_{lim}$ for pure SF_6 (for which we observed no electron detachment under our experimental conditions) from the measured total current wave forms such as those in Fig. 14. In Fig. 14 the initial electron current is designated by I_1 and the total current at the end of the electron drift time is designated by I_2; I_2 is made up of two components, one due to ions (I_3) and another due to electrons (I_2-I_3). From a determination of I_1 and (I_2-I_3) we calculated the quantity $R=[(I_2-I_3)-I_1]/I_1$ and plotted it as a function of E/N. The E/N value for which $R=0$ determines the $(E/N)_{lim}$. In Fig. 15 we show the plot of R vs E/N for two temperatures (300 and 550 K). The lines through the experimental points are linear least squares fits to these points and the intersection of this line with the E/N axis is the $(E/N)_{lim}$ value for that temperature. The $(E/N)_{lim}$ values determined in this manner for 300, 400, 500, 550, and 600 K are plotted in Fig. 16.
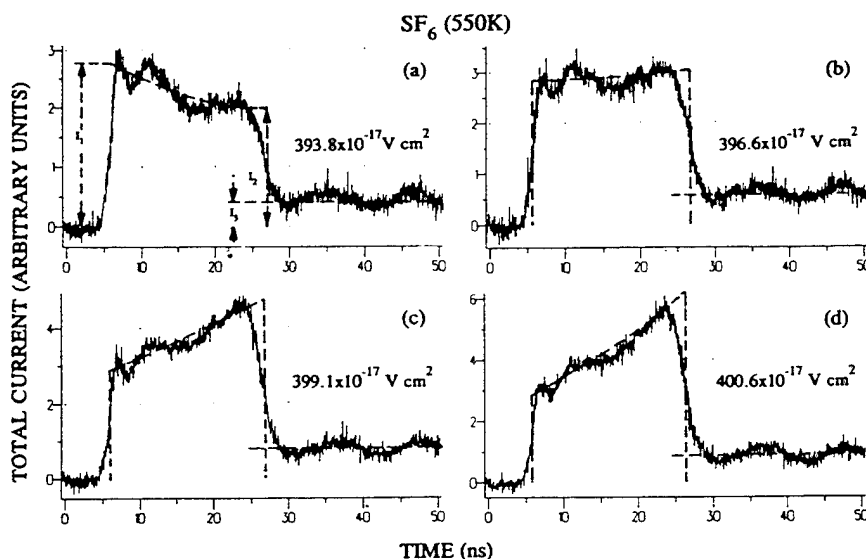
FIG. 14. Total current wave forms for pure SF_6 at four values of E/N around the $(E/N)_{lim}$ at fixed T (550 K) (see the text).
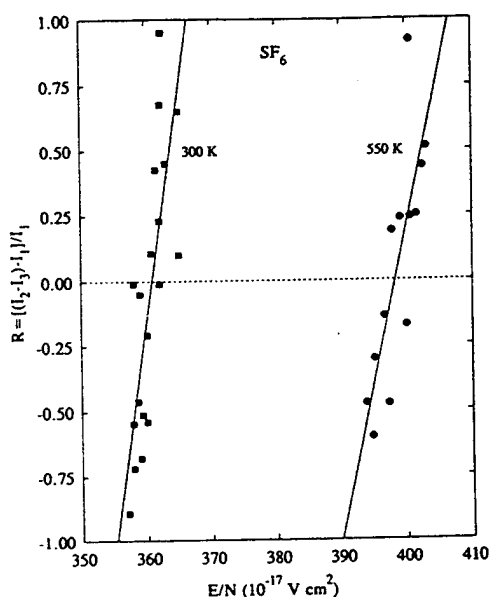
J. Chem. Phys., Vol. 99, No. 11, 1 December 1993

68

FIG. 15. The ratio $R = [(I_2-I_3) - I_1]/I_1$ for pure SF_6 as a function of E/N for 300 and 550 K (see the text).

ment to SF_6 with increasing T (which is the dominant electron attachment process at high E/N). The effect of the presence of an electron detachment process (autodetachment or collisional detachment) would tend to decrease the value of $(E/N)_{lim}$ for a fixed T since there would be more electrons ejected back into the medium released from the negative ions. In this investigation for all the temperatures studied and for E/N values up to $(E/N)_{lim}$ there was no evidence of electron detachment occurring in SF_6.

It is also interesting to note that for temperatures higher than 500 K we observed loss of SF_6 molecules from the chamber. This was probably due to some reaction[47] of SF_6 with the hot copper gaskets we used in the cell forming CuF_2. This problem was eliminated when we used gold plated copper gaskets to seal the cell.

ACKNOWLEDGMENTS

The room temperature value of $(E/N)_{lim}$ determined in this study agrees very well with that reported by other authors.[19] From Fig. 16 it can be seen that the $(E/N)_{lim}$ for SF_6 increases monotonically with increasing T. This we attribute to the increase in the dissociative electron attach-

[1] L. G. Christophorou and S. R. Hunter, in *Electron–Molecule Interactions and Their Applications*, edited by L. G. Christophorou (Academic, Orlando, 1984), Vol 2, Chap. 5.

[2] R. N. Compton, L. G. Christophorou, G. S. Hurst, and P. W. Reinhardt, J. Chem. Phys. 45, 4634 (1966).

[3] B. H. Mahan and C. E. Young, J. Chem. Phys. 44, 2192 (1966).

[4] F. C. Fehsenfeld, J. Chem. Phys. 53, 2000 (1970).

[5] D. Spence and G. J. Schulz, J. Chem. Phys. 58, 1800 (1973).

[6] L. G. Christophorou, D. L. McCorkle, and J. G. Carter, J. Chem. Phys. 54, 253 (1971); 57, 2228 (1972).

[7] K. M. Bansal and R. W. Fessenden, J. Chem. Phys. 59, 1760 (1973).

[8] L. E. Kline, D. K. Davies, C. L. Chen, and P. J. Chantry, J. Appl. Phys. 50, 6789 (1979).

[9] R. W. Crompton and G. N. Haddad, Aust. J. Phys. 36, 15 (1983).

[10] D. Smith, N. G. Adams, and E. Alge, J. Phys. B: At. Mol. Phys. 17, 461 (1984).

[11] Z. Lj Petrović and R. W. Crompton, J. Phys. B: At. Mol. Phys. 17, 2777 (1985).

[12] O. J. Orient and A. Chutjian, Phys. Rev. A 34, 1841 (1986).

[13] S. R. Hunter, J. G. Carter, and L. G. Christophorou, J. Chem. Phys. 90, 4879 (1989).

[14] L. G. Christophorou, D. L. McCorkle, and A. A. Christodoulides, in Ref. 1, Vol 1, Chap. 6.

[15] D. Klar, M. W. Ruf, and H. Hotop, Aust. J. Phys. 45, 263 (1992).

[16] A. A. Christodoulides, L. G. Christophorou, R. Y. Pai, and C. M. Tung, J. Chem. Phys. 70, 1156 (1979).

[17] W. W. Brandt and T. Honda, J. Appl. Phys. 60, 1505 (1986).

[18] S. Salimian, C. B. Cooper, R. Norton, and J. Bacon, Appl. Phys. Lett. 51, 1083 (1987).

[19] L. G. Christophorou and L. A. Pinnaduwage, IEEE Trans. Electr. Insul. 25, 55 (1990).

[20] W. F. Schmidt and R. J. Van Brunt, in *Gaseous Dielectrics III*, edited by L. G. Christophorou (Pergamon, New York, 1982), p. 561.

[21] F. Pinnekamp and N. Wiegart, in *Gaseous Dielectrics IV*, edited by L. G. Christophorou (Pergamon, New York, 1984), p. 91.

[22] N. Wiegart, IEEE Trans. Electr. Insul. 20, 587 (1985).

[23] J. K. Olthoff, R. J. Van Brunt, Y. Wang, R. L. Champion, and L. D. Doverspike, J. Chem. Phys. 91, 2261 (1989).

[24] W. T. Naff, C. D. Cooper, and R. N. Compton, J. Chem. Phys. 49, 2784 (1968).

[25] D. Edelson, J. Griffiths, and K. B. McAfee, Jr., J. Chem. Phys. 37, 917 (1962).

FIG. 16. Limiting electric field strength $(E/N)_{lim}$ values for SF_6 as a function of temperature. The dashed line through the experimental points is a linear least squares fit to the data.

J. Chem. Phys., Vol. 99, No. 11, 1 December 1993

69

[26] A. D. Appelhans and J. E. Delmore, J. Chem. Phys. **88**, 5561 (1988).

[27] L. G. Christophorou, Adv. Electron. Electron Phys. **46**, 55 (1978).

[28] B. Lehmann, Z. Naturforsch. Teil A **25**, 1755 (1970).

[29] M. Fenzlaff, R. Gerhard, and E. Illenberger, J. Chem. Phys. **88**, 149 (1988).

[30] I. Sauers, L. G. Christophorou, and J. G. Carter, J. Chem. Phys. **71**, 3016 (1979).

[31] C. L. Chen and P. J. Chantry, J. Chem. Phys. **71**, 3897 (1979).

[32] In contrast to these findings, another swarm study (Ref. 10) found that $(k_a)_{th}$ initially increases as T is raised from room temperature to 455 K and subsequently decreases as T is further raised to 590 K.

[33] P. G. Datskos, L. G. Christophorou, and J. G. Carter, J. Chem. Phys. **98**, 7875 (1993).

[34] L. G. H. Huxley and R. W. Crompton, *The Diffusion and Drift of Electrons in Gases* (Willey–Interscience, New York, 1974).

[35] S. R. Hunter and L. G. Christophorou, in Ref. 1. Vol 2, Chap. 3.

[36] A. V. Phelps and L. C. Pitchford, Phys. Rev. A **31**, 2932 (1985).

[37] L. Frommhold, Fortschr. Phys. **12**, 597 (1964).

[38] C. Wen, Ph.D. dissertation, Eindhoven University of Technology, The Netherlands, 1989.

[39] C. Wen and J. M. Wetzer, IEEE Trans. Electr. Insul. **23**, 999 (1988); **24**, 143 (1989).

[40] T. H. Teich, in *Gaseous Dielectrics VI*, edited by L. G. Christophorou and I. Sauers (Plenum, New York, 1991), p. 215.

[41] P. Langevin, Ann. Chim. Phys. **5**, 245 (1905).

[42] H. H. Glaassen, G. L. Goodman, J. H. Holloway, and H. Selig, J. Chem. Phys. **53**, 341 (1970).

[43] J. R. Nielsen, M. Z. El-Sabban, and M. Alpert, J. Chem. Phys. **23**, 324 (1955).

[44] L. G. Christophorou, D. L. McCorkle, and A. A. Christodoulides, in Ref. 1, Vol 2, Chap. 6.

[45] E. P. Grimsrud, S. Chowdhury, and P. Kebarle, J. Chem. Phys. **83**, 1059 (1985).

[46] L. G. Christophorou, D. L. McCorkle, and V. E. Anderson, J. Phys. B. At. Mol. Phys. **4**, 1163 (1971).

[47] See discussion at the end of: L. G. Christophorou, R. A. Mathis, S. R. Hunter, and J. G. Carter, in *Gaseous Dielectrics V*, edited by L. G. Christophorou and D. W. Bouldin (Pergamon, New York, 1988), p. 88.

70

5.4. Dependence of the Dielectric Strength of Gases on Temperature as a Result of the Variation with Temperature of their Electron Attachment and Detachment Properties

It has been shown by us earlier [J. Appl. Phys. 63, 52 (1988)] that the limiting uniform field breakdown strength $(E / N)_{lim}$ of electronegative gases which at low electron energies form parent negative ions decreases with increasing gas temperature and for molecules that capture electrons only dissociatively the $(E / N)_{lim}$ increases with increasing T. The decrease in $(E / N)_{lim}$ with increasing T is related to increases in the heat-activated electron detachment which is likely for dielectric gases which capture electrons forming parent anions, while the increase in the dielectric strength with increasing gas temperature follows the T-dependence of the dissociative electron attachment. In the present study, we have been able to determine the limiting electric field strength $(E / N)_{lim}$ in pure SF_6 as a function of T. We did this by locating the value of E/ N (at each temperature) at which the electron attachment coefficient equals the electron impact ionization coefficient. The so determined values of $(E / N)_{lim}$ are given in the preceding paper; they progressively increase from 362.7×10^{-17} V cm^2 at 300 K to a value of 411.5×10^{-17} Vcm^2 at 600 K, that is, an increase of about 14 %. For SF_6 electron attachment is only dissociative at high energies.

These results are fully discussed in the publication reproduced above and in the publications listed in Section 3

6. Electron Attachment to Electronically Excited Molecules

As we have seen in Section 5, electron attachment to molecules which are rotationally / vibrationally excited (thermally or via infrared-laser excitation) shows profound differences compared to the unexcited molecules. These differences depend on the amount of internal excitation and on the mode--dissociative or non-dissociative-- of electron attachment. Generally, increases in the ro-vibrational molecular energy increase the cross section for dissociative electron attachment. We have observed that even larger increases in the cross sections for dissociative electron attachment occur when the molecules are electronically excited. A review of this most interesting new knowledge has been undertaken and is given in Appendix A.

We continued the investigations of electron attachment to electronically excited long- and short-lived excited electronic states of molecules produced directly or indirectly by laser irradiation. These studies showed that the cross sections for dissociative electron attachment to electronically excited molecules usually are many orders of magnitude larger than those for the ground-state molecules. Under this contract we studied dissociative electron attachment to laser-irradiated hydrogen, silane, and methane.

6.1. Hydrogen

Our observation of enhanced H⁻ production in laser irradiated H was further documented by conducting additional photodetachment and ion mobility measurements and analyses. These new findings were integrated with our earlier study on hydrogen and along with their implications for negative ion and neutral beam technologies were described in a paper that has been published in the Journal of Applied Physics. This paper was given earlier (pages 10-18).

The verification of H⁻ production in ultraviolet-laser-irradiated hydrogen has interesting implications for negative ion and neutral beam sources, possible new electron attachment

72

mechanisms for hydrogen discharge sources, and lasing mechanisms of Al following

photoionization in the presence of hydrogen. This last application has been discussed in some

detail in a Physical Review article which is reproduced here also (pages 74-79).

Lasing in Al following photoionization and neutralization in the presence of H₂: The role of H⁻

John F. Kielkopf

Department of Physics, University of Louisville, Louisville, Kentucky 40292

Lal A. Pinnaduwage and Loucas G. Christophorou

Atomic, Molecular, and High Voltage Physics Group, Health Sciences Research Division,
Oak Ridge National Laboratory, Oak Ridge, Tennessee 37831-6122
and Department of Physics, University of Tennessee, Knoxville, Tennessee 37996
(Received 11 November 1993)

Atomic Al develops a population inversion and stimulated emission in the resonance lines when a solid target in a H₂ buffer gas is irradiated with ArF 1930-Å laser light. We present experimental evidence that the H⁻ ion is responsible for this effect, through charge-neutralizing collisions with Al⁺.

PACS number(s): 34.50.Gb, 34.50.Rk, 32.70.−n

I. INTRODUCTION

In the experiments of Kielkopf [1], an ArF 1930-Å excimer laser pulse was focused with a cylindrical lens on a solid Al target in the presence of H₂. Lasing in the $3s4s\ ^2S_{1/2}$-$3s3p\ ^2P_{3/2}$ (3692 Å) transition in Al was observed in the direction of the focal line, perpendicular to the ArF laser axis. Previously, Erlandson and Cool [2] had reported lasing in a segmented discharge in H₂ when it was irradiated by an ArF laser. Although the fundamental physical processes were probably the same in both experiments, the presence of a discharge for the experiments reported in Ref. [2] complicates the interpretation because there were sources of excitation, dissociation, and ionization other than the 1930 Å laser light; however, lasing in Al occurred only when the ArF pump laser light was present. Here we will concentrate on analyzing the observations of Ref. [1], report additional spectroscopic measurements, and describe the use of a photodetachment probe laser to study the importance of H⁻.

This negative ion was proposed in Ref. [1] as a possible agent for the excitation of Al, but at the time there was no direct evidence that H⁻ was present after the ArF excitation pulse passed through the H₂ buffer gas. This situation changed recently when Pinnaduwage and Christophorou observed efficient H⁻ formation in ArF laser irradiated H₂ [3], as shown by the results reproduced in Fig. 1. At high enough laser intensities almost all the electrons produced by means of ArF photoionization of H₂ are converted to H⁻ ions by attachment to concomitantly produced superexcited H₂, or some other attaching species produced by way of those superexcited states. It has been pointed out that Al itself is efficiently ionized by the ArF radiation [1]. In addition to the photoionization of the outer electron, there is a resonant inner-shell $3s3p$-$3p^2$ excitation followed by autoionization as illustrated in the energy level diagram of Fig. 2. In contrast to previous observations of population inversions in laser-produced plasmas referred to in Ref. [1], where the lower state of the transition was an excited state which depop-

ulated rapidly through radiative processes, in the present case the lower level was the ground state. The depopulation of the $3s3p$ ground state here was achieved because of efficient ionization of the Al ground state by the ArF laser. Based on these facts, we propose that the lasing $4s$ state of Al was produced by a neutralizing recombination
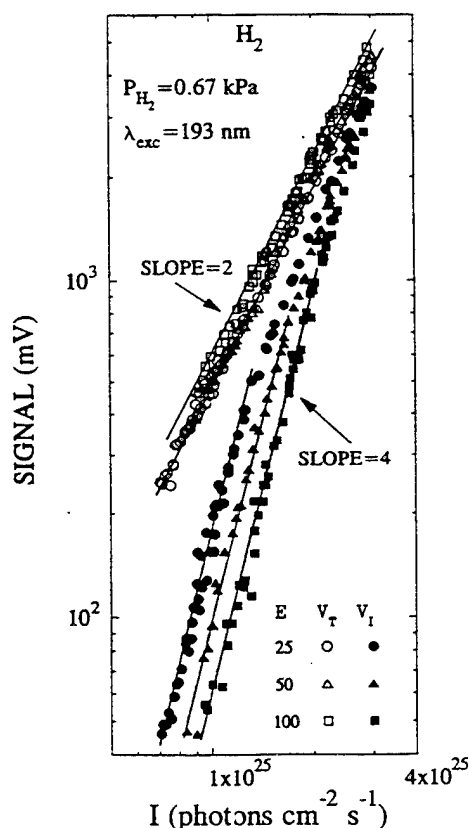

FIG. 1. Dependence of the measured total (V_T) and negative-ion (V_I) signals from H₂ on ArF excimer laser irradiance (I), as reported in Ref. [3]. Experimental parameters are indicated in the figure.
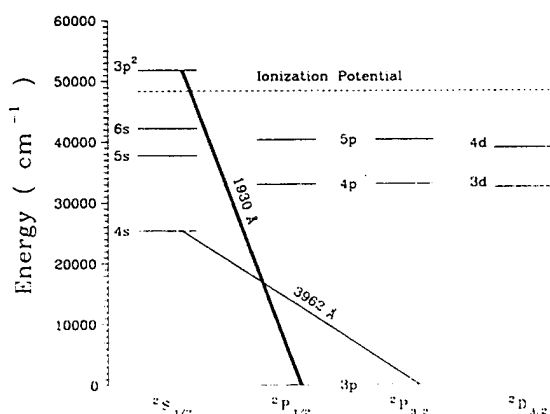
FIG. 2. Energy levels of neutral Al. An ArF laser at 1930 Å excites the autoionizing $3p^2$ $^2S_{1/2}$ level which produces a high concentration of Al^+. Stimulated emission is observed in the $4s$ $^2S_{1/2} - 3p$ $^2P_{3/2}$ component of the doublet due to a population inversion of the $4s$ state relative to the $3p$ ground state.

of H^- and Al^+.

The process which interests us, charge-neutralization collisions

$$Al^+ + H^- \rightarrow Al(4s) + H(1s) \tag{1}$$
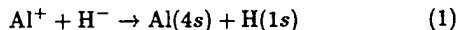
in a gas with an initially high population of Al^+ and H^- ions, would lead to a nonthermal population of neutral Al atoms in the excited $4s$ state. Figure 3 shows the low-lying atomic states, and the relevant neutral and ionic potential-energy curves. Although the cross section is not known, potential curves for the interaction of Al and H were reported recently in a full configuration-interaction benchmark calculation by Bauschlicher and Langhoff [4],
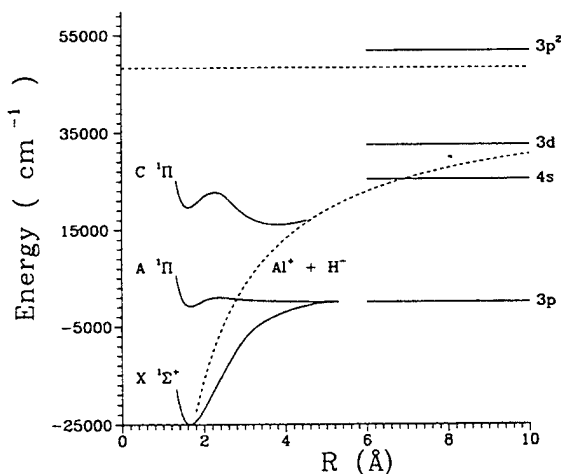
FIG. 3. Potential-energy curves for AlH from the calculations of Matos, Malmqvist, and Roos. The low-lying states are shown relative to the asymptotic atomic states. The C $^1\Pi$ state is ionic around 4 Å, where the ion pair $Al^+ + H^-$ and the neutral pair $Al(4s) + H(1s)$ asymptotes both contribute, but also has $4s$ atomic-state character.

and in a complete active space self-consistent field calculation by Matos, Malmqvist, and Roos [5]. Both calculations showed that the C $^1\Sigma$ state correlates with an Al atom in the $3s^2$ $4s$ state and a H atom in the $1s$ state around the inner minimum, but that the outer minimum is ionic. Therefore, through a crossing of the neutral and ionic potentials, $Al^+ + H^-$ may interact and yield the upper state of the lasing transition.

First, we briefly summarize the previous experiments [1]. An Al rod machined flat on one end was inserted into a vacuum chamber through a sliding O-ring seal. The axis of the rod was along the optical axis of the excimer laser. A 5-cm-diam positive cylindrical lens with a focal length of 10.3 cm focused the laser beam through a fused silica window on the vacuum chamber to a line on the end of the aluminum rod. The cylindrical focusing lens could be rotated about the optical axis of the excimer laser to make the focal line coincide with the optical axis of a scanning vacuum monochromator. The ArF pulse energy inside the vacuum chamber was estimated to be 400 ± 100 mJ.

The target was irradiated after the vacuum system was evacuated with a diffusion pump and backfilled with more than 200 torr of H_2. Within a few nanoseconds following the ArF pulse, an intense blue emission with speckle could be seen by looking through a viewport exactly along the focal line at the Al target. The Al laser beam divergence was quite small because a spot less than 7 mm in diameter showed on a fluorescent screen placed at the viewport. The spot had a well-defined boundary consistent with high gain along the focal line. Spectroscopic measurements showed that the stimulated emission originated in the $3s4s$ $^2S_{1/2}$ state, with gain only in the stronger 3962 Å transition of the doublet to $3s3p$ $^2P_{3/2}$. A search from 1150 Å to 5400 Å showed weak lines arising from $5s$ and $3d$ states, but no other Al I lines. While scattered 1930 Å excimer laser light was seen, lines of Al II, AlH, and H_2 were absent.

Those observations were based on spectra taken primarily along or close to the focal line axis. The absence of AlH and H_2 lines is crucial if alternative hypotheses for the excitation mechanism are to be eliminated. For these reasons we decided to reinvestigate the spectrum, concentrating on the emission 90° from the focal line axis, and making an effort to minimize ArF scattered light so as to increase the sensitivity of detection. Observations with N_2 and He buffer gases were also made to look for evidence of population inversion when H^- could not be present. Finally, as a test of the hypothesis that lasing was caused by charge-neutralization collisions of Al^+ with H^-, we studied the emission when H^- was removed by a second photodetaching laser.

II. NEW EXPERIMENTAL RESULTS

A. Spectra

The system was the same as that described in Ref. [1], with the addition of baffles to minimize scattered light, and a second monochromator to observe emission

perpendicular to the focal line. An iris diaphragm was added along the ArF laser axis inside the vacuum chamber about halfway between the cylindrical lens and the Al target. This diaphragm blocked a portion of the incident ArF beam that would not have illuminated the target, and minimized multiple reflections between the target and the entrance window. The target rod also was extended to trap the light which missed the rod so that it would not scatter back to the spectrometers. Emission along the focal line was directed exactly into a pair of electroformed baffles [6], and through them into a 0.2 m focal length, 4 Å resolution vacuum monochromator. The baffles limited considerably the contributions to the on-axis spectrometer from regions just in front of the Al target, so that that instrument detected only the highly directional emission responsible for the blue spot. Light emitted perpendicular to the focal line was collimated with a 2.5 cm focal length sapphire lens, and reflected to a matching lens that imaged the region on the entrance slit of another 0.25 m scanning monochromator. The light extending about 2 mm in front of the target was integrated in taking the spectra from this perpendicular view.

Part of the ArF incident pump light illuminated a sodium salicylate fluorescent screen, and the fluorescence was detected with a photodiode that triggered gated integrators to measure the signal from the monochromator photomultipliers at specific time delays following excitation. Signals from both instruments were recorded digitally under computer control.

Spectra of the lasing line region with H_2 buffer gas are in Figs. 4 and 5. Along the focal line of the ArF laser, as noted in Ref. [1], the transition at 3962 Å is very strong and the other doublet component is barely detectable. This is very clearly shown in Fig. 4. Without gain in the plasma the intensity ratio of these lines would be 2:1, but instead it is of the order of 50:1 or greater. Later,
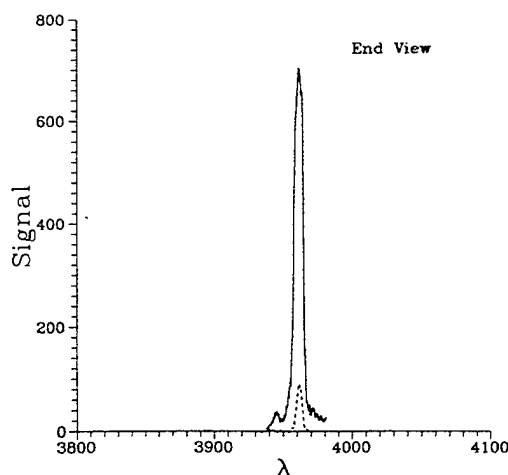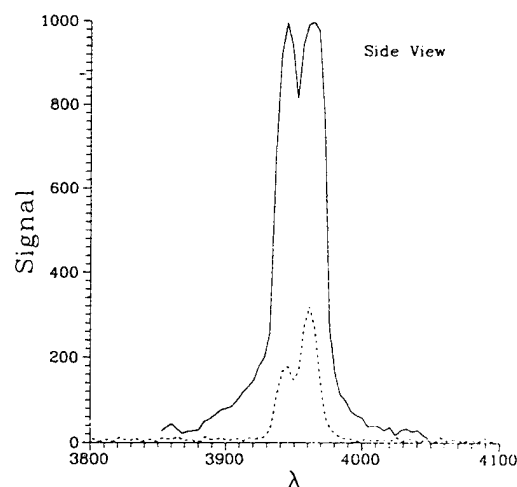

FIG. 5. The spectrum of the 4s-3p transition of Al in a H_2 buffer emitted perpendicular to the lasing axis. Spectra recorded when the 20 ns ArF laser was on (—), and 200 ns later (- - -), are both shown. The doublet intensity ratio of 1:1 during excitation means that the Al resonance line emission is optically thick. After 200 ns the ratio is the canonical 2:1 when the Al density is less. The signal is in arbitrary units. The wavelength is in Å.

with a delay of 200 ns, the Al is still lasing. This is a noteworthy result: lasing does not require the concurrent presence of ArF 1930 Å light, but results from a process that is started by the ArF laser and continues for some time afterward. This rules out photodissociation of AlH as a mechanism and supports our view that the inversion results from a neutralization pump involving H^-. The spectrum monitored perpendicular to the focal line is illustrated in Fig. 5. It shows emission that is optically thick in the resonance lines with an apparent intensity ratio of 1:1. After 200 ns the intensity ratio from the side is closer to 2:1, while the on-axis emission is still entirely in the one stronger doublet component.

Spectra were recorded in the visible and near ultraviolet with an EMI 9789Q uv-sensitive photomultiplier, and in the vacuum ultraviolet with an EMI type G solar blind photomultiplier which is insensitive to the Al laser light. Along the focal line of the ArF laser, only two spectral features were seen between 1150 Å and 6000 Å: the Al laser emission and scattered light from the ArF pump. Figure 6 shows a composite of scans covering these features. Neither other spontaneous Al lines nor emission from H_2 were detected along the axis. Because these measurements were made through the axial baffle which restricted the field of view, we conclude that emission from other excited states in Al occurs mostly in the space in front of the Al target. Since the $3d - 4p$ transition is strong in the spectra taken at 90°, but is not seen at 0° along the focal line axis, we conclude that the $3d$ state is not sufficiently populated to produce stimulated emission and gain.

Lasing in Al had been observed when H_2 was replaced with D_2, but not with He [1]. In the new experiments, no lasing was observed when H_2 was replaced by He or N_2. This latter observation helps to rule out electron recom-

FIG. 4. The spectrum of the 4s-3p transition of Al in a H_2 buffer emitted along the lasing axis. Spectra recorded during the 20 ns ArF laser was on (—), and 200 ns laser (- - -), are both shown. The $4s\,^2S_{1/2}$-$3p\,^2P_{3/2}$ component is far stronger because of stimulated emission and gain along the focal line. The signal is in arbitrary units. The wavelength is in Å.
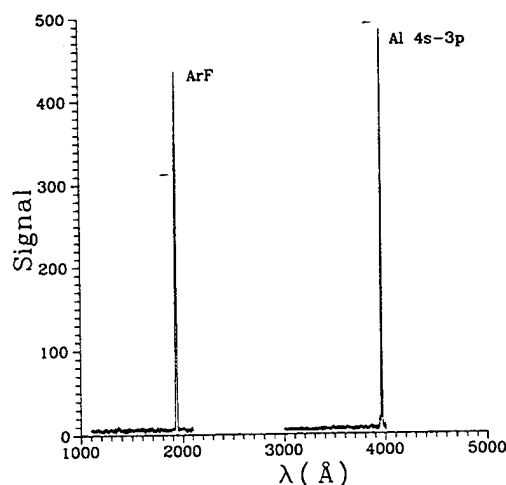
FIG. 6. The spectrum emitted along the ArF focal line from the vacuum ultraviolet through the blue. Only the scattered ArF pump light and the stimulated 4s-3p Al transition are detected. The signal is in arbitrary units

bination with Al^+ as a possible mechanism of populating the lasing neutral Al state, as discussed below. Side view spectra for H_2, N_2, and He buffer gases taken promptly following the ArF excitation are shown in Fig. 7. Lasing occurs only with H_2, but Al I emission is detected for all the gases. To eliminate the contributions from the ArF scattered light to these spectra, some of which are in the second order (at 2λ), we digitally subtracted the N_2 buffer gas spectra from the He and H_2 spectra, since N_2 produced the least Al emission, but an identical ArF background. The result for H_2 is shown in Fig. 8. The difference spectra allow the sensitive detection of several atomic lines of Al: all the transitions we observe terminate on $3p$ and originate in the $3d$, $4d$, $5d$, $4s$, $5s$, and
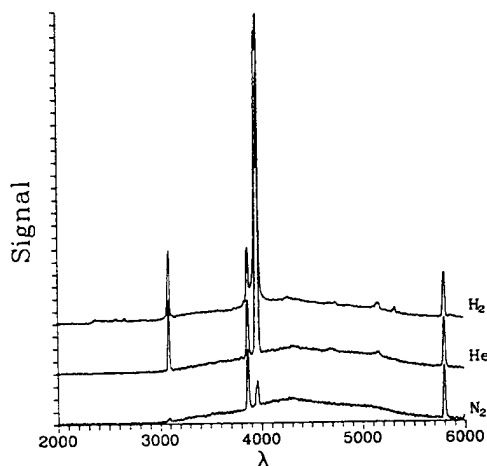
FIG. 7. Spectra perpendicular to the focal-line axis with H_2, He, and N_2 buffer gases. Lasing in Al occurs only for H_2. The underlying continuum and several of the lines originate in the ArF pump laser. The signal is in arbitrary units with spectra displaced vertically for clarity. The wavelength is in Å.
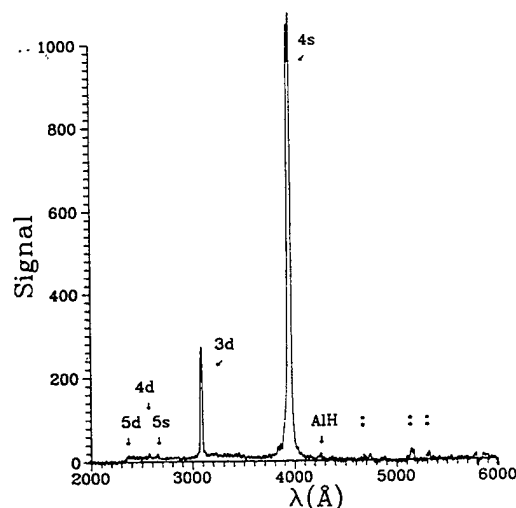
FIG. 8. The spectrum perpendicular to the lasing (focal-line) axis with a H_2 buffer after subtraction of the N_2 buffer spectrum to cancel scattered light from the ArF pump laser. Transitions from several excited states of neutral Al to the ground $3p$ are identified, as is the weak (0-0) band of AlH. Above 4500 Å the features which appear are in the second order at 2λ. The signal is in arbitrary units.

$6s$ excited states. Only the transitions from $4s$ and $3d$ are significant. The AlH molecular bands are largely, but not entirely, absent. The $A \rightarrow X$ (0 − 0) band of AlH is barely detectable in the region from 4245 to 4265 Å. The extreme weakness of the molecular emission, compared to emission from the atomic $3d$ state, which does not even invert, again demonstrates that the AlH molecule is not a factor in producing population inversion.

B. Photodetachment of H⁻

From an experimental point of view, one unfortunate aspect of a hypothesis that H^- is involved in a collisional process in a dense gas is that direct spectroscopic detection is not possible because it is a "dark" ion without a characteristic emission spectrum in a laboratory plasma. While the analysis and observations we have presented thus far demonstrate unquestionably that H^- is a good candidate, the proof depends on eliminating all other possibilities. However, we can test this hypothesis by removing the H^-, while other conditions remain constant, to see whether the stimulated emission disappears too. A convenient way to modulate the H^- concentration is to use a photodetachment reaction

$$H^- + h\nu \rightarrow H(1s) + e^- . \qquad (2)$$
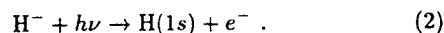
For wavelengths shorter than the threshold at 16 439 Å, the cross section for this process increases to a maximum of 4×10^{-17} cm^2 at 9620 Å [7,8]. The beam from a neodymium yttrium aluminum garnet (Nd:YAG) laser at 1064 nm is close to the optimum wavelength.

A Continuum Surelite II YAG laser produced 700 mJ at its fundamental wavelength. The 6-mm-diam beam

was directed into a KDP crystal to generate the second (green) harmonic, and 300 mJ of the residual infrared 1064 nm was separated by dichroic mirrors. A small fraction of the second harmonic was also present in the separated beam and provided a convenient tracer. The infrared beam was directed to an ultraviolet grade fluorescence-free fused quartz microscope slide inserted at 45° into the 1930 Å ArF excimer laser beam. Approximately 8% of the infrared reflected from the front and back faces of this beamsplitter and went along the ArF laser optical axis toward the 12.5 cm focal length cylindrical lens, which imaged both beams onto the Al target. The ultraviolet ArF beam was sharply focused onto the target to optimize lasing in the Al resonance line. The infrared YAG beam was therefore slightly defocused and broadly illuminated the region through which the ArF beam had passed.

Both lasers were controlled by a Stanford Model 535 Digital Delay Generator with relative triggering jitter of ± 10 ns, within the combined pulse widths of 20 ns at 1930 Å and 5 ns at 1064 nm. The 24 mJ infrared photodetaching pulse was delayed about 10 ns after the ultraviolet pump pulse. The self-collimated beam from the Al laser developed along the focal line axis, at 90° to the ArF laser beam axis, and exited the chamber through a fused silica window. About 40 cm from the window the spot size from this beam was 5 mm. It was observed visually on a fluorescent uranium glass filter in the path. The spatial overlap of the pump and photodetachment beams was optimized to make the two appear to strike the same place on the target, and fine adjustment was made to create the biggest decrease in Al lasing when the photodetachment beam was turned on.

A Hewlett Packard 5082-4220 photodiode with a 0.5-mm-diam sensitive area was inserted in the Al laser beam instead of the uranium glass screen. The small surface area insured that the diode sampled only the highly directional emission from the target. With its output buffered by an EG&G Ortec 575 amplifier, the response time constant of the detector was ≈ 1 μs, integrating over the entire Al lasing episode. The shaped pulse was sampled, averaged over 10 laser shots at 10 Hz, digitized, and recorded. A typical run record is shown in Fig. 9. The YAG beam was blocked and unblocked manually to produce the chopping shown in the figure. When the YAG beam was on, the Al lasing was completely eliminated. The residual signal was only scattered background light from the infrared YAG. When the YAG beam was off, the Al lasing was strong and stable, with some shot-to-shot variation at the high signal levels in the figure. From these observations it is apparent that 24 mJ of infrared YAG light is sufficient to completely quench the lasing process in the ArF irradiated Al/H_2 system.

III. CONCLUSIONS

The spectroscopic measurements, particularly the absence of prominent emission from AlH, the total absence of H_2 emission, and the continuation of lasing up to ≈ 200 ns when the ArF pump is off, suggest a secondary
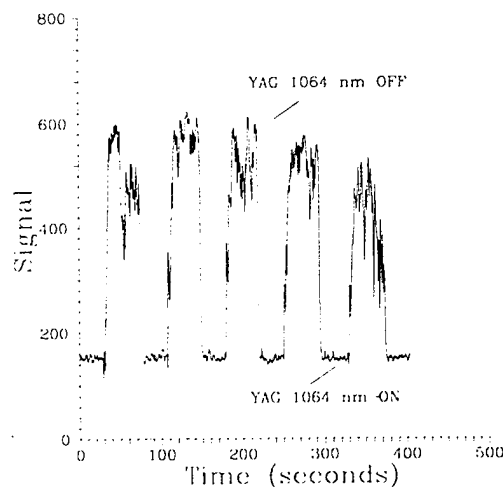

FIG. 9. The dependence of the total 3862 Å $4s\ ^2S_{1/2}$-$3p\ ^2P_{3/2}$ stimulated emission on a simultaneous 1064 nm YAG laser pulse. The 24 mJ YAG 1064 nm probe laser was focused colinearly with the ArF 1930Å excitation laser on the Al target. The signal shows that the stimulated Al laser emission along the focal line disappears whenever the H^- ion is photodetached by infrared illumination. The signal is in arbitrary units.

role for several previously proposed mechanisms for the production of the population inversion in the Al $4s$ state. Photodissociation of AlH, possibly produced by reactive collisions, cannot be important because the molecule is barely detectable, and because lasing continues for over 200 ns after the ArF pulse terminates. This agrees with the conclusions of Ref. [1] that efficient photoionization of Al, followed by recombination, aided in some way by H_2, is the likely mechanism for exciting Al to the $4s$ state. Two possible recombination partners were suggested in Ref. [1]: e^- or H^-. We consider these possibilities in turn.

The stimulated emission appears promptly, within a few nanoseconds, following the ArF pump pulse. This suggests that if recombination of Al^+ is the mechanism, it must be very fast. Radiative recombination with electrons is too slow. It is ruled out by the prompt Al lasing. Three-body recombination, where the third body is an electron, is negligible at electron densities less than 10^{21} cm^{-3}, which is the case here. Neutral stabilized three-body recombination, where the third body is an atom, has a room temperature three-body rate coefficient of the order of 10^{-27} cm^6 s^{-1} [9]. For molecular gases it can be orders of magnitude larger [10] due to the efficient removal of energy by densely spaced ro-vibrational levels. Depending on the nature of the buffer gas, the rate can be as large as 2.7×10^{-23} cm^6 s^{-1} for H_2O. The three-body rate coefficient for H_2 is not known. Therefore, even though the stimulated emission was not observed when H_2 was replaced by He, the possibility existed that neutral stabilized three-body recombination could be strong enough to account for the stimulated emission in the presence of H_2. As a test, in the new experiments, we looked for population inversion with a N_2 buffer gas. The ro-

vibrational levels of N_2 are more densely spaced than those in H_2, and the neutral stabilized electron recombination should be more efficient with N_2 than with H_2. Since we found that stimulated emission is absent with N_2, electron recombination can be ruled out. This new result, together with the new photodetachment experiment, firmly establishes H^- as the partner for Al^+ in the charge neutralization collisions leading to the lasing neutral state of Al.

Indeed, based on the work in Ref. [3], H^- formation in ArF irradiated H_2 is so efficient that there may not be enough free electrons to recombine with Al^+ even if the cross section is large. As can be seen in Fig. 1, at high enough ArF intensities almost all the electrons are converted to H^- ions. In the experiments, ≈ 400 mJ of ArF pulse energy was focused into an area of $\approx 10^{-4}$ cm^2. The corresponding irradiance was $\approx 10^{30}$ photons cm^2 s^{-1}. Since the ArF intensity in the experiments of Ref. [3] was much smaller, $\approx 10^{25}$ photons cm^2 s^{-1}, it is clear that here the conversion of free electrons to H^- ions would be complete. The electron attachment constant for ArF laser-irradiated H_2 is estimated to be $> 10^{-6}$ cm^{3}s^{-1} [3]. Electron attachment to high electronic excited states of H_2 produced by ArF irradiation is believed to be responsible for this efficient H^- formation [3].

The lowest vibrational level ($v = 0$) of the $^1\Sigma_g^+$ ground electronic state of H_2, which is exclusively populated at room temperature, attaches electrons only weakly; the maximum electron attachment rate constant is $\approx 10^{-14}$ cm^{3}s^{-1} [11]. Electron attachment to high vibrational states of $^1\Sigma_g^+$ can have rate constants of up to $\approx 10^{-8}$ cm^3 s^{-1} [12,13]. However, this possibility for H^- formation in ArF irradiated H_2 was ruled out in Ref. [3]. Since $(2 + 1)$-photon ionization of H_2 at the ArF laser line proceeds through a two-photon resonance with the E, F $^1\Sigma_g^+$ state, in principle it is possible that high vibrational states of $^1\Sigma_g^+$ are indirectly populated by the

E, F $^1\Sigma_g^+ \to B$ $^1\Sigma_u^+ \to X$ $^1\Sigma_g^+$ radiative transitions. The present experiments rule out a significant rate of formation of high vibrational states of $^1\Sigma_g^+$ by this process, since the Lyman band B $^1\Sigma_u^+ \to X$ $^1\Sigma_g^+$ emission in the vacuum ultraviolet is not observed. It would appear strongly in the 1600 Å region of Fig. 6.

In addition to the efficient formation of H^- ions at the ArF focal line, a large fraction of the laser ablated Al atoms will be photoionized to form Al^+ ions through the autoionization coincidence shown in the energy level diagram of Fig. 2. Most of these Al^+ ions must be recombining with H^- to achieve the population inversion of the upper $4s$ state with respect to the $3p$ ground state.

Finally, we note that Al laser emission with slightly lower intensity was observed when D_2 was substituted for H_2 [1]. This is consistent with the observation of D^- formation in ArF laser irradiated D_2 [14], which is qualitatively similar, but less efficient, compared to H^- formation in ArF laser irradiated H_2.

ACKNOWLEDGMENTS

[1] J. Kielkopf, J. Opt. Soc. Am. 8, 212 (1991).

[2] A. C. Erlandson and T. A. Cool, J. Appl. Phys. 56, 1325 (1984).

[3] L. A. Pinnaduwage and L. G. Christophorou, Phys. Rev. Lett. 70, 754 (1993).

[4] C. W. Bauschlicher, Jr. and S. R. Langhoff, J. Chem. Phys. 89, 2116 (1988).

[5] J. M. O. Matos, Per-Åke Malmqvist, and B. O. Roos, J. Chem. Phys. 86, 5032 (1987).

[6] J. E. Butler, Appl. Opt. 21, 3617 (1982).

[7] K. R. Lykke, K. K. Murray, and W. C. Lineberger, Phys. Rev. A 43, 6104 (1991).

[8] J. T. Broad and W. P. Reinhardt, Phys. Rev. A 14, 2159 (1976).

[9] Y. S. Cao and R. Johnsen, J. Chem. Phys. 94, 5443 (1991).

[10] J. M. Warmen, E. S. Sennhauser, and D. A. Armstrong, J. Chem. Phys. 70, 995 (1979).

[11] G. J. Schulz and R. K. Asundi, Phys. Rev. 158, 25 (1961).

[12] J. M. Wadehra, Phys. Rev. A 29, 106 (1984).

[13] A. P. Hickman, Phys. Rev. A 43, 3495 (1991).

[14] L. A. Pinnaduwage and L. G. Christophorou, J. Appl. Phys. (to be published).

6.2. Silane

We have observed enhanced electron attachment to ArF-excimer-laser-irradiated silane The experimental measurements are consistent with highly-excited states of silane or its photofragments (produced directly or indirectly via laser irradiation) are responsible for the observed electron attachment. Since such excited states may be populated in silane plasmas, these findings may explain the recently reported large negative ion densities in silane plasmas. These basic measurements are discussed in a paper published in Applied Physics Letters. In this paper the implications of these findings for silane plasmas are elaborated upon, also. The paper is reproduced below (pages 81-83).

Enhanced negative ion formation in ultraviolet-laser irradiated silane: Implications for plasma deposition of amorphous silicon

Lal A. Pinnaduwage, Madhavi Z. Martin, and Loucas G. Christophorou

Atomic, Molecular, and High Voltage Physics Group, Oak Ridge National Laboratory, Oak Ridge, Tennessee 37831-6122 and Department of Physics, University of Tennessee, Knoxville, Tennessee 37996

Observation of enhanced electron attachment to ArF-excimer-laser irradiated silane is reported. Evidence is presented that highly excited electronic states of silane or its photofragments are responsible for the observed enhanced electron attachment. Since such electronically excited states may be produced in silane plasmas (by direct electron impact or by excitation transfer via metastable states of rare gases that are commonly used in silane discharges), the possible significance of this electron attachment process for negative ion formation in silane plasmas is indicated. © *1994 American Institute of Physics.*

Large concentrations of negative ions have been shown (see Ref. 1, and references therein) to exist in radio frequency (rf) glow discharges of silane (SiH_4) and its mixtures used for plasma deposition. Electron attachment measurements on the ground electronic state of silane conducted under low-pressure, single-collision conditions,[2] show that the maximum electron attachment cross section is in the range of 10^{-19} to 10^{-18} cm^2 occurring at electron energies of ~8 eV. A high-pressure (~1 kPa) electron swarm experiment[3] with pure silane also confirmed weak electron attachment to silane in its ground electronic state.

At the first glance it may appear that large negative ion densities that exist in continuous silane discharges may be due to accumulation over long times, especially since it has been established that negative ions are confined to the center of the discharge by the plasma sheath. However, direct electron density measurements inside the discharge volume[4] show that the electrons are lost rapidly via attachment.

It is, therefore, quite likely that an additional, more efficient, electron attachment process occurs in silane rf plasmas. Based on our observation of enhanced negative ion formation in ArF-excimer-laser irradiated silane described below, we point out that electron attachment to electronically excited silane and/or its excited fragments produced in a rf discharge may be a significant channel for negative ion formation in silane discharges.

The technique and the apparatus used in the present experiments have been described earlier.[5] Briefly, the gas under study is irradiated with a laser pulse which produces electrons via multiphoton ionization; some of these electrons are converted to negative ions via attachment. The negative ions and the unattached electrons are separated from positive ions resulting from photoionization using a three-electrode configuration:[5] The laser pulse propagates between two of the three electrodes and the negative or positive charges produced in the interaction region are extracted to the adjoining detection region through a grid in the middle electrode by applying appropriately oriented electric fields in the two regions. In the "negative mode," signal components due to the unattached electrons and negative ions can be distinguished since they travel with different drift velocities; a "break" in the signal wave form is easily seen (see Fig. 1) when the total pressure in the chamber exceeds ~0.1 kPa.

In the present experiments, silane (ionization threshold ~11.0 eV, Ref. 6) was irradiated with an ArF-excimer-laser (wavelength=193 nm, photon energy=6.4 eV). In order to keep the total pressure above 0.1 kPa, a 3.2% silane/nitrogen gas mixture (ultrahigh purity from Matheson Gas Products) was used. At the ArF laser intensities employed, N_2 (electronic excitation threshold ~8.4 eV,[7] ionization threshold ~15.8 eV, Ref. 7) did not absorb laser radiation.

Typical signal wave forms at three laser intensities, I, are shown in Fig. 1. At low I [Fig. 1(a)], no appreciable negative ion signal exists; this clearly shows electron attachment to ground state silane during the electron drift was negligible. However, as I is increased, higher fractions of photoelectrons are converted to negative ions [Figs. 1(b) and 1(c)] due to the increase in the number density of the excited species.

The dependence of the total signal, V_T, and the negative ion signal, V_I, on I is shown in a log–log plot in Fig. 2. The V_T is the sum of V_I and V_E, the signal due to unattached electrons (also see Fig. 1). It must be noted that V_T should be proportional to the number density of electrons initially produced via laser photoionization, and some of them are attached to excited species produced by the same laser pulse.

From Fig. 2, it is seen that V_T increases as I^2 (up to ~4×10^{24} photons cm^{-2} s^{-1}) indicating two-photon ionization of silane as expected. At large I (>4×10^{24} photons cm^{-2} s^{-1} for the data of Fig. 2), the slope of the $V_T(I)$ curve deviates from the quadratic dependence. This is due to the incomplete collection of charges due to space-charge effects.[5] As in Ref. 5, corrections for space-charge effects on V_T and V_I were carried out by forcing the total signal to follow the quadratic dependence (broken line in Fig. 2), and then calculating the "normalized" ion signal assuming fractional transmission through the grid to be the same for negative ions and electrons.[5]

It is seen from Fig. 2 that the measured (up to I~4×10^{24} photons cm^{-2} s^{-1}) and "normalized" V_I vary as I^4. This is consistent with negative ion formation via attachment of an electron produced via two-photon ionization to an excited molecule produced via two-photon excitation, viz.
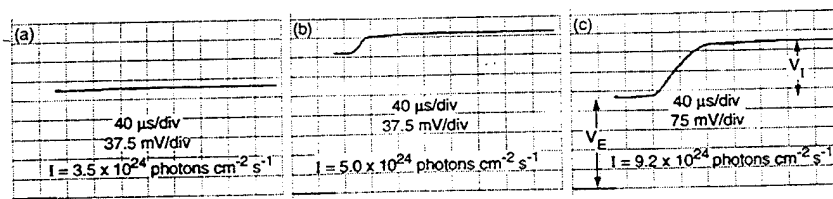
81

FIG. 1. Typical signal wave forms taken at different laser intensities. The signals due to unattached electrons, V_E, were too fast to be digitized at the time scales shown, and, therefore, appear as vertical lines. The partial pressures of silane and nitrogen were 21.3 Pa with 0.67 kPa, respectively, and the applied electric field was 25 V cm^{-1}. A laser intensity value of 10^{24} photons cm^{-2} s^{-2} corresponds to a fluence of $\sim$10.2 mJ cm^{-2}.

$$2h\nu + SiH_4 \rightarrow SiH_4^+ + e, \tag{1}$$

$$2h\nu + SiH_4 \rightarrow SiH_4^{**}, \tag{2}$$

$$e + SiH_4^{**} \text{ (or } X) \rightarrow \text{negative ion} + \text{neutral radical.} \tag{3}$$

SiH_4^{**} indicates an excited state of silane lying above its ionization threshold called a superexcited state (SES),[5] and X denotes a possible electron attaching excited species produced indirectly via SES, (see below). The identities and the relative abundances of negative ions produced are not known; however, SiH_3^-, SiH_2^-, SiH^-, Si^-, and H^- are likely candidates.[2]

Measurements conducted at different pressures, P, of silane (with other parameters kept constant) showed that $V_T \propto P$ and $V_I \propto P^2$. The linear dependence of V_T on P is

consistent with initial electron production via photoionization of silane. The quadratic dependence of V_I on P confirms that for each negative ion two silane molecules are needed, one to produce the attaching electron and the second to produce the excited molecule.

It is possible that the electron attaching species is not a SES of silane but either a comparatively low-lying electronic state of silane populated indirectly (via internal conversion or collisions), or an electronically excited fragment of silane populated via dissociation of SES. Electron attachment to ground state radicals can be ruled out since we did not observe an enhancement in negative ion formation with repetitive pulsing of the laser (at 10-ms time delay). Negative ion formation processes via an ion-pair process involving the SES can also be ruled out since this should yield $V_I \propto I^2 P$ instead of the observed dependence, $V_I \propto I^4 P^2$.

Electronically excited silane or its excited fragments can be produced via electron impact in silane discharges. In the case of silane/rare gas mixtures commonly used in deposition discharges, energy transfer from metastable states of the rare gases will enhance those excited state populations; it was recently shown[8] that the metastable state number density in an argon discharge decreased by more than an order of magnitude when 4% silane was added to the discharge. Electron attachment to excited states populated in discharges may in fact be of common occurrence; we have pointed out the possibility of a similar mechanism for H^- formation in H_2 discharges.[9]

Negative ions have been shown (see Refs. 1, 10, and 11, and references therein) to be the likely precursors of particulate formation in gas discharges; also, there are some indications[10-12] that negative ions may be involved in film deposition. In the present experiments, the negative ion signal decreased rapidly when the applied electric field in the interaction region was increased (as explained in Ref. 5, this could be due to the field-induced electron detachment from the transient parent negative ion). This effect may be observable in rf discharges as well, for example, by applying a static electric field superimposed on the rf field; if so, this may lead to a better control of film quality and/or deposition rate in silane discharges.
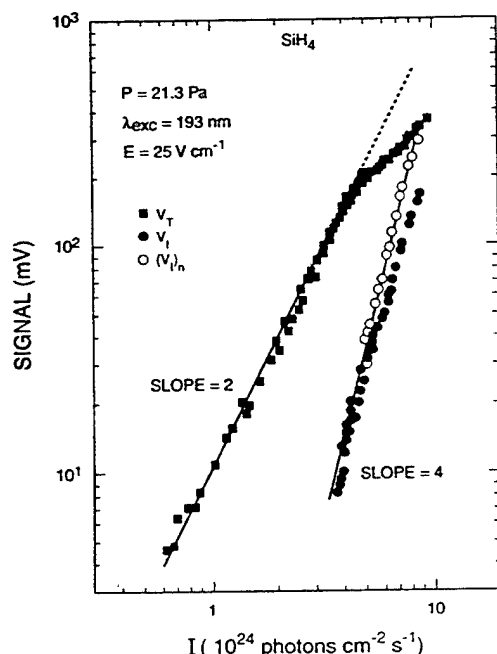
FIG. 2. Laser intensity I, dependence of the measured total V_T, and negative ion V_I, and normalized negative ion $(V_I)_n$ signals for the experimental parameters indicated in the figure; nitrogen pressure was 0.67 kPa.

Pinnaduwage, Martin, and Christophorou

82

[1] A. A. Howling, L. Sansonnens, J. L. Dorier, and Ch. Hollenstein, J. Appl. Phys. **75**, 1340 (1994). –

[2] S. K. Srivastava, E. Krishnakumar, and A. C. de A. e Souza, Int. J. Mass Spectrom. Ion Processes **107**, 83 (1991), and references therein.

[3] M. Shimozuma and H. Tagashira, J. Phys. D **19**, L179 (1986).

[4] C. B. Fledderman, J. H. Beberman, and J. T. Verdeyen, J. Appl. Phys. **58**, 1344 (1985); J. T. Verdeyen, J. H. Beberman, and L. J. Overzet, J. Vac. Sci. Technol. A **8**, 1851 (1990); M. Shiratani, T. Fukuzawa, K. Eto, and Y. Watanabe, Jpn. J. Appl. Phys. **31**, L1791 (1992).

[5] L. A. Pinnaduwage, L. G. Christophorou, and A. P. Bitouni, J. Chem. Phys. **95**, 274 (1991).

[6] J. Berkowitz, J. P. Green, H. Cho, and B. Ruščić, J. Chem. Phys. **86**, 1235 (1987).

[7] S. Opitz, D. Proch, T. Trickl, and K. L. Kompa, Chem. Phys. **143**, 305 (1990).

[8] L. Sansonnens, A. A. Howling, Ch. Hollenstein, J.-L. Dorier, and U. Kroll, J. Phys. D **27**, 1406 (1994).

[9] L. A. Pinnaduwage and L. G. Christophorou, J. Appl. Phys. **76**, 46 (1994).

[10] A. Garscadden, in *Nonequilibrium Processes in Partially Ionized Gases*, edited by M. Capitelli and J. N. Bardsley (Plenum, New York, 1990), p. 541.

[11] A. Lloret, E. Bertran, J. L. Andujar, A. Canillas, and J. L. Morenza, J. Appl. Phys. **69**, 632 (1991).

[12] L. J. Overzet and J. T. Verdeyen, Appl. Phys. Lett. **48**, 695 (1986).

Appl. Phys. Lett., Vol. 65, No. 20, 14 November 1994

83

Pinnaduwage, Martin, and Christophorou   2573

6.3. Methane

We have directed our studies of electron attachment to electronically excited states of molecules to the case of methane in view of its usage in many applications including plasma deposition of carbon films. We have observed enhanced electron attachment to ArF-excimer-laser irradiated methane. Preliminary evidence has been obtained indicating that laser-excited superexcited states of methane (or other excited states to which these convert) are responsible for the observed enhanced attachment, and that predominantly H^- ions are produced via this process. These findings and their possible significance for plasma processing discharges using methane or its mixtures have been outlined in a paper that has just been accepted for publication in Contributions to Plasma Physics (pages 84-96).

Enhanced Negative Ion Formation in ArF-Laser-Irradiated Methane:
Possible Implications for Plasma Processing Discharges

Lal A. Pinnaduwage[1,2], Madhavi Z. Martin[1,2], and Loucas G. Christophorou[2,3]

[1]Health Sciences Research Division, Oak Ridge National Laboratory, P. O. Box 2008, Oak Ridge, TN 37831-6122
[2]Department of Physics, University of Tennessee, Knoxville, TN 37996
[3]National Institute of Standards and Technology, Gaithersburg, MD 20899

Abstract

Observation of enhanced electron attachment to ArF-excimer-laser irradiated methane is reported. Preliminary evidence is presented that laser-excited superexcited states of CH_4 (or other excited states to which these convert) are responsible for the observed enhanced electron attachment, and, that predominantly H^- ions are produced via this process. The possible significance of this process for plasma processing discharges using CH_4 and its mixtures is indicated.

I. INTRODUCTION

Methane has recently received much attention due to its usage in plasma deposition of carbon films (refs. 1, 2, 3, and references therein) and in diffuse discharge switches (refs. 3, 4, and references therein). The mechanism(s) involved for carbon deposition in methane discharges is still far from being clear [1,3], even though methane is one of the few gases used in plasma processing that have reasonably complete sets of electron collision data [2,5].

The presence of high concentrations of negative ions in processing discharges and their effects in such discharges have attracted attention of basic and applied researchers only recently (see the references in [6]). In this paper, we wish to point out the possible importance of electron attachment to electronically-excited states of methane in plasma processing discharges of methane and its mixtures. Electron attachment to methane in its ground electronic state is extremely weak [2,7], having a maximum cross section of $\sim 10^{-19}$ cm^2 [7] around 10 eV electron energy. Therefore, the large number densities of negative ions that have been recently observed [8] in a CH$_4$/Ar discharge could be due to enhanced electron attachment to highly-excited states of CH$_4$ produced in the discharge. Such an efficient dissociative attachment process will not only produce large numbers of negative ions but also complementary radicals.

II. EXPERIMENTAL

The experimental technique and the apparatus have been described in detail earlier [9], and will be outlined briefly here: The experiments were conducted in an electron swarm apparatus at room temperature and at pressures of 4-40 kPa. However, unlike in conventional electron swarm experiments where electron attachment occurred during the drift of the electrons, in these

experiments electron attachment to laser-excited molecules occurred within the duration of the laser pulse ($\sim 10^{-8}$ s), see below and Ref. 9. In the experiments reported here, a single laser pulse excited, by two-photon absorption, the CH_4 molecules to an energy above the ionization threshold; this process resulted in photoionization of CH_4 and the in the formation of superexcited states (SES); the SES are electronically excited states of a molecule lying above the ionization threshold [9], and are expected to have short lifetimes of $\leq 10^{-9}$ s. The electrons resulted from photoionization of CH_4 attached to the concomittantly produced SES or other excited states to which SES internally converted.

The negative ions and the unattached electrons were separated from the positive ions (which resulted from photoionization), using a three-electrode configuration [9]: The laser pulse propagated between two of the three electrodes and the negative or positive charges produced in the interaction region were extracted to the adjoining detection region through a grid in the middle electrode by appropriately directed electric fields in the two regions. In the present experiments, the gap in the interaction region was 1 cm; the "thickness" of the laser beam was ~ 0.1 cm and the distance from the closest edge of the laser beam to the grid in the middle electrode was ~ 0.1 cm; the gap in the detection region was 0.67 cm. The same electric field values were maintained in the interaction and detection regions. In the "negative mode," where negatively charged particles were monitored, signal components due to the unattached electrons and negative ions could be distinguished since they travelled with different drift velocities; a "break" in the signal wave form was easily seen (see Fig. 1) when the total pressure in the chamber exceeded ~ 1 kPa.

In the present experiments, methane (ionization threshold ≤ 12.6 eV [10]) was irradiated with the ArF line (wavelength = 193 nm, photon energy = 6.4 eV) from Lambda Physik Lextra 50 excimer

laser (pulse duration ~ 10 ns (FWHM)). The energy of the lowest-excited singlet state of CH_4 is at ~ 8.5 eV [11], and thus a non-resonant, two-photon absorption process led to the excitation of CH_4 above its ionization threshold. A uniform cross section of the laser output was reduced in cross sectional area by a telescopic arrangement using two lenses of focal lengths 45 and 10 cm; over the length of the interaction region (~ 9 cm), the beam cross section was ~ 0.07 cm^2. A fraction of the laser energy was monitored using a beam splitter; the monitored energy was precalibrated against the pulse energy in the interaction region. The signal wave forms were recorded with a Tektronix DG450 digitizer. Methane of quoted purity of 99.995% from Matheson Chemical Company was used in most experiments; two other samples of CH_4 of 99.995% and 99.95% purity levels were shown to yield consistent results.

Typical signal wave forms for pure CH_4 at a pressure of 20 kPa are shown in Fig. 1(a) and Fig. 1(b). It must be noted that the electrons produced via laser photoionization (over a thin strip of ~ 0.1 cm width) propagated as an electron swarm to the detection region; however, electron attachment to laser-excited molecules occurred only within the laser-irradiated region immediately following the laser pulse. At low laser intensities, excited state population was small and no significant negative ion formation occurred as shown in Fig. 1(a). It is also clear from Fig. 1(a) that electron attachment to ground state CH_4 during the drift of electrons in the interaction and detection regions was negligible, consistent with previous electron attachment measurements an ground state CH_4 [2,7].
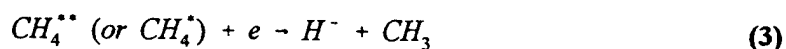
However, when the laser intensity was increased, significant negative ion signal appeared, as shown in Fig. 1(b). Since the E/N values (E is the applied electric field and N is the gas number density) was the same (~ 5 x 10^{-18} V cm^2) for Fig. 1(a) and Fig. 1(b), the negative ion signal in Fig. 1(b) was entirely due to electron attachment to excited states produced by the laser pulse. Since the

electrons moved out of the laser irradiated region (width ~ 0.1 cm) within ~ 5×10^{-8} s, electron attachment to excited molecules must have occurred during that time. This provides an upper bound for the electron attachment time; in fact, since we observed negative ion formation at an E/N value of ~ 2×10^{-17} V cm^2, where the drift velocity of electrons is ~ 1×10^7 cm s^{-1}, the electron attachment time must be < 10^{-8} s. Therefore, this is an extremely efficient electron attachment process, similar to electron attachment to SES of other molecules we have studied [6,9,12]. It is emphasized that the electrons that did not attach during this time would to exposed only to unexcited, ground state CH_4 molecules during their drift in the unirradiated regions, and thus will not contribute significantly to negative ion formation (this is evident from Fig. 1(a)).

In previous studies [12,13] we had shown that ArF-excimer-laser irradiated H_2 yielded large amounts of H$^-$ ions. In order to check the identity of the negative ions produced in ArF-laser-irradiated methane in the present high-pressure study, we conducted the following experiment: A small amount of H_2 (0.48 kPa) was added to 20 kPa of CH_4; for the mixture, a negative ion signal level comparable to that in Fig. 1(b) for pure CH_4 at 20 kPa was obtained at a lower laser intensity since H$^-$ ions from H_2 also contributed. The resulted wave form for the mixture is shown in Fig. 1(c). At the laser intensity of Fig. 1(c), the ion signal in pure CH_4 was less than half the ion signal of Fig. 1(c); thus, about half of the ion signal in Fig. 1(c) was due to H$^-$ ions from H_2. The drift times of the negative ions in Fig. 1(b) and 1(c) are comparable (it was necessary to compare similar ion signal levels, since the measured ion drift times depended on the signal strength due to space-charge effects [13]). If the negative ions due to CH_4 are heavier than H$^-$ (for example CH_2^-, see Ref. 7), the added H$^-$ ions due to H_2 should appear in the wave form in Fig. 1(c) at smaller drift times, i.e., two distinct ion components should be present in Fig. 1(c). Since the drift times indicated by the wave forms in

Fig. 1(b) and Fig. 1(c) are close, we conclude that predominantly H$^-$ ions are produced via electron attachment to laser-excited CH$_4$.

The dependence of the total signal, V$_T$, and the negative ion signal, V$_I$, on I is shown in a log-log plot in Fig. 2. The V$_T$ is the sum of V$_I$ and V$_E$, the signal due to unattached electrons, see Fig. 1. The V$_T$ should be proportional to the number density of electrons initially produced via laser photoionization, and some of these electrons are converted to excited species produced by the same laser pulse. Photoionization of CH$_4$ (ionization threshold ~ 12.6 eV) should occur via a two-photon process, and thus one would expect the slope of V$_T$ vs. I curve for CH$_4$ on a log-log plot to be 2. However, as seen in Fig. 2 the experimental curve for pure CH$_4$ had a slope of less than 2. This was due to photoelectron emission at the grid by the laser pulse. When He (or N$_2$ or Ar) was added to CH$_4$, the photoemission decreased (due to the lowering of the E/N value) as expected and the V$_T$ curve for the mixture became closer to the expected curve of slope 2 as seen in Figure 2. It is important to note that the negative ion signal for this CH$_4$/He mixture was higher than that for pure CH$_4$. The reason for this is not clear and is being investigated. No such enhancement in ion signal was observed when N$_2$ or Ar was added to CH$_4$. The V$_I$ in Fig. 2 increased as I^4. This is consistent with negative ion formation by attachment of an electron produced via two-photon ionization to an excited molecule produced via two-photon excitation. Therefore, the following sequence of events is consistent with the experimental observations:

$$CH_4 + 2h\upsilon \rightarrow CH_4^* + e \qquad\qquad (1)$$

$$CH_4 + 2h\upsilon \rightarrow \overline{CH_4^{**}} \qquad\qquad (2)$$

$$CH_4^{**} \; (or \; CH_4^*) + e \rightarrow H^- + CH_3 \qquad\qquad (3)$$

where, CH_4^{**} is a SES of CH_4, and CH_4^* is an excited state of CH_4 lying below SES.

Measurements conducted at different pressures, P, of CH_4 (with other parameters kept constant) showed that $V_T \alpha \, P$ and $V_I \alpha \, P^2$. The linear dependence of V_T on P is consistent with initial electron production via photoionization of CH_4. The quadratic dependence of V_I on P confirms that to form each negative ion, two CH_4 molecules are needed: one to produce the attaching electron and the second to produce the excited molecule.

Since neither the lifetimes of the SES excited nor the two-photon excitation cross section for CH_4 at the ArF laser line are known it is not possible to estimate a cross section for the electron attachment processes involved. However, a lower limit for the cross section can be estimated as follows: if we take a nominal value of 10^{-47} cm^4 s^{-1} for the nonresonant two-photon excitation cross section for CH_4 at the ArF laser line, the maximum number density of SES produced by a laser pulse of $I \sim 3 \times 10^{24}$ photons cm^{-2} s^{-1} for the data of Fig. 2 would be $\sim 10^{12}$ cm^{-3}. Now, if we assume that the SES populated, or the species to which they converge following their formation (e.g., high Rydberg states), do not decay during the passage of the electrons through the laser-irradiated area (i.e., lifetime $> 10^{-8}$ s), then for the data shown in Fig. 2 at $I \sim 3 \times 10^{24}$ photons cm^{-2} s^{-1}, an electron

attachment cross section of ~ 10^{-10} cm^2 is estimated. Therefore, it is highly unlikely that such a large

cross section can be associated with ground state radicals that may be produced via laser irradiation.

It is possible, but still not likely, that the observed electron attachment was due to low-lying excited

states of radicals produced via dissociation of the SES. We also note that, since the ionization

threshold of CH$_4$ is ~ 12.6 eV and since the two-photon energy for the ArF laser line is 12.8 eV, the

attaching electrons would have energies of $\lesssim 0.2$ eV.

III.   IMPLICATIONS FOR PLASMA PROCESSING DISCHARGES

Large amounts of negative ions (of the same order of magnitude as positive ions) have been

extracted from radio frequency (rf) discharges of SiH$_4$ (see references in [6]), and of CF$_4$ [14]. Even

though no such studies have been reported to our knowledge for CH$_4$ discharges, efficient H$^-$

formation was recently reported [8] for a CH$_4$/Ar pin-hollow cathode discharge. All of the above

three molecules attach electrons weakly in their ground electronic states. We believe that electron

attachment to excited electronic states of these molecules is responsible for the observed efficient

negative ion formation in the above mentioned discharges.

In addition to the results of CH$_4$ presented here, we earlier reported enhanced electron

attachment to laser-excited SiH$_4$ [6]. In both cases, the responsible excited states are believed to be

SES or high-lying Rydberg states to which they decay. Even though the SES are believed to have

sub-ns lifetimes, the Rydberg states can have much longer lifetimes; independently of the lifetimes of

the attaching states the large number densities populated via laser excitation together with the

enormous electron attachment cross sections ($> 10^{-12}$ cm^2) associated with these states, made it

possible for electron attachment to occur [9]. It is unlikely that such high number densities of SES

would be produced in processing discharges. However, it is quite likely that significant numbers of highly-excited states (Rydberg states) lying just below the ionization threshold are populated in such discharges. Such states can be populated via direct electron impact; in addition, in gas mixtures involving rare gases energy transfer from metastable states of the rare gases will enhance those excited state populations [6]. Since highly-excited Rydberg states can have lifetimes in the μs range [15], it is possible that negative ions in these discharges originate mainly from electron attachment to such highly-excited states.

Negative ions have been shown (see for example, Refs. 16-18) to be the likely precursors of particulate formation in gas discharges. Therefore, particulate formation observed in processing discharges using gases such as CH_4 and SiH_4 may have its origin in electron attachment to excited states. By understanding the basic electron attachment process involved, it may be possible to control particulate formation in such discharges.

ACKNOWLEDGMENT

REFERENCES

1. J. C. Angus, P. Koidl, and S. Domitz, "Carbon Thin Films," in Plasma Deposited Thin Films (Ed. By J. Mort and F. Jansen) CRC Press, Boca Raton, 1986, pp. 89-128.

2. D. K. Davis, L. E. Kline, and W. E. Bies, "Measurements of Swarm Parameters and Derived Electron Collision Cross Sections in Methane," *J. Appl. Phys.* **65**, 3311-3323 (1989).

3. A. von Keudell and W. Möller, "A Combined Plasma-Surface Model for the Deposition of C:H Films From a Methane Plasma," *J. Appl. Phys.* **75**, 7718-7727 (1994).

4. S. R. Hunter, J. G. Carter, and L. G. Christophorou, "Electron Transport Measurements in Methane Using an Improved Pulsed Townsend Technique," *J. Appl. Phys.* **60**, 24-35 (1986).

5. W. L. Morgan, "A Critical Evaluation of Low-Energy Electron Impact Cross Sections for Plasma Processing Modeling II.CH_4, SiH_4, and CH_4," *Plasma Chem. and Plasma Proc.* **12**, 478-493 (1992).

6. L. A. Pinnaduwage, M. Z. Martin, and L. G. Christophorou, "Enhanced Negative Ion Formation in Ultraviolet-Laser Irradiated Silane: Implications for Plasma Deposition of Amorphous Silicon," *Appl. Phys. Lett.* **65**, 2571-2573 (1994).

7. T. E. Sharp and J. T. Dowell, "Isotope Effects in Dissociative Attachment of Electrons in Methane," *J. Chem. Phys.* **46**, 1530-1531 (1967).

8. . S. Iizuka, T. Koizumi, T. Takada, and N. Sato, "Effect of Electron Temperature on Negative Hydrogen Ion Production in a Low-Pressure Ar Discharge Plasma with Methane," *Appl. Phys. Lett.* **63**, 1619-1621 (1993).

9. L. A. Pinnaduwage, L. G. Christophorou, and A. P. Bitouni, "Enhanced Electron Attachment to Superexcited States of Saturated Tertiary Amines," *J. Chem. Phys.* **95**, 274-287 (1991).

10. W. A. Chupka and J. Berkowitz, "Photoionization of Methane: Ionization Potential and Proton Affinity of CH_4," *J. Chem. Phys.* **54**, 4256-4259 (1971).

11. C. Winstead, Q. Sun, V. McKoy, J. L. S. Lino, and M. A. P. Lima, "Electronic Excitation of CH_4 by Low-Energy Electron Impact," *J. Chem. Phys.* **98**, 2132-2137 (1993).

12. L. A. Pinnaduwage and L. G. Christophorou, "H^- Formation in Laser-Excited Molecular Hydrogen," *Phys. Rev. Lett.* **70**, 754 (1993).

13. L. A. Pinnaduwage and L. G. Christophorou, "Verification of H^- Formation in Ultraviolet-Laser-Irradiated Hydrogen: Implications for Negative Ion and Neutral Beam Technologies," *J. Appl. Phys.* **76**, 46 (1994).

14. Y. Lin and L. J. Overzet, "Negative and Positive Ions From CF_4 and CF_4/O_2 RF Discharges in Etching Si," *Appl. Phys. Lett.* **62**, 675 (1993).

15. R. F. Stebbing and F. B. Dunning (Eds.), Rydberg States of Atoms and Molecules, Cambridge University Press, 1983.

16. A. Garscadden, "Effects Due to Negative Ions and Particles in Plasmas," in Nonquilibrium Processes in Partially Ionized Gases, (M. Capitelli and J. N. Bardsley, Eds.), Plenum Press, New York, 1990, pp. 541-550.

17. S. J. Choi and M. J. Kushner, "The Role of Negative Ions in the Formation of Particles in Low-Pressure Plasmas," *J. Appl. Phys.* **74**, 853 (1993).

18. A. A. Howling, L. Sansonnens, J.-L. Dorier, and Ch. Hollenstein, "Time-Resolved Measurements of Highly Polymerized Negative Ions in Radio Frequency Silane Plasma Deposition Experiments," *J. Appl. Phys.* **75**, 1340 (1994).

ORNL-DWG 95M-4860

(a)
4 ms/div
40 mV/div
$I = 4 \times 10^{23}$ ph.cm^{-2}s^{-1}
CH$_4$

(b)
4 ms/div
100 mV/div
$I = 17 \times 10^{23}$ ph.cm^{-2}s^{-1}
CH$_4$
V_E
V_I

(c)
4 ms/div
100 mV/div
$I = 10 \times 10^{23}$ ph.cm^{-2}s^{-1}
CH$_4$ + H$_2$
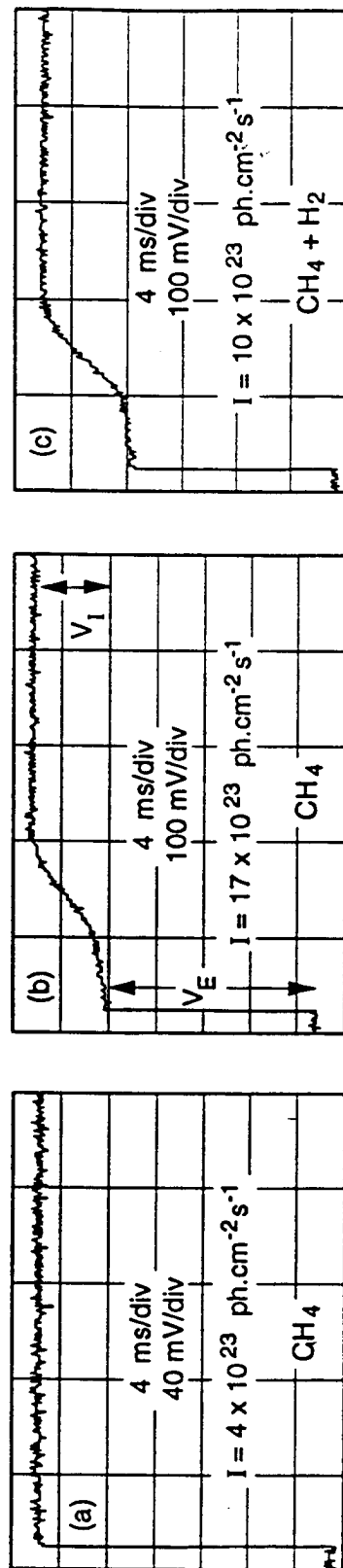
Fig. 1:   Signal versus time wave forms for CH$_4$ and CH$_4$/H$_2$ mixtures irradiated by ArF excimer

laser. The signals due to unattached electrons, V_E, were too fast to be digitized at the time

scales shown, and, therefore, appear as vertical lines. Wave forms in Fig. 1(a) and Fig. 1(b)

are for pure CH$_4$ at 20 kPa; wave form in Fig. 1(c) is for a mixture of 0.48 kPa H$_2$ and 20

kPa of CH$_4$. About half of the ion signal in Fig. 1(c) is due to H$^+$ ions from H$_2$. The applied

electric field was 25 V cm^{-1} for all three wave forms.
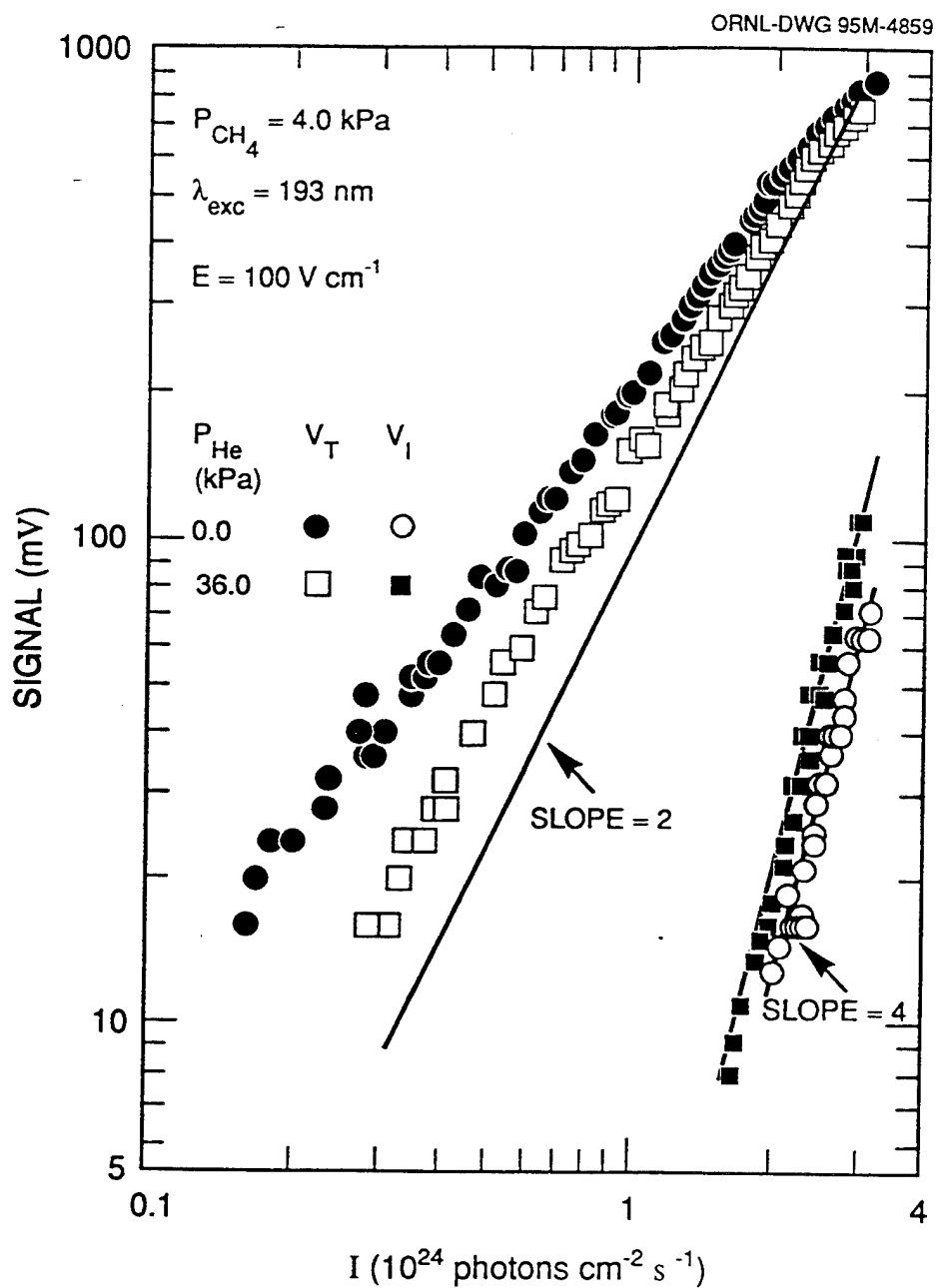
95

Fig. 2: Laser intensity, I, dependence of the measured total, V_T, and negative ion V_I, signals for the experimental parameters indicated in the figure. The figure shows data for pure CH_4 (circles) and for a mixture of CH_4 and He (squares).

6.4. A Possible New Mechanism Involved in Nonuniform Field Breakdown in Gaseous Dielectrics

Even though the electrical breakdown of gases under uniform field conditions is fairly well understood in terms of the Townsend breakdown theory, a consistent model for nonuniform field breakdown is not available at present. The breakdown voltage estimated by the Townsend theory for a nonuniform gap coincides with the corona onset voltage, but the actual breakdown may occur at a higher voltage depending on the gas composition, gas pressure, electrode configuration, etc.; this is called "corona stabilization." The existing electron attachment and breakdown data, especially on the observation that under static or impulse nonuniform field conditions certain additives (e.g., amines) with low ionization thresholds to an insulating gas (e.g., SF_6) can increase the breakdown voltage over certain pressure ranges, have generally been attributed to enhanced space charges introduced by the additive. However, recent studies suggest that space charge effects cannot always explain the experimental observations. In a paper published in the book gaseous Dielectrics VII (see Section 3), we explored the possibility that efficient electron attachment to the highly excited states of the additive (produced via electron impact) might be the reason for the enhanced stability. In particular, our measurements on enhanced electron attachment to triethylanine which has been used as an additive in corona stabilization experiments. seem to be consistent with this proposed mechanism.

6. Review Papers

Parts of the research conducted under this contract have been reviewed in the following two papers which are reproduced, respectively, as Appendix A and Appendix B.

1. L. G. Christophorou, L. A. Pinnaduwage, and P. G. Datskos, "Electron Attachment to Excited Molecules," In <u>Linking the Gaseous and the Condensed Phases of Matter: The Behavior of Slow Electrons</u> , L.G.Christophorou, E. Illenberger, and W. F. Schmidt (Eds.) NATO ASI Series, Plenum Press, New York, 1994, pp.415-442.

2. L. G. Christophorou, R. Van Brunt, and J. Olthoff, "Fundamental Processes in Gas Discharges," Invited lectures, In <u>Proceedings of the Xith International Conference on Gas Discharges and Their Applications</u>, (In Press).

APPENDIX A

L. G. Christophorou, L. A. Pinnaduwage, and P. G. Datskos, "Electron Attachment to Excited Molecules," In <u>Linking the Gaseous and the Condensed Phases of Matter: The Behavior of Slow Electrons</u> , L.G.Christophorou, E. Illenberger, and W. F. Schmidt (Eds.) NATO ASI Series, Plenum Press, New York, 1994, pp.415-442.

ELECTRON ATTACHMENT TO EXCITED MOLECULES[1]

Loucas G. Christophorou, Lal A. Pinnaduwage, and Panos G. Datskos

Atomic, Molecular, and High Voltage Physics Group, Health and Safety Research Division, Oak Ridge National Laboratory, Post Office Box 2008, Oak Ridge, Tennessee 37831-6122, and Department of Physics, The University of Tennessee, Knoxville, Tennessee, 37996

ABSTRACT

Studies on electron attachment to molecules rotationally/vibrationally excited thermally or via infrared-laser excitation showed that the effect of internal energy of a molecule on its electron attachment properties depends on the mode--dissociative or nondissociative--of electron attachment. They quantified the effect of the internal energy of the molecule on the rate of destruction (by autodissociation or by autodetachment) of its parent transient anion. Generally, increases in ro-vibrational molecular energy increase the cross section for dissociative electron attachment and decrease the effective cross section for parent anion formation due mainly to increased autodetachment. These findings and their understanding are discussed. A discussion is given, also, of recent investigations of electron attachment to electronically excited molecules, especially photoenhanced dissociative electron attachment to long- and short-lived excited electronic states of molecules produced directly or indirectly by laser irradiation. These studies showed that the cross sections for dissociative electron attachment to electronically excited molecules usually are many orders of magnitude larger than those for the ground-state molecules. The new techniques that have been developed for such studies are briefly described also.

415

INTRODUCTION

Studies of electron attachment to ground-state molecules trace back many decades; they led to significant knowledge on and to an understanding of the various electron attachment processes and their dependence on molecular structure and the electron energy[1-6]. In contrast, studies of electron attachment to "hot" (ro-vibrationally excited) molecules (e.g., see Refs. 4, 7, and 8 and subsequent discussion in this chapter) and especially to electronically excited molecules (e.g., see Ref. 8, and later in this chapter) are more recent and more limited; they have shown that the cross sections for electron attachment to molecules depend rather strongly on the internal energy content of the molecules and in many instances are exceedingly large (almost macroscopic!).

Studies of electron attachment to excited molecules are of fundamental significance (e.g., theory of collision processes and the structure of matter; energy loss mechanisms and cross sections; plasma, electron, ion, and laser physics and chemistry; radiation and life sciences) and of applied/technological significance (e.g., plasmas, lasers, gas discharges, pulsed power switches, optogalvanic effects). Excited molecules are more reactive than are unexcited molecules, making their effect on the properties of many systems significant even when their number densities in such systems are small. The reason for the limited studies on electron attachment to (and, in general, electron interactions with[8]) excited molecules is largely due to the difficulty in producing sufficient numbers of excited molecules to study under controlled experimental conditions, and to the often rapid dissociation of the excited molecules.

ELECTRON ATTACHMENT TO VIBRATIONALLY/ROTATIONALLY EXCITED MOLECULES AND THERMALLY-ENHANCED DETACHMENT FROM POLYATOMIC NEGATIVE IONS

General Considerations

Electron attachment reactions depend strongly on both the kinetic energy, ϵ, of the attached electron and the structure and internal energy, $<\epsilon>_{int}$ of the electron attaching molecule.[1-4] As $<\epsilon>_{int}$ is increased, delicate and often profound changes occur in the electron attaching/detaching properties of the molecule which crucially depend on the molecule itself and the mode (dissociative or nondissociative) of electron attachment (see Refs. 4 and 8 and sources cited later in this chapter).

Within the resonance scattering theory of electron attachment, the electron e, of energy ϵ, is initially captured by the molecule AX--with a cross section $\sigma_o(\epsilon)$--forming a transient negative ion AX^{-*} which, then, decays by attachment (A + X⁻ or AX⁻) or autodetachment $(AX^{(*)} + e)$, viz.,

$$
\begin{array}{c}
\hspace{6cm} A + X^- \hspace{2cm} (1a) \\[0.3cm]
\hspace{4.5cm} p \nearrow \\[0.2cm]
e(\epsilon) + AX \xrightarrow{\sigma_0(\epsilon)} AX^{-*} \\[0.2cm]
\hspace{5cm} \searrow \\[0.3cm]
\hspace{5cm} AX^{(*)} + e(\epsilon') \hspace{1.5cm} (1b)
\end{array}
$$

416·

$$e(\varepsilon) + AX \xrightarrow[\sigma_0'(\varepsilon)]{} AX^{-*} \begin{cases} \xrightarrow{p'} AX^- + \text{energy} & \text{(2a)} \\ \\ \xrightarrow{} AX^{(*)} + e(\varepsilon') & \text{(2b)} \end{cases}$$
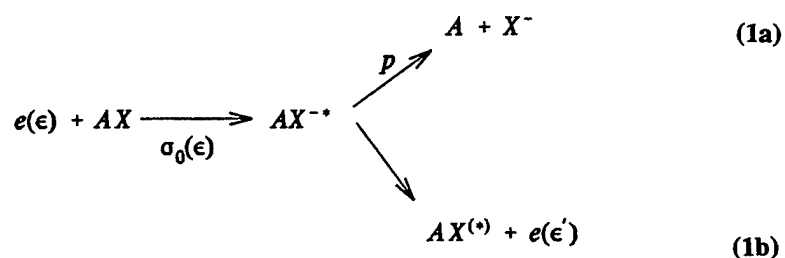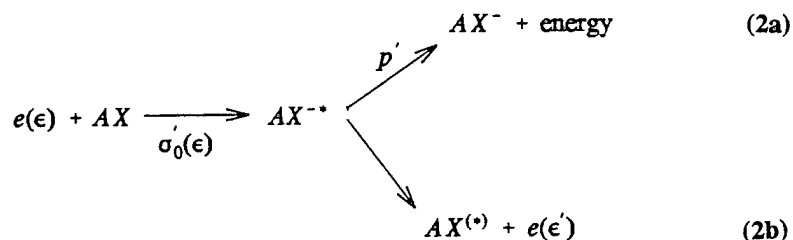
where $\varepsilon'(\leq\varepsilon)$ is the energy of the autodetached electron. The cross section for dissociative electron attachment, σ_{da}, and for nondissociative electron attachment, σ_{nda}, can be written, respectively, as $\sigma_o p$ and $\sigma_o' p'$, where p and p' are the probabilities, respectively, for AX^{-*} to decay producing $A + X^-$, or to become stabilized producing AX^-.

For ground state molecules, the cross sections σ_{da} and σ_{nda} vary by over ten orders of magnitude (from $\sim 10^{-24}$ to $> 10^{-14}$ cm^2) depending on the molecule and the energy position of the negative ion resonance[1,4]. Similarly, the autodetachment lifetimes of the isolated AX^{-*} ions vary by over thirteen orders of magnitude (from $\sim 10^{-15}$ to $> 10^{-2}$ s) (e.g., see Refs. 1, 4, 7, and 9). As the internal energy of the molecule is increased, changes may occur in σ_o and σ_o' due to variations in the Fanck-Condon factors and the fact that as $<\varepsilon>_{int}$ is increased electrons with lower energy can reach the negative ion state. These changes, however, cannot explain the reported dependencies of the attachment cross section on T (e.g., see Refs. 4, 7, 8, 10-24).

For the case of dissociative electron attachment, the reported increases in σ_{da} with increasing T can be largely attributed to the increase of p (Eq. (1)) as T is increased;[4,7,8,10-18] at elevated temperatures electron capture occurs over larger internuclear distances and larger excited-vibrational-state amplitudes.

For the case of nondissociative electron attachment, the reported decreases in the cross section σ_{nda} (or the attachment rate constant, k_{nda}) have been attributed to a decrease in p' (i.e., increased autodetachment) as the anion's internal energy is increased[7,8,19-22]. This, however, requires further scrutiny (see later).

The autodetachment lifetime τ_a of an isolated AX^{-*} metastable negative ion depends on the negative ion state, the internal energy of AX^{-*}, the electron affinity, EA, of AX, and the electronic selection rules and Franck-Condon factors for the transition[7,9]

$$AX^{-*} \xrightarrow{\tau_a} AX^{(*)} + e \qquad (3)$$

Direct measurements of τ_a for reaction (3) as a function of the energy of the captured electron that led to the formation of AX^{-*} have shown that τ_a decreases with ε (e.g., see Ref. 9). In many high-pressure (swarm) experiments, however, AX^{-*} is effectively stabilized by collisions yielding AX^- (reaction (2a)) predominantly in its lowest state of excitation. In such cases the observed apparent decrease in σ_{nda} (or k_{nda}) with T is due to the enhanced probability of autodetachment via the reaction

$$AX^- + heat \longrightarrow AX + e \qquad (4)$$

417

The internal energy of polyatomic negative ions is appreciable even at temperatures within a few hundred degrees above ambient and reaction (4) becomes significant--especially when the EA is small ($\underset{\sim}{<}$ 0.5 eV)--influencing the measured apparent electron attachment (see later and Refs. 19, 21, and 22).

The techniques that have been employed for such studies are conventional electron swarm methods with provisions for heating and temperature control and measurement[11,14,22], and electron impact mass spectrometers with similar provisions[10,12]; measurements dealing only with thermal electron attachment were also made using the flowing afterglow/Langmuir probe technique (e.g., see Refs. 20 and 23). Heating is, of course, the easiest way to increase the internal energy of AX (and AX$^-$), but the resultant ro-vibrational excitation is nonselective. There have been only very few studies which employed selective vibrational excitation of molecules prior to electron attachment, using almost exclusively infrared CO_2 lasers[8,24]. A swarm technique which allows simultaneous determination of the effect of T on both the electron attachment and the electron detachment process has recently been developed and is discussed below.

Dissociative Electron Attachment to "Hot" Molecules

Techniques. As we mentioned above, conventional electron impact mass spectrometers and electron swarm techniques have been employed for the study of dissociative electron attachment to "hot" molecules. The principle of the former is illustrated in Fig. 1. In this particular arrangement, a trochoidal monochrometer is used to produce the monoenergetic electron beam which, subsequently, collides with the excited ("hot") molecules in the iridium chamber. The resulting negative ions were extracted at right angles into a quadrupole mass spectrometer where they are mass analyzed and detected. Temperatures of up to ~ 1200 K were reached in these studies.
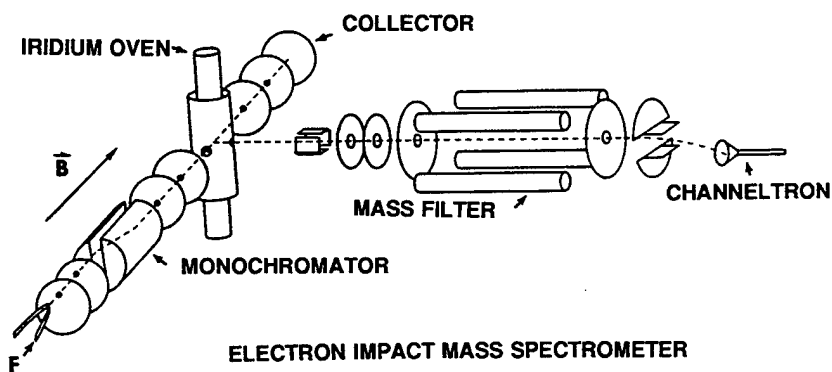
Figure 1. Schematic of an electron impact mass spectrometer[10].

In Fig. 2 is depicted the principle of two electron swarm techniques which have been employed in studies of electron attachment to hot molecules. As is well known[1,4], in electron swarm experiments one deals with high pressures. Electrons are generated in various ways in a plane parallel to the two electrodes (see Fig. 2); they quickly (within a few ns, depending on the gas and its density) attain an equilibrium energy distribution f(ε, E/N, T)

(a)

V_1

CATHODE

d_1

SOURCE   alpha-particle

d_2

ANODE $V_2 = V_1 \dfrac{d_2}{d_1 + d_2}$

C $R = 10^{11} \, \Omega$

VOLTAGE

V_{max}

TIME

(b)

V

CATHODE

e e e e e

LASER PULSE

ANODE

C $R = 10^{11} \, \Omega$

VOLTAGE
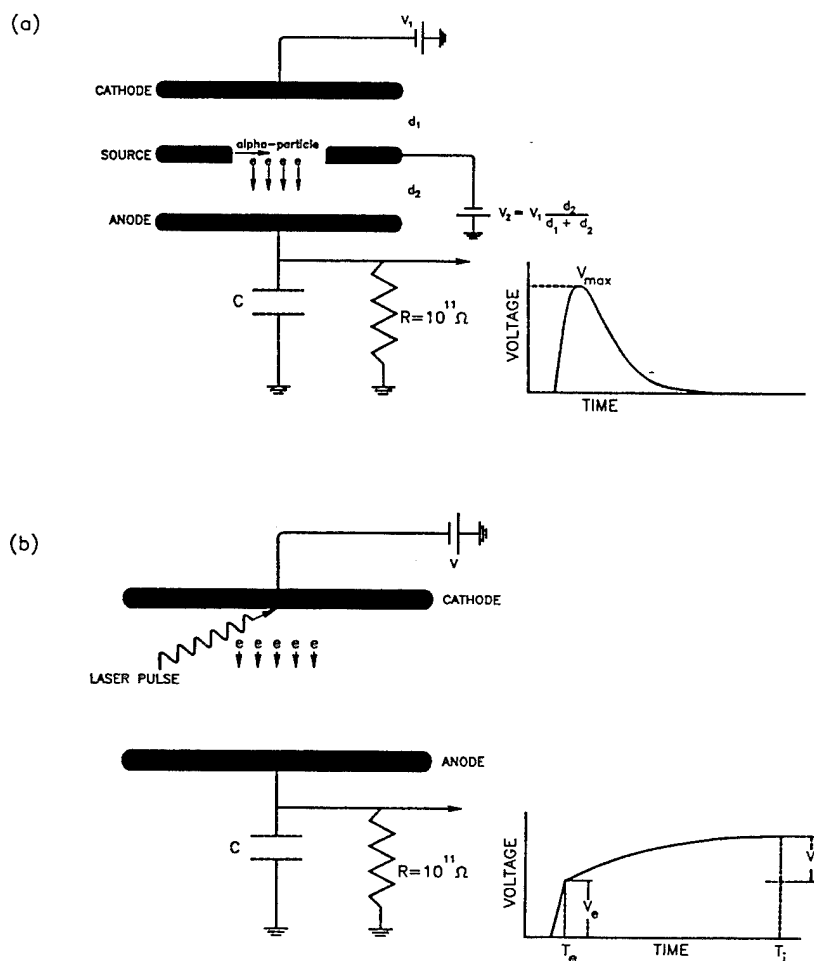
V_e V_i

T_e TIME T_i

Figure 2.   Schematic illustrating the principles of two electron swarm techniques (see the text).

(which depends on the gas, the applied density-reduced electric field E/N and the temperature) and drift, as a swarm, to the anode. As they drift, a fraction is removed from the electron swarm by attachment. The number of electrons removed is measured as a function of E/N (or the mean energy $<\varepsilon>$) and T, and is used to determine $k_a(<\varepsilon>, T)$ from which the attachment cross section σ_a (ε, T) is calculated[1,4]. The various swarm methods differ in the way the initial electrons are produced and the way in which their number is monitored as the swarm drifts to and is collected at the anode[1,4].

In Fig. 2a is shown the principle of the "pulse-shape swarm technique" used extensively by the Oak Ridge National Laboratory group. It is based on the fact that electron attachment modifies appreciably the shape of pulses obtained in ionization chambers. The electron swarm[1,25] (of about 5×10^5 electrons) is produced at a distance d_1 from the cathode every time an α-particle passes through the gas. The α-particle is emitted from a radioactive source (e.g., Cf^{232}) contained in the inner edge of a ring-shaped electrode situated at a distance d_1 from the cathode and at an equipotential. The electron swarm drifts a distance d_2 before reaching the anode. The peak in the <u>induced voltage</u> in the anode electrode is observed

104

through a linear pulse amplifier (which has a known response to a step function) with a multichannel analyzer. At each value of E/N and T this is done for the pure buffer gas (normally Ar or N_2)[1,4] and then again for a mixture of a small quantity of the attaching gas and the buffer gas. From the ratio of the maxima of the pulses due to the induced voltages (see schematic in Fig. 2a) for the two cases, k_a (E/N,T) is determined and from an independent knowledge of $f(\varepsilon,E/N,T)$, $\sigma_a(\varepsilon,T)$ is calculated[4,11,14]. The measured rates and cross sections are <u>total</u>, since no mass analysis is possible in these experiments.

The schematic diagram in Fig. 2b shows the principle of the pulsed Townsend technique which has also been used by the ORNL group for electron-"hot" molecule studies[22,25]. Here a small number of electrons ($<10^6$ electrons/cm^3) is generated photoelectrically at the cathode with a short ($\leq$ 1 ns) UV laser pulse. The photoelectrons quickly reach a steady state and drift--as a swarm--to the anode under E/N. In the presence of electron attachment, the voltage induced in the anode circuit as a function of time (t = 0 $\equiv$ firing of the laser pulse) is as shown schematically in Fig. 2b, i.e., it consists of an initial fast rise due to the unattached electrons and a subsequent slow rise due to the slow-moving negative ions. If N_e and N_i are, respectively, the number of electrons and negative ions reaching the anode and V_e and V_i, are, respectively, the saturated values of the induced voltage due to the motion of electrons and negative ions, then

$$R_v(E/N,T) = \frac{N_e+N_i}{N_e} = \frac{V_e+V_i}{V_e} = \frac{\eta d}{1-\exp(-\eta d)} \quad (5)$$

where d is the drift gap and η(E/N,T) is the unnormalized electron attachment coefficient. From the measured R_v(E/N,T), the η(E/N,T) is determined by an iterative procedure. The total electron attachment rate constant is, then, determined from

$$k_a \ (E/N,T) = \frac{\eta(E/N,T)w_e(E/N,T)}{N_a} \quad (6)$$

where w_e(E/N,T) is the electron drift velocity and N_a is the attaching gas number density.

<u>Representative recent measurements.</u> The rate constant/cross section for dissociative electron attachment generally increases with increasing $<\varepsilon>_{int}$ of the molecule, but the relative increase varies depending on the particular molecule and the position of the negative ion state above the v = 0 level of the neutral molecule. This has been shown for both diatomic (e.g., see Refs. 4, 10, 15-18) and polyatomic (e.g., see Refs. 4, 8, 11-14) molecules. As T increases the probability, p, for reaction (1b) increases profoundly; the transient ion AX^{-*} dissociates faster into A+X$^-$. In Figs. 3 and 4 are shown two recent examples for polyatomic molecules. The variation of k_{da} and σ_{da} with $<\varepsilon>_{int}$ for these two molecules and for the diatomic molecules HCl and DCl are shown in Fig. 5. The $<\varepsilon>_{int}$ for the polyatomic molecules was determined[13,14] by using the expression

$$<\varepsilon>_{int} \approx <\varepsilon>_{vib}(T) = \sum_{i=1}^{N} \frac{\hbar\omega_i}{e^{\hbar\omega_i/kT}-1} \quad (7)$$

where $\hbar\omega_i$ are the vibrational frequencies of the neutral molecule. The use of Eq. (7) to determine $<\varepsilon>_{int}$ reglects the contribution from rotational excitation and takes the internal energy of the molecule to be mainly due to the vibrational excitation above the zero-point energy. The effect of rotational excitation can be seen from the data in Fig. 5c.
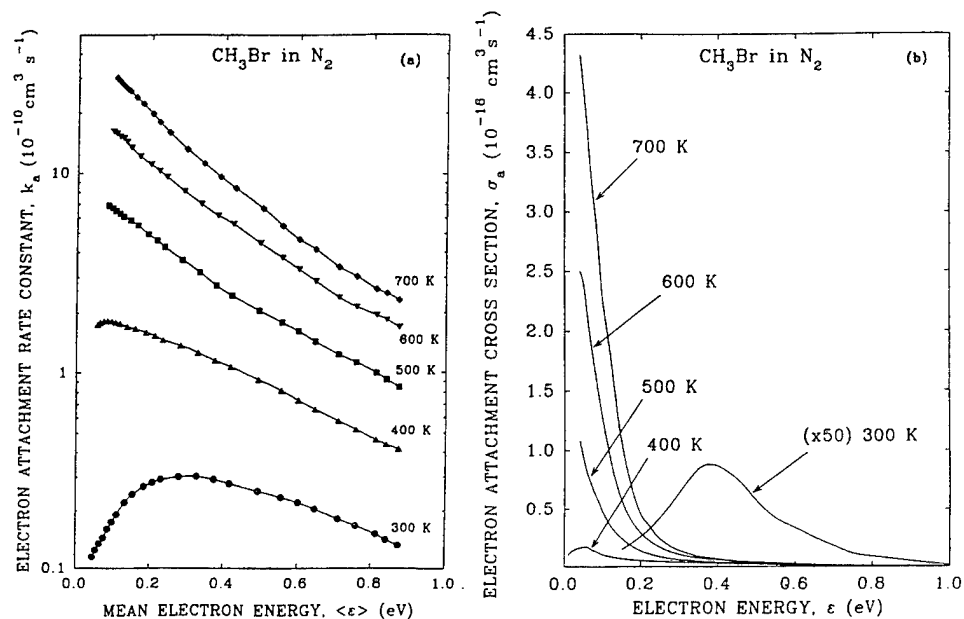
Figure 3. Dissociative electron attachment to CH_3Br at various temperatures. (a) total dissociative electron attachment rate constant k_a as a function of the mean electron energy $<\varepsilon>$. (b) Total dissociative electron attachment cross section σ_a as a function of the electron energy ε (from Ref. 14b).
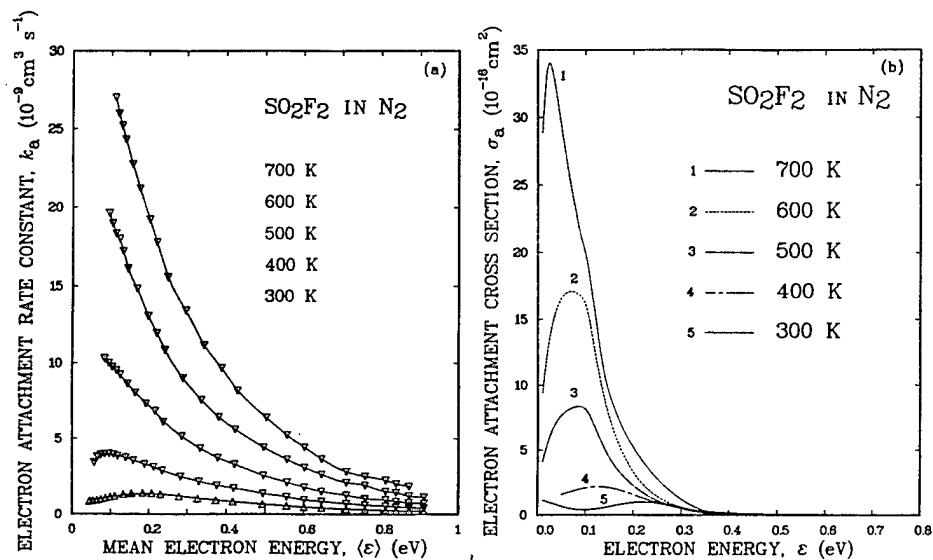
Figure 4. Dissociative electron attachment to SO_2F_2 at various temperatures. (a) k_a vs $<\varepsilon>$; (b) σ_a vs ε (from Ref. 13).

106   421

Nondissociative Electron Attachment to "Hot" Molecules and Thermally-Enhanced Detachment From Polyatomic Negative Ions

While the rate constants/cross sections for dissociative electron attachment to molecules, as a rule, increase with increasing T, just the opposite behavior has been reported for the nondissociative electron attachment reaction (2). The rate constant/cross section for nondissociative electron attachment has been found to decrease with increasing T for a number of molecules (e.g., see Refs. 4, 7, 8, 19-22a). An example of this type of behavior is shown in Fig. 6 for the C_6F_6 molecule which at low electron energies (≤ 1 eV) forms long-lived ($\tau_a \geq 10^{-5}$ s) parent negative ions (see Ref. 19a). The decrease in k_a ($<\varepsilon>$,T) with increasing T has been attributed to an increase in p' and/or a decrease in σ'_o as T increases. As will be discussed below, however, at the high pressures these swarm measurements were made, the long-lived transient anion AX^{-*} is stabilized by collision, and subsequent studies[22]
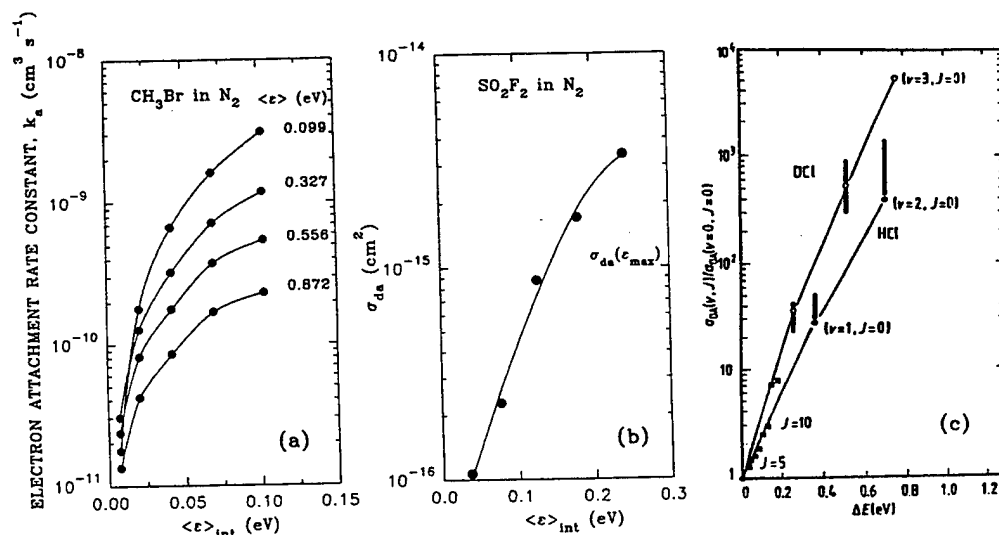
Figure 5. (a) k_a vs $<\varepsilon>_{int}$ for CH_3Br at a number of mean electron energies $<\varepsilon>$ (from Ref. 14b); (b) Variation of the peak cross section σ_{da} (ε_{max}) for SO_2F_2 with $<\varepsilon>_{int}$ (from Ref. 13); (c) σ_{da} (v,j)/σ_{da}(v=0, j=0) versus internal energy for HCl/DCl: error bars (experiment)[10b]; • (HCl, v, j=0); o (DCl; v, j=0); ■ (v=0, j) (calculation for 25 meV above the respective thermodynamic threshold[17]).

showed that the detachment process affects the measurement of k_a as it is conducted in the traditional swarm experiments[19a]. For this reason the data in Fig. 6--and similar other work--represent apparent values of k_a which are influenced by the measurement technique itself.

Recently we employed a new technique via which the effect of T on both the electron attachment and the electron detachment processes can be studied and quantified. This technique is decribed below.

The time-resolved electron swarm technique. This technique allows information on electron attachment and detachment processes to be obtained simultaneously from an analysis of transient electron waveforms. Its principle is shown in Fig. 7. The electron swarm is produced by a narrow ($\sim 6 \times 10^{-10}$ s) N_2 laser pulse which strikes the cathode electrode through a hole in the anode electrode. The electrons drift to the anode under the influence of an applied electric field. As they drift a fraction is removed by attachment forming unstable negative ions which are quickly stabilized, by collision with the buffer gas, forming

422

stable negative ions (M⁻ in Fig. 7). These stabilized anions are subsequently thermally autodetached giving rise to delayed electrons. The motion of those electrons which reach the anode without ever been attached ("prompt" electrons) and those electrons which have been captured and then thermally released ("delayed" electrons) induces a current in the anode circuit which is observed through a 50 Ω resistor to the ground. (For the μs time scales of interest here, the current is solely from the electrons; the contribution from the slowly moving negative ions is negligible and can be neglected). The electron current is given by[26]

$$i_e(t) = \frac{ew_e}{d} \int_{w_i t}^{min(w_e t, d)} \rho_e(x,t)dx \tag{8}$$
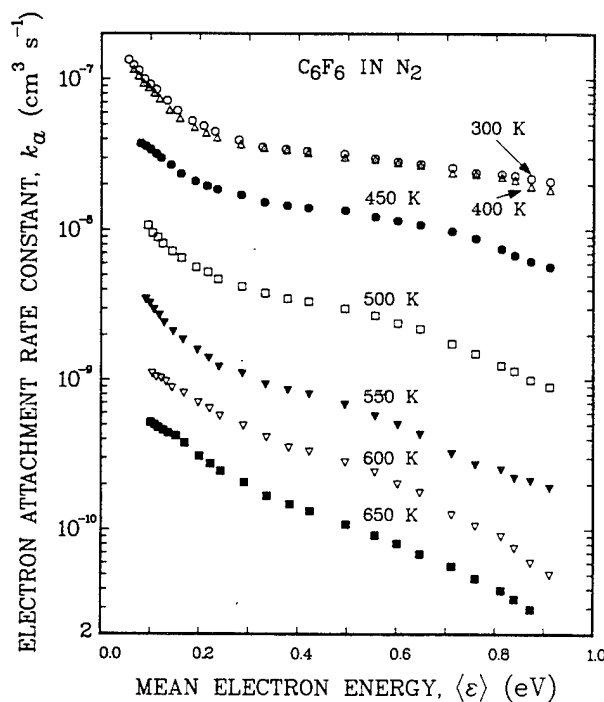
Figure 6. Electron attachment rate constant for C_6F_6 in N_2 buffer gas as a function of the mean electron energy at various temperatures (from Ref. 19a).

where w_e and w_i are the electron and ion drift velocities, d is the drift distance and ρ_e (x,t) is the electron number density given by[26]

$$\rho_e(x,t) = \frac{n_o}{w_e - w_i} \exp\left[-\frac{1}{t_a}\left(\frac{x - w_i t}{w_e - w_i}\right) + \frac{1}{t_d}\left(\frac{x - w_e t}{w_e - w_i}\right)\right]$$

$$x \left\{ \delta\left(\frac{w_e t - x}{w_e - w_i}\right) + \sqrt{\frac{1}{t_d t_d}\frac{x - w_i t}{w_e t - x}} I_1 \left[\frac{2}{(w_e - w_i)} \sqrt{\frac{1}{t_a t_d}(w_e t - x)(x - w_i t)}\right]\right\} \tag{9}$$

423

108
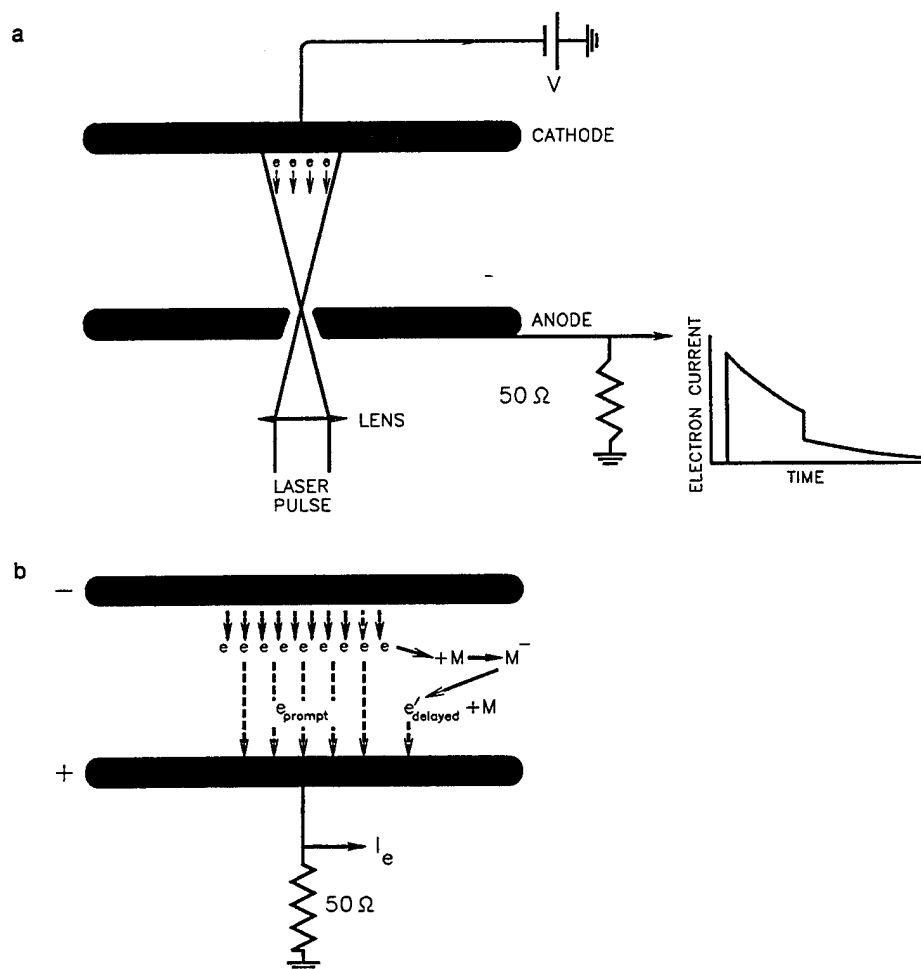
Figure 7. Schematic diagram of the experimental set-up of the time-resolved electron swarm technique (see the text and Ref. 22).

where n_o is the initial electron number density (at x=0), t_a^{-1} and t_d^{-1} are, respectively, the electron attachment and detachment frequencies, $\delta[(w_e t-x)/(w_e-w_i)]$ is a delta function and I_1 is the first order modified Bessel function. Figure 8 shows an example of the recorded waveforms as they were obtained for $C_6F_6^-$. The evolution of the autodetachment process as T is increased is clearly evident. The solid curves (curve 2 in Fig. 8f) are the measured waveforms. The dotted curves (curve 3 in Fig. 8f) represent the contribution to the total electron current when no autodetachment occurs, i.e., when all electrons reaching the anode are prompt. The difference between the total electron current (solid curves) and the dotted curves represents the contribution of the autodetached ("delayed") electrons; this is represented by the dashed curves (curve 4 in Fig. 8f). As T is increased this contribution becomes increasingly more significant; the parent anions autodetach faster.

From such recorded electron current waveforms the t_a^{-1} and t_d^{-1} are obtained--at each T-- using a nonlinear least squares fit. The k_{nda} is, then, obtained from

424

109
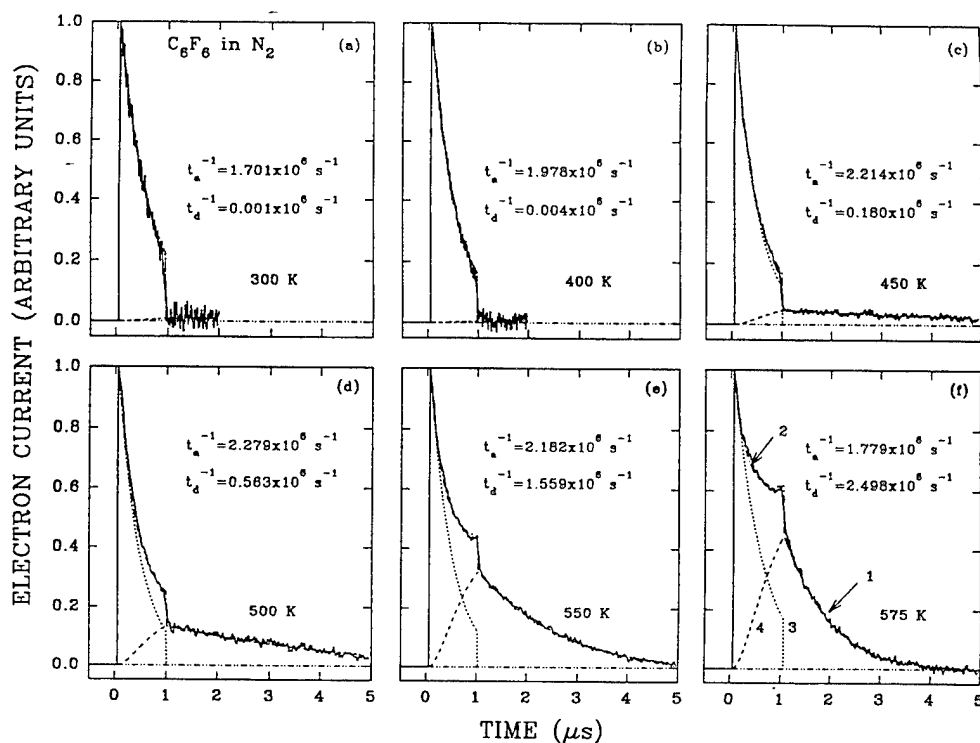
Figure 8. Electron current waveforms for C_6F_6 at T = 300, 400, 450, 500, 550, and 575 K. These waveforms correspond to an E/N = 1.09 x 10^{-17} V cm^2, a mean electron energy <ε> ≈ 0.38 eV, a total gas number density N_T = 9.66 x 10^{19} molecules cm^{-3}, an attaching gas number density N_a = 5.64 x 10^{13} molecules cm^{-3} and an electrode gap d = 0.4183 cm. The solid curves (—) are the experimentally measured electron current waveforms, the dash-dot (-•-•) curves are the calculated electron current waveforms using t_a^{-1} and t_d^{-1} values obtained from the nonlinear least squares fit, the dotted (•••) curves represent the contribution to the total electron current of the initial ("prompt") electrons when only electron attachment is present, and the broken (---) curves are the contribution of the "delayed" (autodetached) electrons.

$$k_{nda} = \frac{1}{t_d N_a} \qquad (10)$$

<u>Nondissociative electron attachment to "hot" molecules/thermally-induced detachment from polyatomic negative ions</u>. The technique described in the preceding section has been applied to the study of C_6F_6 (Ref. 22a) and c-C_4F_6 (Ref. 22b). In Fig. 9 is given the measured k_a(<ε>) for C_6F_6 at various T. Indeed while increases in T affect the k_a(<ε>), the changes are not as profound as indicated by the earlier studies (Fig. 6). The k_a(<ε>) first increases slightly with increasing T and then decreases. This behavior is seen better in Fig. 10a where k_a is plotted as a function of <ε>$_{int}$ for fixed values of the mean electron energy. The <ε>$_{int}$ (T) was determined[22a] by assuming that the vibrational frequencies of the anion and the neutral molecule are the same and using published vibrational frequencies for the neutral molecule and Eq. (7). The rather weak dependence of k_a on T suggests that $σ_o'$ (as $σ_o$) is not a strong function of T. In contrast to this small effect, temperature enhances dramatically the autodetachment of $C_6F_6^-$ (reaction (4)). This is clearly shown in Fig. 10b where the autodetachment frequency t_d^{-1} is seen to increase sharply with increasing <ε>$_{int}$ (the corresponding range of T is 450-575 K).
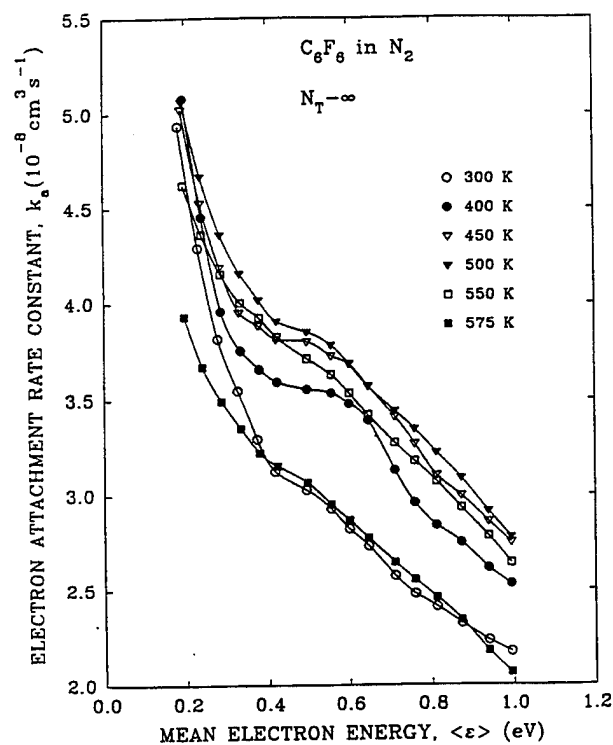
110

425

Figure 9. Electron attachment rate constant for the formation of $C_6F_6^-$ as a function of the mean electron energy at various temperatures (from Ref. 22a).
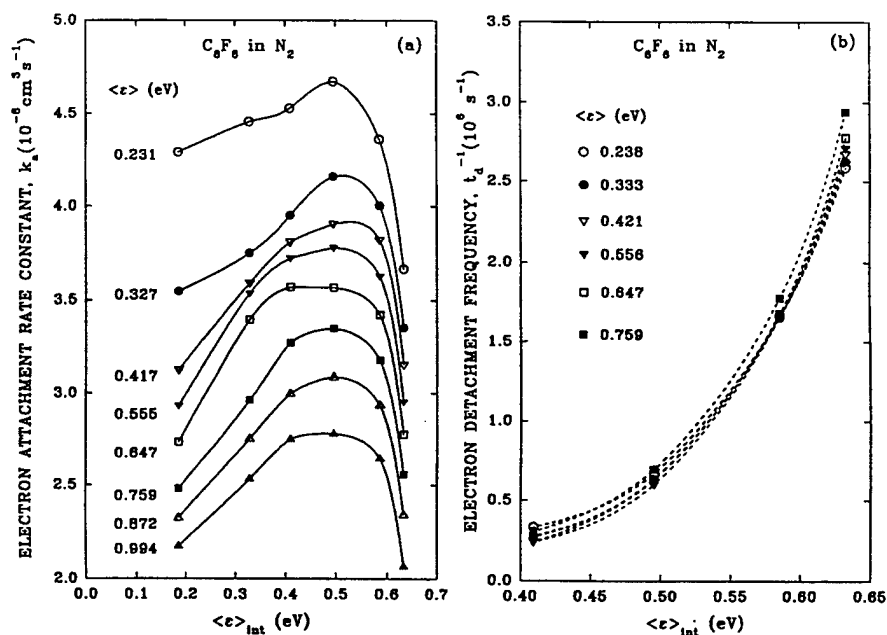

Figure 10. (a) Electron attachment rate constant, k_a (for $N_T \to \infty$) for the formation of $C_6F_6^-$ as a function of $<\varepsilon>_{int}$ for various values of the mean electron energy. (b) Autodetachment frequency, t_d^{-1} (for $N_T \to \infty$) for the formation of $C_6F_6^-$ as a function of $<\varepsilon>_{int}$ for various values of the mean electron energy.

Datskos et al.[22a] assumed that the autodetachment process has an activation energy E^* and that t_d^{-1} is related to T by

$$t_d^{-1} = A \ e^{-E^*/kT} \qquad (11)$$

where A is a constant. From a plot of $\ln(t_d^{-1})$ as a function of T^{-1} (Fig. 11) they obtained a value of E^* equal to 0.477 eV for thermal electrons ($<\varepsilon> \rightarrow 3/2 \ kT$) and for completely
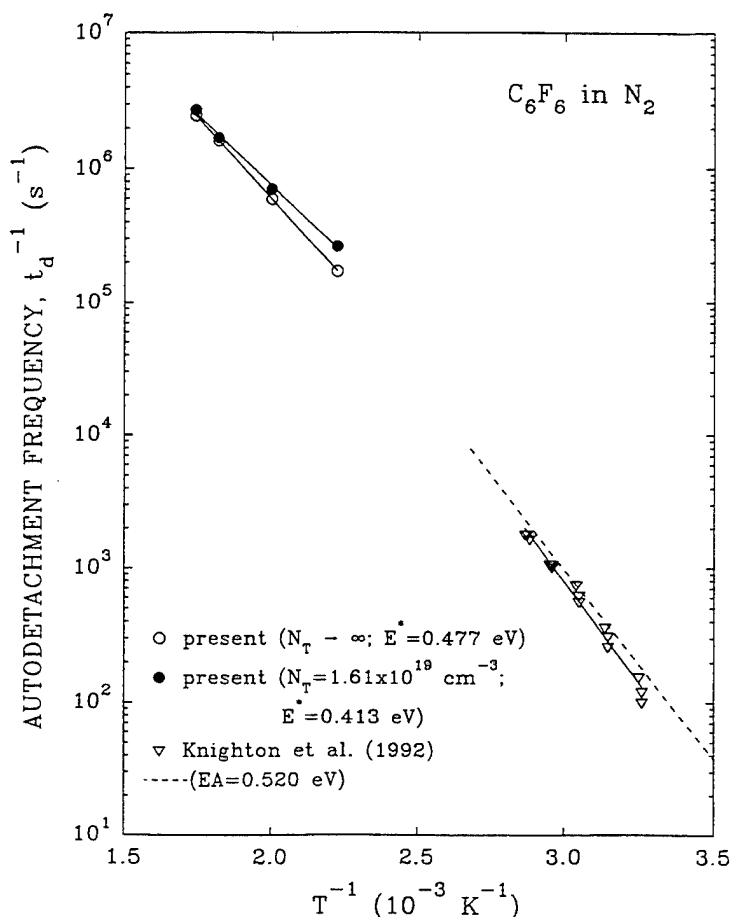
Figure 11. Autodetachment frequency, t_d^{-1} (for $<\varepsilon> \rightarrow 3/2$ kT) for $C_6F_6^-$ as a function of 1/T. The open circles are for $N_T \rightarrow \infty$ and the closed circles for $N_T = 1.61 \times 10^{19}$ molecules cm^{-3}. Also plotted in the figure are the t_d^{-1} data of Ref. 28 extracted from Fig. 9 of that paper. The slope of the solid line through their data corresponds to an E^* of 0.603 eV. The broken line through their data corresponds to an E^* value of 0.52 eV which is the value reported by Ref. 27 for the EA of C_6F_6 [from Ref. 22a].

stabilized $C_6F_6^-$ (i.e., for total pressure $N_T \rightarrow \infty$). This value of E^* would correspond to the case where virtually all negative ions reach the ground electronic state of the neutral molecule adiabatically from the lowest internal energy state of $C_6F_6^-$. It should, thus, compare well--as indeed it does-- with the electron affinity (EA) value of 0.52 eV reported for C_6F_6 by Chowdhury et al.[27] Both of these values were basically determined by looking at the autodetachment reaction (4): that of Ref. 22a by monitoring the autodetached electrons at microsecond and sub-microsecond times and that of Ref. 27 by monitoring the decline of the negative ion number density as a function of time at long (ms) time scales.

112

ELECTRON ATTACHMENT TO ELECTRONICALLY EXCITED MOLECULES

In this section we shall describe briefly recent work on the <u>dissociative</u> attachment of slow electrons to electronically excited molecules prepared by laser light prior to or concomitantly with the generation of the attaching electrons. For these studies new techniques have been devised and are briefly discussed later in this section.

We shall separate these studies into two groups. The first group deals with metastable, long-lived (lifetimes $> 10^{-5}$ s) electronic states produced directly or indirectly (via internal conversion and intersystem crossing from higher-lying excited states initially reached by photoexcitation) by single or multiphoton light absorption, viz.

$$nh\nu(n\geq1) + AX \rightarrow AX^* \xrightarrow{+e} AX^{*-} \begin{cases} \rightarrow AX^{(*)} + e \\ \rightarrow A + X^- \end{cases} \qquad (12)$$
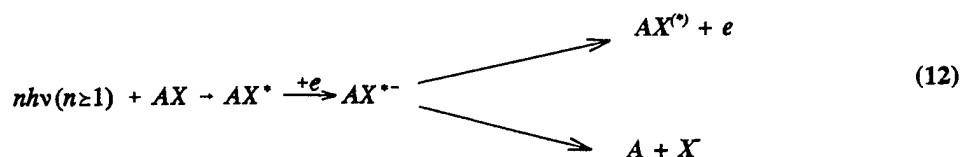
The second group involves short-lived ($< 10^{-6}$ s) or very short-lived (superexcited) electronic states

$$nh\nu(n>1) + AX \rightarrow AX^{**} \xrightarrow{+e} AX^{**-} \begin{cases} \rightarrow AX^{(*)} + e \\ \rightarrow A + X^- \end{cases} \qquad (13)$$
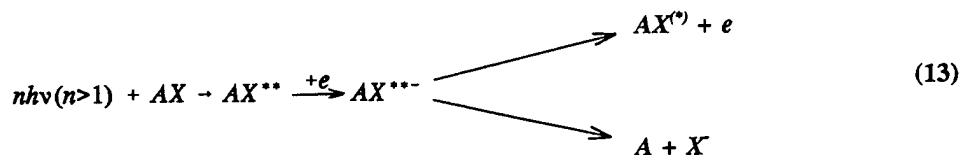
The excited AX^* and superexcited AX^{**} molecules may dissociate into vibrationally or electronically excited neutral fragments. Studies of electron attachment to vibrationally excited photofragments have been reported,[8,29] but, to our knowledge, electron attachment to electronically excited photofragments has not been observed to date.

Prior to discussing the results of these recent studies, it is important to note that electron capture accompanied by simultaneous electronic excitation of the molecule--thus leading to two electrons in normally unfilled molecular orbitals (MOs)--has long been known to manifest itself as resonances in dissociative electron attachment and in electron scattering[1-4,30]. They can be represented by the reaction

$$e_f + AX \rightarrow [AX^*----e_s] \rightarrow AX^{*-} \begin{cases} \rightarrow AX^{(*)} + e \\ \rightarrow A + X^- \end{cases} \qquad (14)$$
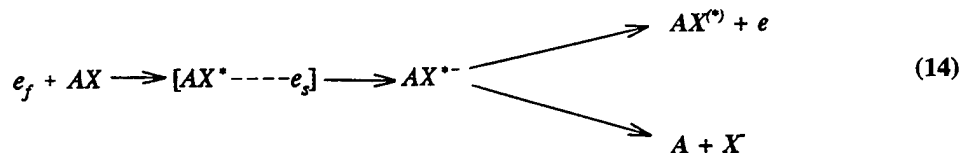
That is, their production involves concomitant electronic excitation of the molecule AX by the "fast" electron e_f which--having lost virtually all of its kinetic energy to exciting electronically the molecule--is "thermalized" in the very vicinity of the electronically excited molecule it produced and is quickly captured by it with a large cross section. The unstable anion AX^{*-} normally decays very quickly (within $< 10^{-12}$ s) by autodetachment and/or autodissociation. It has, however, been found that in certain cases [e.g., p-benzoquinone[31], aromatic hydrocarbon molecules with electron affinities > 0.5 eV (Ref. 32)] the intermediate AX^{*-} lives long enough ($> 10^{-5}$ s) to be detected directly as a parent anion in conventional mass spectrometers. This accounts[31,32] for the observation of negative ion resonances due to long-lived parent negative ions at electron energies well above thermal and with much larger cross sections than at thermal energies.

Experimental Techniques

The observation of electron attachment to electronically excited molecules requires production of an appreciable number of excited molecules and conditions such that electron attachment to the excited molecules occurs within their lifetimes. Since the electronically excited states of most molecules lie a few eV above the ground state, the excimer laser lines are ideal for these studies. With the availability of pulse energies of ~ 100 mJ in 10-20 ns pulses at the XeF (355 nm, 3.5 eV), XeCl (308 nm, 4.0 eV), KrF (248 nm, 5.0 eV), and ArF (193 nm, 6.4 eV), these lines can produce appreciable quantities of low-lying excited states with monophotonic excitation or high-lying excited states with 2- or 3-photon excitation. With the availability of a dye laser pumped by an excimer laser at the XeCl line, wavelength tunability can be obtained from 320 to ~ 1000 nm with pulse energies of ~ 10 mJ.

Depending on the lifetime of the excited state under study, a number of techniques have been developed[33,34,40,42] for electron attachment studies using pulsed lasers. Those techniques that have been developed by the authors are briefly described below.

Measurements on long-lived ($\tau > 10^{-5}$ s) excited states using high-pressure swarm experiments with pulsed lasers. If the lifetime of the excited state under relatively high ambient pressures (1 - 100 kPa) is longer than ~ 10^{-5} s, the experimental arrangement[33,34] shown in Fig. 12 can be employed. The technique is based on the pulsed Townsend method described earlier[22,25]. Depending on the absorption coefficient at the particular laser
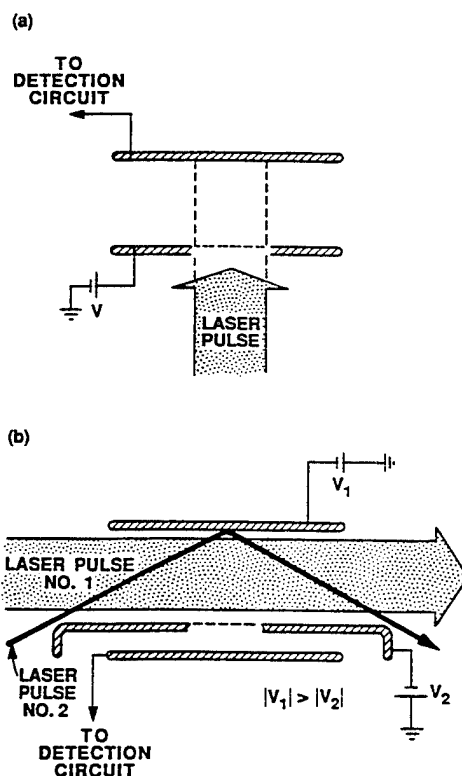
Figure 12. Schematic electrode-laser pulse(s) arrangements used in studies of photoenhanced electron attachment to long-lived (lifetime > 10^{-5} s) electronically excited molecules (see the text and Ref. 34).

114

429

wavelength involved, 0.1 to 100 Pa of the gas under study is mixed with a suitable buffer gas (usually N_2 or Ar) of high pressure (1-100 kPa). In Fig. 12a, a laser pulse enters the interaction region through the gridded bottom electrode, excites the molecules in the interation region, and produces a pulse (or swarm) of electrons at the top electrode. The electron swarm reaches a known steady-state energy distribution within $< 10^{-8}$ s, and drifts through the partially excited gas. The drift time taken by the electrons to reach the bottom electrode is $< 10^{-5}$ s, and thus electron attachment to the excited molecules can take place if the lifetime of the excited molecules is $> 10^{-5}$ s.

The arrangement of Fig. 12b is an improved version of that in Fig. 12a. The production of excited species is decoupled from that of the attaching electrons by using two lasers as shown; thus the time delay between the production of the excited species and the arrival of the attaching electrons in the interaction region can be varied. Furthermore, the use of three electrodes for separating the interaction and the detection regions allows the detection of negatively charged particles unambiguously; by applying suitably oriented electric fields, only the negative charges can be extracted to the bottom detection region through a grid in the middle electrode. This is crucial if positive ions are simultaneously produced (via laser photoionization in the interaction region). However, no direct identification of the negative ions can be made in these experiments although indirect anion identification is possible under certain conditions[35].

Measurements on long-lived ($\tau > 10^{-5}$ s) excited states using electron beam experiments with pulsed lasers. Most excited molecular electronic states undergo collisional destruction in a high pressure environment. If the lifetime of such excited states becomes $< 10^{-5}$ s, the experimental arrangement described in the previous section would not be suitable. Instead, an electron beam apparatus such as shown in Fig. 13 (Ref. 36) can be used to conduct measurements under isolated conditions (pressure $< 10^{-2}$ Pa) where the excited-state lifetime is essentially the radiative lifetime. However, the number of excited species in the collision region is determined by the diffusion of excited molecules out of the collision region (see below and Ref. 36). In the experimental arrangement in Fig. 13 a continuous effusive molecular beam is crossed at right angles with a continuous electron beam (energy resolution ~ 0.1 eV) and a pulsed laser beam, inside a vacuum chamber of base pressure $\sim 10^{-6}$ Pa. The negative ions produced in the interaction region are drawn out by a weak electric field (~ 2 V cm^{-1}) into a quadrupole mass filter and the mass analysed ions are detected with a secondary electron multiplier.

Since the excimer lasers normally used for these experiments have pulse repetition rates of ~ 100 Hz (time delay between consecutive pulses $\sim 10^{4}$ μs), it is important to selectively detect negative ions arriving at the detector within a particular gate time after a preset delay from each laser pulse. The gate delay is associated with the time taken by the (laser-initiated) negative ions to arrive at the detector, and the gate time should be $\le$ minimum $\{\tau, \tau_d\}$, where τ is the lifetime of the excited molecules and τ_d is the time taken by the excited molecules to diffuse out of the interaction region [36].

Measurements on short-lived ($\tau < 10^{-8}$ s) excited states. In order to measure electron attachment to short-lived excited species of lifetime τ produced via a laser pulse of duration τ_L, the electron attachment time, τ_c must be[33]

$$\tau_c < \max \{\tau, \tau_L\} \qquad (15)$$

i.e., electron attachment must occur before the decay of the excited species. For $\tau_L > \tau$, this upper limit is dictated by τ_L since excited species are continuously being produced within the duration of the laser pulse. Therefore, in order to observe electron attachment to short-lived species ($\tau < 10^{-8}$ s) produced by excimer lasers ($\tau_L \sim 10^{-8}$ s), the τ_c must be $< 10^{-8}$ s. Fortunately, the electron attachment cross sections are orders of magnitude larger for the excited states compared to the corresponding ground states making τ_c short.
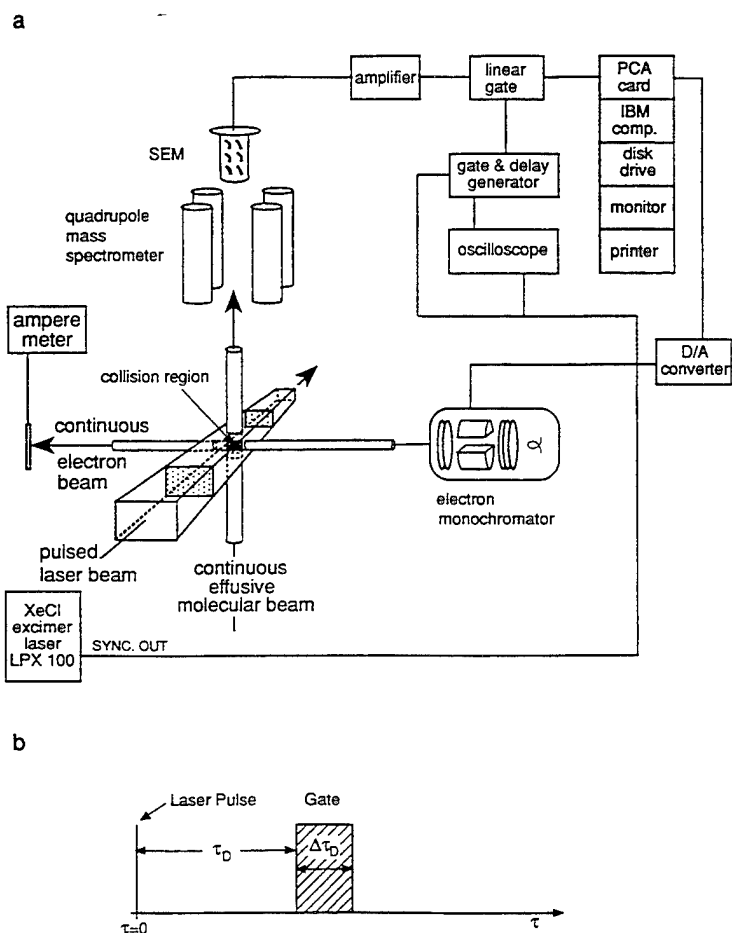
Figure 13. Schematic diagram of an electron spectrometer/mass spectrometer/laser experimental set up and the gate/delay arrangement employed to study electron attachment to electronically excited SO_2 molecules (see the text and Ref. 36).

A technique has been developed[33] to measure electron attachment to short-lived species in a high-pressure (1-50 kPa) environment. The basic idea behind this technique is to produce the excited species and the attaching electrons (via photoionization of the same gas under study or a suitable additive gas) by a single laser pulse (see Fig. 14). Since the excited species and the electrons are produced in close proximity,--depending on the number density and the electron attachment cross section of the excited species--electron attachment can occur in spite of the short τ.

Since in these arrangements positive ions are also produced by photoionization, an inherent requirement of the method is the ability to separate and to detect negative charges (electrons and negative ions) unambiguously. As shown in Fig. 14, this is accomplished by separating the detection region (located between electrodes 2 and 3) from the interaction region (located between electrodes 1 and 2) in a three-electrode arrangement. Charge transmission between the two regions is through a fine grid, which, also, electrically shields the two regions from each other. By applying suitable electric fields in the two regions either positive or negative charges can be extracted to the detection region. In the case of negative charges, the signal components due to electrons and negative ions are distinguished due to the different drift velocities; a "break" in the signal waveform could be easily seen[33,37] when the total pressure in the chamber exceeded ~ 0.1 kPa.

116
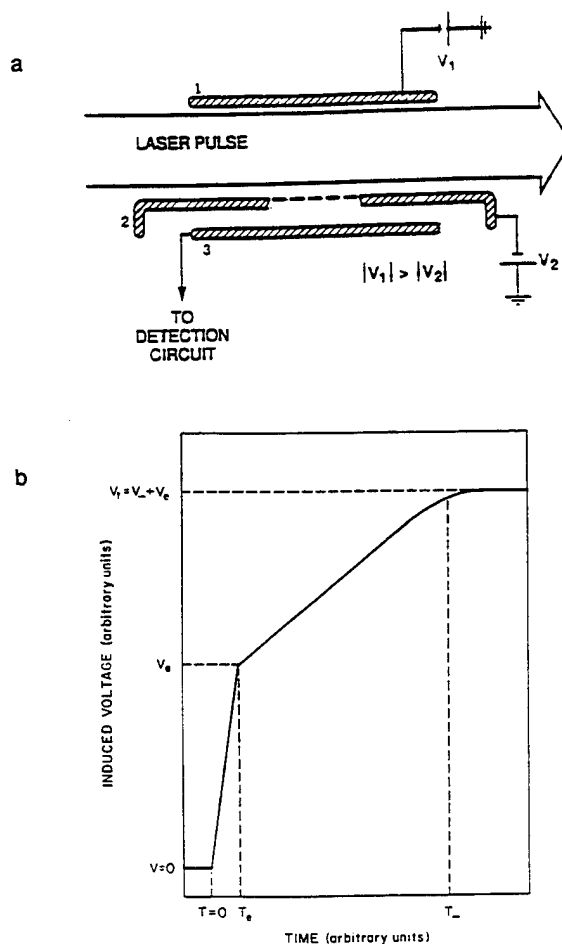
Figure 14. (a) Schematic diagram showing the principle of the technique used to measure electron attachment to short-lived (lifetimes $< 10^{-8}$ s) excited states, and (b) schematic drawing of a typical signal waveform (see the text and Ref. 33).

Dissociative Electron Attachment to Metastable $(\tau \geq 10^{-6}$ s) States

Singlet Oxygen. Electron attachment measurements on pre-prepared electronically-excited molecules was first carried out[38] on the low-lying (excitation energy ~ 1 eV), extremely long-lived (lifetime ~ 2700 s) a $^1\Delta_g$ state of O_2. An electron beam apparatus was employed and the excited molecules produced in a microwave discharge were introduced to the interaction region via a Pyrex tubing; due to the long lifetime of the a $^1\Delta_g$ state, the other aspects of the experiment were the same as for ground state molecules. The cross section for O$^-$ production via the O_2^{-*} ($^2\Pi_u$) state was shown to be ~ 3-4 times larger for the a $^1\Delta_g$ state compared to the $^3\Sigma_g^-$ ground state. Two additional O$^-$ production channels [via the O_2^- ($^2\Sigma_g^+$) state] involving the a $^1\Delta_g$ state were found and studied in two subsequent studies[39,40]. In Fig. 15 are shown the measured[40] cross sections for O$^-$ from the ground state $^3\Sigma_g^-$ of O_2 via the negative ion state $^2\Pi_u$ and from the excited state a $^1\Delta_g$ of O_2 via the negative ion states $^2\Pi_u$ and $^2\Sigma_g^+$.
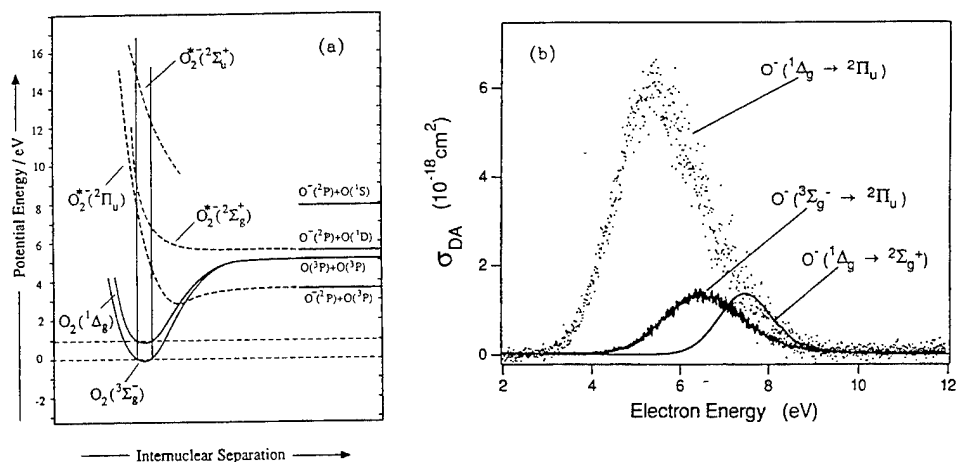
Figure 15. (a) Schematic potential energy diagrams for $O_2(^3\Sigma_g^-)$, $O_2(^1\Delta_g)$, and O_2^- $(^2\Pi_u, {}^2\Sigma_u^+)$. The broken curves refer to the negative ion states relevant to dissociative attachment. (b) Comparison of the cross section for the production of O^- from singlet O_2 via the $^2\Pi_u$ and $^2\Sigma_g^+$ negative ion states with that for O^- from the ground state O_2 via the $^2\Pi_u$ negative ion state (from Ref. 40).

First excited triplet state of thiophenol. The first observation of optically enhanced electron attachment to electronically excited states was reported[34,41] for the first excited triplet state, T_1, of thiophenol (PhSH) using the technique described earlier (Fig. 12a). This state is located ~ 4 eV above the ground state and has a lifetime of ~ 6 ms; it was excited indirectly (via internal conversion (IC) and intersystem crossing (ISC) from higher optically allowed states, S_n) using the 248 nm KrF excimer laser line:

$$PhSH + h\nu(KrF) \longrightarrow PhSH^*(S_n) \quad (optically\text{-}allowed)$$

$$PhSH^*(S_n) \xrightarrow{\ IC\ } PhSH^*(S_1) \xrightarrow{\ ISC\ } PhSH^*(T_1) \tag{16}$$

$$\sim 10^{-13}\ s \qquad\qquad \sim 10^{-11}\text{-}10^{-8}\ s$$
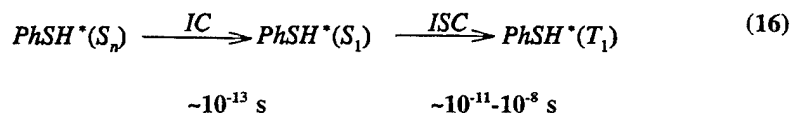
The measured electron attachment coefficient, η/N_a, for the ground and the excited state is shown in Fig. 16: data for curve 1 are for the ground state molecule and were obtained in a separate experiment without using lasers; curve 2 was obtained with 308 nm XeCl excimer laser line and yielded ground state attachment data (the photon energy is 4 eV at the XeCl line and lies below the first excited singlet state S_1 of PhSH); curve 3 was obtained using the KrF line and shows a large enhancement in electron attachment especially at low E/N values (low electron energy). Since only ~ 1 percent of the molecules are excited by a laser pulse, the actual enhancement in electron attachment at thermal energies was shown[34] to be ~ 10^5. This enhancement was attributed to the dissociative electron attachment to the -PhSH(T_1) state produced indirectly via (16).

The curves 4-7 of Fig. 16 show the measured η/N_a for a double laser pulse experiment where the gas was irradiated with one pulse and electron attachment was measured 12.5 ms later when the attaching electrons were produced by a second similar laser pulse[41]. This
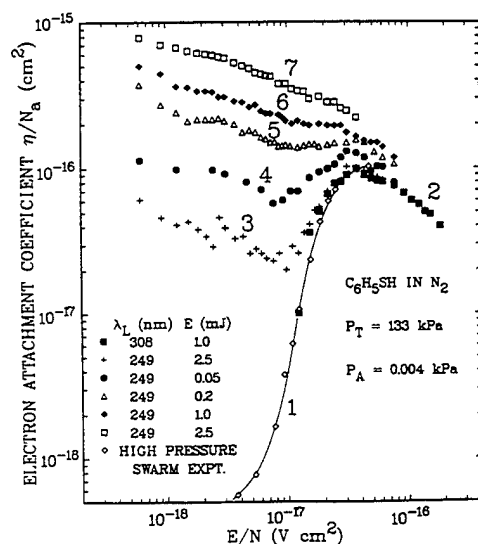
118   433

Figure 16. Electron attachment coefficient η/N_a versus E/N for C_6H_5SH in N_2 for the ground-state (curves 1 and 2) and the first-excited triplet state (curve 3) molecules. Curves 4-7 are photoenhanced attachment due to stable photoproducts formed in a double laser-pulse experiment [see the text and Refs. 34 and 41).

delayed photoenhanced attachment was studied in detail[34] and was shown to be due to electron attachment to diphenyl disulfide ($C_6H_5SSC_6H_5$) produced by the interaction of thiophenoxy radicals ($C_6H_5S^{\cdot}$) formed directly or indirectly via the first laser pulse.

The $A^2\Sigma^+$ state of NO. In this study a pulsed molecular beam was allowed to interact simultaneously with a beam of low energy electrons and a pulsed tunable laser beam[42]. The detector signal was measured with a gated integrator. As the laser wavelength was scanned several peaks appeared for the mass-resolved O^- signal in the wavelength range 226-227 nm. The wavelengths at which this enhancement occurred was shown to correspond to the (0,0) band of the $A^2\Sigma^+$ - X $^2\Pi$ band system of NO; thus, the photonenhanced signal was attributed to dissociative electron attachment to the $A^2\Sigma^+$ ($v = 0$) state of NO. The cross section for this process was estimated[42] to be at least a factor of ten greater than the maximum cross section for the ground state, which is 10^{-18} cm^2 at 8.1 eV.

First excited triplet states of p-benzoquinone and its methylated derivatives. This study was conducted[43] using an electron capture detector (ECD) with a xenon arc lamp as the excitation light source; a monochrometer of 20 nm bandwidth was used for wavelength selection. The ECD current was monitored during the gas chromatographic (GC) introduction of the compound of interest with and without light irradiation. The ECD response was simply the decrease in current due to electron attachment.

Similar to the study on PhSH(T_1) described earlier, the first excited triplet states of p-benzoquinone and its methylated derivatives were populated indirectly via higher-lying, optically-allowed singlet states. The lifetimes of the first excited triplet states of these molecules were ~ 30 μs and were independent of the pressure of the buffer gases argon or nitrogen employed. The estimated enhancement[43] in electron attachment was 10^5 to 10^7 which is quite similar to the enhancement estimated for PhSH(T_1) compared to the ground state.

Low-lying electronically-excited states of SO_2. Recently an electron attachment study[36] on XeCl-laser-irradiated SO_2 was conducted using the electron beam technique outlined

434

earlier (Fig. 13). This investigation identified many of the experimental difficulties associated with electron beam studies of electron attachment to electronically-excited molecules, and illustrated how to overcome such difficulties and extract the relevant information on electron attachment to excited species[36].

Previous electron beam experiments[1,4,44] on the _ground_ electronic state of SO_2 have established the following dissociative attachment channels:

$$
\begin{array}{lll}
 & & \varepsilon_{max}\ (eV) \\
 & O^- + SO & 4.55;7.3 \quad (17a) \\
e + SO_2\ (\tilde{X}^1A_1) \longrightarrow SO_2^{*-} \longrightarrow SO^- + O & 4.85 \quad\ (17b) \\
 & S^- + O_2 & 4.2;7.4 \quad (17c)
\end{array}
$$
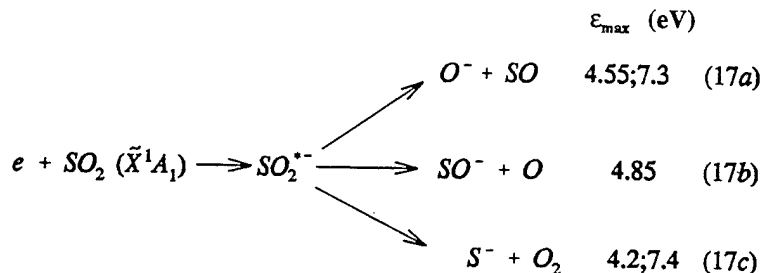
where ε_{max} indicates the electron energies at the peak values of electron attachment cross sections. The maximum cross section for O^- formation (17a) was 2.46×10^{-18} cm^2 at 4.55 eV.

In the experiments of Ref. 36, enhanced O^- formation due to XeCl laser irradiation was studied in detail (enhanced SO^- and S^- formation was also observed). Figure 17a shows the O^- ion yield (monitored continuously) in the absence of laser irradiation, where the peaks due to the ground state process (17a above) can be clearly seen. Figure 17b shows the O^- signal with the laser on (laser repetition rate ~ 150 Hz) and with other conditions kept the same as for Fig. 17a; while the ground state process has not significantly changed, the laser-induced signal at electron energy of < 0.5 eV can hardly be seen without 100-fold amplification. This is due to the discrimination of the photoenhanced signal against the ground state signal by more than a factor of 1000: the ground state process generated O^- continuously while the photoenhanced process contributed only during a few μs per each laser pulse. This short time window available for electrons to interact with excited molecules is due to two factors, (i) decay of excited states, and (ii) the escape of excited states from the interaction region; the actual time available for collisions is the smaller of these two times. This was confirmed in an experiment[36] where the photoenhanced O^- signal was detected only during a 1 μs gate time following different time delays from the firing of the laser. Even though the lifetimes of the relevant excited states were > 50 μs (see below), the photoenhanced signal prevailed only for ~ 4.5 μs following the firing of the laser; this compared well with the estimated[36] "escape time" of ~ 4 μs.

When gated experiments were conducted where the O^- signal was detected only for a few μs following each laser pulse (with laser beam blocked and unblocked) the photoenhanced signal became more prominent, see the solid line of Fig. 17c; when this experimental curve was corrected for the variation of the electron beam current with electron energy, the dotted line of Fig. 17c was obtained. However, since only a fraction of SO_2 molecules are excited by each laser pulse, the photoenhanced signal shown by the dotted line is still not a good presentation of the actual enhancement. The peak cross section for the photoenhanced O^- formation was estimated[36] to be at least 2 orders of magnitude larger than the peak cross section (2.46×10^{-18} cm^2) for O^- formation from the ground state.

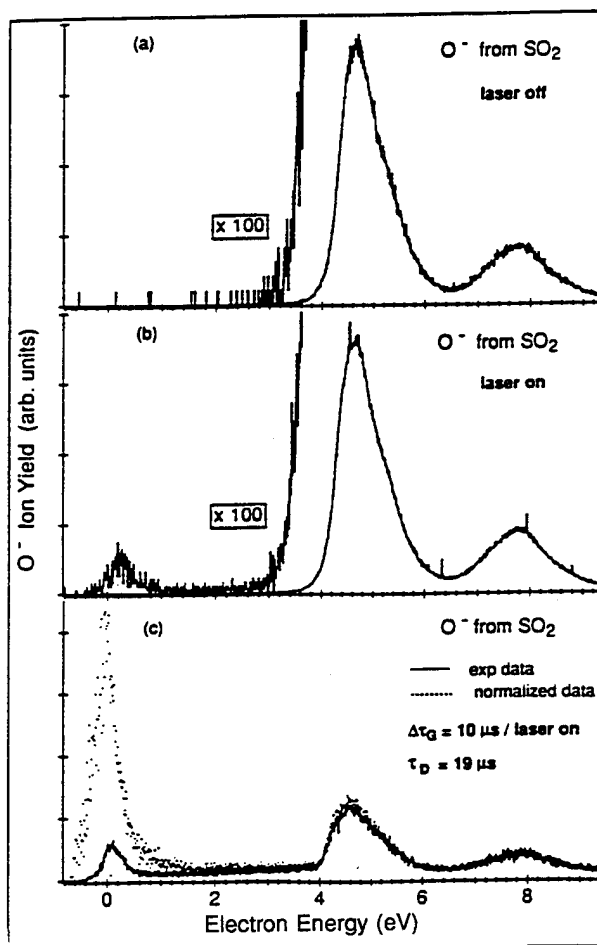This observed photoenhanced O^- signal from XeCl-laser-irradiated SO_2 was attributed to the reaction :

Figure 17. Relative cross section for the production of O⁻ from SO₂ as a function of the electron energy. (a) Ground state SO₂ (laser off). (b) Ground and excited SO₂; laser on (308 nm XeCl excimer laser) but no gating; (c) as in (b), but with a gate of 10 µs and a time delay (between the firing of the laser and the negative ion detection) of 3 µs: (---) experimental data; (--•-•) experimental data corrected for the variation of the electron current with energy and normalized at 8 eV (see the text and Ref. 36).
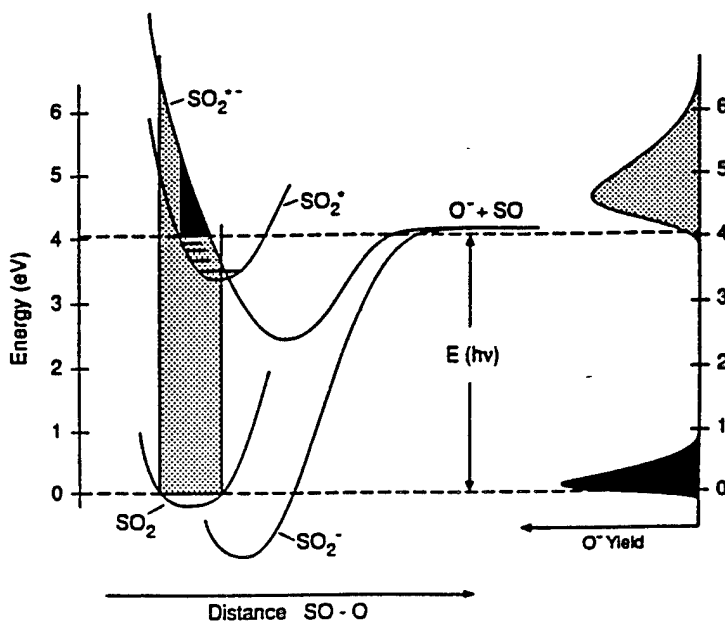
Figure 18. Schematic potential energy diagrams illustrating electron attachment to ground SO_2 and electronically excited SO_2^* (see the text and Ref. 36).

$$h\nu(308nm) + SO_2 \longrightarrow SO_2^*(^1B_1 \ or \ ^1A_2) \xrightarrow{+e(<0.5eV)} SO_2^{*-} \longrightarrow O^- + SO \quad (18)$$
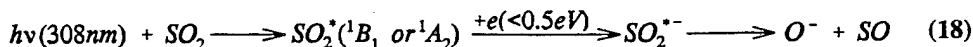
i.e., dissociative electron attachment to the $^1B_1$ or $^1A_2$ states of SO_2 with lifetimes 50 and 80-530 μs respectively[36,45]. Figure 18 shows a schematic potential energy diagram illustrating electron attachment to SO_2 and electronically-excited SO_2^*. The electron energy required for the transition from SO_2^* to SO_2^{*-} is small, and thus the photoenhanced signal (shaded region of Fig. 18) appears at close to zero energy. The photoenhanced resonance is also narrower, due to the change in the equillibrium distance for SO_2^* compared to SO_2[36].

SO_2 is a "Douglas molecule,"[45] and along with other such molecules (e.g., CS_2, NO_2) are good candidates to study since they have long-lived electronically-excited states which do not readily dissociate when excited by easily available laser wavelengths.

Dissociative Electron Attachment to Short-Lived ($\tau < 10^{-8}$ s) States

Very efficient electron attachment to superexcited states, SESs, (electronically excited states lying above the first ionization threshold of molecules) was also reported[33]. Even though these highly energy rich states are short-lived, the presence of low-energy electrons in their close vicinity together with their implied extraordinarily large cross sections for electron attachment make it possible for electron attachment to occur within the short lifetimes of the SESs.

Triethylamine. This and other methylated amine compounds do not attach electrons significantly in their ground electronic states (electron attachment rate constants $< 10^{-11}$ cm^3 s^{-1} at electron energies < 1 eV). However, with excimer laser irradiation (at the KrF, KrCl, and ArF lines) efficient negative ion formation was observed in these compounds. Based on extensive experimental studies[33] on the dependencies of the total (electron plus negative ion) and negative ion signals on the laser fluence, amine partial pressure, buffer gas pressure

437

122

and the applied electric field this laser enhanced electron attachment was attributed to the laser-excited superexcited states of these molecules.

Due to the space limitations we only wish to point out one unique aspect of these studies involving short-lived excited species. The dependence of the negative ion signal on the applied electric field at the KrF line is shown in Fig. 19 for triethylamine; these data were taken with two different buffer gases (Ar and N_2) and over a range of pressure (1.33 to 66.7 kPa). It is clear that the negative ion signal depends only on E, and does not depend significantly on either the identity of the buffer gas or the E/P (i.e., E/N) value. In a conventional electron swarm experiment, one would expect a different behavior, since an
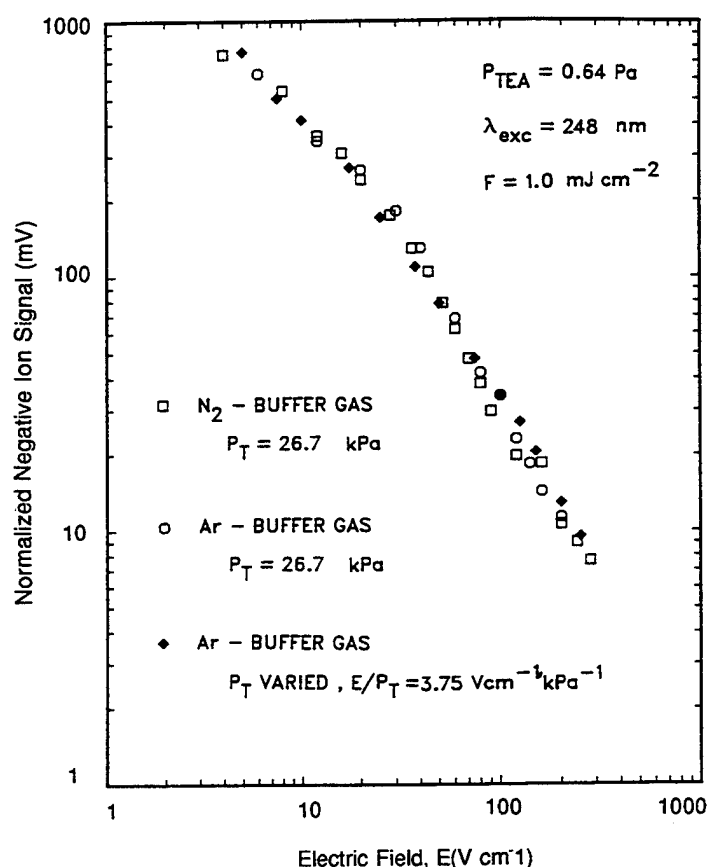
Figure 19. Electric field dependence of the normalized negative ion signal in laser irradiated triethylamine for the experimental parameters shown in the figure (see the text and Ref. 33).

electron allowed to reach steady-state conditions (within ~ 10^{-6} - 10^{-8} s) would have very different energies under these different conditions. In the present case, the electrons are attached just after they are produced (via photoionization) and well before any significant energy exchange occurs via collisions with the buffer gas. The electron attachment time must be less than the duration of the laser pulse which is ~ 10^{-8} s.

Nitric Oxide. In NO, electron attachment to the superexcited states was observed using the KrF excimer laser line and also at several wavelengths from a dye laser pumped by a

XeCl excimer laser[37]. In the case of dye-laser irradiation, resonance enhanced multiphoton ionization (REMPI) experiments were conducted first to determine the resonance wavelengths for optimum ionization signal. Since the attaching electrons in this technique are produced via photoionization, it is essential to have a large enough number of electrons (~ 10^{-8}) per laser pulse[33] to quantify the measurements.

Similar to the amine compounds, no significant buffer gas pressure dependence was observed at 454.433 nm dye laser radiation, and the laser fluence dependence for negative ion formation was consistent with electron attachment to SESs. However, in the case of the KrF line the negative ion signal increased with the increase of buffer gas pressure, even though the total signal (and hence photoionization signal) did not depend on the buffer gas pressure. At the KrF line, the excess energy of the ionized electron is ~ 0.7 eV, and the collision time with N_2 at the pressures employed is < 10^{-10} s (Ref. 37). Thus, there was enough time for the electron to lose some energy via collisions and therefore to attach more efficiently. Previous photoelectron energy measurements had shown[46] that while near-zero-
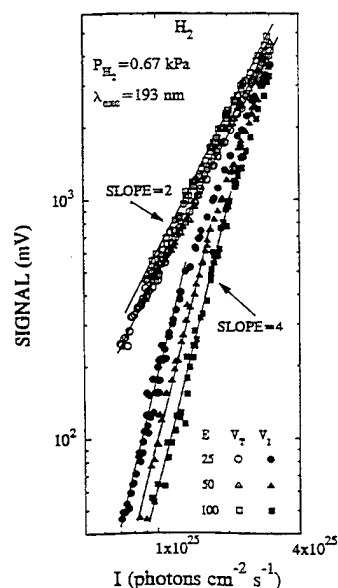
Figure 20. Laser intensity, I dependence of the measured total, V_T, and negative ion, I_I, signal for H_2 for the experimental parameters shown in the figure (see the text and Ref. 47).

energy electrons were produced at the dye-laser wavelength,--and hence energy loss was not needed--they were not produced at the KrF line.

Hydrogen and Deuterium. Due to their comparatively high ionization thresholds (~ 15.4 eV) it was not possible to obtain high ionization yield for H_2 and D_2 via frequency-doubled dye laser radiation. However, due to the serendipitous coincidence of the 2-photon energy of the ArF excimer laser line with the E,F $^1\Sigma_g^+$ ($\upsilon = 6$) state, it was possible to carry out qualitative measurements at that laser line.

The laser intensity I dependence of the total signal and the negative ion signal are shown in Fig. 20 for H_2 irradiated by the ArF laser. The apparent I^2 dependence observed for the

124

3-photon photoionization process is due to the strong photon absorption from the E,F state[47]; since the excitation of a SES in turn should be an apparent 2-photon process, the observed I^4 dependence for negative ion formation is consistent with the attachment of an electron produced via photoionization to a molecule in SES, or an attaching species produced via a SES. Qualitatively similar results were obtained for D_2.

Nitrogen. No photoenhanced electron attachment was observed for N_2 (Ref. 47). This is to be expected since neither N_2 nor N can bind an extra electron.

CONCLUDING REMARKS

The internal energy of molecules plays a crucial role in determining their electron attachment properties. Dissociative electron attachment to "hot" (rotationally/vibrationally excited) molecules, and especially to electronically excited molecules, can be orders of magnitude larger than for ground state molecules. Nondissociative electron attachment to "hot" molecules decreases due to enhanced autodetachment. The experimental techniques that are now available for the systematic study of electron-energy rich molecule collisions will undoubtedly enrich our understanding[2] and increase the potential of this new knowledge for applications such as those involving optical switching, control or modulation of the impedance characteristics of gaseous matter.

REFERENCES

1. Christophorou, L. G., "Atomic and Molecular Radiation Physics," *Wiley-Interscience*, New York (1971).

2. Massey, H.S.W., "Negative Ions," *Cambridge University Press*, London (1976).

3. Smirnov, B. M., "Negative Ions," *McGraw-Hill*, New York (1982).

4. Christophorou, L. G., McCorkle, D. L., and Christodoulides, A. A., Electron Attachment Processes, in "Electron Molecule Interactions and Their Applications," L. G. Christophorou (Ed.), *Academic Press*, New York, 1984, Vol. 1, Chapt. 6.

5. Klar, D., Ruf, M.-W., and Hotop, H., Attachment of Electrons to Molecules at meV Resolution, *Austr. J. Phys.* 45:263 (1992).

6. Illenberger, E., Electron-Attachment Reactions in Molecular Clusters, *Chem. Rev.* 92:1589 (1992).

7. Christophorou, L.G., Electron Attachment and Detachment Processes in Electronegative Gases, *Cotrib. Plasma Phys.* 27:237 (1987).

8. Christophorou, L. G., Electron-Excited Molecule Interactions, in "Invited Papers, Proc. XXth Intern. Conf. Ionization Phenomena in Gases," V. Palleschi, D. P. Singh, and M. Vaselli (Eds.), Institute of Atomic and Molecular Physics, CNR, Pisa, Italy, July 8-12, 1991, pp. 3-13.

9. Christophorou, L. G., The Lifetimes of Metastable Negative Ions, *Adv. Electr. Electron Phys.*, 46:55 (1978).

10. Allan, M. and Wong, S. F., (a) Effect of Vibrational and Rotational Excitation on Dissociative Attachment to Hydrogen, *Phys. Rev. Lett.* 41:1791 (1978); (b) Dissociative Attachment from Vibrationally and Rotationally Excited HCl and HF, *J. Chem. Phys.* 74:1687 (1981).

11. Spyrou, S. M., and Christophorou, L. G., Effect of Temperature on the Dissociative Electron Attachment to $CClF_3$ and C_2F_6, *J. Chem. Phys.* 82:2620 (1985).

---

[2]The scattering of slow electrons from excited atoms is greatly enhanced compared to ground state atoms principally because of the larger polarizabilities of the excited states[48].

12. Chantry, P. J. and Chen, C. L., Ionization and Temperature Dependent Attachment Cross Section Measurements in C_3F_8 and C_2H_3Cl, *J. Chem. Phys.* 90:2585 (1989).

13. Datskos, P. G. and Christophorou, L. G., Variation with Temperature of the Electron Attachment to SO_2F_2, *J. Chem. Phys.* 90:2626 (1989).

14. Datskos, P. G., Christophorou, L. G., and Carter, J. G., (a) Temperature Enhanced Electron Attachment to CH_3Cl, *Chem. Phys. Lett.* 168:324 (1990); (b) Effect of Temperature on the Attachment of Slow ($<$ 1 eV) Electrons to CH_3Br, *J. Chem. Phys.* 97:9031 (1992).

15. O'Malley, T. F., Calculation of Dissociative Attachment to Hot O_2, *Phys. Rev.* 155:59 (1967).

16. Bardsley, J. N. and Wadehra, J. M., (a) Dissociative Attachment and Vibrational Excitation in Low-Energy Collisions of Electrons with H_2 and D_2, *Phys. Rev. A* 20:1398 (1979); (b) Dissociative Attachment to HCl, DCl, and F_2, *J.Chem. Phys.* 78:7227 (1983).

17. Teillet-Billy, D. and Gauyacq, J. P., Dissociative Attachment in e-HCl, DCl Collisions, *J. Phys. B* 17:4041 (1984).

18. Hickman, A.P., Dissociative Attachment of Electrons to Vibrationally Excited H_2, *Phys. Rev. A* 43:3495 (1991).

19. Spyrou, S. M. and Christophorou, L. G., (a) Effect of Temperature on Nondissociative Electron Attachment to Perfluorobenzene, *J. Chem. Phys.* 82:1048 (1985); (b) Effect of Temperature on the Dissociative and Nondissociative Electron Attachment to C_3F_8, *J. Chem. Phys.* 83:2829 (1985).

20. Adams, N. G., Smith, D., Alge, E., and Burdon, J., Anomalous Temperature Dependence of the Coefficient of Electron Attachment to Hexafluorobenzene, *Chem. Phys. Lett.* 116:460 (1985).

21. Christodoulides, A.A., Christophorou, L. G., and McCorkle, D. L., Effect of Temperature on the Low-Energy ($<$ 1 eV) Electron Attachment to Perfluorobutane (c-C_4F_8), *Chem. Phys. Lett.* 139:350 (1987).

22. Datskos, P. G., Christophorou, L. G., and Carter, J. G., (a) Temperature Enhanced Electron Detachment From $C_6F_6^-$ Negative Ions, *J. Chem. Phys.* 98:7875 (1993); (b) Temperature Dependence of Electron Attachment and Detachment in SF_6 and c-C_4F_6, *J. Chem. Phys.* (submitted).

23. (a) Alge, E., Adams, N. G., and Smith, D., Rate Coefficients for the Attachment Reactions of Electrons with c-C_7F_{14}, CH_3Br, CF_3Br, CH_2Br_2, and CH_3I Determined Between 200 and 600 K Using the FALP Technique, *J. Phys. B* 17:3827 (1984).

24. Chen, C. L. and Chantry, P. J., Photon-Enhanced Dissociative Electron Attachment in SF_6 and Its Isotopic Selectivity, *J. Chem. Phys.* 71:3897 (1979).

25. Hunter, S. R., Carter, J. G., and Christophorou, L. G., Electron Transport Measurements in Methane Using an Improved Townsend Technique, *J. Appl. Phys.* 60:24 (1986).

26. Wen, C. and Wetzer, J.M., (a) Electron Avalanches Influenced by Detachment and Conversion . Processes, *IEEE Trans. Electr. Insul.* 23:999 (1988); (b) Time-Resolved Avalanches Current Waveforms in Octafluorocyclobutane, *IEEE Trans. Electr. Insul.* 24:143 (1989).

27. Chowdhury, S., Grimsrud, E. P., Heinis, T., and Kebarle, P., Electron Affinities of Perfluorobenzene and Perfluorophenyl Compounds, *J.Am. Chem. Soc.* 108: 3630 (1986).

28. Knighton, W. B., Bognar, J. A., and Grimsrud, E. P., Thermal Electron Detachment Rate Constants for the Molecular Anion of Perfluorobenzene, *Chem. Phys.Lett.* 192:522 (1992).

29. Rossi, M. J., Helm, H., and Lorents, D. C., Photoenhanced Electron Attachment to Vinylchloride and Trifluoroethylene at 193 nm, *Appl. Phys. Lett.* 47:576 (1985).

30. Schulz, G. J., Resonances in Electron Impact on Diatomic Molecules, *Rev. Mod. Phys.* 45:423 (1973).

31. (a) Christophorou, L. G., Carter, J. G., and Christodoulides, A. A., Long-Lived Parent Negative Ions in p-Benzoquinone Formed by Electron Capture in the Field of the Ground and Excited States, *Chem. Phys.Lett.* 3:237 (1969); (b) Collins, P. M., Christophorou, L.G., Chaney, E. L., and Carter, J. G., Energy Dependence of the Electron Attachment Cross Section and the Transient Negative Ion Lifetime for p-Benzoquinone and 1,4-Naphthoquinone, *Chem. Phys. Lett.* 4:646 (1970).

32. Tobita, S., Meinke, M., Illenberger, E., Christophorou, L. G., Baumgärtel, H., and Leach, S., Polycyclic Aromatic Hydrocarbons: Negative Ion Formation Following Low Energy (0-15 eV) Electron Impact, *Chem. Phys.* 161:501 (1992).

33. Pinnaduwage, L. A., Christophorou, L. G., and Bitouni, A. P., Enhanced Electron Attachment to Superexcited States of Saturated Tertiary Amines, *J. Chem. Phys.* 95:274 (1991).

34. Pinnaduwage, L. A., Christophorou, L. G., and Hunter, S. R., Optically Enhanced Electron Attachment to Thiophenol, *J. Chem. Phys.* 90:6275 (1989).

35. Pinnaduwage, L. A. and Christophorou, L. G., Verification of H⁻ Formation in UV Laser Irradiated Hydrogen; Implication for Negative Ion and Neutral Beam Technology, *J. Appl. Phys.* (submitted, 1993).

36. Jaffke, T., Hashemi, R., Christophorou, L. G., Illenberger, E., Baumgärtel, H., and Pinnaduwage, L. A., Photoenhanced Dissociative Electron Attachment to SO_2, *Chem. Phys. Lett.* 203:21 (1993).

37. Pinnaduwage, L. A. and Christophorou, L. G., Enhanced Electron Attachment to Superexcited States of Nitric Oxide, *Chem. Phys. Lett.* 186:4 (1991); erratum 189:486 (1992).

38. Burrow, P. D., Dissociative Attachment From the $O_2(a\ ^1\Delta_g)$ State, *J. Chem. Phys.* 59:4922 (1973).

39. Belić, D. S. and Hall, R.I., Dissociative Electron Attachment to Metastable Oxygen (a $^1\Delta_g$), *J. Phys. B* 14:365 (1981).

40. Jaffke, T., Meinke, M., Hashemi, R., Christophorou, L. G., and Illenberger, E., Dissociative Electron Attachment to Singlet Oxygen, *Chem. Phys. Lett.* 193:62 (1992).

41. Christophorou, L. G., Hunter, S. R., Pinnaduwage, L. A., Carter, J. G., Christodoulides, A. A., and Spyrou, S. M., Optically Enhanced Electron Attachment, *Phys. Rev. Lett.* 58:1316 (1987).

42. Kuo, C. T., Ono, Y., Hardwick, J. L., and Moseley, J. T., Dissociative Attachment of Electrons to the A $^2\Sigma^+$ State of Nitric Oxide, *J. Phys. Chem.* 92:5072 (1988).

43. Mock, R. S. and Grimsrud, E. P., Optically Enhanced Electron Capture by p-Benzoquinone and Its Methylated Derivatives, *J.Phys. Chem.* 94:3550 (1990).

44. Spyrou, S. M., Sauers, I., and Christophorou, L. G., Dissociative Electron Attachment to SO_2, *J. Chem. Phys.* 84:239 (1986).

45. Okabe, H., "Photochemistry of Small Molecules," *Wiley*, New York, (1978).

46. Miller, J. C. and Compton, R. N., Multiphoton Ionization Studies of Ultracold Nitric Oxide, *J.Chem. Phys.* 84:675 (1986).

47. Pinnaduwage, L. A. and Christophorou, L. G., H⁻ Formation in Laser-Excited Molecular Hydrogen, *Phys. Rev. Lett.* 70:754 (1993).

48. Christophorou, L. G. and Illenberger, E., Scattering of Slow Electrons From Excited Atoms: The Dominant Role of the Polarization Potential, *Phys. Lett. A.* 173:78 (1993).

442

APPENDIX B

L. G. Christophorou, R. Van Brunt, and J. Olthoff, "Fundamental Processes in Gas Discharges," Invited lectures, In <u>Proceedings of the Xith International Conference on Gas Discharges and Their Applications</u>, (In Press).

FUNDAMENTAL PROCESSES IN GAS DISCHARGES

L. G. Christophorou[1,2], R. J. Van Brunt[2] and J. K. Olthoff[2]

[1] Department of Physics, The University of Tennessee, Knoxville, TN 37996
[2] Electricity Division, Electrical and Electronics Engineering Laboratory, National Institute of Standards and Technology, Gaithersburg, MD 20899

ABSTRACT

Recent aspects of fundamental processes in gas discharges are discussed. These include the effect of internal energy of excitation of atoms and molecules on their interactions with slow electrons, the effect of temperature on electron attachment and detachment processes, photodissociation of molecules and photodetachment of anions, and interactions involved in discharge byproduct formation and discharge diagnostics. Reference is also made to fundamental processes in gas discharge materials used in plasma processing.

INTRODUCTION

In this paper an overview is given of recent developments in identifying fundamental processes underpinning the behavior of gas discharges and their applications. Many such processes involve neutral species, positive and negative ions, electrons, and photons. Collectively these processes control the behavior and characteristics of the discharge and its uses. While the study of such processes traces back many decades, fundamental advances have been made recently in certain areas which open up new possibilities, both basic and applied. These are the ones this paper focusses on. We especially emphasize the following: (i) the effect of internal energy of excitation of atoms and molecules on their interactions with slow electrons, (ii) the effect of temperature (rovibrational energy for molecules) on their electron attachment and detachment properties, (iii) photon-molecule and photon-anion interactions and the study of radicals, (iv) basic interactions involved in discharge byproduct formation and discharge diagnostics, and (v) the effect of the medium on fundamental reactions. Reference is also made to a few recent findings on fundamental processes in gas discharge materials used in plasma processing (e.g., silane and halocarbons).

EFFECT OF INTERNAL ENERGY OF EXCITATION OF ATOMS AND MOLECULES ON THEIR INTERACTIONS WITH SLOW ELECTRONS

The interactions of slow electrons with atoms and molecules are functions of not only the kinetic energy of the electron and the target atom or molecule, but also of the internal energy of the latter. While the study of the interactions of slow electrons with ground state atoms and molecules traces back many decades, the study of the interactions of slow electrons with excited

atoms and molecules as a function of their internal energy (electronic and/or rovibrational for molecules) is more recent and more limited. In the past, experimental studies on electron-excited target interactions have been difficult because, the excited species are often short-lived and chemically reactive and because it is difficult to produce sufficient numbers of excited species to study under controlled conditions. Today, however, such studies are becoming increasingly more feasible through the use lasers.

Excited species are of interest in gas discharges (for instance, the importance of the formation and destruction of rare-gas-atom metastables has long been recognized). Recent studies, referred to in this paper, have shown that the cross sections for electron-atom/molecule interactions depend rather strongly on the internal energy content of the atom/molecule and in many instances the cross sections are several orders of magnitude larger than for the ground states, and hence even a small percentage of excited species present in the discharge can alter its behavior. Such knowledge on electron-excited atom/molecule interactions offers unique opportunities for changing the electrical properties of gaseous matter by the use of lasers and has potential applications in other applied areas such as in the development of ultrasensitive analytical instruments.

Examples of these new reactions are given in this section (see, also [1-3]). The limited experimental and theoretical studies to date on slow electron-excited atom/molecule collisions show many and often profound changes in the cross sections for electron scattering, ionization, attachment and detachment. Especially profound are the reported increases in the cross sections for electron scattering from electronically excited atoms and the cross sections for dissociative electron attachment to electronically excited molecules.

Electron Scattering from Excited Atoms and Molecules

In Fig. 1 are compared [4] the total electron scattering cross sections for the ground state CO_2 and for the vibrationally excited CO_2 molecules [mostly in the low-lying (0.083 eV) 01^10 bending mode]. The bending CO_2 vibration has an associated electric dipole moment and it was suggested [4] that the enhancement in the electron scattering cross section is due to the electron-electric dipole moment interaction associated with this bond. The cross sections for slow electron-electric dipole scattering are known to be large [5].
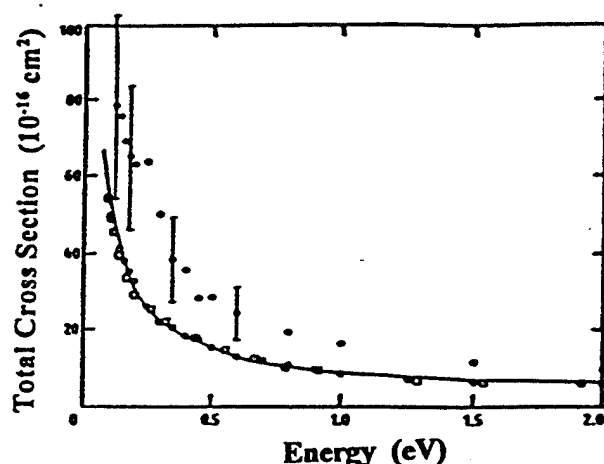
However significant the effects of vibrational excitation on the cross section for electron scattering are, they are much smaller compared to those involving electronically excited atoms and molecules. This can be seen (Fig.2) from the measurements on singlet O_2 where the cross section for excitation of the $b^1\Sigma^+_g$ state of O_2 from the excited state $O_2^*(a^1\Delta_g)$ is more than ten times larger than from the ground state $O_2(X^3\Sigma^-_g)$ [6]. It is further dramatized by the more extensive data on excited atoms (Figs. 3 and 4).

In Fig. 3 are compared the momentum transfer cross section, σ_m, for electron-ground state argon atom [Ar(3 ^{1}S)] scattering [7] with the cross section for elastic scattering of electrons from the
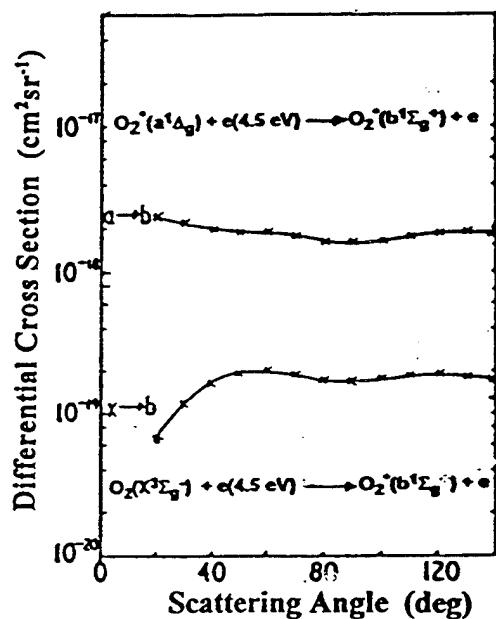
excited argon atom $Ar^*(4^3P_2)$, σ^*_e, calculated by Robinson [8]; the latter cross section exceeds the former substantially [around the Ramsauer-Townsend (R.-T) minimum by about 10^4 times]. The R.-T minimum — so prominent a feature in the cross section for electron scattering from the ground state of the heavier rare gas atoms — is entirely absent from the cross sections for electron scattering from the excited state(s) of the rare gas atoms. This is a consequence of the much larger electric dipole polarizability, α, of the excited state ($\alpha = 318.2\ a_0^3$ [9]; $a_0 = $ Bohr radius) compared to that of the ground state atom ($\alpha = 11.07\ a_0^3$ [9]), and the resultant dominant role of the electron-induced dipole polarization potential in the scattering. The results of a number of calculations clearly show that the cross sections for scattering of slow electrons from excited atoms are large and that they are characterized by a large contribution of higher angular momenta, L, to the total cross section as opposed to the cross sections for electron scattering by ground-state atoms where most of the contributing partial waves have small L values.

The dominant role of the dipole polarizability in electron scattering can be seen from the measurements of the differential electron scattering cross sections from ground and excited atoms. Thus, measurements [10] of the differential electron scattering cross section for excitation by 30 eV electrons of the 2^3P excited state of He from the metastable state 2^3S and from the ground state (1^1S) of He showed (Fig.4) that the cross section for the excited state is up to 10^5 times larger compared to the ground state. The maximum enhancement is for small angles (forward scattering) as is to be expected for the distant
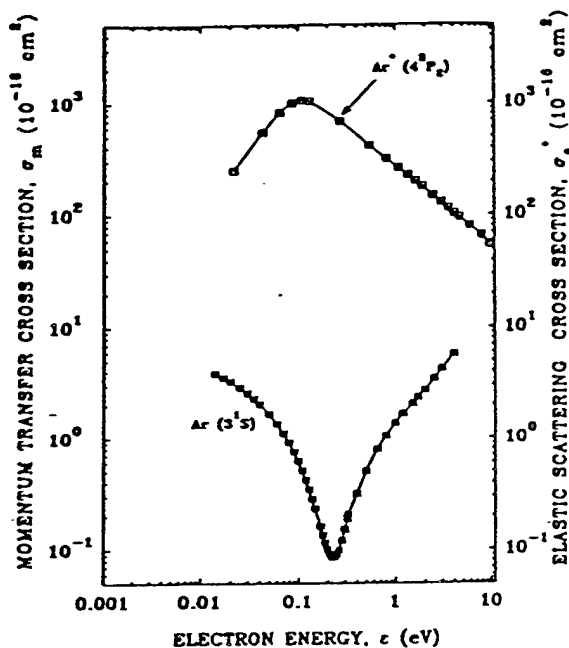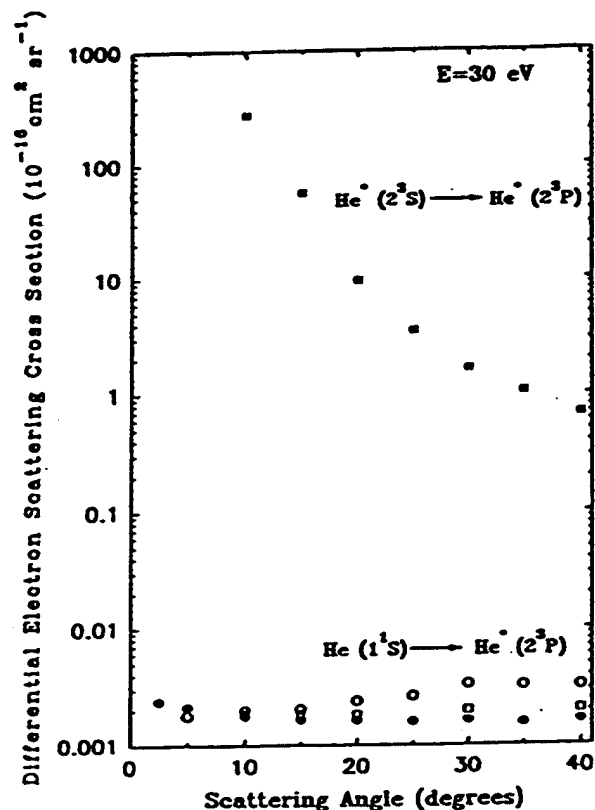
130

Fig. 4 Differential electron scattering cross section as a function of scattering angle for the excitation of the 2^3P state of He from the excited state 2^3S (see [10]) and from the ground state 1^1S (from [2]) of the He atom by 30 eV electrons
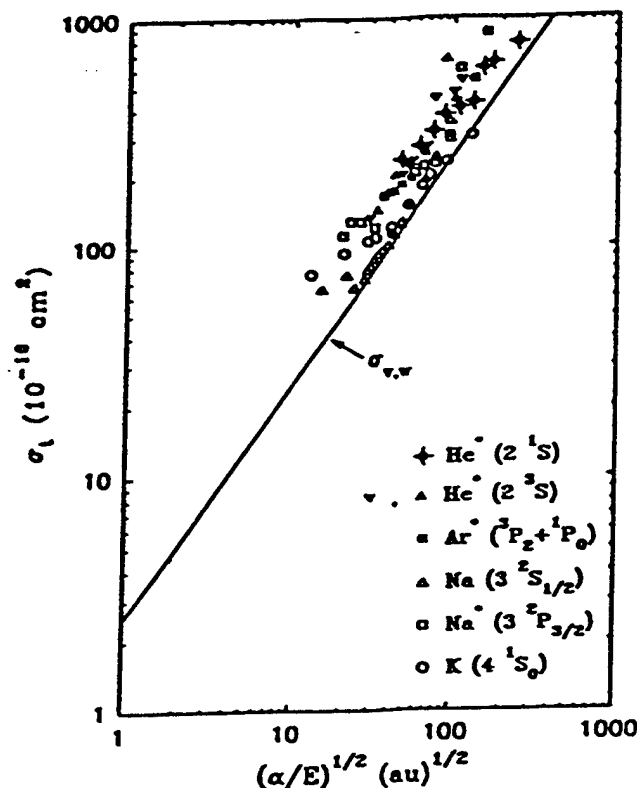
Fig. 5 Total electron scattering cross section plotted versus $(\alpha/\varepsilon)^{1/2}$ for a number of ground state and excited atoms (see the text and [9])
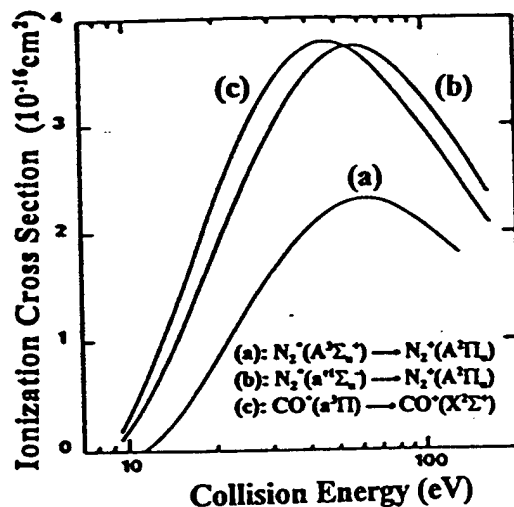
collisions involved in the electron-induced dipole scattering ([$\alpha(\text{He } (1^1S)) = 1.38 \, a_0^3$; $\alpha(\text{He}^*(2^3S)) = 315 \, a_0^3$ [9]). Actually, it has been shown [9] that the Vogt-Wannier "limiting case formula"

$$\sigma_{v,w} = 2.487 \times 10^{-16} \, (\alpha/\varepsilon)^{1/2} \qquad (1)$$

(where α and the electron energy,ε, are in atomic units and $\sigma_{v,w}$ in cm^2), obtained by considering the interaction between an electron and an atom to be simply the polarization function [11]

$$V(R) = -1/2 \, (e^2\alpha/R^4) \qquad (2)$$

predicts reasonably well the magnitude of the total scattering cross section (see Fig. 5). Clearly the large electron scattering cross sections for the excited states are largely due to the large α of the excited atoms (see, also, [1] and [2]).

Electron Impact Ionization of Excited Atoms and Molecules

There are no data that we know of on the electron impact ionization cross section σ_i of *vibrationally* excited molecules and those on *electronically* excited molecules are very limited [1,12]. In Fig. 6 are presented the results of a binary encounter approximation calculation [12b] for ionization of the metastables

Fig. 6 Calculated electron impact ionization cross sections for the metastables $N_2^*(A^3\Sigma_u^+)$, $N_2^*(a' \, ^1\Sigma_u^-)$ and $CO^*(a^3\Pi)$ (from [12b])

$N^*_2 (A^3\Sigma^+_u)$, $N^*_2 (a^1\Sigma^-_u)$ and $CO^*(a^3\Pi)$. These are generally higher than those for the corresponding ground state species; the peak values of the total ionization cross section for the ground state molecules are 2.5×10^{-16} cm^2 for N_2 and

131

2.6×10^{-16} cm^2 for CO [13]. Both theory and experiment have shown [2] that σ_i is larger for excited atoms compared to ground state atoms as can be seen from Fig. 7; the lower ionization thresholds and the higher dipole polarizabilities of the excited species cause a shift of the cross section maximum to lower energies which, in turn, affects the rate coefficients of the various discharge processes.

Electron Attachment to Excited Molecules

The internal energy of molecules plays a crucial role in determining their electron attachment (and detachment, see next Section) properties [1,3,16]. It has been known for sometime (e.g., see [1,3,5,16]) that the cross sections for *dissociative electron attachment* to "hot" (rovibrationally excited molecules) can be very much larger than for the ground state molecules. The increase is a function of the internal energy of the molecule and the relative positions of the potential energy curves (surfaces) of the dissociating negative ion state and the ground state; as the internal energy of the molecule increases, lower energy electrons are captured for which the cross sections are larger and the resultant transient anions dissociate faster. A recent example of such profound effects is shown in Fig. 8 [17]. It has, also, been known that *nondissociative electron attachment* to hot molecules decreases with increasing temperature due to enhanced autodetachment of the transient anion as its internal energy is increased [3,18]. The effect of temperature on electron attachment and detachment processes has been well studied recently with a

number of new techniques. In Fig. 9 is depicted the principle of one such new method, namely the *time-resolved electron swarm technique* [18]. This technique allows information on electron attachment and detachment processes to be obtained simultaneously from an analysis of transient electron waveforms. The electron swarm is produced by a narrow N$_2$ laser pulse
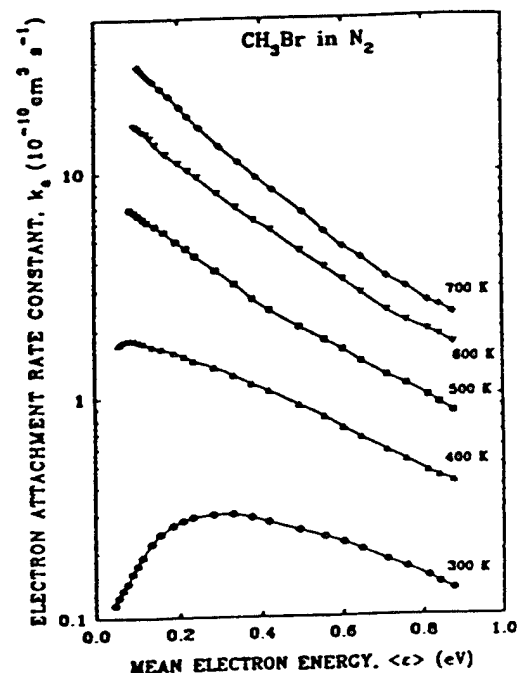

Fig. 8 Total dissociative electron attachment rate constant for CH$_3$Br as a function of the mean electron energy at various temperatures [17]
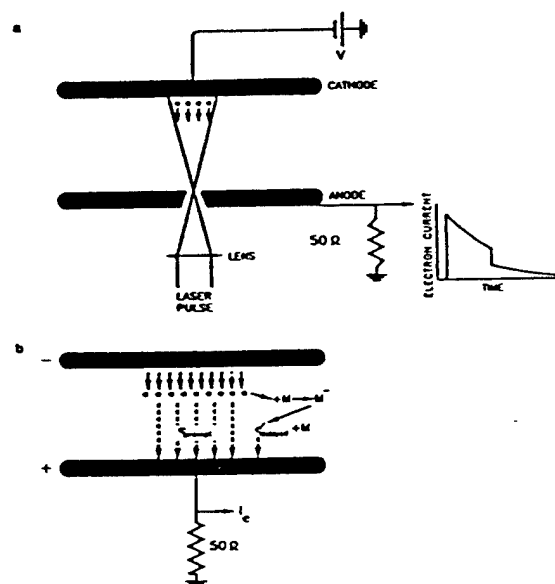

Fig. 7 Electron impact ionization cross section of the ground-state helium atom He(1^{1}S) (., [14]) and the excited helium He*(2^{3}S) (o, ■, [15])

Fig. 9 Schematic diagram of the principle of the time-resolved electron swarm technique (see [18] for details)

132

which strikes the cathode electrode through a hole in the anode electrode. The electrons drift to the anode under the influence of an applied electric field. As they drift a fraction is removed by attachment forming unstable negative ions which are quickly stabilized by collisions with the buffer gas, forming stable negative ions. Subsequently, these stabilized anions are thermally autodetached giving rise to delayed electrons. The motion of those electrons which reach the anode without ever been attached ("prompt" electrons) and those electrons which have been captured and then released ("delayed" electrons) induces a current in the anode circuit which is observed through a 50 Ω resistor to the ground. The electron current is given by [18,19]

$$i_e(t) = ew_e / d \int_{w_i t}^{min(w_e t, d)} \rho_e(x, t) \, dx \qquad (3)$$

where $\rho_e(x,t)$ is the electron number density; w_e and w_i are the electron and ion drift velocities and d is the drift distance. An example of the recorded waveforms as they were obtained for $c\text{-}C_4F_6^-$ is shown in Fig. 10. The solid curves [curve 1; Fig.10d] are the experimentally measured total electron currents as a function of time; the dash-dot curves [curve 2; Fig.10d] are the calculated electron current waveforms for the t_a^{-1} and t_d^{-1} obtained from a fit to Eq. 3 and the values of t_a^{-1} and t_d^{-1} given in the figure to curves 1; the dotted curves [curve 3; Fig.10d] represent the contribution to the total electron current of the initial (prompt) electron swarm when only electron attachment occurs, and the broken curves [curve 4; Fig. 10d] represent the contribution to the total electron current from the autodetached ("delayed") electrons. As T is increased this latter contribution becomes increasingly more significant; the parent anions autodetach faster. From recorded electron current waveforms such as in Fig. 10, the electron attachment frequency t_a^{-1} and the electron detachment frequency t_d^{-1} are obtained at each temperature using a nonlinear least squares fit; $t_a^{-1} = k_aN_a$ where k_a is the nondissociative electron attachment rate constant and N_a is the attaching gas number density. In Figs. 11a and 11b are shown, respectively, the k_a for $c\text{-}C_4F_6^-$ formation and the t_d^{-1} for $c\text{-}C_4F_6^-$ destruction by electron autoejection as a function of the mean electron energy and the gas temperature. Clearly while the electron attachment rate constant is little affected by increasing T above ambient, the electron detachment frequency t_d^{-1} is increased dramatically as T is raised from 450 to 600 K. The latter is also shown in Fig. 11c where t_d^{-1} is plotted as a function of the internal energy of the $c\text{-}C_4F_6^-$ anion. The heat-enhanced autodetachment has an activation energy of 0.237 eV for $c\text{-}C_4F_6^-$ and 0.477 eV for $C_6F_6^-$ [18]; it is a strong function of the electron affinity of the molecule. Thus, in sharp contrast to the profound increases in the thermally-induced autodestruction of the parent anions $c\text{-}C_4F_6^-$ and $C_6F_6^-$ with increasing T, no thermally-induced autodetachment was observed for SF_6^- up to 600 K. This is understood on the basis of the larger electron affinity (1.05 eV [20]) of the SF_6 molecule. At least up to 600 K, the collisionally stabilized SF_6^-

is stable with respect to autodetachment ($t_d^{-1} < 0.001 \times 10^6 \, s^{-1}$ [18])·

On the basis of these results, then, it can be concluded that there is littlte effect of T on the k_a of parent anion formation but there is a profound effect of T on the autodetachment frequency which increases with T; this increase, however, depends rather strongly on the binding of the extra electron in the anion. These findings are significant for the modelling of gas discharges and for understanding the behavior of gaseous dielectrics especially under conditions where electron detachment is a source of gas-breakdown-initiating electrons.

Recent studies [3,21] on electron attachment to electronically excited molecules—prepared by laser light prior to or concomitantly with the generation of the attaching electrons—have shown that the cross section for *dissociative electron attachment* to electronically excited molecules can be orders of magnitude larger than for the ground state molecules. A number of techniques have been developed for these studies and their principle is shown in Fig. 12·

The first group (Figs 12a-c) deals with electron attachment to excited electronic states— poduced directly or indirectly from higher-lying excited states reached initially by single or multiple photon absorption— studied in high pressure (1 to 100 kPa) gas mixtures using a pulsed Townsend technique [21a,b,c]. In Fig. 12a, a laser pulse enters the interaction region through the gridded bottom electrode, produces excited molecules M^* in the interaction region, and generates a pulse of electrons at the top electrode. The electron swarm reaches a known steady-state energy distribution within $<10^{-8}$ s, and drifts through the partially excited gas. The drift time taken by the electrons to reach the bottom electrode is $< 10^{-5}$ s, and thus electron attachment to the excited states can take place if the lifetime τ of the excited molecules is $> 10^{-5}$ s.

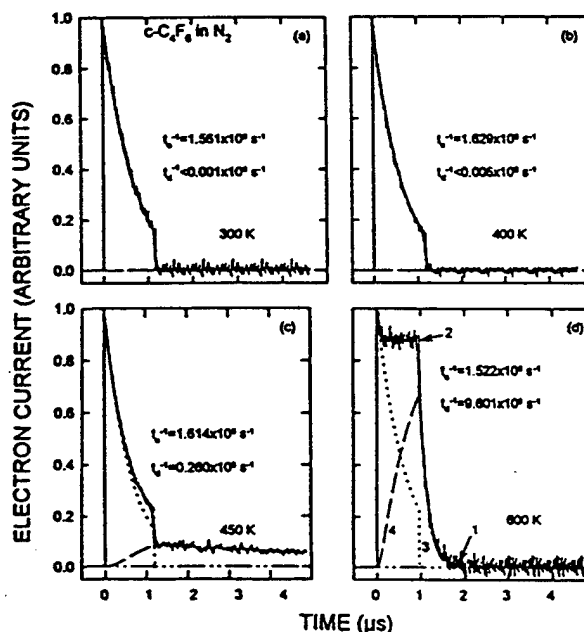Fig. 10 Electron current waveforms for $c\text{-}C_4F_6$ in N_2 at T = 300, 400, 450 and 600 K. All waveforms are for E/N = 1.24×10^{-17} Vcm^2; N_T = 6.44×10^{19} molecules cm^{-3} [18]
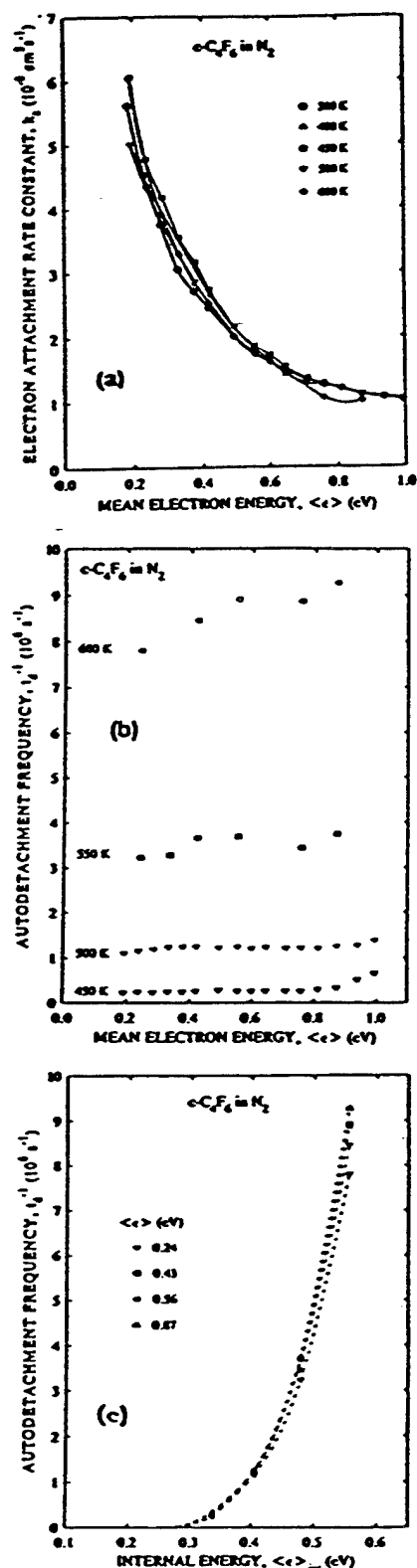
133

Fig. 11 a. Electron attachment rate constant k_a for c-C_4F_6 as a function of the mean electron energy $<\varepsilon>$, at various temperatures

b. Autodetachment frequency t_d^{-1} for c-$C_4F_6^-$ as a function of the mean electron energy at 450, 500, 550 and 600 K.

c. Autodetachment frequency t_d^{-1} for c-$C_4F_6^-$ as a function of the internal energy of the anion for four values of the mean electron energy [18]
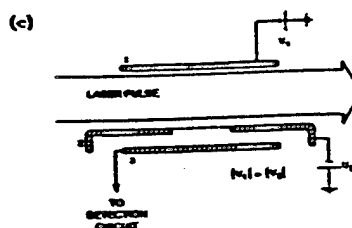
ELECTRON ATTACHMENT TO ELECTRONICALLY-EXCITED MOLECULES

Electron Swarm Experiments:

—Electrons brought to the excited molecules M* within $\tau_M^*(\geq 10^{-5}s)$

(a)

(b)
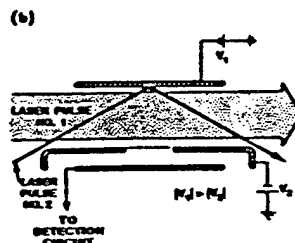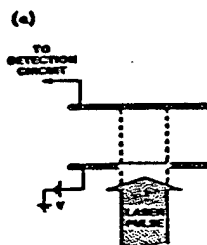
— Electrons produced concomitantly with and in the vicinity of M* $(\tau_M^* < 10^{-6} s)$

(c)

Electron Beam Experiments

(4)
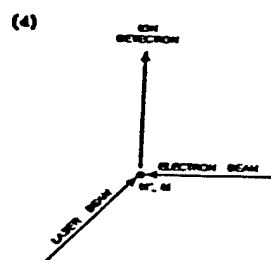
—Proper Synchronization of laser and electron beams

$-\tau_{detection} < min. \{ \tau_M^* ; \tau_{diffusion} \}$

Fig. 12 Principles of novel electron swarm and electron beam techniques for the study of electron attachment to electronically excited molecules (see the text and [3],[21])

134

The arrangement of Fig.12b is an improved version of that in Fig. 12a. The production of excited species is decoupled from that of the attaching electrons by using two lasers as shown; thus the time delay between the production of the excited species and the arrival of the attaching electrons in the interaction region can be varied. Furthermore, the use of three electrodes for separating the interaction and the detection regions allows the detection of negatively charged particles unambiguously.

In these two arrangements the electrons are brought to the excited molecules M^* within the lifetime τ_M^* of M^* which must be $> 10^{-5}$ s. By contrast, in Fig. 12c the principle of another swarm technique is illustrated which has been developed [21 b,c] to measure electron attachment to short-lived excited states ($\tau_M^* < 10^{-8}$ s) in a high-pressure (1 to100 kPa) environment. The electrons are produced concomitantly with and in the vicinity of the excited molecules M^* (via photoionization of the same gas under study or a suitable additive gas) by a single laser pulse (Fig.12c). Since the excited species and the electrons are produced in close proximity, electron attachment can occur in spite of the short τ_M^*.

The second group of techniques (Fig. 12d) deals with long-lived ($\tau_M^* > 10^{-5}$ s) excited electronic states under single collision conditions (pressures $< 10^{-4}$ torr) using electron beams and pulsed lasers. They require proper synchronization of the laser and the electron beams. In the only such experimental study to date [21d], the electron beam was continuous and the laser beam was an excimer laser pulse having repetition rates of < 150 Hz. In this experiment it was important to selectively detect negative ions arriving at the detector within a particular gate time $\Delta\tau_G$ after a preset delay time τ_D from each laser pulse. The gate delay is associated with the time taken by the (laser-initiated) negative ions to arrive at the detector, and the gate time should be $<$ minimum (τ_M^*, τ_D), where τ_M^* is the lifetime of the excited molecules and τ_D is the time taken by the excited molecules to diffuse out of the interaction region. (See details in [3, 21d]).

Examples of the new information obtained by these three types of novel experiments represented by Figs 12a,b, Fig. 12c, and Fig. 12d are shown, respectively, in Figs 13, 14, and 15. In Fig. 13 is shown the first [21a] observation of optically enhanced dissociative electron attachment to electronically excited states. Curve 1 is the coefficient for dissociative electron attachment to the thiophenol molecule (C_6H_5SH) in the ground state (laser off) as a function of the density reduced electric field E/N ; curve 3 is the measured coefficient for electron attachment to the thiophenol molecule in its first excited triplet state, reached indirectly from higher excited (singlet) states, themselves populated by single photon absorption using the 249 nm KrF excimer line. When the laser photon energy is below the first excited singlet state of the molecule (which is the case for the 308 nm laser line) no enhancement is observed (curve 2 in Fig. 13). The enhancement is actually about 100 times larger than indicated in the figure since the ratio of the excited to the unexcited thiophenol molecules was about 0.01 under the experimental conditions of reference 21a.

In Fig.14 are shown the large negative ion signals observed when H_2 was irradiated with the ArF laser line (192 nm) and its dependence on the laser intensity I. Virtually no anions are formed from ground state H_2 at room temperature; the rate constant for H^- production at 3.75 eV is $< 10^{-14}$ cm^{3}s^{-1} (see p. 455 of [5]). The large negative ion signals under laser irradiation were interpreted as resulting from electron attachment to high-
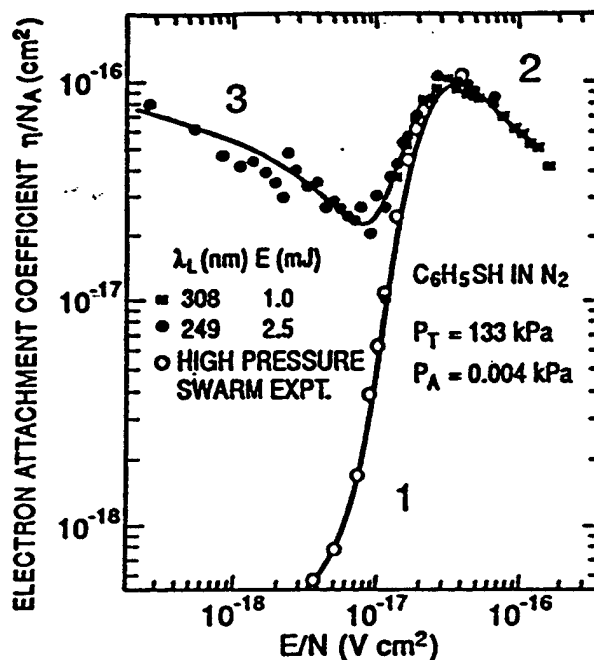

Fig. 13 Electron attachment coefficient η/N_a versus E/N for C_6H_5SH in N_2 for the ground state (curves 1 and 2) and the first excited triplet state (curve 3) of the molecule [21a]
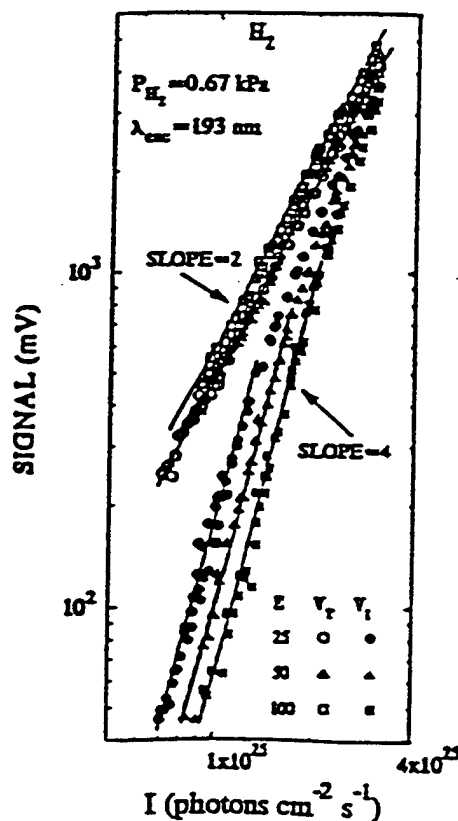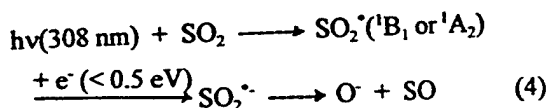

Fig. 14 Laser intensity ,I, dependence of the measured total (V_T) and negative ion(V_I) signal for H_2 under the experimental conditions shown in the figure (see the text and [21c])

lying excited states of H_2 which are reached by three-photon absorption; they indicated that the rate constants for electron attachment to such states (or to lower-lying excited states to which these decay) are enormous: $> 10^{-6}$ cm^{3}s^{-1} [21c,22]. Cross sections of such magnitude can have profound implications in many technologies (e.g., negative ion and neutral particle beams [22], H_2 discharges [23], lasing mechanisms [24]). The observation of laser enhanced dissociative electron attachment to SiH_4 [25], CH_4 [26] and other molecules [3] points to their possible significance in plasma deposition and materials processing and to the possible development of ultrasensitive analytical instruments.

In Fig. 15 is compared the cross section for O$^-$ production from SO_2 in the ground state (Fig.15a) and under laser irradiation (XeCl line; 308 nm) (Fig. 15b). The O$^-$ signal with the laser on was obtained at a laser repetition rate of 150 Hz; the rest of the experimental conditions were as for Fig. 15a. It is evident that under laser irradiation in addition to the ground-state processes (Fig. 15a) an intense peak appears at near-zero energy which was attributed [21d] to the reaction

$$h\nu(308 \text{ nm}) + SO_2 \longrightarrow SO_2^*(^1B_1 \text{ or } ^1A_2)$$
$$\xrightarrow{+ e^- (< 0.5 \text{ eV})} SO_2^{*-} \longrightarrow O^- + SO \qquad (4)$$

The electron energy required for the transition from $SO_2^*(^1B_1$ or $^1A_2)$ to SO_2^{*-} is small, and thus the photoenhanced signal appears at close to zero energy. The photoenhanced resonance is also narrower, due to the change in the equilibrium distance of SO_2^* compared to SO_2. The broken
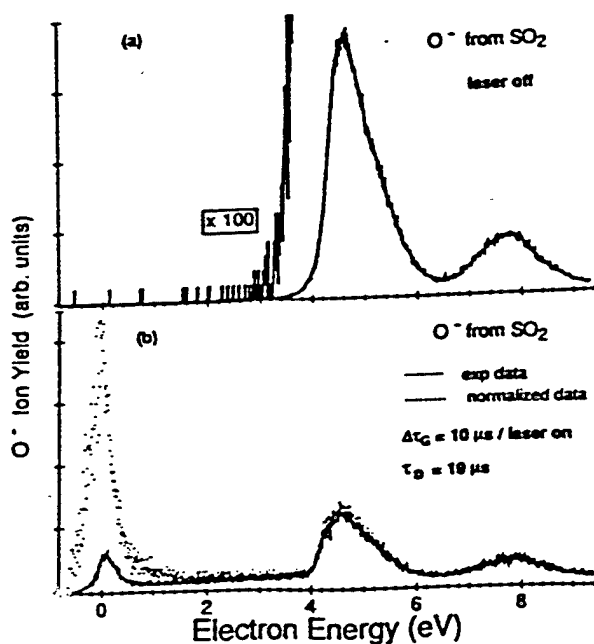
curve in Fig. 15b is the experimental data corrected for the variation of the electron current with electron energy and normalized at 8 eV (see [21d]). The intensity of the near-zero energy peak is very much larger than is indicated in the figure because only a small fraction of the SO_2 molecules are excited by each laser pulse. The peak cross section value for the photoenhanced O$^-$ signal was estimated [21d] to be at least 2 to 3 orders of magnitude larger than the peak cross section value (2.46×10^{-18} cm^2) for O$^-$ from the ground state.

These observations may have implications for the behavior of SO_2 and other similar-type pollutants in the atmosphere.

PHOTON-ANION AND PHOTON-MOLECULE INTERACTIONS AND THE STUDY OF RADICALS

Photodetachment and photodissociation are two photoprocesses of interest to gas discharges. The former creates free electrons and the latter free radicals.

Photodetachment

A significant recent accomplishment has been the development of new techniques for the study of photodetachment processes in both the gas [27-31] and the other states of matter (e.g., see [30]). The method described in [30] and [31] is particularly sensitive and can provide accurate measurement of absolute photodetachment cross sections $\sigma_{pd}(\nu)$ and photodetachment energetics. In Fig. 16 are presented the results of [31] for the reaction

$$SF_6^- + h\nu \longrightarrow SF_6 + e \qquad (5)$$

The photodetachment cross section has a threshold at 3.16 eV which is about three times larger than the electron affinity of the SF_6 molecule (about 1.05 eV). The magnitude of the
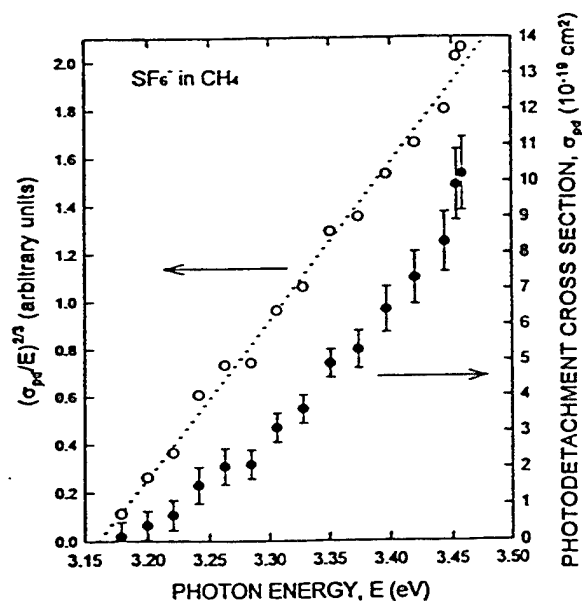

Fig. 15 Relative cross section for the production of O$^-$ from SO_2 as a function of electron energy for ground state SO_2 molecules (Fig.15a) and for a mixture of ground and excited SO_2 molecules (Fig.15b) (See the text and [21d])

Fig. 16 (.) Photodetachment cross section $\sigma_{pd}(E)$ for SF_6^- in a buffer gas (CH_4) as a function of photon energy E. (o) A plot of $(\sigma_{pd}(E) / E)^{2/3}$ versus E consistent with a threshold value of 3.16 eV [31]

photodetachment cross section increases from the threshold to 1.0×10^{-18} cm^2 at a photon energy of 3.46 eV. The small size of the measured photodetachment cross section is attributed to the large relaxation in the equilibrium internuclear positions of SF$_6^-$ compared to SF$_6$.

Photodissociation

A most interesting study of this fundamental process is that on the photodissociation of freons under collisionless conditions using lasers: CHFCl$_2$ [32], CHCl$_3$ [32], CF$_2$BrCl [33], CFCl$_3$ [34], CF$_2$Cl$_2$ [35] and the radical CHCl$_2$ [32]. These studies provided absolute cross section data and photodissociation quantum yields for specific radicals which can allow the controlled photoproduction of radicals for further study. Such investigations are important in view of the use of these freon compounds in plasma processing of materials. In Table 1 are listed pertinent findings by these workers. The high yields for the reactions given in the Table clearly show that at the laser light wavelength (193 nm) used, the decay of the excited states of these freons is via the C -Cl fission. (See, also, a review of absolute cross sections for photoabsorption, partial photoionization and ionic photofragmentation processes for a number of molecules in [36]).

Table 1: Photodissociation of freons by 193 nm laser light

Photodissociation Reaction	Photodissociation Cross Section (10^{-18} cm^2)	Photodissociation Quantum Yield	Reference
CF$_2$Cl$_2$ + hv → CF$_2$Cl + Cl	~ 3.5	~ 1	33
CFCl$_3$ + hv → CFCl$_2$ + Cl	14	~ 1	34
CHFCl$_2$ + hv → CHFCl + Cl	2	~ 1	32
CHCl$_3$ + hv → CHCl$_2$ + Cl	8	~ 1	32

Radicals

The study of radicals, especially those radicals which are of technological significance, is rather demanding. Very little is known, for example, about their electron attachment, scattering and impact ionization properties. Efforts are under way at the authors' laboratory to study electron attachment to radicals and recently significant results have been reported [37-40] on electron impact ionization of radicals of interest to plasma etching and deposition. For example, the free radicals CF$_3$, CF$_2$, and CF were prepared [37-40] by near-resonant charge transfer reactions of CF$_3^+$, CF$_2^+$ and CF$^+$ with various species (e.g., Xe) and the positive ions produced by electron impact on them have been identified and quantified. These radicals and their ions are most abundant and reactive species that result from the dissociation of CF$_4$.

In Fig. 17a are shown [37] the absolute cross sections for dissociative ionization of CF$_x$ (x = 1-3) free radicals of CF$_3$; the molecular fragment ionization (CF$_2^+$, CF$^+$ from CF$_3$) cross section exceeds the parent ionization cross section (CF$_3^+$ from CF$_3$). In Fig. 17b are presented absolute cross sections for the parent ionization of the CF$_x$ (x = 1-3) radicals by electron impact [38]. These results are important in modeling discharges of the CF$_4$ gas.
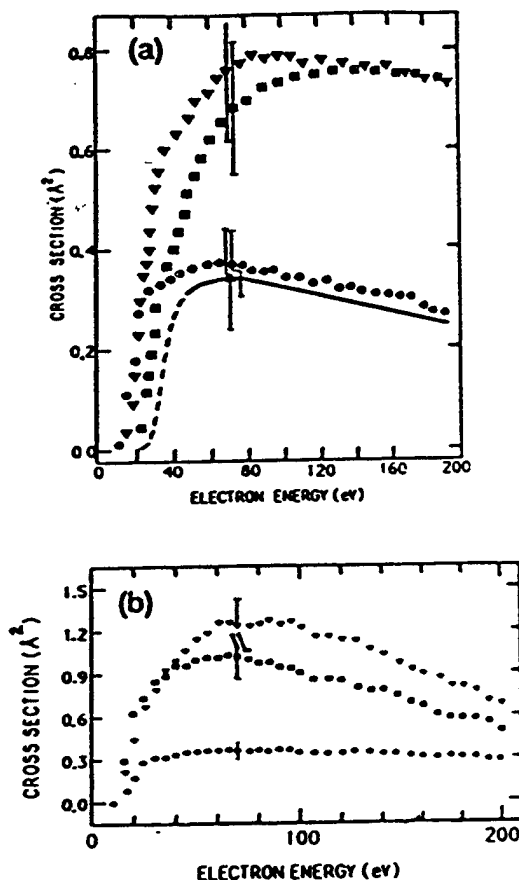

Fig. 17 a. Absolute electron-impact ionization cross section for the formation of CF$_3^+$ parent ions (.) and CF$_2^+$ (▼) and CF$^+$ (■) fragment ions from CF$_3$ as a function of electron energy. Also shown (▲) is the absolute cross section for the formation of F$^-$ at 70 eV. The energy dependence of the F$^-$ cross section is indicated by the solid line above 50 eV and by the broken line below 50 eV [37] b. Absolute electron- impact ionization cross section for the formation of the CF$_x$ (x = 1 to 3) parent ions as a function of electron energy; (.) CF$_3^+$, (■) CF$_2^+$ and (▼) CF$^+$ (from [38]).

ANION PROCESSES INVOLVING SF$_6$ DISCHARGE BYPRODUCTS

When electrical discharges occur in SF$_6$ or in mixtures of this gas with O$_2$ and H$_2$O, a host of stable or quasi-stable electronegative byproducts are formed which include such species as SOF$_2$, SO$_2$F$_2$, SOF$_4$, SO$_2$, S$_2$OF$_{10}$, S$_2$O$_2$F$_{10}$, SF$_4$, and S$_2$F$_{10}$ [41,42]. The cross sections for total electron scattering and electron attachment processes have recently been measured for these species [43-45]. Shown in Fig. 18 are the dissociative electron attachment rate coefficients as a function of E/N for SF$_6$, SOF$_2$, SO$_2$F$_2$, SF$_4$, and SO$_2$ in SF$_6$ which were calculated from directly measured cross sections in an electron beam apparatus [43]. Although the dissociative attachment rates for the byproducts indicated in Fig. 18, as well as the rates for SOF$_4$ (not shown in the figure) fall below the values for SF$_6$, the rates are still high enough that the dielectric strength of SF$_6$ is not measurably reduced when small amounts of these compounds are present.
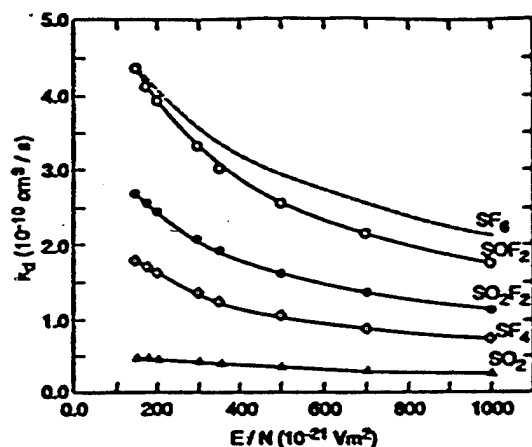
137

Fig. 18 Calculated total dissociative electron attachment rate coefficients for SF_6 and its discharge byproducts SOF_2, SO_2F_2, SF_4 and SO_2 in SF_6 as a function of E/N [43]

Fig. 19 Electron energy dependence of the total cross section for dissociative electron attachment to S_2OF_{10} (long dashed line), $S_2O_2F_{10}$ (short dashed line) and SF_6 (solid line) in comparison with the calculated maximum s-wave capture limit ($\pi \lambda^2$) [45]

The byproducts S_2F_{10}, S_2OF_{10}, and $S_2O_2F_{10}$, on the other hand, have electron attachment cross sections and corresponding electron attachment rate constants that are significantly higher than those for SF_6. Figure 19 shows the measured [45] electron energy dependence of the absolute cross sections for dissociative electron attachment to S_2OF_{10}, $S_2O_2F_{10}$, and SF_6 compared to the calculated maximum s-wave capture limit ($\pi \lambda^2$) corresponding to the Wigner threshold condition [46].The cross sections for both S_2OF_{10} and $S_2O_2F_{10}$ are anomalously high, exceeding the s-wave limit at 0.1 eV by more than an order of magnitude. In the case of these molecules, there is reason to question the applicability of partial-wave analysis and therefore the s-wave limit to electron scattering because the electron-molecule interaction potentials are not likely to satisfy the requirement of spherical symmetry. It should be kept in mind that these are relatively large, asymmetric molecules that likely have multicentered interaction potentials.

The dissociative electron attachment cross section for S_2F_{10} also exhibits somewhat unusual behavior as is illustrated by the results shown in Fig. 20 which indicate a significant cross section for electron impact energies up to 11 eV. For all other SF_6 oxidation byproducts it is found that electron attachment occurs at electron energies below 8.0 eV [43,45]. The higher energy electron attachment resonances above 4 eV do not contribute significantly to the electron attachment rate for E/N less than 10^{-18} Vm^2 corresponding to typical discharge conditions in SF_6. This accounts for the relatively low rates for SO_2 seen in Fig. 18, because its ground-state dissociative electron attachment cross section is peaked near 5 eV (see Fig. 15). It is also interesting to note that SF_6^- formation contributes significantly to the S_2F_{10} dissociative attachment process at low energies below 1 eV. The experimental results [43-45] show that dissociative electron attachment is the predominant electron attachment process that occurs for all SF_6 byproducts mentioned above, and therefore, the electron attachment process will contribute to the destruction of these species in a discharge.

In assessing the role of anion processes in SF_6 discharges there are other unusual characteristics of the anion chemistry in this gas that should be pointed out. The first concerns the anomalously high collisional detachment threshold energies that have been observed [47] for the ions F^-, SF_5^-, and SF_6^- that result from electron attachment to SF_6. The measured collisional detachment cross sections for these three ions are shown in Fig. 21 and indicate that SF_6^- and SF_5^- both have detachment thresholds at about 90 eV and F^- at about 8 eV. Because of these high thresholds, the negative ions formed directly form SF_6 will not detach by collision under
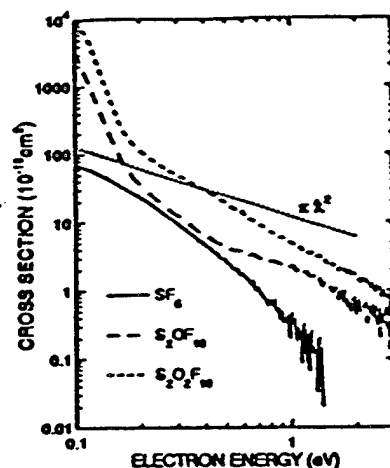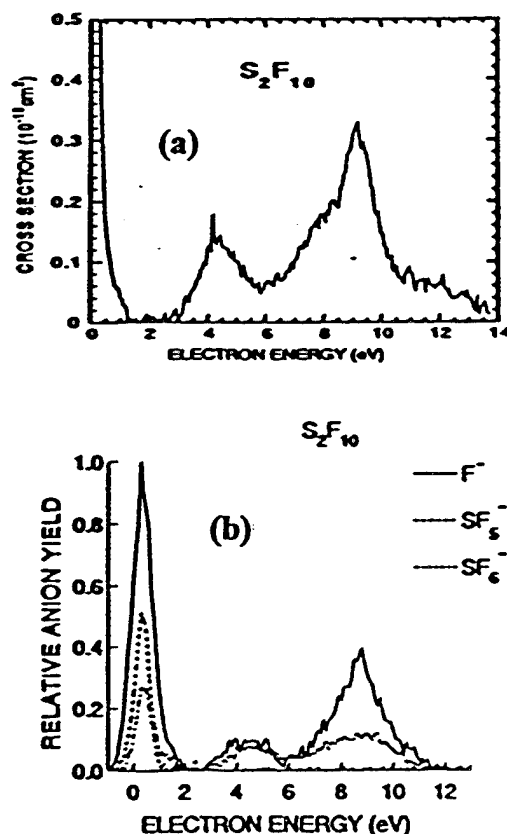

Fig. 20 a. Electron energy dependence of the cross section for dissociative electron attachment to S_2F_{10} [45]
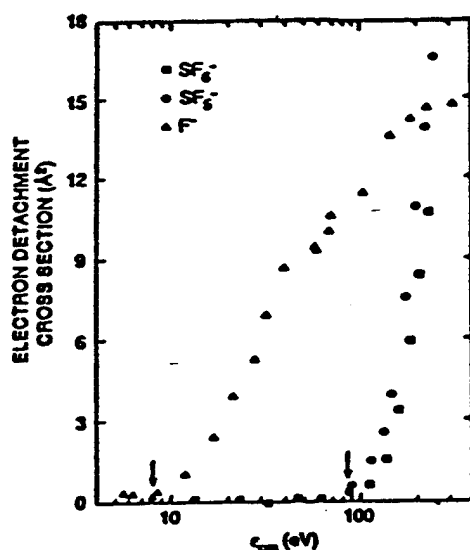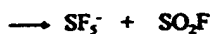b. Electron energy dependence of the relative anion yields from dissociative electron attachment to S_2F_{10} [45]

138

Fig. 21 Collisional electron detachment cross sections for F⁻, SF₅⁻, and SF₆⁻ on SF₆ target gas as a function of the center-of-mass energy [47]

ELECTRON SCATTERING CROSS SECTIONS FOR SILANE AND HALOCARBONS

In this section we refer to two recent studies dealing with the determination of electron scattering cross sections for polyatomic molecules of technological interest. The first study is on SiH_4 and is prototypical of the continuous effort to obtain consistent sets of low-energy electron scattering cross sections for the various elastic and inelastic processes for polyatomic molecules using electron swarm transport coefficients and Boltzmann transport equation analysis or Monte Carlo computations. In Fig.22 is shown the set of cross sections obtained recently [52] for SiH_4 by the use of Monte Carlo calculations and transport data in SiH_4-He mixtures. The authors emphasized the significance of using electron transport data on SiH_4 in a "non-Ramsauer buffer gas" (He) to achieve consistency in the derived cross sections. Cross section sets of this type are important in identifying and quantifying the precursors and the mechanisms in thin film technology using SiH_4 gas [52].

The second study is on halocarbons CF_4, $CClF_3$, CCl_2F_2, CCl_3F and CCl_4 [53] and is prototypical of efforts to measure electron scattering cross sections over wide energy ranges using monoenergetic electron beams. The measurements of this investigation on the total electron scattering cross sections from 10 to 4000 eV are shown in Fig. 23 (see, also, [54] and [55]).
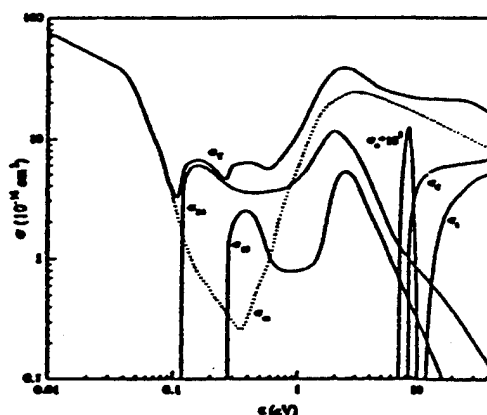
typical discharge conditions. It can, therefore, be concluded that collisional detachment processes in SF_6 that are important for determining discharge initiation probability, will be controlled by anions associated with impurities such as OH⁻ from H_2O [48]. Once discharge byproducts appear in the gas, they can become important in controlling the anion chemistry through such fast reactions as:

$$SF_6^- + SOF_4 \longrightarrow SOF_5^- + SF_5$$

$$SF_6^- + SO_2 \longrightarrow SO_2F^- + SF_5$$

$$\longrightarrow SF_5^- + SO_2F$$

$$\longrightarrow SO_2F_2^- + SF_4$$

which have high rates that approach the theoretical collision limit at low temperatures or at low E/N [49, 50]. In a decomposed gas in which oxyfluoride byproducts are present, the predominant initial SF_6^- anion will rapidly convert to other ions such as SOF_5^-. At the present time, little is known about the collisional detachment rates of the oxyfluoride-type anions.

Fig. 22 Electron collision cross sections for SiH_4; the subscripts T, m, 24, 13, a, d, i correspond to the total (elastic + inelastic), momentum transfer, first vibrational, second vibrational, attachment, dissociation and ionization cross sections respectively [52].

EFFECT OF MEDIUM ON GAS-PHASE REACTIONS; INTERACTIONS ON SURFACES

Many fundamental reactions depend on the density and nature of the medium in which they occur. The behavior, for example, of slow electrons in matter depends on the state of matter. In addition, the surface often acts as a catalyst and the cross sections for and energetics of reactions occurring on the surface differ from -- and affect-- those in the gas. These processes need detailed investigation as do clustering phenomena involving neutrals and/or charged particles. The topic is of current interest (e.g., see [16] and [51]).

CONCLUSION

New methods and experimental techniques provide basic knowledge which allows a deeper understanding of fundamental gas discharge processes. This knowledge opens up new possibilities for applications.
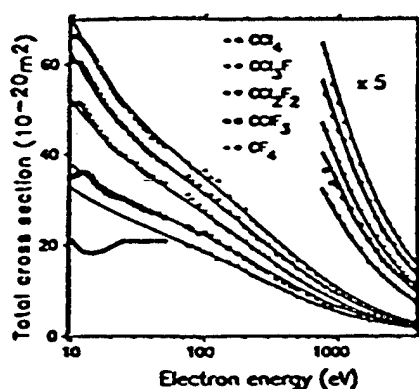
Fig. 23 Total cross sections for electron scattering from chlorofluoromethanes in the energy range 10 to 4000 eV. Points are experimental data and curves are semiempirical fits (from [53])

REFERENCES

[1] Christophorou, L. G., In XXth Intern. Conf. on Phenomena in Ionized Gases. Palleschi, V., Singh, D. P. and Vaselli, M., (Editors), (Pisa: Instituto di Fisica Atomica e Molecolare), Invited Papers, p. 3, 1991.

[2] Trajmar, S. and Nickel, J. C., in Adv. Atom. Mol. Opt. Phys., Bates, D. R. and Bederson, B. (Editors), Academic, Orlando, FA, p. 45, 1993.

[3] Christophorou, L. G., Pinnaduwage, L. A. and Datskos, P. G., in Linking the Gaseous and Condensed Phases of Matter. Christophorou, L. G., Illenberger, E., and Schmidt, W. F.(Editors), Plenum, New York, p. 415, 1994.

[4] a. Buckman, S.J., Elford, M. T., Newmam, D. S., J. Phys B20, p. 5175, 1987.
b. Fersch, J., Masche, C., Raith, W., Wiemann, L., Phys Rev. A 40, p. 5407, 1989.
c. Johnstone, W. M., Mason, N. J.and Newell, W. R., J. Phys. B 26, p. L147, 1993.

[5] Christophorou, L.G., Atomic and Molecular Radiation Physics, Wiley-Interscience, New York, 1971.

[6] Hall, R. I. and Trajmar, S., J. Phys. B 8, p. L293, 1975.

[7] Milloy, H. B., Crompton, R. W., Rees, J. A. and Robertson, A. G., Austr. J. Phys. 30, p. 61, 1977.

[8] Robinson, E. J., Phys. Rev. 182, p. 196, 1969.

[9] Christophorou, L. G. and Illenberger, E., Phys. Lett. A173, p. 78, 1993.

[10] Muller-Fiedler, R., Schlemmer, P., Jung, K., Hotop, H. and Ehrhardt, H., J. Phys. B 17, p. 259, 1984.

[11] Vogt, E. and Wannier, G. H., Phys. Rev. 95, p. 1190, 1954.

[12] a. McCann, K. J., Flannery, M. R., and Hazi, A., Appl. Phys. Lett. 34, p. 543, 1979.
b. Ton-That, D. and Flannery, M. R., Phys. Rev. A 15, p. 517, 1977.
c. Armentrout, P. B., Tarr, S. M., Dori, A. and Freund, R. S., J. Chem. Phys. 75, p. 2786, 1981.

[13] Ref. 5, pp. 390,391.

[14] Krishnakumar, E. and Srivastava, S. K., J. Phys. B 21, p. 1055, 1988.

[15] Dixon, A. J., Harrison, M. F. A. and Smith, A. C. H., J. Phys. B 9, p.2617, 1976.

[16] Christophorou, L. G., McCorkle, D. L. and Christodoulides, A. A., in Electron-Molecule Interactions and Their Applications. Christophorou, L. G.(Editor) Academic, Orlando, FA, Vol. 1, Chapter 6, 1984.

[17] Datskos, P. G., Christophorou, L. G. and Carter, J. G., J. Chem. Phys. 97, p. 9031, 1993.

[18] a. Datskos, P. G., Christophorou, L. G. and Carter, J. G., J. Chem. Phys. 99, p. 8607, 1993.
b. Datskos, P. G., Christophorou, L. G. and Carter, J. G., J. Chem. Phys. 98, p. 7875, 1993.
c. Christophorou, L. G. and Datskos, P. G., Intern. J. Mass Spectr. Ion Processes, in press.

[19] Wen, C. and Wetzer, J. M., IEEE Trans. Electr. Insul. 23, p. 999, 1988; 24, p. 143, 1989.

[20] Grimsrud, E. P., Chowdhury, S. and Kebarle, P., J. Chem. Phys. 83, p. 1059, 1985

[21] See, for example:
a. Christophorou, L. G., Hunter, S. R., Pinnaduwage, L. A., Carter, J. G., Christodoulides, A. A. and Spyrou, S. M., Phys. Rev. Lett. 58, p. 1316, 1987.
b. Pinnaduwage, L. A., Christophorou, L. G. and Hunter, S. R., J. Chem. Phys. 90, p. 6275, 1989.
c. Pinnaduwage, L. A. and Christophorou, L. G., Phys. Rev. Lett. 70, p.754, 1993.
d. Jaffke, T., Hashemi. R., Christophorou, L. G., Illenberger, E., Baumgartel, H., and Pinnaduwage, L. A.,Chem. Phys. Lett. 203, p. 21, 1993.

[22] Pinnaduwage, L. A. and Christophorou, L. G., J. Appl. Phys. 76, p. 46, 1994.

[23] Garscadden, A. and Nagpal., Plasma Source Sci. Technol. (preprint, private communication, August, 1994).

[24] Kielkopf, J. F., Pinnaduwage, L. A. and Christophorou, L. G., Phys. Rev. A 49, p. 2675, 1994.

[25] Pinnaduwage, L. A., Martin, M. Z. and Christophorou, L. G., Appl. Phys. Lett. 65, p. 2571, 1994.

[26] Pinnaduwage, L. A., Martin, M. Z. and Christophorou, L. G., Contributions to Plasma Physics (submitted, February, 1995).

[27] Drzaic, P. S. and Brauman, J. I., J. Amer. Chem. Soc. 104, p. 13, 1982.

[28] Mock, R. S. and Grimsrud, E. P., Chem. Phys. Lett. 184, p. 99, 1991.

[29] Ingolfsson, O., Illenberger, E. Schmidt, W. F., Inten. J. Mass Spectr. Ion Processes 139, p. 103, 1994.

[30] Christophorou, L. G., Datskos, P. G. and Faidas, H., J. Chem. Phys. 101, p. 6728, 1994.

[31] Datskos, P. G., Carter, J. G. and Christophorou, L. G., Chem. Phys. Lett. (in press).

[32] Yang. X., Felder, P. and Huber, J. R., Chem. Phys. 189, p.127, 1994.

[33] Baum, G. and Huber, J. R., Chem. Phys. Lett. 203, p. 261, 1993.

[34] Felder, P. and Demuth, C., Chem. Phys. Lett. 208, p.21, 1993.

[35] Baum, G. and Huber, J. R., Chem. Phys. Lett. 213, p. 427, 1993.

[36] Gallagher, J. W., Brion, C. E., Samson, J. A. R. and Langhoff, P. W., J. Phys. Chem. Ref. Data 17, p. 9, 1988.

[37] Tarnovsky, V., Kurunczi, P., Rogozhnikov, D. and Becker, K., Intern. J. Mass Spectr. Ion Processes 128, p. 181, 1993.

[38] Tarnovsky, V. and Becker. K., J. Chem. Phys. 98, p.7868, 1993.

[39] Tarnovsky, V., Levin, A. and Becker, K., J. Chem. Phys. 100, p. 5626, 1994.

[40] Deutsch, H., Mark, T. D., Tarnovsky, V., Becker, K., Cornelissen, C., Cespiva, L. and Bonacic-Koutecky, V., Intern. J. Mass Spectr. Ion Processes 137, p. 77, 1994.

[41] Sauers, I., Ellis, H. W. and Christophorou, L. G., IEEE Trans. Elec. Insul. 21, p. 111, 1986.

[42] Van Brunt, R. J. and Herron, J. T., Physica Scripta T53, p. 9, 1994.

[43] Wan, H.- X., Moore, J. H., Olthoff, J. K. and Van Brunt, R. J., Plasma Chem. Plasma Proc. 13, p.1, 1993.

[44] Sauers, I., Christophorou, L. G. and Spyrou, S. M., Plasma Chem. Plasma Proc. 13, p. 17, 1993.

[45] Olthoff,J. K., Stricklett, K. L., Van Brunt, R. J., Moore, J. H., Tossell, J. A. and Sauers, I., J. Chem. Phys. 98, p. 9466, 1993.

[46] Wigner, E. P., Phys. Rev. 73, p. 1002, 1948.

[47] Olthoff, J. K., Van Brunt, R. J., Wang, Y., Champion, R. L. and Doverspike, L. D., J. Chem. Phys. 91, p. 2261, 1989.

[48] Van Brunt, R. J., J. Appl. Phys. 59, p. 2314, 1986.

[49] Sieck, L. W. and Van Brunt, R. J., J. Phys. Chem. 91, p. 708, 1988.

[50] Van Brunt, R. J., Sieck, L. W., Sauers, I. and Siddagangappa, M. C., Plasma Chem. Plasma Proc. 8, p. 225, 1988.

[51] See, for example:
a. Christophorou, L. G., Illenberger, E. and Schmidt, W. F., Editors, Linking the Gaseous and the Condensed Phases of Matter, Plenum Press, New York, 1994, and references cited therein.
b. Illenberger, E., Chem. Rev. 92, p. 1589, 1992.
c. Sanche, L., IEEE Trans. Electr. Insul. 28, p. 789, 1993.
d. Christophorou, L. G., in Physical and Chemical Mechanisms in Molecular Radiation Biology, Glass, W. A. and Varma, M. N., Editors, Plenum press, New York, p. 183, 1991.

[52] Nagpal, R. and Garscadden, A., in Gaseous Dielectrics VII, Christophorou, L. G. and James, R. D., Editors, Plenum Press, New York, p. 39, 1995; Phys. Rev. Lett. 73, p. 1598,. 1994.

[53] Zecca, A., Karwasz, G. P. and Prusa, R. S., Phys. Rev. 46, p. 3877, 1992.

[54] Szmytkowski, C., Krzysztofowicz, A. M., Janicki, P. and Rosenthal, L., Chem. Phys. Lett. 199, p. 191, 1992.

[55] Randell, J., Ziesel, J-P., Lunt, S. L., Mrotzek, G. and Field, D., J. Phys. B 26, p.3423, 1993.